



HAL
open science

Climate-Glacier relationship in the monsoon-arid transition zone: A Case study in Himachal Pradesh, India

Farooq Azam Mohd

► **To cite this version:**

Farooq Azam Mohd. Climate-Glacier relationship in the monsoon-arid transition zone: A Case study in Himachal Pradesh, India. Earth Sciences. Université de Grenoble, 2014. English. NNT : 2014GRENU032 . tel-01230980

HAL Id: tel-01230980

<https://theses.hal.science/tel-01230980>

Submitted on 19 Nov 2015

HAL is a multi-disciplinary open access archive for the deposit and dissemination of scientific research documents, whether they are published or not. The documents may come from teaching and research institutions in France or abroad, or from public or private research centers.

L'archive ouverte pluridisciplinaire **HAL**, est destinée au dépôt et à la diffusion de documents scientifiques de niveau recherche, publiés ou non, émanant des établissements d'enseignement et de recherche français ou étrangers, des laboratoires publics ou privés.

THESIS

Submitted to obtain the degree of

DOCTOR OF THE UNIVERSITY OF GRENOBLE

Speciality : **Earth Sciences, Universe and Environment**

Arrêté ministériel : 1 November 2011

Presented by

Mohd Farooq AZAM

Thesis directed by **Patrick Wagnon**

and co-directed by **Christian Vincent & Ramanathan Alagappan**

Prepared in the **Laboratoire de Glaciologie et de Géophysique de l'Environnement/Laboratoire d'Etudes des Transferts en Hydrologie et Environnement, UJF/CNRS**
in **Doctoral school Earth Sciences, Universe and Environment**

Climate-Glacier relationship in the monsoon-arid transition zone: A Case study in Himachal Pradesh, India.

Defended publicly : **17 December 2014,**

Before the jury :

Mr. Gerhard KRINNER

Research Director, CNRS, LGGE (France), President

Mr. Martin HOELZLE

Professor, University of Fribourg (Switzerland), Reporter

Mr. Thomas SCHULER

Assistant Professor, University of Oslo (Norway), Reporter

Mr. Pierre RIBSTEIN

Professor, Pierre-and-Marie-Curie University (France), Examiner

Mr. Claudio SMIRAGLIA

Professor, University of Milano (Italy), Examiner

Mr. Patrick WAGNON

Chargé de recherche, IRD, LTHE (France), Director

Mr. Christian VINCENT

Ingénieur de Recherche, CNRS, LGGE (France), Co-director

Mr. Ramanathan ALAGAPPAN

Professor, Jawaharlal Nehru University (India), Co-guide



Dedicated to:

the victims of Leh flash flood in August 2010,
Kedarnath disaster in June 2013
and J&K flood in September 2014

Abstract

The Hindu-Kush Karakoram Himalaya (HKH) region is the largest snow and ice reservoir on the planet outside the Polar Regions. In the HKH region the mass balance and meteorological observations are sparse and the historical knowledge is mainly concentrated on snout fluctuation records. Hitherto, the understanding of glacier-climate relationship is poor in the HKH region. Therefore, the goal of the present work is to improve the understanding of glacier-climate relationship on a representative glacier 'Chhota Shigri' in the western Himalaya.

A number of in-situ measurements concerning mass balances, surface velocity, ice thickness and meteorology have been collected during and before the present PhD work since 2002. These data sets were first analyzed to understand the glacier behaviour and then used in the models to understand the glacier relationship with climatic variables. Between 2002 and 2013, glacier showed a mass wastage/unsteady-state conditions with a cumulative mass loss of -6.45 m w.e. Further, the ice flux analysis over 2002-2010 suggested that the glacier has experienced a period of steady-state or slightly positive mass balance during the 1990s.

We first reconstructed the annual and seasonal mass balances using a degree day model from simple meteorological variables, precipitation and temperature. This reconstruction allowed us to examine the mass balances between 1969 and 2012. Since 1969, Chhota Shigri showed a moderate mean mass wastage at a rate of -0.30 m w.e. a^{-1} . A period of steady-state between 1986 and 2000, already suggested by ice flux analysis and geodetic measurements, was confirmed. The mass balance evolution of this glacier revealed that the mass wastage is recent and provide a very different pattern than that of usually found in the literature on western Himalayan glaciers. The analysis of decadal time scale mass balances with meteorological variables suggested that winter precipitation and summer temperature are almost equally important drivers controlling the mass balance pattern of this glacier. Second, in order to understand the detailed physical basis of climatic drivers, a surface energy balance study was also performed using the in-situ meteorological data from the ablation area of Chhota Shigri Glacier. Net all-wave radiation was the main heat flux towards surface with 80% contribution while sensible, latent heat and conductive heat fluxes shared 13%, 5% and 2% of total heat flux, respectively. Our study showed that the intensity of snowfall events during the summer-monsoon is among the most important drivers responsible for glacier-wide mass balance evolution of Chhota Shigri Glacier. However, due to the lack of precipitation measurements and the strong precipitation gradient in this region, the distribution of precipitation on the glacier remains unknown and needs further detailed investigations.

Keywords: Himalaya, Glacier, Mass Balance, Steady-State, Energy Balance, Summer-Monsoon, Albedo.

Résumé

La région de l'Hindu-Kush Karakoram Himalaya (HKH) est la plus grande région englacée de la planète, exceptée les calottes polaires. Dans cette région, les mesures météorologiques et de bilans de masse sont sporadiques et les observations glaciologiques concernent essentiellement les mesures de fluctuations des fronts des glaciers. Ainsi, la réponse de ces glaciers aux changements climatiques est très mal connue. Le but de ce travail de thèse est d'améliorer la connaissance de des relations entre les variables météorologiques et les bilans de masse glaciaires à partir de l'étude du glacier Chhota Shigri situé dans l'Ouest de l'Himalaya.

De nombreuses mesures in-situ de bilans de masse, de vitesses d'écoulement, d'épaisseurs et de météorologie ont été réalisées depuis 2002 et au cours de ce PhD. L'analyse de ces observations permet de comprendre le comportement du glacier au regard des fluctuations climatiques. Entre 2002 et 2013, nos observations indiquent une perte de masse cumulée équivalente à une lame d'eau de -6.45 m. Par ailleurs, l'analyse des observations des flux de glace suggèrent que le glacier a connu un état proche d'un état d'équilibre avec des bilans nuls ou légèrement positifs au cours des années 1990.

Nous avons reconstitués les bilans de masse annuels et saisonniers depuis 1969 en utilisant des variables météorologiques. Depuis 1969, les bilans de masse sont faiblement négatifs, équivalents à -0.30 m d'eau par an. Cette reconstitution montre que le glacier était proche de l'état d'équilibre entre 1986 et 2000, ce qui confirme les résultats obtenus à partir de l'analyse des flux de glace et des mesures géodésiques. Cette étude montre également que la perte de masse glaciaire est récente et révèle des fluctuations de bilans de masse avant l'année 2000 très différentes de ce que l'on trouve dans la littérature. L'analyse des bilans de masse à l'échelle décennale révèle que les précipitations hivernales et les températures estivales jouent un rôle sensiblement équivalent. Afin de comprendre plus en détail les variables climatiques qui contrôlent le bilan de masse, une étude a été conduite à partir des flux d'énergie en surface à l'aide de stations météorologiques sur le glacier et à proximité du glacier. Le bilan net de toutes les longueurs d'onde contrôlent 80 % des flux d'énergie entrant en surface alors que les flux de chaleur sensible, latente et conductif contribue pour 13, 5 et 2 % respectivement du flux entrant total. Par ailleurs, notre étude montre que les événements de fortes précipitations au cours de la période de mousson jouent un rôle important sur l'évolution des bilans de masse. Néanmoins, à cause du manque de données de précipitation dans cette région et le fort gradient régional, la répartition des précipitations sur le glacier reste mal connue.

Keywords: Himalaya, Glacier, Bilan de masse, Etat d'équilibre, Bilan d'énergie, Mousson, Albedo.

Acknowledgements

This research was funded by *Institut de recherche pour le Développement (IRD)*, France and supported by *Indo-French Centre for the Promotion of Advanced Research (IFCPAR)* project no. 3900-W1, the *French Service d'Observation GLACIOCLIM* as well as the *Department of Science and Technology (DST)*, Government of India.

My love for the mountains dates back to early years of my childhood. My obsession for mountains led me to incessant encounters with the glaciers where the fact endowed upon me to understand the declining health of the Himalaya by contributing in the field of glaciology. The eagerness to contribute to the glacier research took proper shape with my supervisors Patrick and Christian to whom I owe my deepest reverence. Besides, being true mentors they always kept a friendly environment. The several visits to Christian's family were always refreshing. I would also like to express my gratitude to Prof. AL Ramanathan who provided me amenities in *Jawaharlal Nehru University (JNU)*, New Delhi as well as for the field expeditions on Chhota Shigri Glacier. Great thanks to Yves for providing the computer machine to carry out this work. The numerous field expeditions with Patrick, Christian, Jose, Yves, Parmanand, Linda, Chatterjee, Arindan and Thupstan were really motivational and rewarding. The night discussions with Jose at Chhota Shigri Glacier camps have been source of motivation.

I appreciate the discussion and company of my LGGE-LTHE friends Ruben, Alvaro, Saehee, Miral, Adrien, Julie, Max, Helene, Luis, and Romain. How can I forget my old pals, Shariq, Hilal and Bhupi, they are the ones who have been there through my bumpy rides and joyous pursuits. Thanks to Raj for improving the contents of my research articles. A special thanks to *International Centre for Integrated Mountain Development (ICIMOD)* for providing me an office to work with Patrick during my visit in Nepal. Words fail to express my gratitude for Vincent Favier, Adina Racoviteanu, Etienne Berthier, Renoj Thayyen, Antoine Rabatel, D. P. Dobhal, Tobias Bolch, Michael Zemp, Delphine Six, Armelle Philip, Rakesh Bhambri, Samjwal Bajracharya, Johannes Oerlemans and Jean Luc Jaffrezo who always rendered a helping hand. I sincerely thank to LGGE-LTHE directors Thierry Lebel and Paolo Laj and administrative staff for ensuring necessary facilities in carrying out this work. *Geological Survey of India (GSI)* provided the published literature on Himalayan glaciers and *Indian Meteorological Department (IMD)* provided the meteorological data from Bhuntar meteorological station.

I would also like to acknowledge the continuous assistance of Adhikari Ji during several expeditions and all the Nepalese porters without whom the glacier expeditions cannot be imagined in the Himalayas. At last I feel grateful to all people who directly or indirectly supported this work.

مجھے اِس مقام تک پہنچانے میں میرے والدین کا جو تعاون اور قربانیاں میرے ساتھ رہیں ان کو بیان کرنے کے لئے صرف الفاظ کافی نہیں ہیں۔ میری شریک حیات نزہت قاضی نے جتنے ٹھوس اور پُر عزم الفاظ میں مسلسل میری حوصلہ افزائی کی ہے وہ اپنے آپ میں مثالی حیثیت رکھتی ہے۔ دونوں بہنوں، زینت یاسمین، عائشہ ناز اور بھائی، طارق نیّر کی بے لوث محبت اور اپنائیت اس درمیان میری ذہنی آسودگی کے لئے ایک لازوال سرمایہ ثابت ہوئی نیز طارق کی موسیقی اور گلوکاری میرے لئے ریسرچ کے اس سفر میں چلتے چلتے تازہ دم ہونے کا بہترین وسیلہ بنی۔

میں اللہ تبارک و تعالیٰ کے حضور سجدۂ شکر ادا کرتا ہوں کہ اس نے ریسرچ کے اس کام کو میرے لئے آسان فرمایا اور تکمیل تک پہنچانے کی توفیق بخشی۔

Mohd. Farooq Azam



View of mid-ablation area of Chhota Shigri Glacier from the lateral moraine during the peak ablation season

Contents

Abstract	i
Résumé	iii
Acknowledgements	v
Contents	vii

1 Current knowledge of glaciers in the region of Hindu-Kush Karakoram Himalaya.....	1
1.1 Controversy about the future of the Himalayan glaciers	1
1.2 Importance of glaciers in the HKH region	2
1.3 Climate dynamics and glacier regimes.....	3
1.4 Evolution of climate in the HKH region.....	4
1.4.1 Temperature changes	4
1.4.2 Precipitation changes	4
1.5 Glacier surface mass balance processes	5
1.5.1 Mass balance of a glacier	5
1.5.2 Hydrological year and seasonal mass changes	5
1.5.3 Surface energy balance of a glacier	6
1.6 Methods for estimating the mass balance	7
1.6.1 Glaciological method	7
1.6.2 Geodetic Method	8
1.6.3 Hydrological method	8
1.6.4 Gravitational method	8
1.7 Glacier changes in the HKH region	9
1.7.1 Glacier fluctuations over the last 170 years.....	9
1.7.2 Mass Balance changes	12
1.7.2.1 Mass Balance changes at glacier scale	12
1.7.2.2 Mass Balance changes at regional scale.....	15
1.8 Summary	16
1.9 Objectives and organization of the thesis.....	16

2 Meteorological conditions and mass balances of Chhota Shigri Glacier19

Executive summary 19

2.1 Background and Introduction..... 20

2.2 Study site and AWS-M description..... 20

2.3 Hydrological year and field measurements to assess the mass balances 23

 2.3.1 Delineation of the hydrological year..... 23

 2.3.2 Measurement network to measure the glacier-wide mass balance with
 the glaciological method..... 23

2.4 Meteorological conditions and characterization of the seasons on Chhota
Shigri Glacier 24

 2.4.1 Air temperature and relative humidity 24

 2.4.2 Precipitation 25

 2.4.3 Incoming short and long wave radiations 27

 2.4.4 Wind regimes 28

2.5 Annual and Seasonal mass balance..... 29

 2.5.1 Annual point mass balances as a function of altitude..... 29

 2.5.2 Annual vertical mass balance gradients..... 30

 2.5.3 Annual and cumulative glacier-wide mass balances 32

 2.5.4 ELA and AAR..... 33

 2.5.5 Seasonal glacier-wide mass balances 35

2.6 Conclusion 38

3 Dynamic behaviour of Chhota Shigri Glacier41

Executive summary 41

Abstract..... 42

3.1 Introduction..... 43

3.2 Site description and methodology 45

 3.2.1 Site description..... 45

 3.2.2 Mass balance..... 45

 3.2.3 Surface velocity 45

 3.2.4 Ice thickness..... 46

3.3 Data analysis and results..... 46

 3.3.1 Glacier-wide mass balance and mass balance profile 46

 3.3.2 Ice thicknesses and cross-sectional areas..... 48

 3.3.3 Ice velocity 50

 3.3.4 Ice fluxes from kinematic method 51

 3.3.5 Ice fluxes obtained from surface mass balance..... 52

3.4 Discussion 52

 3.4.1 Null to slightly positive mass balance during the 1990s inferred from
 ice fluxes..... 54

3.4.2	Glacier dynamics starting to adjust to 21 st century negative mass balance.....	55
3.5	Conclusion.....	57
4	Mass balance reconstruction of Chhota Shigri Glacier.....	59
	Executive summary.....	59
	Abstract.....	60
4.1	Introduction.....	61
4.2	Study site.....	62
4.3	Data and climatic settings.....	62
4.3.1	Mass-balance data.....	62
4.3.2	Meteorological data.....	64
4.3.2.1	Air temperature.....	64
4.3.2.2	Precipitation.....	65
4.3.3	Climatic setting.....	66
4.4	Methods.....	66
4.4.1	Model description.....	66
4.4.2	Parameter analysis.....	67
4.4.2.1	Temperature lapse rate (LR).....	67
4.4.2.2	Degree-day factors.....	69
4.4.2.3	Precipitation gradient.....	70
4.4.3	Model calibration.....	71
4.5	Results.....	72
4.5.1	MB as a function of altitude.....	72
4.5.2	Annual mass balance.....	74
4.5.2.1	Cumulative mass balance since 1969.....	74
4.5.2.2	Error analysis.....	74
4.5.3	Seasonal mass balance.....	76
4.6	Discussion.....	77
4.6.1	Mass balance pattern and climatic drivers.....	77
4.6.2	Comparison with other studies.....	79
4.6.3	MB sensitivity to temperature and precipitation.....	79
4.7	Conclusion.....	81
	Appendix.....	83
	Hydrological year and mass balance evolution.....	84
5	Processes governing the mass balance of Chhota Shigri Glacier.....	85
	Executive summary.....	85
	Abstract.....	87
5.1	Introduction.....	88
5.2	Data and climatic settings.....	90

5.2.1	Study site and AWSs description	90
5.2.2	Meteorological data and corrections.....	92
5.2.3	Accumulation and ablation data	94
5.2.4	Climatic settings.....	95
5.2.4.1	Characterization of the seasons	95
5.2.4.2	Influence of ISM and MLW.....	97
5.2.4.3	Representativeness of 2012/13 hydrological year	98
5.3	Methodology: SEB calculations	99
5.3.1	SEB equation.....	99
5.3.2	Conduction into the ice/snow	100
5.3.3	Turbulent fluxes.....	101
5.3.3.1	Turbulent flux calculations	101
5.3.3.2	Roughness parameters.....	103
5.4	Results	103
5.4.1	Analysis of the meteorological conditions at AWS-G	103
5.4.2	Mean values of the SEB components	108
5.4.3	Model validation.....	110
5.4.4	Mean diurnal cycle of the meteorological variables and SEB components.....	112
5.5	Discussion.....	114
5.5.1	Control of the summer-monsoon snowfalls on melting	114
5.5.1.1	Comparison between 2012 and 2013 melting periods	114
5.5.1.2	Impact of the summer-monsoon snowfalls on glacier-wide mass balance.....	117
5.5.2	Comparison of the SEB of Chhota Shigri Glacier with that of other glaciers in the High Mountain Asia	118
5.6	Conclusion	121
6	General conclusions and perspectives.....	123
	References.....	129
	List of tables	149
	List of figures.....	151

CHAPTER 1

Current knowledge of glaciers in the region of Hindu-Kush, Karakoram and Himalaya

The Hindu-Kush Karakoram Himalaya (HKH) region comprises the biggest mountain range on the Earth and is home to the highest peaks of the world. This mountain range, stretching east to west over 2,500 km, covers a glacierized area of almost 40,800 km² (Bolch et al., 2012). The HKH region, with the largest snow and ice cover in the world outside the Polar Regions and being the birthplace of some of the largest rivers in Asia, is aptly called as the “Third Pole” or “Water Tower of Asia”. Glacierized basins form the headwaters of almost all the major rivers in the HKH mainland (Armstrong, 2010). The glaciers of the HKH region contain some of the longest and largest mid-latitude/sub-tropical glaciers of the world (Sarikaya et al., 2012) such as Siachen, Baltoro, Gangotri glaciers. The important snow and ice reserves of the HKH influence the flow of several rivers and streams that converge into the three foremost river systems of the region: the Brahmaputra in eastern, the Ganges in central and the Indus in western part of the HKH region (Fig. 1.1).

1.1 Controversy about the future of the Himalayan glaciers

The contradictory statement about the Himalayan glaciers that “*the likelihood of them disappearing by the year 2035 or perhaps sooner is very high if the Earth keeps warming at the current rate*” in the Intergovernmental Panel on Climate Change (IPCC) Fourth Assessment Report (Parry et al., 2007) provoked interests in scientific community and highlighted important research gaps and areas where scientific investigation is critically important. However, emerging evidence advocates that such statements were, at best, exaggerated. At least part of the problem is lack of the data that fostered the controversies. The contradictory statement of “disappearing Himalayan glaciers” by 2035 was found to be wrong of course, since it requires 25 times greater loss of mass over the period 1999 to 2035 compared to the estimated rate over 1960 to 1999 and error was originated from a typing mistake of “2350” (Cogley et al., 2010). Nevertheless some studies reported high rates of retreat of the Himalayan glaciers over the last decades (Bolch et al., 2012). Such trends are commonly based on a few sporadic and short periods, and they might not capture the complex behavior of glacier-climate relationship.

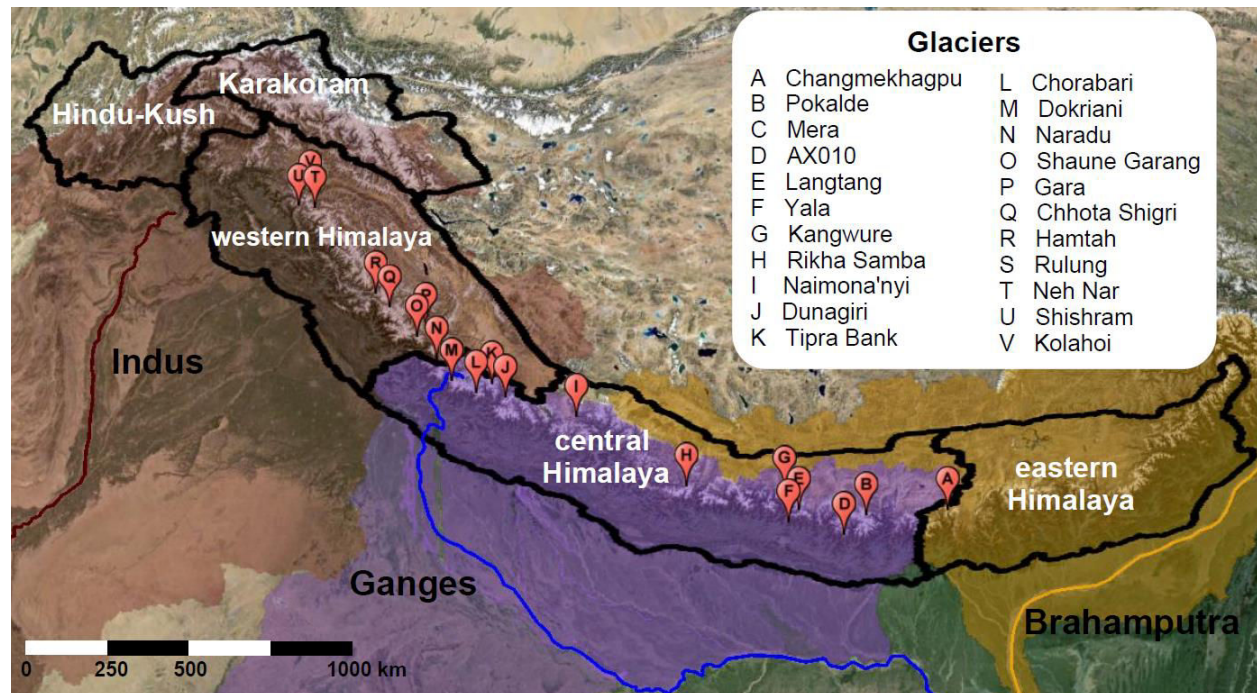


Figure 1.1. Map of the Hindu-Kush Karakoram Himalayan region showing the location of three major river basins. The base map comes from Google Earth, the basin boundaries are provided by *International Centre for Integrated Mountain Development (ICIMOD)* and the boundary shape is provided by Dr. Tobias Bolch (*University of Zurich*). The balloons A-V show the location of the glaciers surveyed by glaciological method in the whole HKH region.

1.2 Importance of glaciers in the HKH region

The demand for global fresh water is continuously increasing due to the growing population and industrialization. The role of snow and ice in high mountain areas of the world as an important source of freshwater has been highlighted by several studies (e.g., [Kaser et al., 2010](#); [Immerzeel et al., 2010](#)). Rivers originating in the HKH region are among the most melt-water dependent river systems on the Earth, yet large human populations depend on their resources downstream ([Schaner et al., 2012](#)). Nevertheless the contribution of melt-water to measured discharge decreased substantially towards lowland locations ([Racoviteanu et al., 2013](#)). The HKH glaciers play a crucial but irregular role with varying contribution of glacier and snow melt to the total runoff in the water supply of Asia's main river basins ([Immerzeel et al., 2012a](#)). [Lutz et al. \(2014\)](#), covering whole of the HKH region (based on 1x1 km grid, daily time step model), showed that in the upper Indus Basin (mean of all 1x1 km grids), stream flow is dominated by glacier melt water, contributing almost 40.6% of the total runoff while in upper Ganges and upper Brahmaputra basins contribution is much lower with values of 11.5 and 15.9%, respectively. The relative percentage of glacier melt water to the total runoff is an indicator of vulnerability of the river systems to the future climate changes. Thus the future evolution of the glacier melt water is

more crucial in the upper Indus Basin than Ganga and Brahmaputra basins. Furthermore, the increasing amount of total runoff is directly linked with the natural hazards such as flood, Glacial Lake Outburst Flood (GLOF) down to the river basins; therefore, monitoring of the HKH glaciers is a key issue of the present day.

1.3 Climate dynamics and glacier regimes

The HKH region experiences diverse climate and hydrology from east to west that are controlled by the Indian Summer Monsoon (ISM) and Mid-Latitude Westerlies (MLW) circulation systems, which transport precipitations to this region in the summer (May to October) and winter (November to April) periods, respectively. These circulation systems are controlled by the Inter-Tropical Convergence Zone (ITCZ) (Bookhagen and Burbank, 2010). The high Sun inclination during the summer heats up the Indian subcontinent considerably, generating low pressure area over the northern and central Indian subcontinent. Consequently, to fill this void, the ISM arises and brings moisture from the Indian Ocean towards the HKH range in the north. The HKH range acts as a barrier to the monsoon winds, causing maximum precipitation on the South slopes of the Himalaya from June to September (Shrestha et al., 1999; Gautam et al., 2009) with an east-west gradient in monsoon intensity, providing higher summer precipitation amounts in the eastern and central Himalaya (eastern Tibetan plateau, Nepal and Garhwal Himalaya) than in the western Himalaya, Hindu-Kush and Karakoram ranges. In contrast, during the winter, the ITCZ moves southwards due to the changing insolation and westerly winds, out-blowing from dry source areas with moisture from the Mediterranean, Black, and Caspian seas. Therefore, depending on their geographical situation and regional orography, the glaciers in the HKH region are subjected to different climatic regimes.

Three climatic zones can be distinguished based on the relative amount of precipitation: (1) the “monsoon influenced” zone in the eastern and central Himalaya, with maximum precipitation amounts in the summer, characterized by “summer-accumulation” type glaciers (Ageta and Higuchi, 1984). These glaciers experience maximum accumulation and ablation in the summer due to high monsoonal precipitation and temperature (Wagnon et al., 2013); (2) the “monsoon-arid transition zone” (western Himalaya, Lahaul-Spiti and Ladakh), receiving precipitation from monsoon in the summer and MLW in winters (Bookhagen and Burbank, 2010) and (3) the “snow dominant alpine region” (Hindu-Kush and Karakoram), with maximum precipitation during the winter (Thayyen and Gergan, 2010), characterized by “winter-accumulation-type” glaciers (Benn and Owen, 1998). Because of the strong topography of the HKH region, local climate might influence the atmospheric circulations. Through orographic and leeward effects, extremely dry inner valleys can co-exist to adjacent mountain slopes receiving much more precipitation (Eriksson et al., 2009).

1.4 Evolution of climate in the HKH region

1.4.1 Temperature changes

Given the dependency of a large population of the world on the HKH river systems, there is a big concern about the impact of climate change on regional cryosphere. Over the last century, [Bhutiya et al. \(2007\)](#) and [Dash et al. \(2007\)](#) found a warming of 1.60 °C in the northwest and 0.98 °C in western Himalayan regions, respectively. [Dash et al. \(2007\)](#) also indicated an accelerated warming after 1972 in the northwest and western Himalayan regions. On a long-term climate scale, microwave satellite measurements of tropospheric temperature from 1979 to 2007 also indicated an accelerated annual mean warming over the whole Hindu-Kush Himalayan region (0.21 ± 0.08 °C/decade) with the maximum warming localized over the western Himalaya (0.26 ± 0.09 °C/decade) ([Gautam et al., 2010](#)). This enhanced tropospheric warming has been observed mainly in the pre-monsoon (April- June) and was associated with radiative heating from increased absorbing (coarse) dust aerosols in the atmosphere over the Indo-Gangetic Plain ([Gautam et al., 2010](#)). In the upper Indus Basin, [Fowler and Archer \(2006\)](#) reported increasing trends in winter temperature between 1961 and 2000 with varying warming rates of 0.07-0.51 °C/decade in annual mean temperature. In the Karakoram region, [Dimri and Dash \(2010\)](#) found a decrease in winter temperatures in the accumulation zone and an increase in winter temperatures in the ablation zone of the Siachen Glacier between 1984 and 2006. This contrast over the same glacier gives rise to the hypothesis that, in sensitive ecoregions such as glacial regions, changes in temperature are more likely to be governed by local dynamics than by regional or global trends ([Singh et al., 2011](#)). In conclusion, temperature trends over the HKH region consistently show a warming trend in agreement with Fourth Assessment Report of the IPCC ([IPCC, 2007](#)) which stated that the global mean surface air temperature is increased by 0.74°C over the last century. Nevertheless, the rate of temperature change in the HKH region varies in different periods depending on the climatic regions and seasons.

1.4.2 Precipitation changes

It is expected that changes in temperature due to climate change in the atmosphere might lead to changes in the pattern of precipitation. However, physical processes influencing precipitation are much more complex and give rise to large variability in precipitation trends in different regions. For example, [Bhutiya et al. \(2010\)](#) reported a decreasing trend in average annual and monsoon rainfall in the northwest Indian Himalaya from 1866 to 2006. Similarly, [Dimri and Dash \(2012\)](#) reported decreasing trends in winter precipitation (December-February) in the western Himalaya for 1975-2006; however the trends were not consistent. This inconsistency is due to the highly variable precipitation events, which are difficult to detect in such terrain or due to sparse network of observing stations in the western Himalaya. In contrast to the Himalayan range, increasing trends in winter precipitation were reported from 1961 to 1999 in the upper Indus Basin (Karakoram) at Skardu and Dir stations, with increase of 18 and 16% per decade, respectively

(Fowler and Archer, 2005). The contrasting behaviour of precipitation trends over Karakoram can be explained by the steep regional orography that plays dominant role in precipitation forming process than the large scale circulation (Dimri, 2004).

1.5 Glacier surface mass balance processes

1.5.1 Mass balance of a glacier

Changes in glacier mass are a key subject of glacier monitoring, providing important information for assessing climatic changes, water resources and sea level rise (Zemp et al., 2013). Mass gain (accumulation) or loss (ablation) can take place on the glacier surface, within the body of the glacier, or at the glacier-bedrock interface (Kaser et al., 2003). A glacier accumulates mass from different sources: snowfall, redistribution of snow by wind, avalanches, re-sublimation, condensation or freezing of rain/melt water percolating inside the glacier. With the passage of time, the accumulated snow transformed first to firn (density between 400 and 830 kg m⁻³) and then ice (density between 830 and 910 kg m⁻³) (Cuffey and Paterson, 2010). A glacier also loses mass through different processes called ablation that includes melting, snow drift, calving and sublimation. Mass changes on the glacier surface dominate the mass balance (MB) and the englacial and sub-glacial processes are, in most cases, ignored (Cuffey and Paterson, 2010). On the upper reaches of the glacier, the accumulation processes dominate while on the lower part, the ablation processes take over. These two zones are separated by a boundary where the annual balance is zero and is defined as the equilibrium line. The altitude of the equilibrium line (ELA, Equilibrium Line Altitude) can vary from one year to another. ELA can be measured directly or estimated from remote sensing as the altitude of the snowline at the end of the ablation period (Rabatel et al., 2005).

Glacier-wide annual mass balance (B_a) can be defined as the difference between the accumulation and ablation (Cuffey and Paterson, 2010). If the sum of ablation is equal to that of accumulation, the glacier is in balance state. The mass changes are converted in water equivalent meters (m w.e.) to make an easy comparison amid glaciers. The surface B_a of a glacier directly reflects signal of all meteorological processes affecting the glacier's health. The range of physical processes involved is complex and can only be described by the surface energy balance studies.

1.5.2 Hydrological year and seasonal mass changes

The hydrological/MB year is defined as the time between one minimum of glacier mass to the next, which, in mid-latitudes, occurs in autumn. Ideally, B_a of a glacier should be monitored at the beginning of each hydrological year but this is almost impossible in the HKH region because of harsh conditions that make the access difficult. Practically, B_a is calculated over a period slightly differing from the hydrological year. In the HKH region, a seasonal time resolution corresponding to winter and summer seasons is also used to determine the important climatic factors driving the annual B_a (Wagnon et al., 2013; Azam et al., 2014a).

1.5.3 Surface energy balance of a glacier

The energy balance study over a glacier surface concerns the interaction between atmosphere and the surface (Garratt, 1999). Figure 1.2 is the pictorial representation of different processes over a glacier surface. Assuming a lack of horizontal energy flux transfers, for a unit of volume of a glacier (a depth from the surface where no significant heat fluxes are found) and for a unit of time, the surface energy balance can be expressed by Eq. 1.1 (Oke, 1987, p. 90):

$$SWI - SWO + LWI - LWO + H + LE + G + P - F_{\text{surface}} = 0 \quad (1.1)$$

Where SWI, SWO, LWI and LWO are the short-wave incoming, short-wave outgoing, long-wave incoming and long-wave outgoing radiation fluxes, respectively. H and LE are the sensible and latent turbulent heat fluxes, respectively. G is the conductive heat flux in the snow/ice and P is the heat supplied by precipitation. F_{surface} is the net heat flux available at glacier surface. By convention all the fluxes ($W m^{-2}$) towards the surface are taken as positive and vice-versa, except for the outgoing radiation terms that are kept positive, but assigned a minus sign, because they are always directed away from the surface. The details about surface energy balance can be found in Wagnon et al. (1999) and Favier et al. (2011).

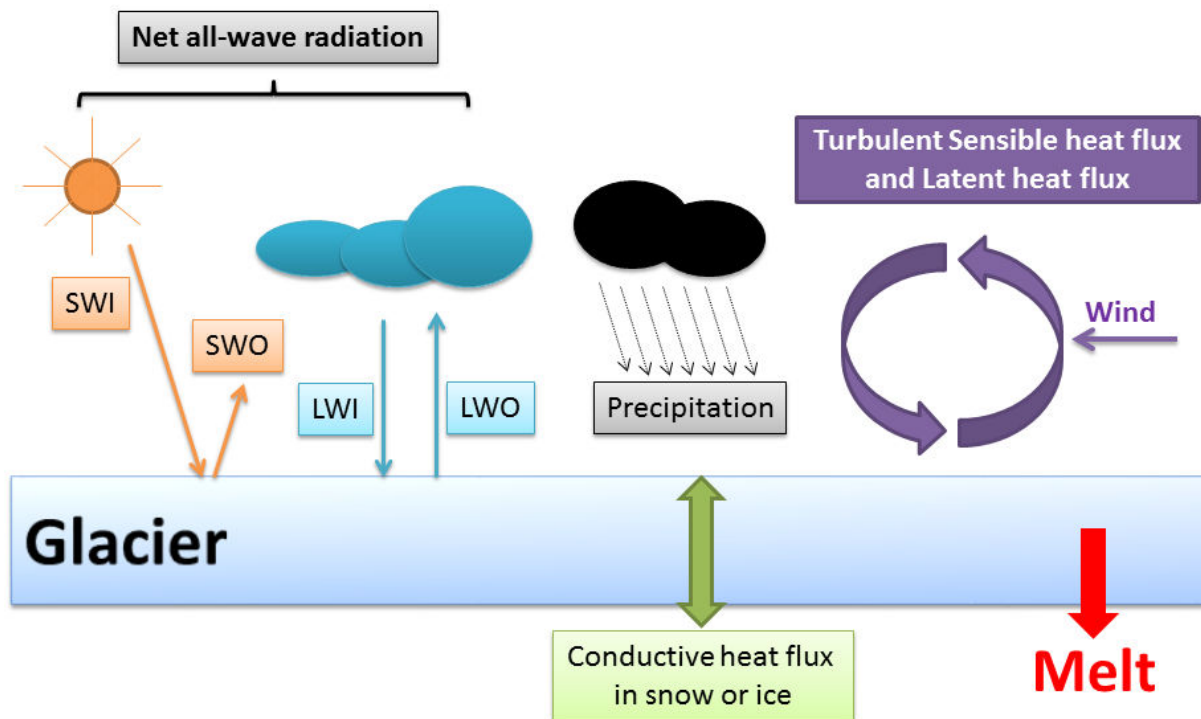


Figure 1.2. The processes determining the energy flux at the glacier-atmosphere interface.

1.6 Methods for estimating the mass balance

There are several methods to determine the mass changes of a glacier or glacierized area over a specific period. All the methods provide uncertain results; therefore, the best approach is to use more than one method (Cuffey and Paterson, 2010). Generally the four following types of methods have been used worldwide:

1.6.1 Glaciological method

The glaciological or direct method is the conventional way of measuring B_a of a glacier, and it involves using stakes in the ablation zone and coring or snow pits in the accumulation zone (Østrem and Brugman, 1991). In ablation zone, the stake emergence is measured whereas in accumulation zone, both the density and thickness of the annual accumulation layer are measured. On temperate glaciers, the bottom of the annual accumulation layer can be located either by visual inspection of the dirt layer that corresponds to last summer surface or by locating the artificially colored layer of the preceding year. The latter method provides a better accuracy in the measurements (Wagnon et al., 2013). In the ablation zone, a network of stakes drilled in the ice is used. The distance between the top of the stake and the glacier surface is measured at the beginning and end of the hydrological year. The surface height difference at each stake provides the thickness added or removed that is converted into point mass change (m w.e.) by multiplying the density of snow/ice. Extrapolation of these accumulation and ablation point measurements over the entire glacier area gives rise to the glacier-wide mass balance, B_a according to Eq. 1.2:

$$B_a = \frac{1}{S} \int b_i \cdot s_i \quad (1.2)$$

where b_i (kg m^{-2}) and s_i (m^2) are the altitudinal MB and altitudinal surface area at different elevation of the glacier, respectively. Since the glaciological method needs an enormous amount of man power and is quite challenging specially in the harsh terrain of the HKH region, the chosen glaciers are, generally, small in size that raises the question of their regional representativeness (Vincent et al., 2013). However, it still provides valuable information on the temporal variability of B_a if the monitoring is continuous over several years (Vincent et al., 2004). The error attributed to B_a measured by the glaciological method can be estimated following Thibert et al. (2008), who conducted a variance analysis on all potential sources of errors related to either the measurements themselves (ice/snow density, core length, stake height determination, liquid-water content of the snow, snow height) or the sampling network (*i.e.* density and representativeness of the stake network). The resulting error is therefore specific for each glacier and is for instance equal to ± 0.28 w.e. a^{-1} on Mera Glacier (Wagnon et al., 2013) or ± 0.40 m w.e. a^{-1} on Chhota Shigri Glacier (Azam et al., 2012).

1.6.2 Geodetic Method

The geodetic method, also called photogrammetric or volumetric method, involves comparing two glacier surface elevation datasets from topographic maps or digital elevation models to determine the volume change over the considered time interval (generally 5-10 years) for a single glacier or a large glacierized area. By applying the density of snow/ice at different parts of the glacier, the volume change can be converted into mass change. Geodetic method is now frequently used to calculate the elevation changes and regional MBs of the glaciers world-wide (e.g., [Berthier et al., 2007](#); [Bolch et al., 2011](#); [Kääb et al., 2012](#); [Gardelle et al., 2013](#)). The main drawback of the geodetic method is that it doesn't provide the annual or seasonal glacier surface mass balances, which are necessary to understand the glacier-climate relationship. However, this method is adequate at regional scales, and it overcomes the problem of representativeness of a single glacier for large regions. The geodetic method is a useful complementary method to the glaciological method since it covers a larger time span (e.g., 10 years) and in turn can be used to cross check or correct the traditional glaciological results ([Thibert et al., 2008](#); [Zemp et al., 2013](#)).

1.6.3 Hydrological method

By neglecting the amount of ice or snow lost by sublimation and evaporation, the glacier mass balance $B_{n,H}$ can be calculated from the difference between precipitation and discharge at the outlet of basin ([Sicart et al., 2007](#)) according to Eq. 1.3:

$$B_{n,H} = R - \frac{1}{S} [D - (S_b - S)c_e R] \quad (1.3)$$

where S is the glacier surface area (m^2), S_b is the total surface area of the basin (m^2) and c_e is the runoff coefficient of the surface not covered by the glacier. R ($m a^{-1}$) is the average of the storage rain gauges in the basin while D ($m^3 a^{-1}$) is the discharge monitored at the basin outlet. Estimation of MB of a glacier by this method is quite challenging, as the adequate sampling of precipitation and discharge are difficult to record throughout the year ([Cuffey and Paterson, 2010](#)). Indeed, precipitation in high-elevation catchments is one of the largest unknown of mountain hydrology because it is highly variable and observations are lacking ([Immerzeel et al., 2012b](#)). The spatial variability of precipitation is even harder to assess at large basin scale.

1.6.4 Gravitational method

This method has recently been developed with the introduction of the Gravity Recovery and Climate Experiment (GRACE) program in 2002. GRACE satellite mission has provided monthly, global gravity field solutions since its launch allowing users to calculate mass variations at the Earth's surface. GRACE has been used to monitor the MB of glaciers and ice caps, as well as of Antarctica and Greenland ([Luthcke et al., 2008](#); [Riva et al., 2010](#); [Jacob et al., 2012](#); [Gardner et al., 2013](#)). Nevertheless GRACE provides the mass changes over large areas, it has large uncertainties

(Jacob et al., 2012; Gardner et al., 2013), and therefore, this method cannot be used for individual glacier.

1.7 Glacier changes in the HKH region

The observed worldwide glacier retreat over the 20th century is a strong indication of global warming (Dyurgerov and Meier, 2000). Existing knowledge of the glacier changes in the HKH region is limited by the fact that most of the reports are of fluctuations in snout position and the B_a observations are scarce. The main reason of insufficiency of B_a data is the data collection that is often challenging because of vast glacierized area, high altitude, rugged terrain, extreme climatic conditions, political issues of boundaries, etc. Fluctuations of a glacier are not only a reaction to climatic forcing (e.g., Leysinger et al., 2004; Oerlemans, 2005; Lüthi and Boudier, 2010; Leclercq and Oerlemans, 2012), but also to specific topographical features such as the length, area, glacier slope, glacier bedrock slope, surroundings, and the type of glacier (debris-covered or clean). Consequently, extracting the climate signal from glacier fluctuations is not straightforward and the glacier length change (*i.e.* the advance or retreat) is an indirect, delayed and filtered signal to a change in climate. On the contrary the glacier B_a (*i.e.* the change in thickness/volume) is the direct and un-delayed response to the annual atmospheric conditions (Haeberli and Hoelzle, 1995). Glacier length change records have been used to infer B_a variations in several studies (e.g., Klok and Oerlemans, 2003; Steiner et al., 2008). Recently Lüthi et al. (2010) introduced a novel method to infer the glacier volume changes from glacier length records applying their method on 13 selected glaciers in the Swiss Alps.

1.7.1 Glacier fluctuations over the last 170 years

Purdon (1861) and Godwin-Austen (1864) started surveying and mapping the Himalayan glaciers in the early nineteenth century using the plane-table survey and heavy theodolites. Since the beginning of the 20th century, *Survey of India* (SOI) together with *Geological Survey of India* (GSI) produced topographical maps at different scales for several glaciers using plane table, terrestrial photogrammetry and aerial photographs combined with field work (e.g., Longstaff, 1910; Auden, 1937; Chaujar, 1989; Survey of India, 2005). However these maps are not in the public domain and some contain errors due to the time of the year when the survey had been conducted leading to some erroneous glacier delineations in case of snow cover (Bhambri et al., 2009). Glacier maps constitute valuable records of glacio-geomorphic features (Ashwell, 1982). Moreover, in second half the 20th century the revolutionized introduction of satellites provided images of glacierized areas around the globe. Comparison of these latest satellite images with old maps allows to quantify the glacier snout fluctuations, area, volume or mass changes (e.g., Berthier et al., 2007; Bolch et al., 2008; Kääb et al., 2012; Bahmbri et al., 2013; Gardelle et al., 2013; Racoviteanu et al., 2014).

Table 1.1. Snout fluctuation records for some selected glaciers from the HKH region. See Fig. 1.3 for recession evolution.

Glacier	Basin	Period	No. of observations	Recession rate (m a ⁻¹)	References
Eastern Himalaya					
Rathong	Sikkim	1976-2005	4	-18.2	Raina (2009)
S.Lohank	Sikkim	1962-2008	5	-42.2	Govindha Raj et al. (2013)
Zemu	Sikkim	1909-2005	5	-9.0	Raina (2009)
Central Himalaya					
Khumbu	Dudh Koshi Basin	1960-2006	5	-18.3	Bajracharya and Mool (2009)
Imja	Dudh Koshi Basin	1960-2006	5	-60.5	Bajracharya and Mool (2009)
Rongbuk	Qomolangma	1966-2004	5	-8.8	Jiawen et al. (2006)
East Rongbuk	Qomolangma	1966-2004	5	-6.0	Jiawen et al. (2006)
AX010	Shorong Himal	1978-2004	9	-6.7	Fujita et al. (2001a); Shrestha and Shrestha (2004)
Rikha Samba	Hidden Valley	1974-1999	4	-12.0	Fujita et al. (2001b)
Shunkalpa	Garhwal Himalaya	1886-1957	4	-7.3	Cotter and Brown (1907); Jangpangi (1958)
Pindari	Garhwal Himalaya	1845-2010	8	-18.7	Tewari (1973); Bali et al. (2013)
Gangotri	Garhwal Himalaya	1842-2010	10	-11.0	Auden (1937); Naithani et al. (2001); Kargel et al. (2011); Bhambri et al. (2012)
Chaurabari	Garhwal Himalaya	1962-2010	10	-6.8	Dobhal et al. (2013)
Milam	Garhwal Himalaya	1849-2006	9	-17.0	Cotter and Brown (1907); Mason (1938); Govindha Raj (2011)
Tipra	Garhwal Himalaya	1962-2008	4	-14.4	Mehta et al. (2011)
Western Himalaya					
Bara Shigri	Lahaul-Spiti	1906-1995	4	-29.8	GSI (1999)
Chhota Shigri	Lahaul-Spiti	1962-2010	3	-7.0	GSI (1999); Azam et al. (2012)
Gangstang	Lahaul-Spiti	1963-2008	3	-29.7	Sangewar (2011)
Kolahoi	Jhelum Basin	1857-1961	3	-15.7	Odell (1963)
Gepang Gath	Lahaul-Spiti	1965-2012	6	-19.7	Mukhtar and Prakash (2013)
Hamtah	Lahaul-Spiti	1980-2010	5	-16.8	Pandey et al. (2011)
Raikot	Nanga Parbat	1934-2007	10	-2.8	Schmidt and Nusser (2009)
Karakoram					
Siachen	Karakoram	1862-2005	7	1.5	Ganjoo (2009)
Biofo	Karakoram	1850-2020	13	-8.6	Hewitt (2011)
Minapin	Karakoram	1887-2002	16	8.6	Hewitt (2011)
Central Rimo	Karakoram	1930-2011	6	-21.0	Bhambri et al. (2013)
Hispar	Karakoram	1892-2004	7	-39.0	Hewitt (2011)
Aktash	Karakoram	1974-2011	9	17.0	Bhambri et al. (2013)
Panmah	Karakoram	1855-2010	5	0.1	Hewitt (2011)
Baltoro	Karakoram	1855-2010	13	-2.4	Hewitt (2011)

Historical records of glacier fluctuations in the HKH region dates back to last 170 years. The main longest records concerning the glacier fluctuation come from mid-nineteen century for Milam (Cotter and Brown, 1907), Gangotri (Auden, 1937), Pindari (Cotter and Brown, 1907), Siachen (Ganjoo, 2010) and Baltoro (Hewitt, 2011) glaciers. Here, an up-to-date compilation of glacier fluctuations in the HKH region is made. Table 1.1 and Fig. 1.3 show some of the longest studies for snout fluctuation in the whole HKH region.

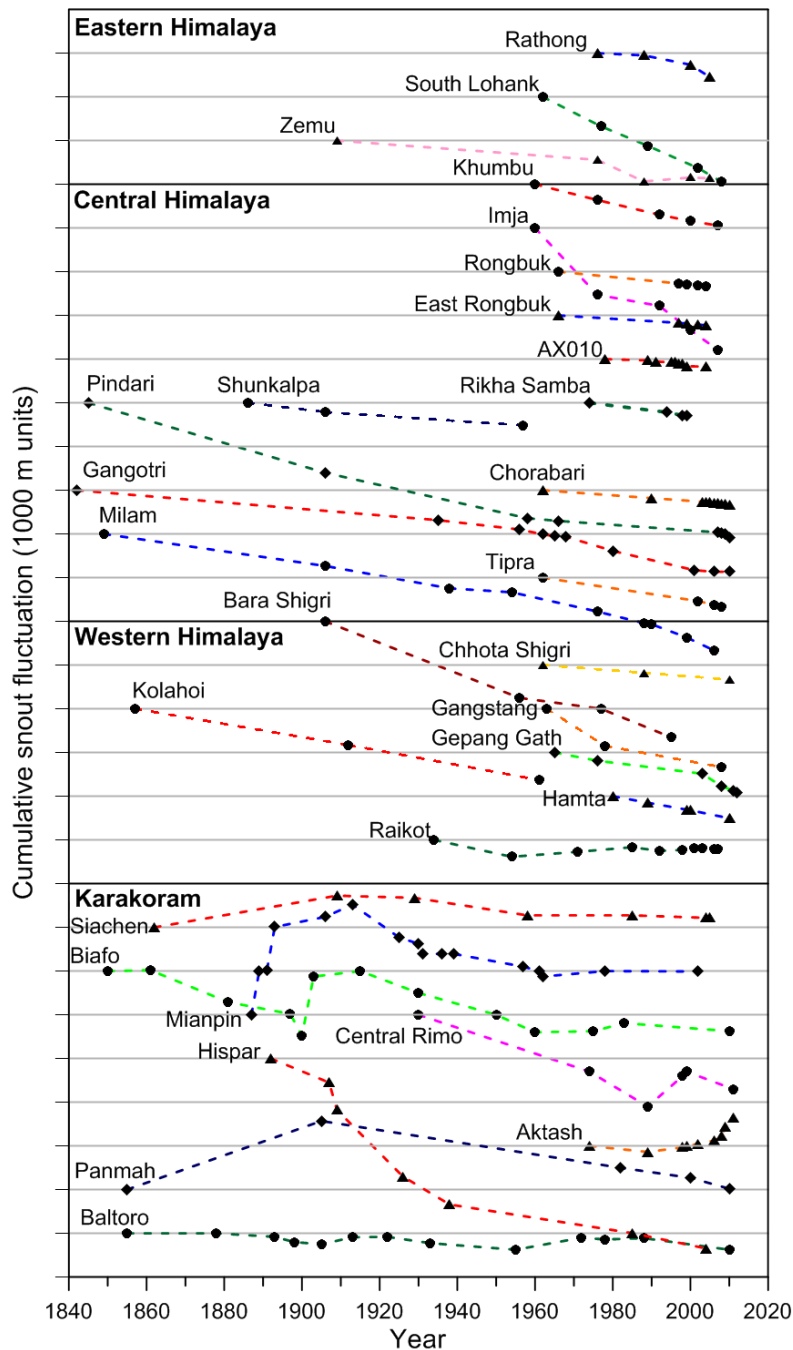


Figure 1.3. The recession evolution for some selected glaciers in the HKH region over the last 170 years.

Several studies involving field based and satellite imagery reported that a majority of glaciers in the Himalayan range are retreating (e.g., Kulkarni et al., 2007; Bajracharya and Mool, 2009; Raina, 2009; Sangewar, 2011; Panday et al., 2011; Kamp et al., 2011). Glacier retreat (Fig. 1.3) seems to be consistent with increasing temperature trends reported in other studies (e.g., Shrestha et al., 1999; Yang et al., 2006; Dash et al., 2007; Bhutiyani et al., 2007; Immerzeel, 2008; Singh et al., 2008; Dimri and Dash, 2012) and decreasing precipitation trends (e.g., Bhutiyani et al., 2010; Dimri and Dash, 2012) over the Himalayan range. In contrast to the Himalayan glaciers, a complicated picture emerges from the Karakoram (west to the Himalaya) glaciers (Fig. 1.3) where large, often rapid, advances and retreats occurred, more or less out of phase with one another (Hewitt, 2011; Bhambri et al., 2013). The climatic conditions which make Karakoram glaciers different from the Himalayan glaciers could be attributed firstly to extreme vertical topography (300 m/km), that is exceptional even in comparison to the Himalaya (Mayewski and Jeschke, 1979), that enhances precipitation in the source area, and secondly to the extensive/thick debris cover of most of the glaciers (Hewitt, 2005; Scherler et al., 2011) that reduces the ablation. Several studies also reported cooler summers, greater summer cloudiness, snow covers and decreasing trends in maximum and minimum temperatures (Fowler and Archer, 2005; Shekhar et al., 2010; Scherler et al., 2011). These conditions can also reduce the average ablation rates or the duration of the ablation season (Hewitt, 2011).

1.7.2 Mass Balance changes

1.7.2.1 Mass Balance changes at glacier scale

Table 1.2 and Fig. 1.4 present an up-to-date compilation of all the published annual B_a data to overview glacier changes in the HKH region. Most of the work has been done using glaciological method with the exception of Langtang (Tangborn and Rana, 2000) and Siachen (Bhutiyani, 1999) glaciers where MBs were calculated by temperature index and hydrological methods, respectively. Chhota Shigri Glacier B_a has been observed using both the glaciological and temperature index methods since 2002 and 1969, respectively (Wagnon et al., 2007; Azam et al., 2012 & 2014a). In the HKH region, B_a data series are mainly reported from Indian (covering western as well as parts of central and eastern Himalaya) and Nepalese Himalaya. To date, no documentation about surface B_a is available from the Hindu-Kush and Karakoram regions. However, in the Himalaya, several B_a studies were started during the seventies but were discontinued after some years. The field based B_a data from the HKH is greatly underrepresented considering the relative large glacierized area in this mountain range in comparison to other regions. Only 22 glaciers, covering an area of ~110 km² out of 40,800 km² of the total glacierized area of the HKH region, have been surveyed. Most of the glaciers in the HKH region are in recession.

Table 1.2. Glacier-wide mass balance observations from the HKH region.

Glacier name	Location	Area (km ²)	Period	Mean B _a (m w. e. a ⁻¹)	References
Eastern Himalaya					
1. Changmexhangpu Sikkim, India	27°57'N 88°41'E	4.5	1979-1986	-0.38	Raina (2009)
Central Himalaya					
2. AX010 Shorang Himal, Nepal	27°42'N 86°34'E	0.6	1995-1999	-0.60	Ageta et al. (2001)
3. Yala Langtang Valley, Nepal	28°14'N 85°36'E	1.6	2011-2012	-0.89	Baral et al. (2014)
4. Mera Dudh Koshi Basin, Nepal	27°70'N 86°90'E	5.1	2007-2012	-0.08	Wagnon et al. (2013)
5. Pokalde Khumbu Valley, Nepal	27°90'N 86°80'E	0.1	2009-2012	-0.72	Wagnon et al. (2013)
6. Rikha Samba Hidden Valley, Nepal	28°82'N 83°49'E	4.6	1998-1999	-0.75	Fujita et al. (2001b)
7. Kangwure Xixiabangma Region, China	28°27'N 85°45'E	1.9	1991-1993 2009-2011	-0.45 -0.16	Liu et al. (1996) TPE (2012)
8. Chorabari Garhwal Himalaya, India	30°74'N 79°09'E	6.7	2003-2010	-0.73	Dobhal et al. (2013)
9. Dokriani Garhwal Himalaya, India	30°50'N 78°50'E	7.0	1992-1995, 1997-2000	-0.32	Dobhal et al. (2008)
10. Dunagiri Garhwal Himalaya, India	30°33'N 79°54'E	2.6	1984-1990	-1.04	GSI (1992)
11. Tipra Bank Garhwal Himalaya, India	30°44'N 79°41'E	7.0	1981-1988	-0.25	Gautam and Mukherjee (1989)
Western Himalaya					
12. Chhota Shigri Lahaul-Spiti, India	32°28'N 77°52'E	15.7	2002-2013	-0.67	Wagnon et al. (2007); Azam et al. (2012)
13. Hamtah Lahaul-Spiti, India	32°24'N 77°37'E	3.2	2000-2009	-1.46	GSI (2011)
14. Gara Baspa Basin, India	31°28'N 78°25'E	5.2	1974-1983	-0.33	Sangewar and Siddiqui (2007)
15. Gor-Garang Baspa Basin, India	31°37'N 78°49'E	2.0	1976-1985	-0.38	Sangewar and Siddiqui (2007)
16. Kolahoi Jhelum Basin, India	34°20'N 75°47'E	11.9	1983-1984	-0.27	Dyurgerov and Meier (2005)
17. Naradu, Baspa Basin, India	31°20'N 78°27'E	4.6	2000-2003	-0.40	Koul and Ganjoo (2010)
18. Neh Nar Jhelum Basin, India	34°16'N 75°52'E	1.7	1975-1984	-0.53	Raina and Srivastava (2008)
19. Naimona'nyi West Himalaya, China	30°27'N 81°20'E	7.8	2004-2006, 2007-2010	-0.56	TPE (2012)
20. Rulung Zaskar Range, India	31°11'N 78°00'E	1.1	1980-1981	-0.11	Srivastava et al. (2001)
21. Shaune Garang Baspa basin, India	31°17'N 78°20'E	4.9	1981-1991	-0.42	GSI (1992)
22. Shishram Jhelum Basin, India	34°20'N 75°43'E	9.9	1983-1984	-0.29	Dyurgerov and Meier (2005)

The glaciological MB observations, available from the HKH glaciers, are mostly limited to the period 1975–1990 (Table 1.2), when glaciers often experienced negative B_a (Fig. 1.4). During the nineties, the glaciological MBs are available only for the AX010, Rikha Samba, Kangwure and Dokriani glaciers but, unfortunately, these measurements are either short (<5 years) or discontinuous (Dokriani Glacier) and provide an incomplete picture of glacier change. Currently Chhota Shigri, Chorabari, Dokriani, Hamtah, Mera, Pokalde, Yala, and Rikha Samba glaciers are the glaciers where continuous B_a observations are being conducted in the HKH region.

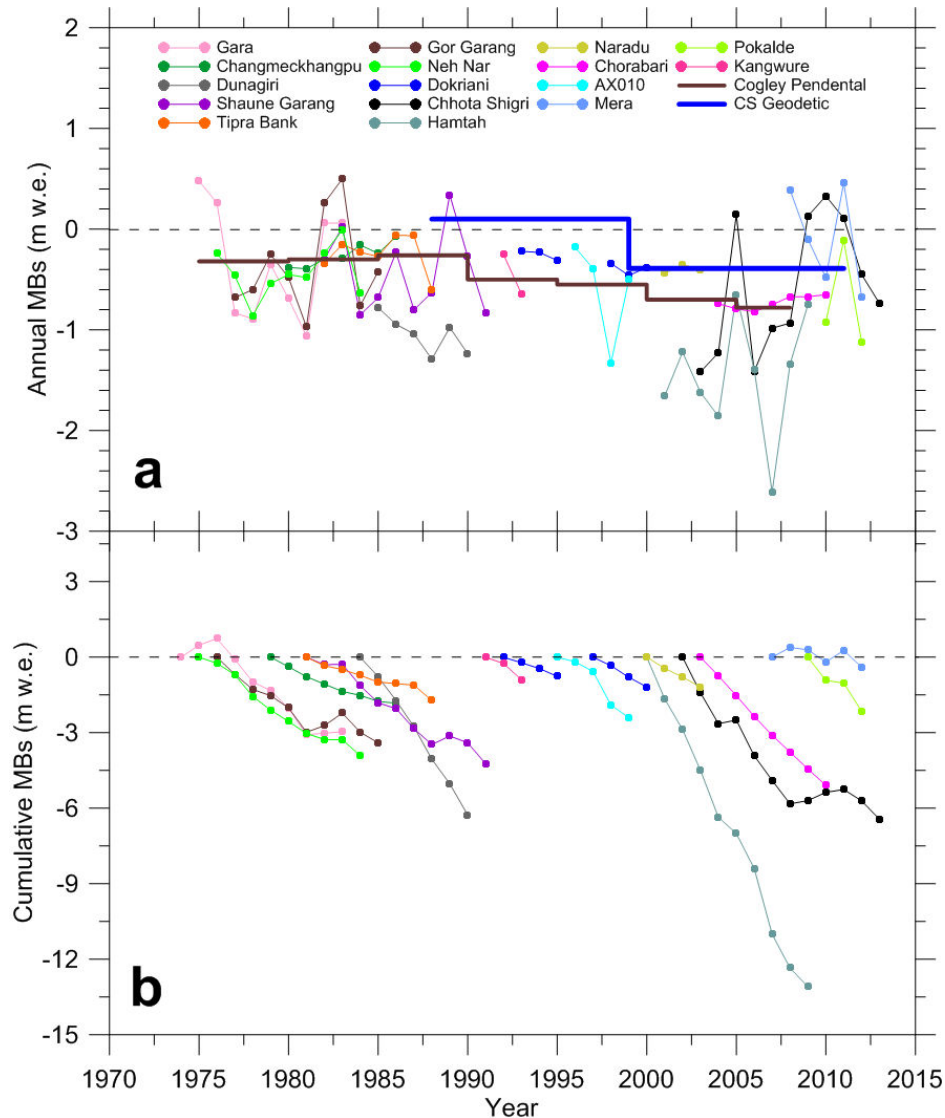


Figure 1.4. Glacier annual glacier-wide mass balances in the Hindu-Kush Karakoram Himalayan region. (a) Annual MB of glaciers with more than one year of observations. The dark brown and blue thick lines correspond to the pentadal Himalaya–Karakoram averages from Cogley (2011) and decadal MBs of Chhota Shigri Glacier from Vincent et al. (2013), respectively (b) cumulative MBs.

Figure 4a also includes the pentadal average MBs for the HKH region (Cogley, 2011). The scarcity of B_a observations (Table 1.2) available to compute the pentadal average gives a large weight to individual B_a measurements, some of them being questionable (Vincent et al., 2013). Due to a difficult access to the accumulation areas, it seems that some glaciers are probably surveyed only in their lower part (which is not always clearly mentioned in the sources), making B_a biased negatively. This could be the case for Hamtah Glacier that shows the strong negative field B_a (Fig. 1.4) which are not consistent with space-borne measurements. For this glacier, Vincent et al. (2013) measured a geodetic MB of -0.45 ± 0.16 m w. e. a^{-1} during 1999–2011, whereas the mean glaciological B_a was -1.46 m w. e. a^{-1} during 2000–2009 (Table 1.2). Consequently, some of the ground-based observational data and thus the average MBs in the HKH region are probably biased negatively (Vincent et al., 2013). Gardner et al. (2013) also suggested that most of the assessments have overestimated global mass losses because of the interpolation of sparse glaciological measurements that are not representative for the largest glacierized regions and tend to be located in the sub-regions where mass loss is greater than in their region as a whole.

1.7.2.2 Mass Balance changes at regional scale

Recently, with the evolution of satellite imageries, several studies have been conducted to calculate the mass changes of glacierized regions worldwide. Covering a glacierized area of ~ 62 km², Bolch et al. (2011) calculated a MB of -0.32 ± 0.08 m w.e. a^{-1} over 1970–2002 and -0.79 ± 0.52 m w.e. a^{-1} over 2002–2007 period for Khumbu region. Nuimura et al. (2012) covering the same glacierized area of Khumbu region reported a mean MB of -0.45 ± 0.60 m w.e. a^{-1} over 2000–2008 period. Over 6 glacierized areas (Bhutan, Everest, West Nepal, Lahaul & Spiti, Karakoram west and Hindu-Kush) of the HKH region, Kääb et al. (2012) computed the mean mass wastage of -0.21 ± 0.05 m w.e. between 2003 and 2008. Gardelle et al. (2013) provided the most exhaustive region-wide MBs for 9 sub-regions in the HKH and Pamir (west to the HKH region) mountain ranges between 2000 and 2008/2011. The area weighted mean MB showed a mass wastage of -0.14 ± 0.08 m w.e. a^{-1} for all 9 sub-regions (glacierized area of 72251 km²). The region-wide glacier MBs were contrasted with the largest wastage in the western Himalaya (-0.45 ± 0.13 m w.e. a^{-1}), moderate mass losses in the eastern and central Himalaya (-0.22 ± 0.12 m w.e. a^{-1} to -0.33 ± 0.14 m w.e. a^{-1}), least mass losses in Hindu-Kush region (-0.12 ± 0.16 m w.e. a^{-1}) and mass gain in the Karakoram east, Karakoram west and Pamir sub-regions ($+0.11 \pm 0.14$, $+0.09 \pm 0.18$, $+0.14 \pm 0.14$ m w.e. a^{-1} , respectively). Although the region-wide MBs show the contrasting pattern over the HKH region during the first decade of the present century, these region-wide MBs are two to three times less negative than the estimated global average for glaciers and ice caps (Kääb et al., 2012; Gardelle et al., 2013).

1.8 Summary

This chapter can be summarized as follows: (1) the historical knowledge of the HKH glaciers mainly comes from the snout fluctuations but, unfortunately, it is a poor indicator of climate change given that the snout fluctuations also depend on several variables which are not related to climate such as the length, area, glacier slope, glacier bedrock slope, surroundings, and the type of glacier (debris-covered or clean), (2) the in-situ surface B_a measurements have been started on some selected glaciers in the western Himalaya during the 1970s but discontinued after some years. Very limited B_a studies are available over the 1990s from the central Himalaya and with the beginning of 21st century some new studies have started in different parts of the Himalaya. Besides, these limited measurements mostly come from small glaciers and are expected to be biased negatively. Till date no B_a study is reported from the Hindu-Kush and Karakoram parts. In addition, (3) our knowledge of region-wide glacier mass changes in the HKH region has been improved significantly over the last years mainly because of geodetic measurements from satellite images. A contrasting pattern of glacier mass loss over the entire HKH region, depending on the climatic settings of the different parts of the range, is revealed from the remote sensing studies. Unfortunately these geodetic mass budgets do not allow us to analyze the climatic variables such as temperature and precipitation responsible for the glacier MB evolution. Consequently, the best way to understand the climatic drivers responsible for glacier MB evolution is to measure the surface B_a (accumulation and ablation) and to analyze this with the meteorological data. Certainly understanding the present and past behaviour of these glaciers towards climatic conditions is the key foundation to predict the future of glacierized areas in the HKH region. Therefore, the present situation demands to understand the behaviour of some selected glaciers over the entire HKH range, with different climatic regimes, towards the present and past climatic conditions in order to get an overview about the whole HKH mountain range.

1.9 Objectives and organization of the thesis

Keeping the main knowledge gaps about the HKH glaciers in mind, a representative glacier 'Chhota Shigri' in the western Himalaya, India, has been selected for the present research work. The annual surface B_a of this glacier has been measured since 2002 using glaciological method. Moreover ice thickness, ice flow velocities, seasonal MB measurements and meteorological data have been collected before and during this PhD work.

The main motive of this thesis is to analyze the sensitivity of Chhota Shigri Glacier B_a to climate change and to understand which meteorological variables drive B_a of the glaciers in the western Himalayan region. In order to achieve this motive, the following objectives are set for this research work:

- to understand the local meteorological conditions at glacier scale using in-situ meteorological data from an Automatic Weather Station (AWS-M) located on the western moraine on Chhota Shigri Glacier
- to study the annual and the seasonal mass balances for understanding the seasonal characteristics of Chhota Shigri Glacier
- to analyze the present imbalance state of Chhota Shigri Glacier from ice thickness changes and ice flow velocity measurements performed over the last decade and at the end of the 1980s
- to reconstruct the long term time series of mass balance for understanding the past behaviour of Chhota Shigri Glacier towards climatic variables
- to analyze the relationship between the meteorological variables and the surface mass balance in order to understand which meteorological variables drive the surface mass balance of Chhota Shigri Glacier. For this purpose, the processes controlling the surface mass balance are analyzed using detailed surface energy balance approach

In order to address all the objectives listed above, the present manuscript is organized as follow. After this first **Chapter**, giving an overview of the status of the HKH glaciers and highlighting the main knowledge gaps in the glaciological research of the HKH region, **Chapter 2** provides the details of the meteorological conditions and in-situ annual and seasonal MBs on Chhota Shigri Glacier. **Chapter 3** discusses the dynamic conditions of Chhota Shigri Glacier by analyzing the ice fluxes calculated from the surface MB and ice thickness-velocity methods. **Chapter 4** presents the reconstruction of long-term time series of annual and seasonal glacier-wide MBs for Chhota Shigri Glacier using a temperature index model with an accumulation model. The reconstructed series provides a basis to study the climate-glacier interaction over last four decades as well as some principle processes governing B_a of Chhota Shigri Glacier. **Chapter 5** focuses on further understanding of the melt processes with a detailed physical basis at point scale using a surface energy balance model with in-situ Automatic Weather Station (AWS-G) data from the ablation area of Chhota Shigri Glacier. **Chapter 6** presents the overall conclusion and perspectives of this thesis.

Three of the chapters presented in this PhD thesis are already published articles and one is under process.

CHAPTER 2

Meteorological conditions and mass balances of Chhota Shigri Glacier

Executive summary

Chapter 1 highlighted the main knowledge and data gaps in our present understanding of the glaciers in the Hindu-Kush Karakoram Himalayan region. Chapter 2 aims at characterizing the different climatic and seasonal regimes in the region of Chhota Shigri Glacier and analyzes the annual and seasonal mass balances of this glacier. On Chhota Shigri Glacier, the characterization of seasons was done using the data from the automatic weather station operating on the western moraine at 4863 m a.s.l. since 18 August 2009. The annual mass balances have been measured continuously since 2002 using the glaciological method. In May 2009, the mass balance observations were also started at seasonal scale. The annual and seasonal mass balances were then analyzed with meteorological conditions in order to understand the role of winter and summer glacier-wide mass balances for annual glacier-wide mass balance of Chhota Shigri Glacier. This glacier is a representative glacier for Lahaul and Spiti Valley ([Berthier et al., 2007](#); [Vincent et al., 2013](#)). Therefore the characterization of seasons as well as the control of meteorological conditions on seasonal and thus annual mass balances can be generalized over the whole Lahaul and Spiti Valley.

2.1 Background and Introduction

After some preliminary work conducted during the latter part of the 1980s (Ramanathan et al., 2011), glaciological research has been started again on Chhota Shigri Glacier under an Indo-French collaboration in 2002. As a master student, I joined the glaciological research team of *Jawaharlal Nehru University*, New Delhi, India in 2008 and visited Chhota Shigri Glacier for the first time in October 2008. Since then, I have been involved in most of the expeditions to this glacier with Indian as well as French collaborators. In 2011, I enrolled in PhD in France and started organizing and leading several expeditions in order to collect the required data for this present thesis. The expeditions on Chhota Shigri Glacier were mainly related to annual and seasonal mass balance observations, surface ice velocity from stake displacement measurements, glacier ice thickness from ground penetrating Radar measurements, annual thickness fluctuations of cross sectional surface profiles with differential global positioning system, installation of hydrological station, installation and maintenance of automatic weather stations and installation of automatic precipitation gauge. With these measurements, Chhota Shigri Glacier is the only “tier-2” type glacier (Paul et al., 2007) in the Lahaul and Spiti Valley (western Himalaya).

Contrary to the Alps, the expeditions in the Himalayas are greatly challenging. The interiority of the glaciers makes the access difficult. The expeditions for Chhota Shigri Glacier are prepared at the town of Manali, which is 100 km far by road from the glacier base camp. The only access road to Chhota Shigri Glacier is through Rohtang Pass (3978 m a.s.l.; literally *pile of corpses*) and often closed because of landslides from steep mountain slopes. In such situation, sometimes, the expeditions are continued on foot with heavy loads carried as back pack to reach the glacier base camp. Besides, weather forecast is not available for this region making the expedition even more challenging. Moreover, expeditions can only be carried out between May and October because the Rohtang pass is completely covered by snow beyond this time window.

This chapter presents the meteorological and glaciological data collected during and before the present PhD. The main goals are (1) to characterize the seasons and local meteorology on Chhota Shigri Glacier using the glacier-side Automatic Weather Station (AWS-M) data since 18 August 2009 (2) to discuss the eleven years (2002-2013) of specific annual glacier-wide mass balance (B_a) and 4 years (2009-2013) of seasonal (winter and summer) glacier-wide mass balances (B_w and B_s), and (3) to analyze the meteorological control on seasonal and annual mass balances.

2.2 Study site and AWS-M description

Chhota Shigri Glacier (32.28 N, 77.58 E) is a valley-type, non-surging glacier located in the Chandra-Bhaga river basin of Lahaul and Spiti Valley, Pir Panjal range, western Himalaya (Fig. 2.1). This glacier extends from 6263 to 4050 m a.s.l. with a total length of 9 km and area of 15.7 km² (Wagnon et al., 2007). Its snout is well defined, lying in a narrow valley and giving birth to a single pro-glacial stream feeding Chandra River, one of the tributaries of Indus river system.

Chhota Shigri Glacier is mainly oriented north-south in its ablation area but its tributaries and accumulation area have a variety of orientations (Fig. 2.1). The ablation area is made up of two main flows, one coming from the eastern side of the accumulation area and flowing on the right bank of the glacier (eastern flank) and the second coming from the western side and flowing on the left bank (western flank). The lower ablation area (<4500 m a.s.l.) is covered by debris representing 3.4% of the total surface area (Vincent et al., 2013). The debris layer is highly heterogeneous, from a few millimeter sized sand particles to big boulders exceeding sometimes several meters.

AWS-M is located off-glacier on a western lateral moraine (4863 m a.s.l.) on a flat rocky surface and has been functioning continuously since 18 August 2009. The meteorological variables were measured at 30-sec time step, except for wind direction (instantaneous values every 30-min) and the data was stored in a Campbell CR1000 data logger as hourly means for 18 August 2009-22 May 2010 period and 30-min means after 22 May 2010. AWS-M was checked and maintained regularly during the summer field expeditions. At the glacier base camp (3850 m a.s.l., 2 km north of the glacier snout), an all-weather precipitation gauge with a hanging weighing transducer (Geonor T-200B) has been operating continuously since 12 July 2012 (Fig. 2.1). The Geonor T-200B sensor is suitable for both solid and liquid precipitation measurements. Table 2.1 gives the list of meteorological variables with the sensor specifications.

Table 2.1. Measurement specifications for AWS-M located at 4863 m a.s.l. on the western lateral moraine of Chhota Shigri Glacier and precipitation gauge installed at base camp (3850 m a.s.l.). Variable symbols are also given.

Variable	symbol (unit)	sensor	stated accuracy
air temperature	T_{air} (°C)	Campbell HC-S3-XT	±0.1 at 0 °C
relative humidity	RH (%)	Campbell HC-S3-XT	±1.5% at 23 °C
wind speed	u (m s ⁻¹)	05103-10-L	±0.3 m s ⁻¹
wind direction	WD (degree)	05103-10-L	±3 degree
short wave incoming and outgoing	SWI, SWO (W m ⁻²)	Kipp & Zonen CNR-1	±10% daily total
long wave incoming and outgoing	LWI, LWO (W m ⁻²)	Kipp & Zonen CNR-1	±10% daily total
surface temperature	T_{surf} (°C)	IRR-P	±0.5 °C
Precipitation	P (mm)	Geonor T-200B	±0.6 mm

The AWS-M meteorological records have very small data gaps (generally <1%) suggesting good data continuity. T_{air} , u and WD showed 0.003%, 0.29%, and 0.07% data gaps, respectively. These gaps were filled by linear interpolation using the adjacent data. Only one long gap exists in LWI and LWO radiation data between 18 August 2009 and 22 May 2010. Moreover internal temperature sensor of CNR-1 did not work during the four-year period of observation. Thanks to the surface temperature (T_{surf}) data from IRR-P sensor, the LWO could be assessed using the

Stefan-Boltzmann equation assuming the emissivity of the surface as unity ($LWO = \sigma T_{\text{surf}}^4$ with $\sigma = 5.67 \cdot 10^{-8} \text{ W m}^{-2} \text{ K}^{-4}$), and comparing this LWO with the uncorrected value of LWO recorded by AWS-M, we could retrieve CNR-1 internal temperature.

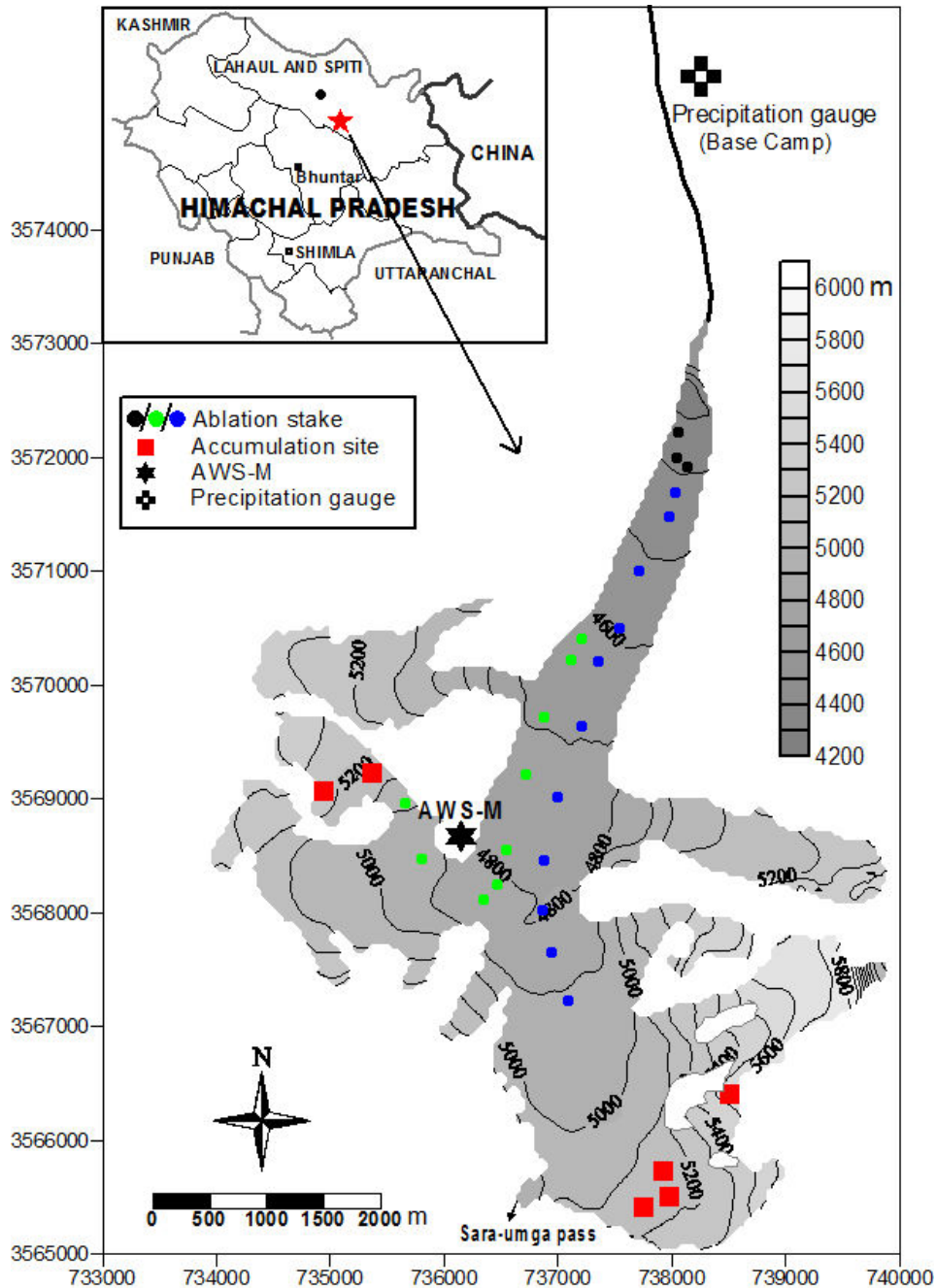


Figure 2.1. Map of Chhota Shigri Glacier showing the ablation stakes in debris cover area (black dots), in eastern flank (blue dots), in western flank (green dots), accumulation sites (red squares), AWS-M (black star) and precipitation gauge (black cross). The map coordinates are in the UTM43 (north) World Geodetic System 1984 (WGS84) reference system.

2.3 Hydrological year and field measurements to assess the mass balances

2.3.1 Delineation of the hydrological year

Kaser et al. (2003) defined the hydrological balance year as the time between one minimum of glacier mass to the next, which, in mid-latitudes, generally occurs in autumn. The glaciers in the Lahaul and Spiti Valley (western Himalaya) are influenced by Mid-Latitude Westerlies (MLW) during winter and by Indian Summer Monsoon (ISM) during summer (section 1.3). The precipitation data at high altitudes in the Himalayas is extremely rare. The automatic precipitation gauge installed on 12 July 2012 at Chhota Shigri Glacier base camp (3850 m a.s.l., Fig. 2.1) provides the only recorded local precipitation data for this glacier (Fig. 2.2, Table 2.2). In order to analyze the contribution of MLW and ISM circulations to the annual precipitation sum at glacier base camp, the year is divided into summer (May to October) and winter (November to April) months. MLW (November to April) provided 79% while ISM (May to October) contributed only 21% to the annual precipitation (976 mm) at Chhota Shigri Glacier base camp between October 2012 and September 2013. Therefore, unlike the summer-accumulation type glaciers (Ageta and Higuchi, 1984) in central Himalaya, Chhota Shigri Glacier receives most of its precipitation during winter months. Given that October and November are the driest months in this region (Prasad and Roy, 2005; Datt et al., 2008) and the access is restricted after 15 October, the hydrological year can be defined from 1st October to 30th September of the following year on this glacier. Nevertheless one year precipitation record is quite short and the relative contribution of precipitation, which is likely to change from one year to another, should be considered cautiously. The issue of hydrological/mass balance (MB) year is dealt thoroughly in Chapter 4 (appendix) using the long term reconstructed daily MB series.

2.3.2 Measurement network to measure the glacier-wide mass balances with the glaciological method

Annual glacier-wide surface MB measurements have been carried out on Chhota Shigri Glacier since 2002 at the end of September or beginning of October using the direct glaciological method (Peterson, 1994). Ablation is measured through a stake farm distributed between 4300 and 5000 m a.s.l. (Fig. 2.1) whereas in the accumulation area, the net annual accumulation is obtained by drilling cores or pits between 5160 and 5550 m a.s.l. The total number of stakes was changed from year to year but every year a minimum of 22 stakes was maintained to get enough ablation measurements for MB calculations. Eco-friendly bamboo pieces of 2-m length linked with metallic wire were used and inserted vertically downward up to 8-10 m deep in the glacier. In the accumulation area, the number of sampled sites is limited due to the difficult access and high elevation; still five-six sites were measured every year to have enough accumulation measurements (Fig. 2.1). A blue powder mixed with saw dust was spread over the glacier surface (2-m radius) to mark the annual horizon in accumulation area besides a Recco avalanche reflector

put at accumulation sites in order to locate the marked points using Recco detector in the following year. The details of mass balance methodology can be found in [Wagnon et al. \(2007\)](#). In October 2013, the electronic balance failed; consequently, the core densities could not be calculated. It is known that from one year to another, at specific location, accumulation thickness varies but the density along the depth remains almost the same. Therefore at each accumulation site, the mean vertical density along every pit was assumed equal to the mean depth-averaged density of every corresponding accumulation site from the years before. These resulting mean densities together with corresponding accumulation thicknesses were used to obtain the annual accumulation at each site for October 2013.

The overall error in B_a , calculated following [Thibert et al. \(2008\)](#), comes from a variance analysis applied to all types of errors (ice/snow density, core length, stake height determination, liquid-water content of the snow, snow height). Applying these errors at different altitudinal ranges using Eq (1.2), the uncertainty on B_a is ± 0.40 m w.e. a^{-1} . The details of error estimation are provided in Chapter 3 (section 3.3.1). The uncertainties in the seasonal glacier-wide mass balances are likely to be different. Given the limited time frame of this PhD, these uncertainties could not be assessed yet.

2.4 Meteorological conditions and characterization of the seasons on Chhota Shigri Glacier

2.4.1 Air temperature and relative humidity

Figure 2.2 displays the daily temporal variation in T_{air} , RH, u , SWI and LWI during the measuring period from 18 August 2009 to 30 September 2013 recorded by the AWS-M and daily precipitation sums at glacier base camp recorded by the precipitation gauge between 12 July 2012 and 30 September 2013. The meteorological data available for more than 4 years have been used to assess local meteorological conditions and to characterize the seasons on Chhota Shigri Glacier. Four hydrological years (1 October 2009 to 30 September 2013) for AWS-M variables and one hydrological year (1 October 2012 to 30 September 2013) for precipitation were selected to analyze the meteorological conditions at seasonal and annual scale (Table 2.2).

Daily means of T_{air} ranged between -22.0 and $+7.3$ °C with a mean value of -5.8 °C while RH ranged between 4 and 96% with a mean value of 51% for the studied period (1 October 2009 to 30 September 2013). The mean T_{air} (-5.8 °C) reflects the high altitude of the AWS-M location. The daily mean u varied from 0.7 to 15.9 m s^{-1} with an annual mean of 4.1 m s^{-1} , over the four hydrological year observation period. A decrease in u during the first half of May and a rapid increase of RH from the last week of May or the first week of June was revealed from daily mean records (Fig. 2.2). These abrupt changes can be considered as the onset of the monsoon. RH continuously increases and achieves the maximum values in August. Furthermore, a sudden

drop in RH and an increase in u , noticed around 20 September, show the sharp decay of the monsoon on Chhota Shigri Glacier.

T_{air} and RH variations are large enough to characterize pronounced seasonal regimes. A warm summer-monsoon with high RH from June to September and a cold winter season, relatively less humid, from December to March were identified (Fig. 2.2). In addition a pre-monsoon from April to May and a post-monsoon from October to November can also be defined. Table 2.2 demonstrates the mean annual and seasonal values of all studied variables for each hydrological year as well as for the whole period (1 October 2009-30 September 2013).

The coldest month was January with a mean T_{air} of $-15.8\text{ }^{\circ}\text{C}$ and the hottest month was August with a mean T_{air} of $4.3\text{ }^{\circ}\text{C}$. The monthly mean T_{air} during winter season was $-13.4\text{ }^{\circ}\text{C}$ and that for the summer-monsoon was $2.5\text{ }^{\circ}\text{C}$, while during pre-monsoon and post-monsoon it was -5.3 and $-7.8\text{ }^{\circ}\text{C}$, respectively (Table 2.2). However the monthly average T_{air} is $>0\text{ }^{\circ}\text{C}$ in at least three months (July to September), T_{air} can drop below the freezing point even in the hottest months of the year (21% days in June, 5% in July, 3% in August and 15% in September). The monthly mean is higher than the annual mean T_{air} ($-5.8\text{ }^{\circ}\text{C}$) between May and October whereas the October mean temperature ($-4.9\text{ }^{\circ}\text{C}$) was closest to the annual mean T_{air} . A sudden change in mean monthly T_{air} characterizes the onset of a new season; and the most evident inter-seasonal change was found between the summer-monsoon and post-monsoon with a difference of $10.3\text{ }^{\circ}\text{C}$ while the minimum difference ($5.6\text{ }^{\circ}\text{C}$) was found between post-monsoon and winter season showing that winter and the summer-monsoon are thermally well distinguished. Compared to 2009/10, 2010/11 and 2011/12, the summer-monsoon of 2012/13 year was relatively warm ($0.7\text{ }^{\circ}\text{C}$ higher than the mean of the four hydrological years) while the 2009/10 winter season was warmer ($0.9\text{ }^{\circ}\text{C}$ higher than the mean of the four hydrological years).

A sudden increase (decrease) in mean monthly RH in June (October) shows the onset (end) of monsoon on Chhota Shigri Glacier. The highest peak in mean monthly humidity was observed in August (74%) while another peak was observed in February (51%) suggesting that Chhota Shigri Glacier is alternately influenced by ISM during the summer-monsoon (mean monsoon RH = 68%) and MLW during winter season (mean winter RH = 42%). Post-monsoon showed the lowest (39%) RH while pre-monsoon showed the RH (52%) closest to the annual mean.

2.4.2 Precipitation

Table 2.2 also shows the seasonal precipitation sums for a complete hydrological year between 1 October 2012 and 30 September 2013 at Chhota Shigri Glacier base camp (3850 m a.s.l.). The observed precipitation during winter season was maximum with a contribution of 71% to the total annual precipitation whereas post-monsoon received minimum precipitation (3% of the annual amount). The contributions of pre-monsoon and summer-monsoon to annual precipitation were only 15% and 12%, respectively. The monthly precipitation sums (not shown in Table 2.2.) were the highest in January and February (183 and 238 mm, respectively) whereas

the lowest were for October and November (14 and 18 mm, respectively). The least precipitation amounts during October and November, in agreement with the regional studies (e.g., Prasad and Roy, 2005; Datt et al., 2008), support the choice of the hydrological year starting from 1st October.

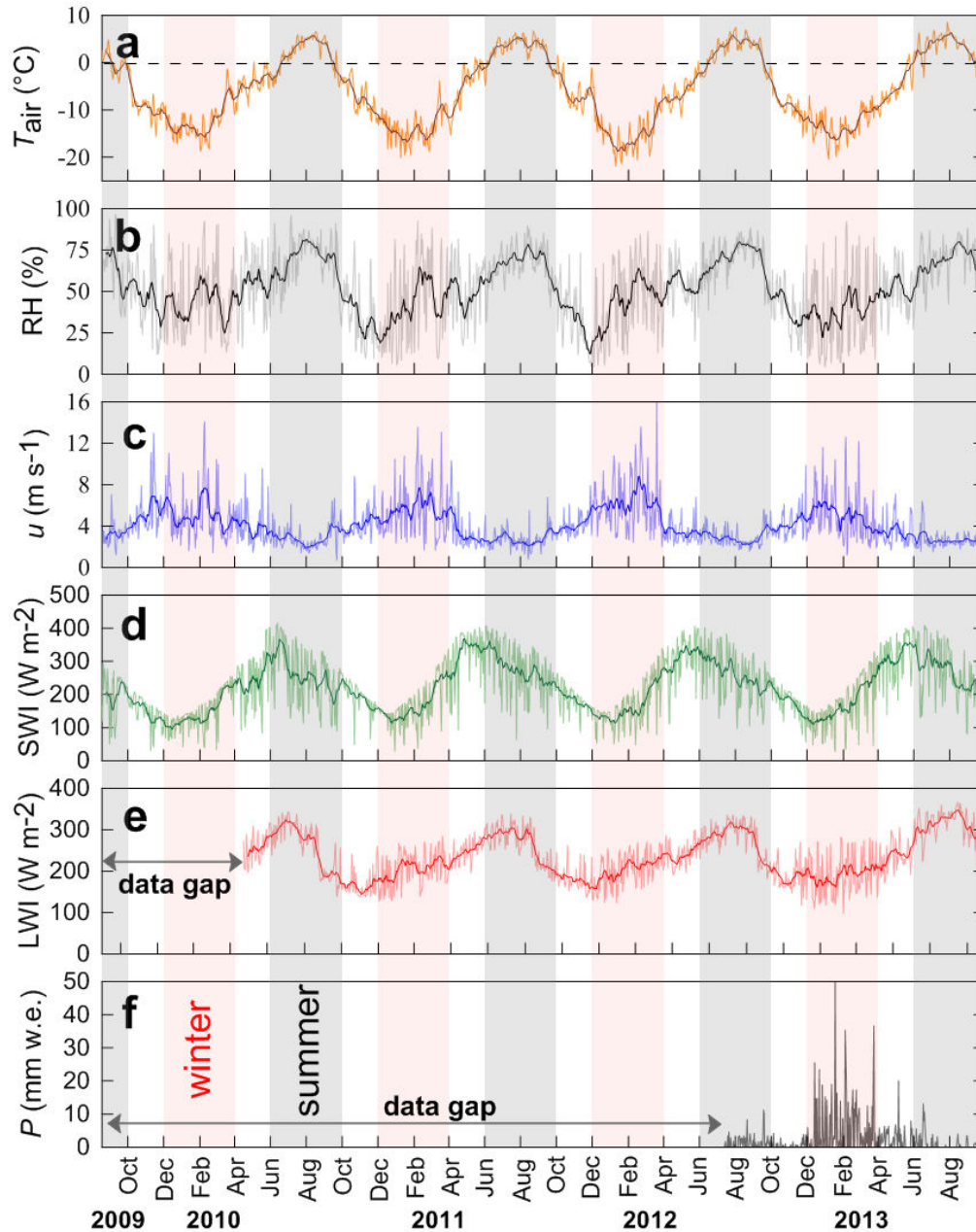


Figure 2.2. Daily means of (a) T_{air} ($^{\circ}\text{C}$), (b) RH (%), (c) u (m s^{-1}), (d) SWI (W m^{-2}) and (e) LWI (W m^{-2}) at AWS-M. T_{air} , RH, u and SWI are the daily means for the full observation period between 18 August 2009 and 30 September 2013 while LWI are the daily means between 23 May 2010 and 30 September 2013. The lowest panel (f) shows the daily precipitation (mm w.e.) between 12 July 2012 and 30 September 2013 at glacier base camp collected by the precipitation gauge. The thick lines in panels a-e are the 15 day running means.

Table 2.2. Mean seasonal values of T_{air} , RH, u , SWI and LWI at AWS-M. T_{air} , RH, u and SWI are the mean seasonal values of four hydrological years between 1 October 2009 and 30 September 2013 while LWI are the mean seasonal values between 1 June 2010 and 30 September 2013. P is the seasonal precipitation for one hydrological year between 1 October 2012 and 30 September 2013 at glacier base camp collected by the precipitation gauge.

Season	Variable	Year				Mean 2009-13
		2009-10	2010-11	2011-12	2012-13	
Post-monsoon (ON)	T_{air} ($^{\circ}\text{C}$)	-8.8	-7.3	-6.1	-9.1	-7.8
	RH (%)	48	35	33	40	39
	u (m s^{-1})	5.1	4.2	4.1	4.2	4.4
	SWI (W m^{-2})	150	191	186	178	176
	LWI (W m^{-2})	-	178	192	192	187
	P (mm w.e.)	-	-	-	32	-
Winter (DJFM)	T_{air} ($^{\circ}\text{C}$)	-12.4	-13.6	-14.5	-13.1	-13.4
	RH (%)	43	41	43	38	42
	u (m s^{-1})	5.1	5.5	6.3	5.0	5.5
	SWI (W m^{-2})	144	168	163	168	161
	LWI (W m^{-2})	-	190	195	190	192
	P (mm w.e.)	-	-	-	679	-
Pre-monsoon (AM)	T_{air} ($^{\circ}\text{C}$)	-4.6	-4.9	-6.1	-5.5	-5.3
	RH (%)	52	50	54	51	52
	u (m s^{-1})	3.9	3.4	3.4	3.5	3.5
	SWI (W m^{-2})	249	323	311	316	299
	LWI (W m^{-2})	-	230	233	231	231
	P (mm w.e.)	-	-	-	148	-
Summer- monsoon (JJAS)	T_{air} ($^{\circ}\text{C}$)	1.9	2.8	2.4	3.3	2.6
	RH (%)	69	67	69	68	68
	u (m s^{-1})	2.9	2.7	2.9	2.7	2.8
	SWI (W m^{-2})	260	277	263	265	266
	LWI (W m^{-2})	280	276	283	308	289
	P (mm w.e.)	-	-	-	117	-
Annual (mean)	T_{air} ($^{\circ}\text{C}$)	-5.7	-5.6	-6.1	-5.7	-5.8
	RH (%)	54	50	52	50	51
	u (m s^{-1})	4.1	4.0	4.3	3.8	4.1
	SWI (W m^{-2})	201	234	225	227	222
	LWI (W m^{-2})	-	224	230	237	230
	P (mm w.e.)	-	-	-	976	-

2.4.3 Incoming short and long wave radiations

The characterization of the seasons on Chhota Shigri Glacier can also be explained by the variation of SWI and LWI. The highest SWI was found during pre-monsoon with a mean annual value of 299 W m^{-2} . As soon as the summer-monsoon starts, T_{air} increases but SWI is reduced by 33 W m^{-2} (summer-monsoonal mean = 266 W m^{-2}) in agreement with high RH (summer-monsoonal mean = 68%) (Fig. 2.2 and Table 2.2). The low values of SWI, during the summer-monsoon, are largely compensated by high values of LWI (summer-monsoonal mean = 289 W m^{-2}) emitted from the summer-monsoonal clouds. Post-monsoon and winter season exhibited more

or less similar conditions, receiving low and almost same SWI (176 and 161 $W m^{-2}$, respectively) and LWI (187 and 192 $W m^{-2}$, respectively). The low SWI and LWI values over these seasons are mainly related to decreasing solar angle (for SWI), and the low values of T_{air} , RH and cloudiness (for LWI), respectively.

2.4.4 Wind regimes

On average u was the highest during the winter season with a mean value of $5.5 m s^{-1}$ and reached up to its maximum value of $6.2 m s^{-1}$ in the month of February. u was also strong in pre-monsoon (mean = $3.5 m s^{-1}$), especially in the month of March (monthly mean = $5.1 m s^{-1}$). u over the summer-monsoon was found quite weak (mean = $2.8 m s^{-1}$) and breezed at its minimum strength particularly in August (monthly mean = $2.4 m s^{-1}$). During post-monsoon, wind gusted at moderate speeds (mean = $4.4 m s^{-1}$) and approached the high speed of wintertime value. The summer-monsoon winds were almost the same for the four hydrological years while the winter wind was the highest in 2011/12 hydrological year.

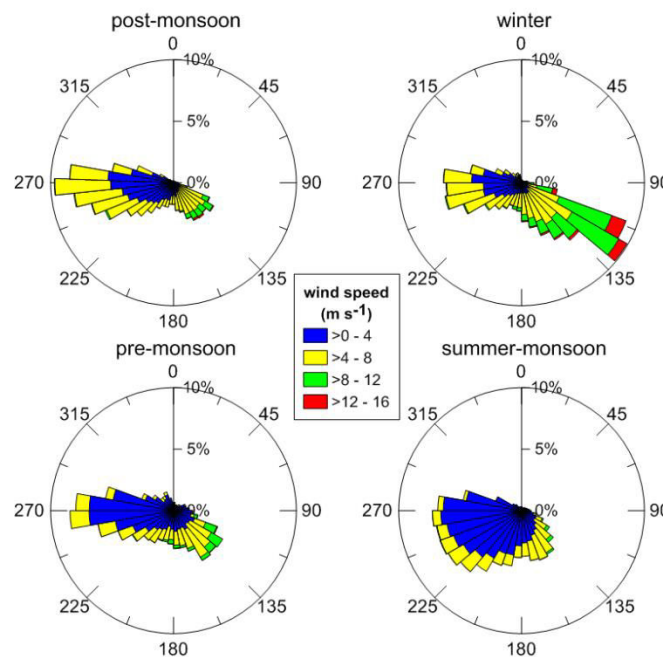


Figure 2.3. Wind rose (direction and intensity of half-hourly average data) at AWS-M for post-monsoon, winter, pre-monsoon and the summer-monsoon over the four hydrological years of observation. The data is hourly average between 1 September 2009 and 22 May 2010. The frequency of wind direction is expressed as percentage for each season (indicated on the radial axes).

Below 4800 m a.s.l., Chhota Shigri Glacier is situated in an almost north-south oriented valley and the AWS-M is located on a west lateral moraine on a rocky surface around 100 m above the main glacier trunk at 4863 m a.s.l. A small and steep cirque tributary glacier is located in the

south-west of AWS-M and the Sara-umga pass is located toward the south (Fig. 2.1). Wind direction measured at AWS-M indicated that there was a persistent down-glacier wind coming from the west in all the seasons (Fig. 2.3), and opposite to it, less strong winds were also observed from south-east direction during all the seasons. The west winds may be because of the steep cirque glacier just above the AWS-M in south-west that can generate katabatic forcing at AWS-M site.

In order to analyze the impact of synoptic scale circulation at AWS-M site, the wind directions at AWS-M were compared with those of 450 hPa pressure level obtained from High Asia Refined Analysis data (HAR, [Maussion et al., 2014](#)) at hourly scale. HAR wind data is available at 10 km resolution for different pressure levels for 2001-2012 period. The pressure level of 450 hPa (equivalent to ~6350 m a.s.l.) has been chosen as representative of the synoptic circulation above the glacier (whose highest elevation is 6263 m a.s.l.). Synoptic (HAR, 450 hPa) wind comes mainly from west or south-west directions, depending on the season (not shown in Fig. 2.3). Given that the AWS-M is located on a western moraine at 4863 m a.s.l., the site is likely to be affected by synoptic scale winds. Therefore at AWS-M the persistent west winds are probably the collective impact of katabatic and synoptic scale winds. During all the seasons, the south-east or south-west winds at AWS-M are probably the impact of synoptic winds. The synoptic winds coming from west are channeled by north-south oriented valley and come from south-east or south-west directions at AWS-M. The south-east winds are more frequent and stronger (up to 15 m s^{-1}) in winter season than during the other seasons. In winter season the AWS-M site as well as south-eastern upper reaches are completely covered by snow that may give rise to cooling to the near-surface air, generating katabatic flow ([Grisogono and Oerlemans, 2002](#)) parallel to the channeled synoptic scale winds thus the strong winds from south-west direction. In conclusion the wind regime at AWS-M site is a combined effect of local katabatic and synoptic scale winds during all the seasons. Upcoming valley wind at AWS-M is absent in all seasons. This is probably because of the long distance (7 km) between snout and AWS-M location that prevents the upcoming valley wind reaching to the AWS-M site.

2.5 Annual and Seasonal mass balance

2.5.1 Annual point mass balances as a function of altitude

Figure 2.4 (panels a–g) shows the point mass balances as a function of altitude for 2006–2013 hydrological years (the details of point mass balances between 2002 and 2006 are given in [Wagnon et al., 2007](#)). Measurements were performed on 30 September 2006, 1 October 2007, 6 October 2008, 9 October 2009, 10 October 2010, 9 October 2011, 10 October 2012 and 6 October 2013, ± 4 days. The black, blue and green dots represent measurements over the debris cover area (<4400 m a.s.l.), eastern flank (the main glacier body) and western flank of the glacier, respectively whereas red dots are the field MBs at 5500/5550 m a.s.l. The elevation of the limit between the debris-covered and the clean-ice area is lower on the eastern flank (4400 m a.s.l.) than on the

western flank (4500 to 4600 m a.s.l.). Panel h (Fig. 2.4) shows the mean altitudinal MBs for each 50-m altitudinal range. From Fig. 2.4 (panels a–h) it is revealed that ablation at the stakes (black dots) in the lowest part of the ablation area is subdued by 2–3 m w.e. a⁻¹ irrespective to their altitude. This is due to the debris cover that has an insulating effect and the deep-narrow valley over this area that in turn induces a reduced incoming short-wave radiation (Wagnon et al., 2007). However, the annual point mass balances are still very negative on the debris covered area with annual values varying between –2 and –5 m w.e. At similar altitudes (generally, >5000 m a.s.l.), the point mass balances in western flank were found lower than those observed in the eastern flank of the glacier (panels a–g, Fig. 2.4). These differences can be explained by the east orientated slopes of western parts that receive more solar radiation and thus likely to have more ablation (Wagnon et al., 2007).

Given the harsh conditions and rugged terrain, the point accumulation measurements at 5500/5550 m a.s.l. could only be measured in 2003, 2004, 2005, 2009 and 2011 years between 2002 and 2013. For the years without accumulation measurements at 5500/5550 m a.s.l., an extrapolation of 5200 m a.s.l. mean MB (3 measurements in eastern part) to the 5500/5550 m a.s.l. was done applying the MB gradient calculated between 5200 and 5500/5550 m a.s.l. from similar MB years. Accumulation measurements, in eastern flank (main glacier) varied between a minimum annual value of 1.0 m w.e. in 2006/07 (extrapolated) and a maximum value of 2.3 m w.e. in 2008/09 (measured) hydrological year.

2.5.2 Annual vertical mass balance gradients

The blue lines in Fig. 2.4 (panels a–g) are the regression lines plotted over annual point MBs measured in the main glacier body (eastern flank) between 4400 and 5200 m a.s.l. (clean-ice area). These regression lines were used to derive the vertical MB gradients for each hydrological year. The annual vertical MB gradients are reported in Table 2.3. Over the 2002–2013 observation period, the annual MB gradient between 4400 and 5200 m a.s.l. showed a standard deviation of 0.09 m w.e. (100m)⁻¹ with a minimum value of 0.52 m w.e. (100m)⁻¹ for 2008/09 and a maximum value of 0.81 m w.e. (100m)⁻¹ for 2011/12 year. The mean vertical MB gradient between 2002 and 2013 was 0.66 m w.e. (100m)⁻¹. Though calculated over 4400 to 4900 m a.s.l. altitudinal range, the mean annual MB gradient of 0.69 m w.e. (100m)⁻¹ between 2002 and 2006 (Wagnon et al., 2007) for Chhota Shigri Glacier is in good agreement with the mean gradient over 2002–2013 period (0.66 m w.e. (100m)⁻¹).

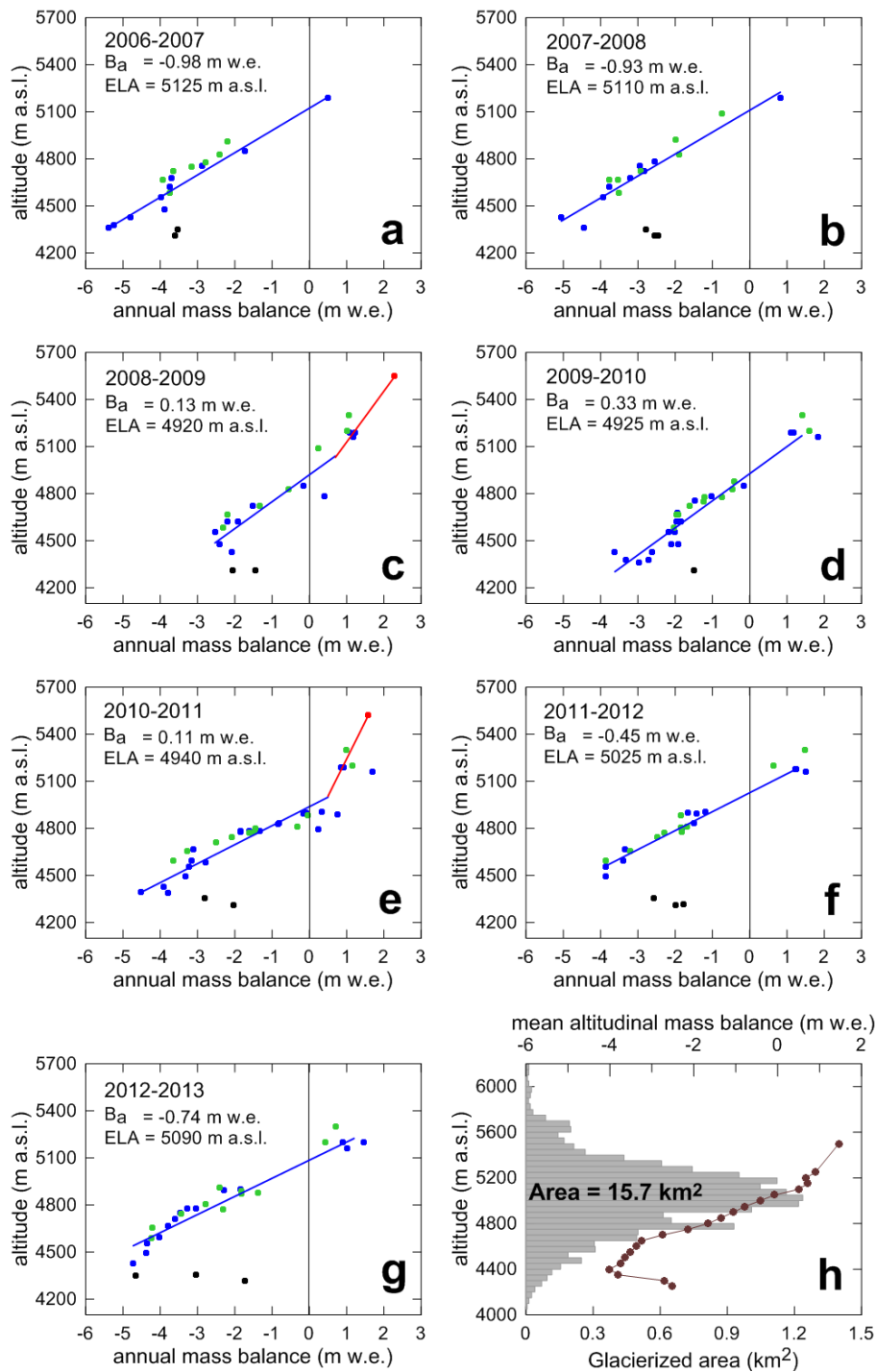


Figure 2.4. Panels a–g show the annual point MB (dots) as a function of altitude derived from field measurements (stakes, drillings or pits) on Chhota Shigri Glacier for seven hydrological years between 2006 and 2013. The black, blue and green dots are the annual point MBs over debris cover area (<4400 m a.s.l.), eastern flank and western flank of glacier, respectively whereas red dots are the MBs at 5500/5550 m a.s.l. B_a and ELA for every year are also displayed on the corresponding panel. Panel h shows the hypsometry (50-m altitudinal ranges) and mean altitudinal MBs (brown dots) of Chhota Shigri Glacier. The mean altitudinal MBs are mean MBs for each 50-m range (e.g., 4400 MB represents the mean MB for 4400–4450 range), except for at 4250 and 5400 where the mean MB are for 4050–4300 and 5400–6250 range, respectively.

The vertical annual MB gradients are also calculated for debris cover (between 4300 and 4400 m a.s.l., (regression lines are not shown in Fig. 2.4) and accumulation area (red regression lines between 5200 and 5500/5550 m a.s.l. in Fig. 2.4) when the MB measurements are available at 5500/5550 m a.s.l. Over the debris cover area, the MB gradients are highly variable (standard deviation = 0.80 m w.e. (100m)⁻¹) with a negative mean value of -2.15 m w.e. (100m)⁻¹ over 2002-2013 observation period. The negative MB gradients can be explained by the thickness of the debris cover that increases with decrease in altitude, therefore, protecting glacier more efficiently at lower altitudes. The high year-to-year variability in MB gradients over debris cover part compared to the main glacier gradients is due to the stake positions and, thus, the debris thickness that can be different from one year to another. The annual vertical MB gradient in accumulation area showed rather less annual variability (standard deviation = 0.08 m w.e. (100m)⁻¹) with a quite low mean value of 0.22 m w.e. (100m)⁻¹ between 2002 and 2013. The mean accumulation MB gradient is calculated using only field observed MB gradients available for 5 years only (Table 2.3).

The MB gradients (Table 2.3) calculated over Chhota Shigri Glacier (main ablation body) are comparable to those observed in the Alps, Nepalese Himalaya or mid-latitude glaciers (e.g., Rabatel et al., 2005; Zemp et al., 2009; Shea et al., 2013; Wagnon et al., 2013). Recently some studies (e.g., Racoviteanu et al., 2013) developed glacier melt models at watershed scale in the Himalayan region based on a single ablation gradient value for MB gradient. Such models can therefore be improved in the future using different MB gradients at different altitudes.

2.5.3 Annual and cumulative glacier-wide mass balances

The annual glacier-wide MBs of Chhota Shigri Glacier between 2002 and 2013 are given in Table 2.3 whereas Fig. 2.5 displays the B_a as well as the cumulative B_a . B_a was often negative except for four years (2004/05, 2008/09, 2009/10 and 2010/11) when it was generally close to balance conditions. B_a varied, with a large inter-annual variability (standard deviation = 0.67 m w.e. a⁻¹), from a minimum value of -1.42±0.40 m w.e. in 2002/03 to a maximum value of +0.33±0.40 m w.e. in 2009/10. The cumulative B_a of Chhota Shigri was -6.45 m w.e. between 2002 and 2013 while the B_a averaged over the same period was -0.59±0.40 m w.e. a⁻¹. With eleven years of B_a measurements, Chhota Shigri Glacier B_a series is the longest continuous B_a series in the HKH region.

Chhota Shigri Glacier has also been studied using remote sensing techniques as it is recognized to be a representative glacier in the Lahaul and Spiti region (Vincent et al., 2013). Gardelle et al. (2013) calculated a mass wastage of -0.39±0.18 m w.e. a⁻¹ for Chhota Shigri Glacier over 1999–2011 period in agreement with field observations (B_a = -0.58±0.40 m w.e. a⁻¹ between 2002 and 2011). For the whole Lahaul and Spiti region the mass wastage was -0.45±0.13 m w.e. a⁻¹ over 1999–2011 period (Gardelle et al., 2013). Nevertheless B_a behavior of this glacier is in contrast to that of neighboring Hamtah Glacier (~13 km west to Chhota Shigri) where a highly negative mean B_a of -1.46 m w.e. a⁻¹ was observed between 2000 and 2009 (Table 1.2; GSI, 2011).

Vincent et al. (2013) calculated a geodetic B_a of -0.45 m w.e. a^{-1} for 1999-2011 period for Hamtah Glacier and suggested that the field B_a series of this glacier is most probably negatively biased because the access to the accumulation area is quite difficult and the field measurements mainly come from ablation area.

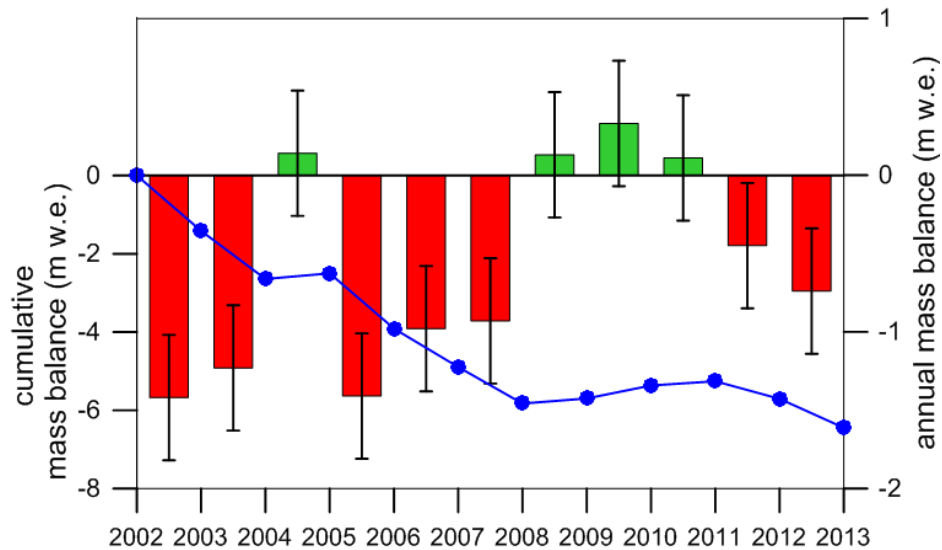


Figure 2.5. Cumulative (blue line) and annual glacier-wide mass balances (red (-) and green (+) histograms) of Chhota Shigri Glacier between 2002 and 2013. Black error bars represent the uncertainty in annual glacier-wide mass balance calculated in Azam et al. (2012).

It is highly recommended to detect potential systematic biases in B_a series obtained from the glaciological method by using satellite derived geodetic B_a (e.g., Thibert et al., 2008; Huss et al., 2009; Zemp et al., 2013). Unfortunately this kind of bias correction in B_a series has never been applied yet on the HKH glaciers. Chhota Shigri Glacier B_a series since 2002 is long enough to apply this correction; therefore, in the future, we will validate B_a derived from field observations with decadal volume changes assessed from geodetic method. Despite the relatively large error bars, year-to-year relative differences are instructive for climatic purposes because annual values refer to the same map, to the same area-elevation distribution function and to the same measurement network (Wagnon et al., 2013).

2.5.4 ELA and AAR

Table 2.3 shows the Equilibrium Line Altitude (ELA) and Accumulation Area Ratio (AAR) for each hydrological year between 2002 and 2013. ELA was calculated using the regression line (blue lines in Fig. 2.4) plotted on annual point MBs in the main glacier body (eastern flank) between 4400 and 5200 m a.s.l. AAR, each year, is then calculated using the ELA of the corresponding year. Over the observation period since 2002, on Chhota Shigri Glacier, ELA varied from a maximum

value of 5235 m a.s.l. in 2002/03 ($B_a = -1.42 \pm 0.40$ m w.e. and AAR = 25%) to a minimum value of 4905 m a.s.l. in 2004/05 ($B_a = +0.14 \pm 0.40$ m w.e. and AAR = 69%) hydrological year. ELA and AAR are well correlated with glacier MB and hence proved to be good indicators of MB change (e.g, [Benn and Lehmkühl, 2000](#); [Cuffey and Paterson, 2010](#)). On Chhota Shigri Glacier, the annual ELA and AAR showed a good agreement with B_a ($r^2 = 0.95$ and 0.94 , respectively) between 2002 and 2013 (Fig. 2.6). The ELA for a zero B_a (ELA₀) was also derived from regression between B_a and ELA over 2002-2013 period and calculated as ~4950 m a.s.l. Similarly AAR₀ was calculated as ~62% for steady state B_a (Fig. 2.6).

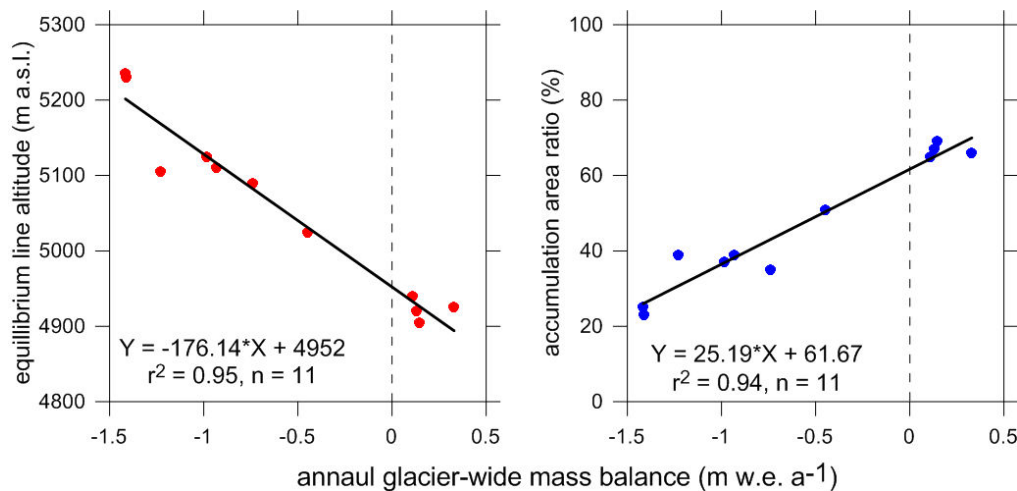


Figure 2.6. The equilibrium line altitude (m a.s.l.) and accumulation area ratio (%) as a function of annual glacier-wide mass balance.

[Rabatel et al. \(2005\)](#) developed a method to calculate B_a using remotely sensed ELA on three glaciers in the French Alps and validated their results with the field based B_a and ELA data. Therefore, the remote sensing method can be applied to the glaciers where no ground data exist, on the scale of a mountain range, if the method is reasonably validated with field observations. Some studies (e.g., [Chaturvedi et al., 2014](#)) used ELA-, AAR-MB relationships to infer the mass changes in the Himalayas. The extensive field data about B_a , ELA and AAR on Chhota Shigri Glacier definitely provide a good opportunity to validate the results of these remote sensing based studies. [Berthier et al. \(2007\)](#), [Gardelle et al. \(2013\)](#) and [Vincent et al. \(2013\)](#) have already used the Chhota Shigri B_a to validate their results of geodetic mass changes for the Lahaul and Spiti region. Recently [Brun et al. \(2014\)](#) reconstructed the annual mass balances of Chhota Shigri and Mera (Everest region, Nepal) glaciers using a relationship between annual minimum albedo averaged over the glacier (retrieved from MODerate Imaging Spectroradiometer, MODIS images) and B_a . Their method worked successfully for Chhota Shigri Glacier because this glacier received maximum precipitation during the winter season, consequently finding the annual minimum

albedo from MODIS images during the summer season was possible as the sky was often clear during the summer season whereas on Mera Glacier the dominant cloudy conditions during the summer season made the retrieval process of annual minimum albedo complex and often inaccurate. Brun et al. (2014) concluded that their method can be applied on the glaciers in the western Himalaya where some years of field based B_a observations are available to calibrate the relationship between B_a and annual minimum albedo. Using this method, they reconstructed Chhota Shigri B_a since 2000, the year from when MODIS images are available.

2.5.5 Seasonal glacier-wide mass balances

On Chhota Shigri Glacier seasonal MB measurements were started in May 2010 to assess the winter (B_w) and summer glacier-wide MBs (B_s) separately. The access to the glacier after winter season depends on the road clearance; therefore, B_w observations could not be carried out on fixed dates. The measurements were carried out on 21 May 2010, 24 June 2011, 20 June 2012 and 6 July 2013, ± 3 days. Azam et al. (2014a) suggested that the average summer ablation period lasts from mid-June to the end of September with 96 ± 18 days and neither ablation nor accumulation is dominant during May-June months therefore no correction was applied to the field B_w for varying measurement dates. However it is considered that varying dates cannot be ignored and their impact is inherited in the overall uncertainty of seasonal MBs especially for the B_w of 2012/13 when the measurements were carried out quite late on 6 July 2013.

Table 2.3 and Fig. 2.7 show the seasonal MBs. B_w ranged from a maximum value of 1.38 m w.e. in 2009/10 to a minimum value of 0.89 in 2012/13 year whereas B_s varied from the highest value of -0.95 m w.e. in 2010/11 to the lowest value of -1.72 m w.e. in 2011/12 year. Between 2009 and 2013, the observed B_a on Chhota Shigri Glacier were slightly positive for 2009/10 (0.33 m w.e.) and 2010/11 (0.11 m w.e.) and negative for 2011/12 (-0.45 m w.e.) and 2012/13 (-0.74 m w.e.) years. Although the seasonal MBs are available only since 2009, this series still provides a good opportunity to analyze the control of the seasonal MBs on B_a . In order to understand the influence of the meteorological conditions on seasonal MBs and in turn on B_a , the annual and seasonal MBs were compared with the meteorological data (Table 2.3 and Fig. 2.7). In-situ temperature (T_{air}) records were available from the AWS-M, operating on the lateral moraine (Fig. 2.1; 4863 m a.s.l.) since 18 August 2009, while precipitation (P) data were taken from the long term time series precipitation record at Bhuntar meteorological station (~50 km south-west of Chhota Shigri Glacier) in this analysis. For a justified comparison, B_a , B_w and B_s were compared with annual, winter and summer T_{air} and P over the exact dates of field measurements.

The relationships between B_a and annual P or T_{air} were quite consistent. The positive B_a years (2009/10 and 2010/11) were associated with higher annual P (167 and 110 mm, respectively) and slightly lower annual mean T_{air} (0.1 and 0.2 °C) than the mean annual averages (1020 mm and -5.8 °C) between 2009 and 2013 whereas negative B_a years (2011/12 and 2012/13) were characterized by lower annual P (195 and 81 mm, respectively) and slightly higher annual mean

T_{air} (0.4°C in 2011/13) or similar T_{air} in 2012/13 than the mean annual averages over the 2009-2013 period. At seasonal scale, B_w did not show any relation with winter P although B_w were consistent with winter T_{air} . (Fig. 2.7). During the high B_w years (2009/10 = 1.38 m w.e. and 2011/12 = 1.27 m w.e.) the mean winter T_{air} were more negative (0.7°C and 0.5°C , respectively) while during the low B_w years (2010/11 = 1.06 and 2012/13 = 0.89 m w.e.) the mean winter T_{air} were less negative (0.4°C and 0.9°C , respectively) than the mean winter T_{air} of -9.4°C between 2009 and 2013. Contrary to B_w , B_s showed a good agreement with summer P : in 2009/10 and 2010/11 years the B_s were less negative (-1.05 m w.e. and -0.95 m w.e., respectively) with higher summer P (294 mm and 21 mm, respectively) whereas in 2011/12 and 2012/13 the B_s were highly negative (-1.72 and -1.63 m w.e.) with lower summer P (70 mm and 244 mm, respectively) than the mean annual summer precipitation of 472 mm between 2009 and 2013. B_s also showed quite consistent relationship with summer mean T_{air} except for the 2010/11 year when summer T_{air} was slightly higher (0.3°C) than the mean summer T_{air} (2.4°C) between 2009 and 2013 but B_s was least negative (-0.95 m w.e.).

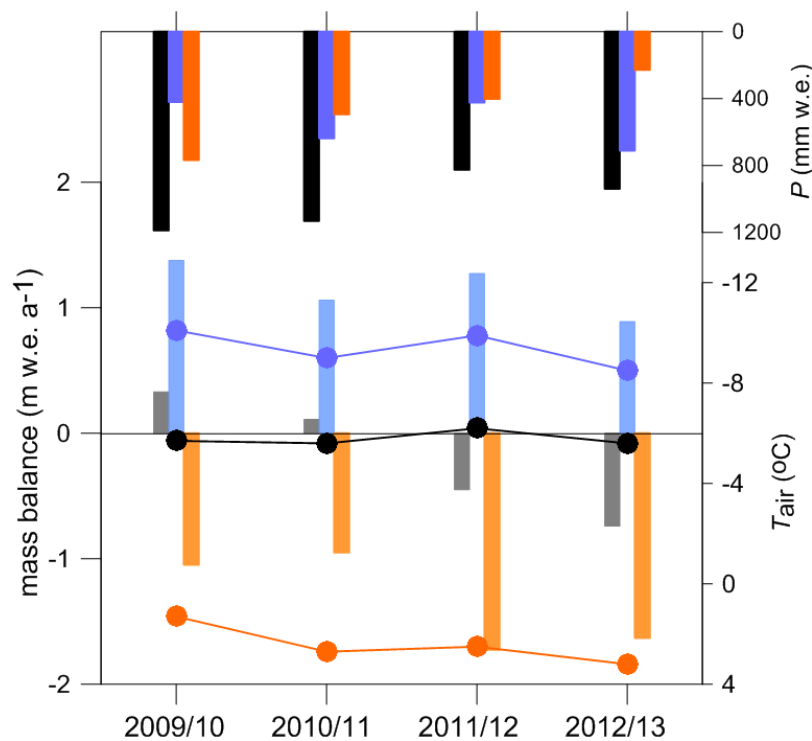


Figure 2.7. Annual, winter and summer mass balances are shown by light black, light blue and light orange histograms. The annual, winter and summer precipitations (temperatures) are shown by black, blue and orange histograms (dots). The mean temperatures are from AWS-M while the precipitations sums are from Bhuntar meteorological station.

Table 2.3. Annual and seasonal MBs, ELA, AAR and MB gradients db/dz (m w.e. (100m)⁻¹) for Chhota Shigri Glacier. The mean and standard deviation (STD) are also displayed for every variable. The uncertainty range for B_a is ± 0.40 m w.e.

	2002/03	2003/04	2004/05	2005/06	2006/07	2007/08	2008/09	2009/10	2010/11	2011/12	2012/13	mean	STD
B_a (m w.e.)	-1.42	-1.23	0.14	-1.41	-0.98	-0.93	0.13	0.33	0.11	-0.45	-0.74	-0.59	0.67
ELA (m a.s.l.)	5235	5105	4905	5230	5125	5110	4920	4925	4940	5025	5090	5055	121
AAR (%)	25	39	69	23	37	39	67	66	65	51	35	47	17
db/dz_{abl} (m w.e. (100m) ⁻¹)	0.62	0.74	0.62	0.61	0.68	0.68	0.52	0.54	0.73	0.81	0.76	0.66	0.09
db/dz_{debris} (m w.e. (100m) ⁻¹)	-3.3	-2.45	-1.66	-1.97	-2.49	-2.81	-0.28	-2.18	-2.68	-1.58	-2.3	-2.15	0.80
db/dz_{acc} (m w.e. (100m) ⁻¹)	0.29	0.18	0.25	-	-	-	0.3	-	0.1	-	-	0.22	0.08
B_w (m w.e.)	-	-	-	-	-	-	-	1.38	1.06	1.27	0.89	1.15	0.22
B_s (m w.e.)	-	-	-	-	-	-	-	-1.05	-0.95	-1.72	-1.63	-1.34	0.40
Meteorological conditions ^a													
Annual temperature (°C)	-	-	-	-	-	-	-	-5.7	-5.6	-6.2	-5.8	-5.8	0.3
Summer temperature (°C)	-	-	-	-	-	-	-	1.3	2.7	2.5	3.2	2.4	0.8
Winter temperature (°C)	-	-	-	-	-	-	-	-10.1	-9.0	-9.9	-8.5	-9.4	0.8
Annual precipitation (mm)	-	-	-	-	-	-	-	1187	1130	825	939	1020	168
Summer precipitation (mm)	-	-	-	-	-	-	-	766	493	402	228	472	225
Winter precipitation (mm)	-	-	-	-	-	-	-	421	637	423	711	548	149

^a = temperature at AWS-M (4863 m a.s.l.) and precipitation at Bhuntar meteorological station (1092 m a.s.l.); for the summer or winter means, the starting and ending dates have been chosen to match the field measurements of B_s and B_w , respectively

Even though the mean summer T_{air} at AWS-M (4863 m a.s.l.) was positive during all the years, daily mean T_{air} occasionally dropped below the freezing point (Fig. 2.2) during summer months, inducing a precipitation phase change from rain to snow. This was probably the case in 2009/10 and 2010/11 positive B_a years, the higher values of summer P than the mean summer P between 2009 and 2013 often provided snow falls on the glacier. These snowfalls changed the surface albedo of the glacier during the high melting period of summer season and consequently the melting was reduced leading to less negative B_s for these years. Given that in 2011/12 and 2012/13 negative B_a years, summer T_{air} were slightly higher and P were lower than the mean annual summer T_{air} and P between 2009 and 2013, the snowfalls were probably sporadic and not big enough to protect the glacier from higher melting. These years were thus characterized by highly negative B_s .

Certainly Chhota Shigri Glacier received maximum precipitation during the winter season (section 2.3), the present analysis suggests that the summer is the key season for this glacier. During summer months the ablation and accumulation coincide and the intensity of summer accumulation controls the B_a evolution through B_s . However we believe that the unclear link between B_w and winter P needs to be clarified and this analysis should be developed with long term comparison of seasonal MB with meteorological variables for a concrete conclusion.

2.6 Conclusion

A 4-year meteorological dataset (since 2009), one of the longest high altitude (4863 m a.s.l.) data sets in this part of the HKH, was used to describe the micrometeorology and to characterize the seasons on Chhota Shigri Glacier. A decrease in wind speed and a rapid increase of RH and LWI from the last week of May or the first week of June suggested the onset of the monsoon, whereas a sudden drop in RH and LWI and an increase in wind speed around 20 September, showed the sharp decay of the monsoon on Chhota Shigri Glacier. A warm summer-monsoon with high RH from June to September and a cold winter season, relatively less humid, from December to March were identified. Additionally a pre-monsoon from April to May and a post-monsoon from October to November were also demarcated.

The annual point MBs at the stakes just above the snout were reduced by 2–3 m w.e. a^{-1} despite their low altitude because of the thick debris cover and deep-narrow valley over this area. Yet the annual point mass balances were still very negative on the debris cover area with annual values varying between –2 and –5 m w.e. The mean vertical annual MB gradient between 4300 and 4400 were negative showing the increasing effect of thick debris with decrease in altitude. In the main ablation part of the glacier (between 4400 and 5200 m a.s.l.), the mean vertical annual MB gradient of 0.66 m w.e. $(100\text{m})^{-1}$ over 2002-2013 period was found similar to those observed in the Alps, Nepalese Himalaya or mid-latitude glaciers. The mean annual vertical MB gradient in accumulation area (between 5200 and 5500/5550 m a.s.l.) was 0.22 m w.e. $(100\text{m})^{-1}$. Chhota Shigri Glacier experienced mass wastage between 2002 and 2013 with a cumulative B_a of –6.45 m w.e. and a mean B_a of -0.59 ± 0.40 m w.e. a^{-1} . This mass wastage was in good agreement with

satellite derived geodetic B_a of -0.39 ± 0.18 m w.e. a^{-1} calculated by [Gardelle et al. \(2013\)](#) for this glacier between 1999 and 2011. ELA_0 for a zero B_a was calculated as 4950 m a.s.l. corresponding to an AAR_0 of 62% using the B_a , ELA and AAR data between 2002 and 2013 period.

The precipitation data at Chhota Shigri Glacier base camp suggested that this glacier received maximum accumulation during the winter months. Nevertheless one year precipitation record is quite short and the relative contribution of precipitation, which is likely to change from one year to another, should be considered cautiously. Besides, the analysis of B_a , B_w and B_s with meteorological variables suggested that during the summer months the ablation and accumulation coincided and the intensity of summer accumulation controls the B_a evolution through controlling the B_s . However we believe that the present analysis, conducted over 4 years only, needs to be supported with long term analyses between seasonal MBs and meteorological variables. The B_a series of Chhota Shigri Glacier since 2002 is one of the longest continuous B_a series in the HKH region. Like each glaciological B_a series, this series may also has some systematic biases; therefore, in the future, we will validate B_a derived from field observations with the decadal volume changes assessed by geodetic method.

CHAPTER 3

Dynamic behaviour of Chhota Shigri Glacier

After:

[Azam, M. F.](#), Wagnon, P., Ramanathan, A.L., Vincent, C., Sharma, P., Arnaud, Y., Linda, A., Pottakkal, J. G., Chevallier, P., Singh, V. B., and Berthier, E.: From balance to imbalance: a shift in the dynamic behaviour of Chhota Shigri Glacier (western Himalaya, India), *J. Glaciol.*, 58, 315–324, doi:10.3189/2012JoG11J123, 2012.

Executive summary

In Chapter 2 glacier-wide mass balances (B_a) of Chhota Shigri Glacier between 2002 and 2013 were discussed. Since 2002 this glacier showed a mean B_a of -0.59 m w.e. a^{-1} . In addition, [Berthier et al. \(2007\)](#) observed a geodetic B_a of -1.02 m w.e. a^{-1} , similarly in a revised study ([Vincent et al., 2013](#)) almost same geodetic B_a of -1.03 m w.e. a^{-1} was observed for this glacier during the period 1999 to 2004; therefore, the mass wastage period can be extended back to 1999. Auspiciously in October 2009, Chhota Shigri Glacier was surveyed for its ice thickness using Ground Penetrating Radar (GPR) at five different cross sections. The GPR measurements confirmed that the thicknesses obtained by gravimetric methods in 1989 ([Dobhal et al., 1995](#)) were almost two fold underestimated as already suspected by [Wagnon et al. \(2007\)](#). Moreover ice thicknesses together with surface ice velocity measurements of 2003/04 allowed assessing the kinematic ice flux at each cross section. On one hand, these kinematic fluxes corresponding to 2003/04 year were much larger than the average fluxes calculated from 2002-2010 surface mass balances (MB); on the other hand, they were close to the theoretical ice fluxes calculated from the surface MB assuming steady-state conditions of the glacier. The latter suggested that the dynamic behaviour of the glacier in 2003/04 was representative for steady-state conditions. Since the dynamic behaviour of the glacier is the result of its mean MB state over the last one or two preceding decades, this glacier has probably been close to equilibrium during the one or two decades before 2003/2004, and at that time, the ice fluxes had not adjusted to the previous year negative MBs. The almost similar ice velocities measured in 1987/88 ([Dobhal et al., 1995](#)) and in 2003/04 as well as the slow terminus retreat of 7 m a^{-1} between 1988 and 2010 also supported this conclusion suggesting that the dynamic behaviour did not change much between 1988 and 2010. Given that [Berthier et al. \(2007\)](#) and [Vincent et al. \(2013\)](#) observed a geodetic B_a of Chhota Shigri Glacier of approximately -1.02 and -1.03 m w.e. a^{-1} , respectively during the period 1999 to 2004, the glacier probably experienced zero to slightly positive B_a conditions between 1988 and the end of the 20th century. However a recent decreasing trend of surface velocities as well as a thinning between 2003/04 and 2009/10 showed that Chhota Shigri Glacier was progressively adjusting to the recent negative B_a but its dynamic behaviour was still far from B_a and climatic conditions between 2002 and 2010.

Abstract

Mass balance and dynamic behaviour of Chhota Shigri Glacier, western Himalaya, India, has been investigated between 2002 and 2010 and compared to data collected in 1987–1989. During the period 2002–2010, the glacier experienced a negative glacier-wide mass balance (B_a) of -0.67 ± 0.40 m w.e. a^{-1} . Between 2003 and 2010, elevation and ice-flow velocities slowly decreased in the ablation area, leading to a 24–37% reduction in ice fluxes, an expected response of the glacier dynamics to its recent negative B_a . The reduced ice fluxes are still far larger than the balance fluxes calculated from the 2002–2010 average surface MBs. Therefore, further slowdown, thinning and terminus retreat of Chhota Shigri Glacier are expected over the next few years. Conversely, the 2003/04 ice fluxes are in good agreement with ice fluxes calculated assuming that B_a is zero. Given the limited velocity change between 1987–1989 and 2003/04 and the small terminus change between 1988 and 2010, we suggest that the glacier has experienced a period of near-zero or slightly positive MB in the 1990s, before shifting to a strong imbalance in the 21st century. This result challenges the generally accepted idea that glaciers in the western Himalaya have been shrinking rapidly for the last few decades.

3.1 Introduction

Although Himalayan glaciers have important social and economic impacts (Barnett et al., 2005), they have not been monitored on a long-term basis and little is known about recent glacier trends or their contribution to local and regional water supplies. Because of this poor knowledge, the controversial statement that “the likelihood of them disappearing by the year 2035 or perhaps sooner is very high if the Earth keeps warming at the current rate” came into existence in the Intergovernmental Panel on Climate Change (IPCC) Fourth Assessment Report (Parry et al., 2007; Cogley et al., 2010). A generally negative B_a of mountain glaciers on a global level is clearly revealed by recent research (Cogley, 2009; Zemp et al., 2009), but the effect of global warming in the Himalaya is still under debate (Yadav et al., 2004; Roy and Balling, 2005). Though temperate glacial MB change is one of the best indicators of climate change (Oerlemans, 2001; Vincent et al., 2004; Ohmura et al., 2007), the paucity of B_a data in the Himalaya makes it difficult to obtain a coherent picture of regional climate-change impacts in this region. In the Indian Himalaya the first MB study started on Gara Glacier, Himachal Pradesh, in September 1974 (Raina et al., 1977) and ended in 1983 (Dobhal et al., 2008). According to Dyurgerov and Meier (2005), eight glaciers in the Indian Himalaya were surveyed for B_a for at least 1 year during the 1980s. Unfortunately each study was restricted to short periods, not more than one decade (Dobhal et al., 2008). Remote-sensing studies were also attempted in this part of the Himalaya, but these either deal with only surface area changes (e.g., Kulkarni et al., 2007; Bhambri et al., 2011) or cover short periods (Kulkarni, 1992; Berthier et al., 2007).

The present study is based on B_a and surface ice flow velocity measurements conducted on Chhota Shigri Glacier, Himachal Pradesh, between 2002 and 2010, and on a comparison with data collected in 1987–1989. In the Hindu-Kush Karakoram Himalayan range, this is one of the longest continuous field MB datasets. In October 2009, a ground-penetrating radar (GPR) survey was also conducted to measure ice thickness. Eight years of B_a measurements, surface ice velocities and ice thickness data provide an opportunity to study the behaviour of this glacier. The main objectives of this paper are (1) to present the recent B_a of Chhota Shigri Glacier, (2) to determine the ice fluxes at five cross sections from thickness and ice velocities and (3) to compare these data with the ice fluxes inferred from cumulative surface MB upstream of the same cross sections. These results give insights into the B_a trend of the glacier over the last two to three decades, and allow us to assess whether it is in equilibrium with the climate of the 21st century.

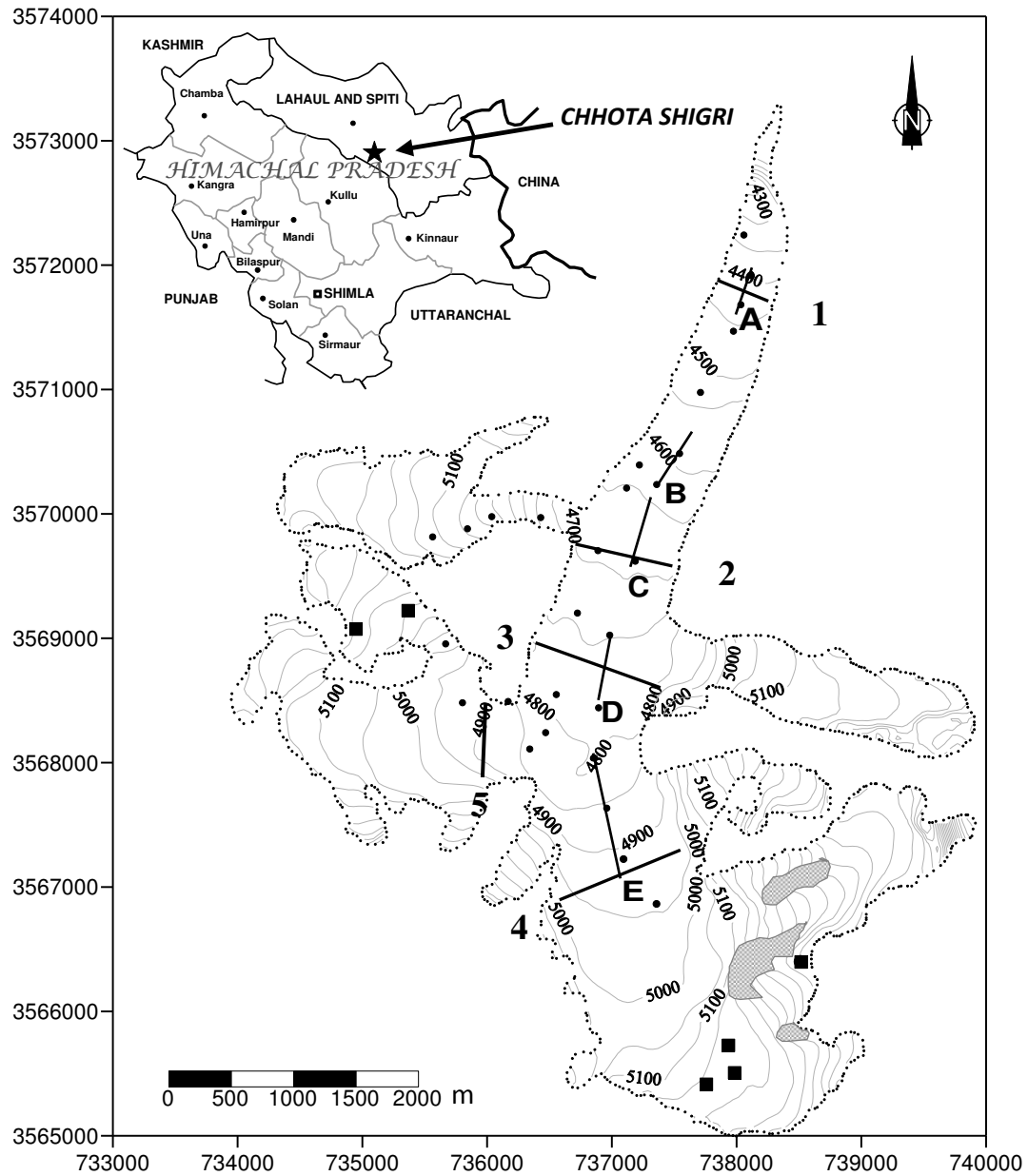


Figure 3.1. Map of Chhota Shigri Glacier with the measured transverse cross-sections (lines 1-5), the ablation stakes (dots) and the accumulation sites (squares). Also shown are longitudinal sections (lines A-E) used to calculate thickness and ice velocity variations (see section 3.4.2). The map (contour lines, glacier delineation) was constructed using a stereoscopic pair of SPOT5 (Système Pour l’Observation de la Terre) images acquired 12 and 13 November 2004 and 21 September 2005 (Wagnon et al., 2007). The map coordinates are in the UTM43 (north) World Geodetic System 1984 (WGS84) reference system.

3.2 Site description and methodology

3.2.1 Site description

Chhota Shigri Glacier (32.2° N and 77.5° E) is a valley-type glacier located in the Chandra-Bhaga River basin of Lahaul and Spiti Valley, Pir Panjal Range, western Himalaya. This glacier extends from 6263 m to ~4050 m a.s.l., is ~9 km long and covers 15.7 km² of area. Its snout is easy to locate from one year to the next because it is well defined, lying in a narrow valley and giving birth to a single proglacial stream. The main orientation of this glacier is north but its tributaries which have a variety of orientations (Fig. 3.1). The lower ablation area (<4500 m a.s.l.) is partly covered by debris representing ~3.4% of the total surface area. This glacier is located in the monsoon-arid transition zone and is influenced by two atmospheric circulation systems: the Indian summer monsoon during summer (July–September) and the northern-hemisphere mid-latitude westerlies during winter (January–April) (Singh et al., 1997; Bookhagen and Burbank, 2006; Gardelle et al., 2011).

3.2.2 Mass balance

The first series of MB measurements on Chhota Shigri Glacier was performed between 1987 and 1989 (Nijampurkar and Rao, 1992; Dobhal et al., 1995; Kumar, 1999). The bedrock topography and surface ice velocity were also surveyed over the same period by gravimetric and stake displacement methods, respectively (Dobhal et al., 1995; Kumar, 1999). The MB observations were reinitiated in 2002. Since that year, B_a measurements have been carried out continuously on Chhota Shigri Glacier at the end of September or the beginning of October using the direct glaciological method (Paterson, 1994). Ablation was measured through a network of ~22 stakes distributed between 4300 and 5000 m a.s.l. (Fig. 3.1), whereas in the accumulation area the net annual accumulation was obtained at six sites (by drilling cores or pits) between 5100 and 5550 m a.s.l. (Wagnon et al., 2007). In the accumulation area, the number of sampled sites is limited due to difficulty of access and the high elevation. B_a is calculated according to:

$$B_a = \sum b_i (s_i / S) \quad (3.1)$$

where b_i is the MB of the altitudinal range i (m w.e. a⁻¹), of map area s_i , and S is the total glacier area. For each altitudinal range, b_i is obtained from the corresponding stake readings or net accumulation measurements.

3.2.3 Surface velocity

Annual surface ice velocities were measured at the end of each ablation season (September–October) by determining the annual stake displacements (~22 stakes) using a differential GPS (DGPS). These geodetic measurements were performed in kinematic mode relative to two fixed

reference points outside the glacier on firm rocks. The accuracy of x (easting), y (northing) and z (elevation) at each stake position is estimated at ± 0.2 m depending mainly on the size of the hole in which the stake was set up. Thus the surface ice velocities measured from stake displacements have an accuracy of ± 0.3 m a⁻¹.

3.2.4 Ice thickness

GPR measurements were conducted in October 2009 to determine ice thickness on five transverse cross sections (Fig. 3.1) between 4400 and 4900 m a.s.l. A pulse radar system (Icefield Instruments, Canada) based on the Narod transmitter (Narod and Clarke, 1994) with separate transmitter and receiver, was used in this study with a frequency centred near 4.2 MHz and an antenna length of 10 m. Transmitter and receiver were towed in snow sledges along the transverse profile, separated by a fixed distance of 20 m, and used to record measurements every 10 m. The positions of the receiver and the transmitter are known through DGPS measurements, within an accuracy of ± 0.1 m. The speed of electromagnetic wave propagation in ice has been assumed to be 167 m μs^{-1} (Hubbard and Glasser, 2005). The field measurements were performed in such a way as to obtain reflections from the glacier bed located more or less in the vertical plane with the measurement points at the glacier surface, allowing the glacier bed to be determined in two dimensions. The bedrock surface was constructed as an envelope of all ellipse functions, which give all the possible reflection positions between sending and receiving antennas. Ice thickness was measured along four transverse profiles (profiles 1–4) on the main glacier trunk and one (profile 5) on a western tributary (Fig. 3.1).

3.3 Data analysis and results

3.3.1 Glacier-wide mass balance and mass balance profile

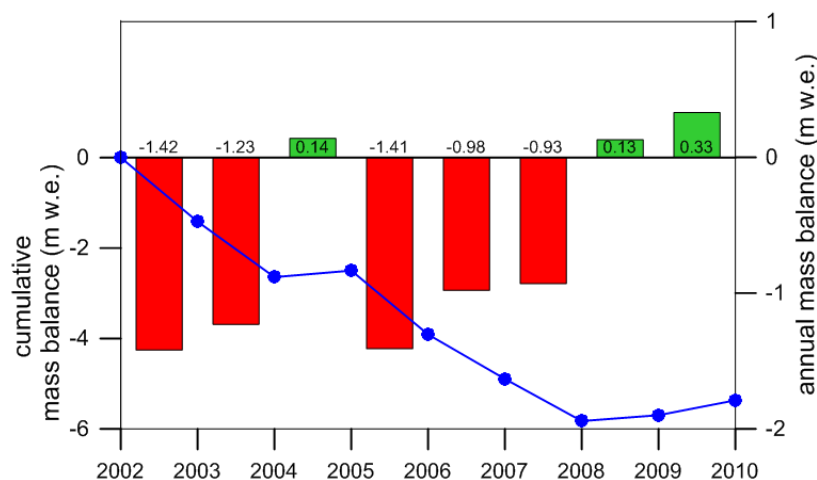


Figure 3.2. Cumulative (blue line) and annual glacier-wide mass balances (red (-) and green (+) histograms) of Chhota Shigri Glacier between 2002 and 2010.

B_a and cumulative B_a of Chhota Shigri Glacier between 2002 and 2010 are plotted in Fig. 3.2. B_a was negative except for three years (2004/05, 2008/09 and 2009/10). It varies from a minimum value of -1.42 m w.e. in 2002/03 to a maximum of $+0.33$ m w.e. in 2009/10. The cumulative B_a of Chhota Shigri is -5.37 m w.e. between 2002 and 2010, while the B_a averaged over the same period is -0.67 m w.e. a^{-1} .

The quantitative uncertainty associated with the glaciological B_a requires a distinction between the accumulation zone and the ablation zone. In the accumulation zone, the surface MB measurements were obtained from shallow boreholes (auger). Therefore, they are based on core length and density determination. In the ablation zone, the measurements have been carried out from ablation stakes. The overall error (standard deviation) on point measurements are estimated at 0.30 m w.e. and 0.15 m w.e. in the accumulation zone and in the ablation zone, respectively. The overall error comes from a variance analysis (Thibert et al., 2008) applied to all types of errors (ice/snow density, core length, stake height determination, liquid-water content of the snow, snow height). Although conducted on a glacier in the Alps, the analysis of Thibert et al. (2008) can be generalized to other glaciers because it is based on measurement errors which are similar on every glacier when using the glaciological method. However, only 6 sites are sampled in the accumulation zone (11.6 km²), and 22 sites in the ablation zone (4.1 km²). The uncaptured spatial variability of surface MB may cause systematic errors on B_a . In the accumulation zone, the spatial variability remains unknown and is probably very high as observed for other glaciers (e.g., Machguth et al., 2006). In the ablation zone, stakes set up at the same altitude show similar values except on the terminal tongue which is debris covered. Consequently, the overall uncertainties on MB profile have been assessed at 0.5 m w.e. in the accumulation zone, 0.25 m w.e. in the white ablation zone and 0.5 m w.e. in the debris covered area of the glacier. Moreover, the surface area estimation also causes systematic error. The uncertainty on the surface area calculated for each altitudinal range is estimated at 5%. Combining these errors at different altitudinal ranges using Eq. 1, the uncertainty on the B_a is ± 0.40 m w.e. a^{-1} . As revealed by other studies (e.g., Vincent, 2002; Thibert et al., 2008; Huss et al., 2009), this estimation confirms that the glaciological method needs to be calibrated by a volumetric method over a long period of monitoring (*i.e.* >5 years) in order to limit the systematic errors and to improve the accuracy of absolute values of B_a . Note that the uncertainty of relative changes in B_a from year to year is smaller than those inherent in B_a , given that the influence of systematic errors can be reduced.

We also calculated the MB profile between 2002 and 2010 (Fig. 3.3). For each altitudinal range, we computed the average of all available measurements. Figure 3.3 shows that melting in the lowest part of the ablation area (<4400 m a.s.l.) is reduced by -1 m w.e. a^{-1} irrespective of its altitude. This is due to the debris cover (approximately 5–10 cm thick debris mixed with isolated rocks) which reduces the melting in this region (Mattson et al., 1993; Wagnon et al., 2007). Moreover the lower part of Chhota Shigri Glacier flows in a north–south oriented deep and

narrow valley (Fig. 3.1), causing the glacier tongue to receive less solar radiation due to the shading effect of the steep valley slopes.

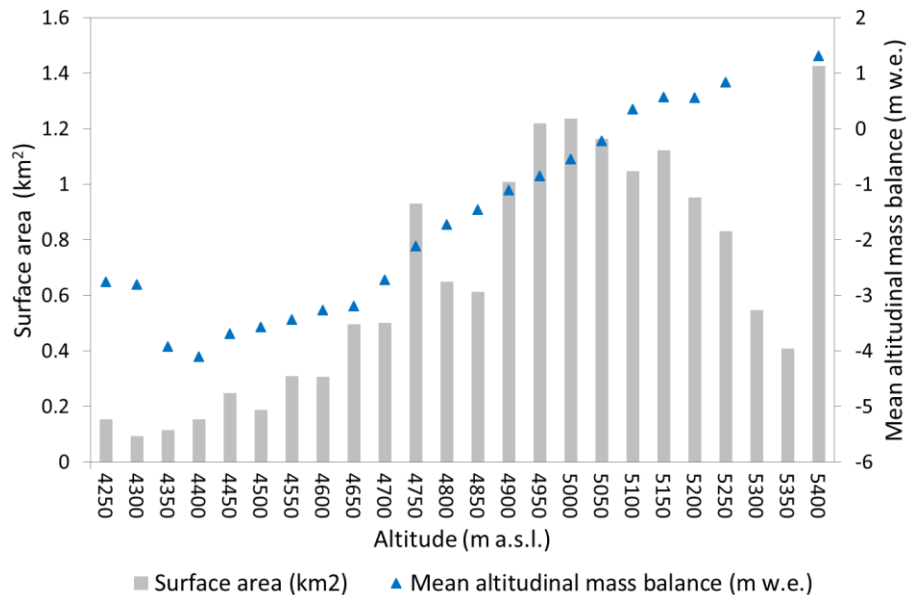


Figure 3.3. The 2002–10 average MB profile and hypsometry of Chhota Shigri Glacier. Altitudinal ranges are of 50m (e.g., 4400 stands for the range 4400–4450 m), except for 4250 and 5400 which stand for 4050–4300 and 5400–6250m respectively.

3.3.2 Ice thicknesses and cross-sectional areas

Thanks to clear reflections, the ice/bedrock interface was generally easy to determine in all profiles. Figure 3.4 provides an example of the radargram obtained at cross section 2. A radar wave velocity of $167 \text{ m } \mu\text{s}^{-1}$ was used to calculate ice thickness at all the profiles. The cross sections obtained from GPR measurements reveal a valley shape with maximum ice thickness greater than 250 m (Fig. 3.5). The centre line ice thickness increases from 124 m at 4400 m a.s.l. (cross section 1 in Fig. 3.1) to 270 m at 4900 m a.s.l. (cross section 4). This confirms that the thicknesses obtained by gravimetric methods in 1989 (Dobhal et al., 1995), twice as low as the present results, were underestimated as proposed by Wagnon et al. (2007). The cross-sectional areas are given in Table 3.1. The accuracy of the calculated ice thickness is determined, in part, by the accuracy of the measurement of the time delays and the antenna spacing. Additional errors may arise because the smooth envelope of the reflection ellipses is only a minimal profile for a deep valley-shape bed topography, with the result that the ellipse equation will be governed by arrivals from reflectors located toward the side and thus not directly beneath the points of observation. Further errors may be introduced by assuming that all reflection points lie in the plane of the profile rather than on an ellipsoid. No errors associated with radar wave velocity variations between snow and

ice have been accounted for because all cross sections were surveyed in the ablation zone or slightly above (with the firn/ice transition depth at the surface or <2 m deep). Hence, the radar wave velocity for ice ($167 \text{ m } \mu\text{s}^{-1}$) was used to calculate all ice depths. The estimated overall uncertainty in ice thickness is $\pm 15 \text{ m}$. Given that the uncertainty in ice surface coordinates is low ($\pm 0.1 \text{ m}$), the uncertainty in cross-sectional areas mainly arises from the uncertainty in ice thickness. The uncertainties in cross-sectional areas are 16%, 9%, 10%, 10% and 15% for cross sections 1, 2, 3, 4 and 5 respectively.

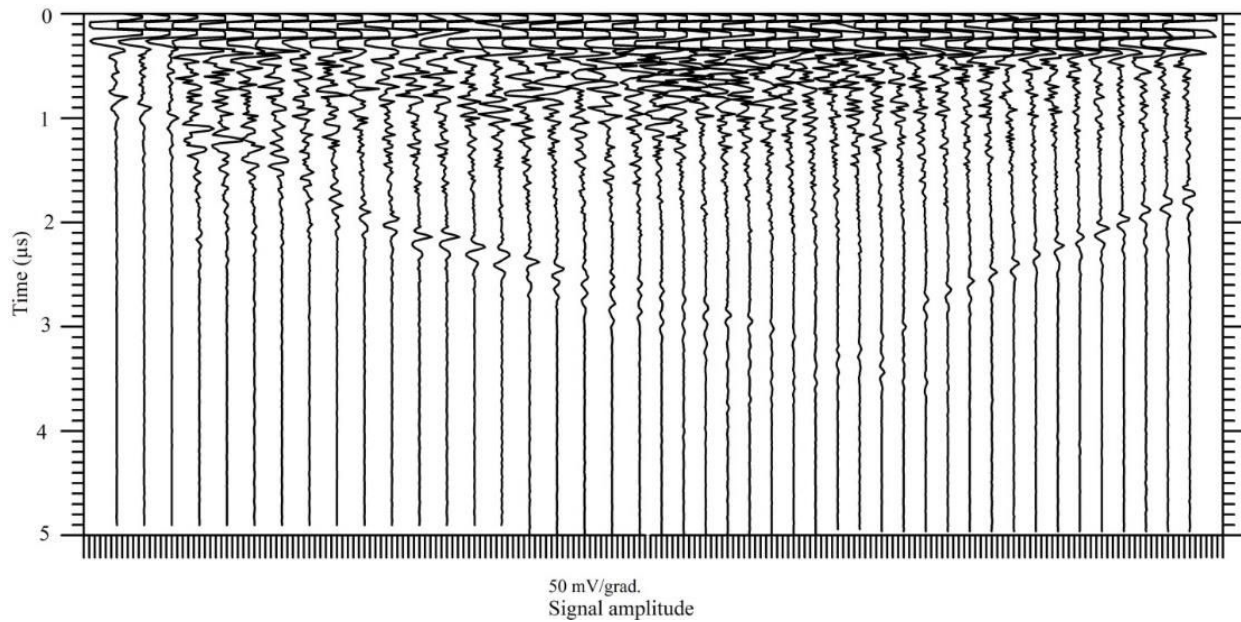


Figure 3.4. Radargram of cross section 2: radar signals plotted side by side from west to east in their true spatial relationship to each other (interval between each signal of 10 m). The x-axis gives the amplitude of each signal (50 mV per graduation); the y-axis is the double-time interval (μs).

Table 3.1. Calculated ice flux, mean surface ice velocity and maximum ice depth at each cross section. The mean surface horizontal ice velocities are from DGPS measurements performed in 2003/04. The satellite-derived mean ice velocities are from the correlation of satellite images acquired on 13 November 2004 and 21 September 2005 (NA: Not available).

Cross section	Altitude m a.s.l.	Cross-sectional area 10^4 m^2	Mean surface ice velocity from field data* m a^{-1}	Satellite-derived mean surface velocity m a^{-1}	Ice flux $10^6 \text{ m}^3 \text{ a}^{-1}$	Max. depth at centre of cross section m
1	4400	4.23 ± 0.68	20.3	NA	0.78 ± 0.21	124
2	4650	12.14 ± 1.09	31.2	30.7	3.41 ± 0.69	240
3	4750	16.49 ± 1.65	29.2	29.2	4.35 ± 0.92	245
4	4900	15.53 ± 1.55	30.1	NA	4.20 ± 0.89	270
5	4850	6.01 ± 0.90	27.1	25.5	1.47 ± 0.38	175

*Centre line velocity X 0.79

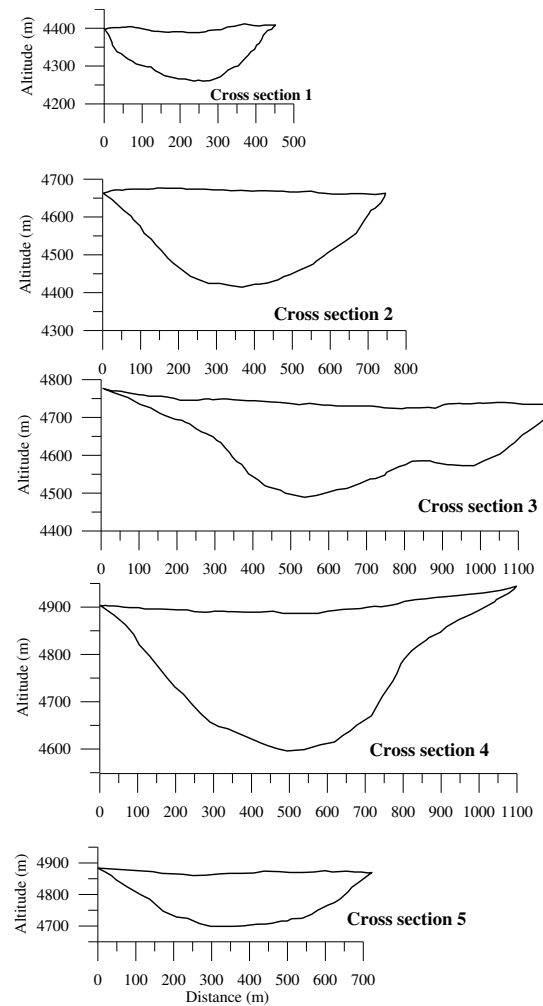


Figure 3.5. Ice depth and surface topography of cross-sections 1-5. The horizontal and vertical scales are the same for all cross-sections. All cross sections are oriented from west to east except cross section 5 which is north-south oriented.

3.3.3 Ice velocity

Annual surface ice velocities were also measured between 2002 and 2010. However, some data gaps exist due to discontinuous DGPS signal, or loss of stakes. The 2003/04 ice velocities were used in this study because they provided the most complete dataset (Fig. 3.6). The centre line horizontal ice velocities at each cross section were calculated by linear interpolation along the centre line between the velocities measured immediately up- and downstream of the cross section (ablation stakes visible in Fig. 3.1). Mean cross-sectional velocities are required to compute the ice fluxes (see section 3.3.4). A map of the surface ice velocity field was derived by correlating SPOT5 images acquired on 13 November 2004 and 21 September 2005 (Berthier et al., 2005). Comparison of the satellite-derived velocities with 16 nearly simultaneous DGPS velocity measurements

shows a mean difference of 0.2 m a^{-1} and a standard deviation of 1.6 m a^{-1} . The ratio between the centre-line horizontal velocity and the mean surface velocity (all extracted from the satellite-derived 2004/05 velocity field) was found to be 0.80 and 0.78 for cross sections 2 and 3 respectively. Reliable velocity measurements could not be made with SPOT5 imagery for other cross sections. Using the mean value of 0.79, the mean horizontal velocity was calculated from the centre-line velocity for each gate cross section (Table 3.1).

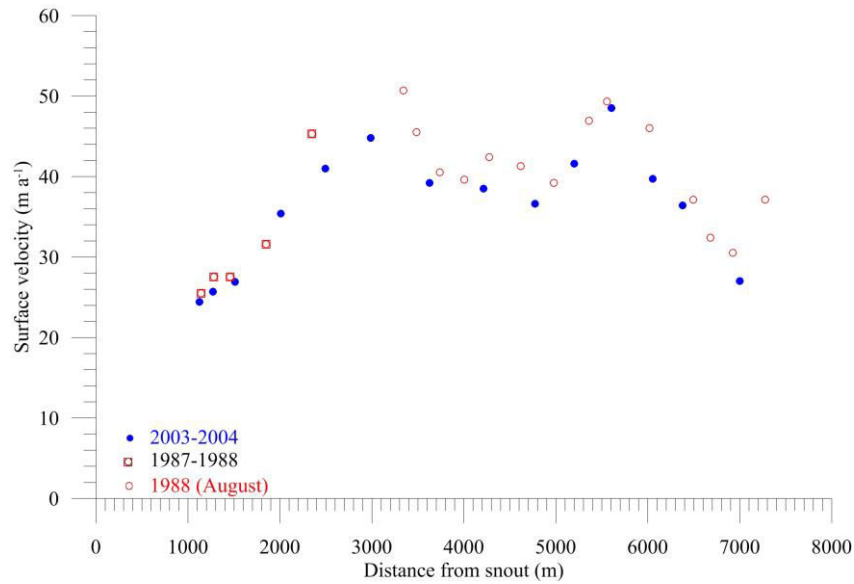


Figure 3.6. Measured ice velocities plotted as a function of the distance from the 2010 terminus position. Measurements were collected along the central flow line.

3.3.4 Ice fluxes from kinematic method

The ice flux Q ($\text{m}^3 \text{ ice a}^{-1}$) through each cross section was calculated using the cross-sectional area S_c (m^2) and depth-averaged horizontal ice velocity U (m a^{-1}).

$$Q = U S_c \quad (3.2)$$

The depth-averaged horizontal ice velocity was derived from the mean surface ice velocity calculated in section 3.3.3. Nye (1965) gives ratios of depth-averaged horizontal ice velocity to mean surface ice velocity varying from 0.8 (no sliding) to 1 (maximum sliding). Here we assume a mean basal sliding, with a constant ratio of 0.9. The calculated ice fluxes and maximum depth at each cross section are given in Table 3.1. The flux through cross section 3 at 4750 m a.s.l. is higher than the flux through cross section 4 at 4900 m a.s.l. This is due to the ice influx from the western part of the glacier (flux through cross section 5) which contributes to cross section 3 and not to cross section 4 (Fig. 3.1).

The largest uncertainty in the depth-averaged horizontal ice velocity results from the ratio between the depth velocity and the surface flow velocity. The estimated factor 0.9 and unknown variations in the basal sliding lead to an uncertainty of roughly $\pm 10\%$ in the calculated flux, which lies within the range of uncertainty of the other variables as discussed by Huss et al. (2007). Consequently, we can infer that depth-averaged horizontal ice velocity at each cross section is known with an accuracy of 1.0–3.0 m a⁻¹ depending on the cross sections. Combining these errors in the cross-sectional area and mean velocity, the uncertainties in the ice fluxes are 0.21, 0.69, 0.92, 0.89 and 0.38 $\times 10^6$ m³ a⁻¹ for cross sections 1, 2, 3, 4 and 5 respectively. We have considered the errors to be systematic, so these uncertainties are probably overestimated.

3.3.5 Ice fluxes obtained from surface mass balance

We also calculated ice fluxes using annual surface MB measured during 2002–10. Although dynamic changes are neglected here, this method allows us to estimate the ice fluxes for each section from MB data according to:

$$Q = \frac{1}{0.9} \sum_z^{z_{\max}} b_i s_i \quad (3.3)$$

where Q is the ice flux (converted into m³ ice a⁻¹ using an ice density of 900 kg m⁻³, hence the factor 1/0.9) at a given elevation, z , and b_i is the annual MB of the altitudinal range i of map area s_i . The altitudinal ranges taken into account in the calculation are located between z and the highest range of the glacier z_{\max} (highest altitude of the glacier area contributing ice to the cross section). We assume that at each point of the glacier above z the surface elevation has remained unchanged from one year to the next.

The ice fluxes calculated from annual MB data at the five cross sections each year are given in Table 3.2, while the average ice fluxes for the 8 years are given in Fig. 3.7. The uncertainties in ice fluxes resulting from surface MB are directly derived from the MB uncertainties (see section 3.3.1) applied to areas contributing to each cross section.

3.4 Discussion

The first and main objective of this section is to discuss the MB change of Chhota Shigri Glacier over the last two to three decades using not only direct B_a observations (over the last 8 years) but also ice-flux analysis. The second goal is to give insights into the specific dynamics and the future retreat of this glacier that can be expected in relation to its recent B_a .

Table 3.2. Ice fluxes (in $10^6 \text{ m}^3 \text{ ice a}^{-1}$), inferred at each cross section from annual MB data.

Cross section	Altitude m a.s.l.	Hydrological year (Oct-Sep)								Mean (2002-2010)
		2002/03	2003/04	2004/05	2005/06	2006/07	2007/08	2008/09	2009/10	
Snout	4050	-22.26	-19.28	2.27	-22.21	-15.59	-14.65	2.06	5.24	-10.55
1	4400	-22.83	-19.55	3.78	-22.65	-15.43	-14.82	3.19	6.84	-10.18
2	4670	-14.31	-11.49	6.57	-14.35	-8.63	-8.21	6.03	8.70	-4.46
3	4735	-9.88	-7.68	6.89	-10.04	-5.45	-5.46	6.16	8.43	-2.13
4	4900	-1.41	-1.36	4.84	-2.30	0.05	-0.16	4.14	5.72	1.19
5	4870	-1.61	-1.30	2.08	-2.19	-0.57	-0.82	1.86	2.80	0.03

Table 3.3. Ice fluxes (in $10^6 \text{ m}^3 \text{ ice a}^{-1}$), obtained at every cross section, using steady-state MB assumption for every surveyed year.

Cross section	Altitude m a.s.l.	Hydrological year (Oct-Sep)								Mean (2002-2010)	Standard deviation
		2002/03	2003/04	2004/05	2005/06	2006/07	2007/08	2008/09	2009/10		
Snout	4050	0.00	0.00	0.00	0.00	0.00	0.00	0.00	0.00	0.00	0
1	4400	1.25	1.32	1.33	1.38	1.43	1.03	0.96	1.17	1.23	0.17
2	4670	5.07	5.30	4.59	4.99	4.94	4.55	4.24	4.14	4.73	0.41
3	4735	6.04	6.11	5.27	5.85	5.70	5.02	4.69	4.68	5.42	0.58
4	4900	5.78	4.87	4.11	4.88	5.09	4.58	3.48	4.02	4.60	0.72
5	4870	2.76	2.48	1.63	2.17	2.49	2.06	1.46	1.77	2.10	0.46

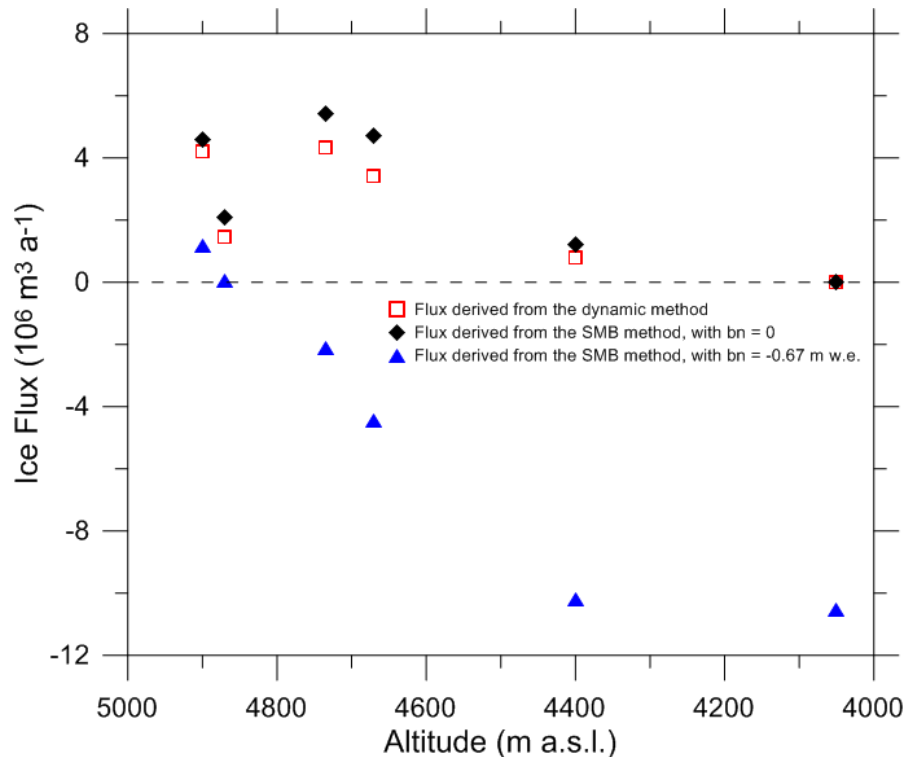


Figure 3.7. Ice fluxes at every cross section derived (i) from 2003/04 ice velocities and section areas (red open squares) and (ii) from MB method for a glacier-wide MB = 0 m w.e. (black squares) or a glacier-wide MB = -0.67 m w.e. (blue triangles).

3.4.1 Null to slightly positive mass balance during the 1990s inferred from ice fluxes

The ice fluxes obtained from the kinematic method using ice thickness and 2003/04 ice velocities are much higher than the average fluxes derived from the 2002-2010 surface MBs, the latter being often negative (Table 3.2). Thus in this section, to assess the mean state of the glacier corresponding to the ice fluxes obtained by the kinematic method, we compare these measured ice fluxes to theoretical ice fluxes calculated from surface MB assuming the glacier to be in steady-state. The B_a obtained by the glaciological method is -0.67 m w.e. a^{-1} over the 2002-2010 period. Consequently, the MB needs to be increased by 0.67 m w.e. a^{-1} , for the glacier to be in steady-state. For each year (over 2002-2010 period), we calculated the theoretical ice flux from MB at each cross section assuming the glacier was in steady-state. For this purpose, every year, a theoretical MB at each elevation has been calculated by subtracting the overall B_a of the same year. For instance, year 2002/03 was characterized by a negative B_a of -1.40 m w.e. so we calculated a new MB profile by adding $+1.40$ m w.e. to the MB at each elevation. In contrast, year 2009/10 was characterized by a positive B_a of $+0.33$ m w.e. so we calculated a new MB profile by subtracting 0.33 m w.e. from the MB at each elevation. The resulting ice fluxes are reported in Table 3.3, together with the mean ice flux at each cross section over the 8 years and the corresponding standard deviations.

These ice fluxes are close to the 2003/04 ice fluxes obtained by the kinematic method (Fig. 3.7) indicating that the dynamic behaviour of the glacier in 2003/04 is representative for steady-state conditions. This suggests that in the years preceding 2003/04, B_a of this glacier has probably been close to zero and that, in 2003/2004, the ice fluxes had not adjusted to previous year negative B_a .

This result is also supported by other observations. First, the ice velocities measured in 1987/88 (Dobhal et al., 1995) are very close to the 2003/04 values (Fig. 3.6) suggesting that the dynamic behaviour of this glacier did not change a lot between 1988 and 2004. Second, the terminus fluctuation measured between 1988 and 2010 show a moderate retreat equal to 155 m, equivalent to only 7 m a⁻¹, in agreement with conditions not far from steady-state. Given that Berthier et al. (2007) observed a geodetic B_a of Chhota Shigri Glacier of approximately -1 m w.e. a⁻¹ during the period 1999 to 2004, the glacier is likely to have experienced a null to slightly positive B_a between 1988 and the end of the 20th century.

3.4.2 Glacier dynamics starting to adjust to 21st century negative B_a

In theory, the response of ice fluxes to surface B_a is immediate (Cuffey and Paterson, 2010, p. 468) but observations show a 1-5 year delay (Vincent et al., 2000; Span and Kuhn, 2003; Vincent et al., 2009). For instance, Span and Kuhn (2003) found synchronous decrease in ice velocity between eight glaciers in the Alps, which are driven by the same MB changes (Vincent et al., 2005). Consequently, the recent dynamic behaviour of Chhota Shigri Glacier should be affected by the negative B_a since 1999. However, the stake network on Chhota Shigri Glacier, originally designed for B_a measurements, is not best suited to accurately compare either the ice velocities or the thickness variations because the measurements have not been performed exactly at the same location every year and they are mainly restricted to the ablation area.

In spite of the above limitation, an attempt has been made to compare ice velocities and elevations from the available stake network. For this purpose, stakes measured at the beginning and at the end of the series have been selected on five short longitudinal cross sections (A, B, C, D and E in Fig. 3.1) along the centre line of the glacier where the network is most dense. The elevations in 2003 and 2010 and the ice velocities in 2003/04 and 2009/10 have been reported on these longitudinal cross sections to deduce thickness and velocity changes in the ablation area (Fig. 3.8, Table 3.4). Although the accuracy of the results is affected by the distance between the point measurements, we can conclude that the part of the glacier below 4750 m a.s.l. is in strong recession. First, the thickness has decreased annually by 0.7 to 1.1 m a⁻¹ over the last seven years. Second, the ice velocities have been reduced by ~7 m a⁻¹ between 2003 and 2010 resulting in a 24 to 37% decrease in the ice fluxes since 2003.

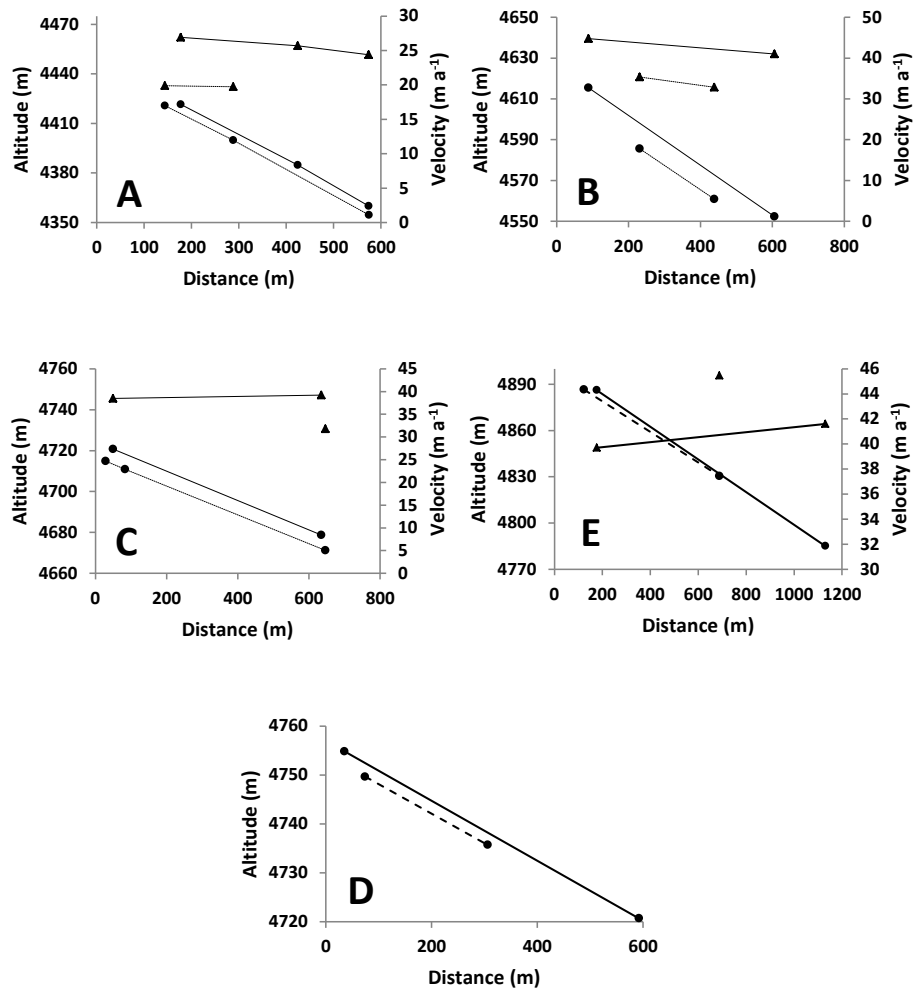


Figure 3.8. Elevation (dots) and surface ice velocity (triangles) between 2003 (continuous lines) and 2010 (dashed lines) along the longitudinal sections A, B, C, D and E shown in Fig. 3.1.

Table 3.4. Thickness and surface velocity changes between 2003 and 2010 on 5 longitudinal cross sections (NA: Not available).

Long. section	Elevation change m	Velocity change m a ⁻¹
A	-5.3	-6.6
B	-8.6	-8.8
C	-7.5	-7.4
D	-2.8	NA
E	-5.6	+4.8

Despite an improvable monitoring network, it may be surmised that the ice fluxes have been affected by the negative B_a during (at least) between 2002 and 2010, and the dynamics of this glacier are progressively adjusting to the negative B_a . Consequently, we expect an accelerated terminus retreat in the coming years. If the B_a remained equal to its 2002-2010 average value in the future, the terminus would retreat by 5.6 km to reach an altitude of 4870 m a.s.l. (altitude where the ice flux is equal to zero) (Table 3.2).

3.5 Conclusion

Chhota Shigri Glacier experienced negative B_a over the 2002-2010 period. B_a of the glacier is estimated at -0.67 m w.e. a^{-1} between 2002 and 2010, revealing strong unsteady-state conditions over this period. Conversely, ice fluxes calculated through 5 transverse cross sections by the kinematic method correspond to near steady-state conditions before 2004. Given that ice velocities measured in 2003/04 are close to those measured in 1988, and that terminus has retreated only 155 m between 1988 and 2010, it seems that the dynamic change was moderate between 1988 and 2004. Therefore, considering that [Berthier et al. \(2007\)](#) observed a negative geodetic B_a of about -1 m w.e. a^{-1} between 1999 and 2004 using satellite images, our analysis suggests that the glacier experienced a period of slightly positive or close to zero B_a at the end of the 20th century, before starting to shrink. As Chhota Shigri Glacier seems to be representative of other glaciers in the Pir Panjal Range ([Berthier et al., 2007](#)), it is possible that many western Himalayan glaciers of northern India experienced growth during the last 10-12 years of the 20th century, before starting to shrink at the beginning of the 21st century.

Since 2003, ice velocities and elevation are decreasing in the ablation area. Our data suggest that the ice fluxes have diminished by 24 to 37% below 4750 m a.s.l. between 2003 and 2010. Even if we account for a 37% decrease in ice fluxes calculated from 2003/04 ice velocities to obtain present ice fluxes values, it remains a very large imbalance with ice fluxes coming from B_a between 2002 and 2010. Thus the present dynamics (thickness and ice velocities) of this glacier are far from B_a and climate conditions between 2002 and 2010, even if it is progressively adjusting. Therefore the glacier is likely to undergo accelerated retreat in the near future.

This glacier is almost free of debris and thus its B_a variations are closely related to climate changes. This glacier has the longest running series of B_a measurements in the Hindu-Kush Karakoram Himalayan range. In the future, the dynamic behaviour and B_a need more detailed investigations, although such field measurements are demanding due to the very high altitude. In order to investigate the annual thickness and the ice velocity changes, we recommend performing elevation and ice velocity measurements on ~ 12 cross sections including some in the accumulation zone. We also recommend measuring the ice velocities from a dense network of stakes to be set up on longitudinal center lines in order to compare the annual velocity changes at the same points. Finally, we recommend calibrating and checking the B_a field measurements from a volumetric method (from photogrammetry or remote sensing techniques).

Acknowledgements

This work has been supported by the IFCPAR/CEFIPRA under the project n°3900-W1 and by the French Service d'Observation GLACIOCLIM as well as the Department of Science and Technology (DST), and Space Application Centre, Government of India. The French National Research Agency through ANR-09-CEP-005-01/PAPRIKA provided DGPS devices to perform field measurements. We thank J. E. Sicart, J. P. Chazarin, our field assistant Mr. B. B. Adhikari and the porters who have been involved in successive field trips, sometimes in harsh conditions. We would also like to thank Dr. D. P. Dobhal for his kind cooperation in answering our queries regarding the earlier research on Chhota Shigri Glacier. E. Berthier acknowledges support from the French Space Agency (CNES) through the TOSCA and ISIS proposal #0507/786 and from the Programme National de Télédétection Spatiale (PNTS). We thank Jawaharlal Nehru University for providing all the facilities to carry out this work. Prof. K. A. Brugger and another anonymous reviewer have provided constructive suggestions and comments which helped to significantly improve the manuscript. They are greatly acknowledged here.

CHAPTER 4

Mass balance reconstruction of Chhota Shigri Glacier since 1969

After:

[Azam, M. F.](#), Wagnon, P., Vincent, C., Ramanathan, AL., Linda, A., and Singh, V. B.: Reconstruction of the annual mass balance of Chhota Shigri Glacier (Western Himalaya, India) since 1969, *Ann. Glaciol.*, 55, 69–80, doi:10.3189/2014AoG66A104, 2014a.

Executive summary

Ice flux analysis in chapter 3 suggested that Chhota Shigri Glacier has experienced a period of steady-state or slightly positive mass balance in the 1990s, before shifting to a strong imbalance in the 21st century. [Vincent et al. \(2013\)](#) calculated the volumetric change of this glacier between 1988 and 2010 using in-situ geodetic measurements. Their results revealed a moderate mass loss over this 2-decade period (-3.8 ± 2.0 m w.e. corresponding to -0.17 ± 0.09 m w.e. a⁻¹). Combining the latter result with field measurements and digital elevation models differencing from satellite images, they deduced a slightly positive or steady-state mass balance between 1988 and 1999 ($+1.0 \pm 2.7$ m w.e. corresponding to $+0.09 \pm 0.24$ m w.e. a⁻¹) and confirmed the chapter 2 results. Given that [Vincent et al. \(2013\)](#) used field geodetic measurements conducted in 1988 and 2010, they could not determine the exact starting and ending years of steady-state or slightly positive mass balance conditions on Chhota Shigri Glacier. Besides, the climatic drivers responsible for the steady-state or slightly positive mass balance conditions between 1988 and 1999 and for the strong imbalance after 1999 were unknown.

In order to answer these questions, in the present chapter the annual mass balances of Chhota Shigri Glacier are reconstructed between 1969 and 2012 applying a degree-day model together with an accumulation model fed by long-term meteorological data recorded at Bhuntar meteorological station (~50 km south of the glacier, 1092 m a.s.l.). This reconstruction allowed us to examine the mass balances since 1969. A period of steady-state between 1986 and 2000 sandwiched between a moderate mass loss period (between 1969 and 1985) and an accelerated mass wastage period (between 2001 and 2012) was defined. The respective mean mass balances for these 3 periods were -0.36 ± 0.36 m w.e. a⁻¹ (1969-85), -0.01 ± 0.36 m w.e. a⁻¹ (1986-2000) and -0.57 ± 0.36 m w.e. a⁻¹ (2001-12) corresponding to a mean mass balance of -0.30 ± 0.36 m w.e. a⁻¹ for this 43-year period. An analysis of these decadal scale mass balances with meteorological variables suggested that winter precipitation and summer temperature are almost equally important drivers controlling the mass balance pattern of this glacier.

Abstract

This study presents a reconstruction of the mass balances (MBs) of Chhota Shigri Glacier, Western Himalaya, India, and discusses the regional climatic drivers responsible for its evolution since 1969. The MBs are reconstructed by a temperature-index and an accumulation model using daily air-temperature and precipitation records from the nearest meteorological station, at Bhuntar meteorological station. The only adjusted parameter is the altitudinal precipitation gradient. The model is calibrated against 10 years of annual altitudinal MB measurements between 2002 and 2012 and decadal cumulative MBs between 1988 and 2010. Three periods were distinguished in the annual glacier-wide mass balance (B_a) series. Periods I (1969–85) and III (2001–12) show significant mass loss at B_a rates of -0.36 ± 0.36 and -0.57 ± 0.36 m w.e. a^{-1} , respectively whereas period II (1986–2000) exhibits steady-state conditions with average B_a of -0.01 ± 0.36 m w.e. a^{-1} . The comparison among these three periods suggests that winter precipitation and summer temperature are almost equally important drivers controlling the B_a pattern of Chhota Shigri Glacier at decadal scale. The sensitivity of the modeled B_a to temperature is -0.52 m w.e. $a^{-1} \text{ } ^\circ\text{C}^{-1}$ whereas sensitivity to precipitation is calculated as 0.16 m w.e. a^{-1} for a 10% change.

4.1 Introduction

Glacier surface MB reflects climatic fluctuations and is important for the assessment of water resources (e.g., [Ohmura et al., 2007](#)). The Himalaya is one of the largest glacierized areas outside the polar regions, with a total glacier coverage of 22,800 km² ([Bolch et al., 2012](#)). Therefore, understanding the evolution of Himalayan glaciers is of great interest in diagnosing the future water availability in these highly populated watersheds (e.g., [Kaser et al., 2010](#); [Thayyen and Gergan, 2010](#); [Prasch et al., 2013](#)). A reliable prediction of glacier behaviour in the future demands an assessment of their response to climate in the past.

Since Intergovernmental Panel on Climate Change (IPCC) dispute ([Parry et al., 2007](#)), the Himalaya have become a focus of research interest, and subsequent ground-based MB (e.g., [Cogley, 2009](#); [Azam et al., 2012](#); [Vincent et al., 2013](#)) as well as remote-sensing studies (e.g., [Bolch et al., 2011, 2012](#); [Gardelle et al., 2012, 2013](#); [Kääb et al., 2012](#)) have been conducted over recent years. Unfortunately, data on recent glacier changes over the Himalaya are sparse, and even sparser as we go back in time (e.g., [Cogley, 2011](#); [Bolch et al., 2012](#)), so the rate at which these glaciers have been changing is still not well assessed. Direct measurements of B_a over the Indian Himalaya are available on a limited number of glaciers (13 glaciers covering ~100 km²) and mostly come from the period 1975-90 ([Vincent et al., 2013](#)). Chhota Shigri Glacier is one of the best observed glaciers in this region for its B_a , surface velocity and geodetic MB. Although B_a since 2002 ([Wagnon et al., 2007](#); [Azam et al., 2012](#)) and geodetic MB since 1988 ([Vincent et al., 2013](#)) are available, it is desirable to have longer series in order to extend our knowledge of the glacier-climate relationship. There is therefore a necessity to reconstruct the B_a of Himalayan glaciers in the past and to assess the impacts of climatic variables on B_a .

Melt models are customary approaches to reconstruct MBs. These models generally fall into two categories: temperature-index models (e.g., [Jóhannesson et al., 1995](#); [Braithwaite and Zhang, 2000](#); [Vincent, 2002](#); [Hock, 2003](#); [Pellicciotti et al., 2005](#); [Zhang et al., 2006](#); [Huss et al., 2008](#)) and energy-balance models (e.g., [Fujita and Ageta, 2000](#); [Hock and Holmgren, 2005](#); [Nemec et al., 2009](#); [Paul, 2010](#); [Mölg et al., 2012](#)). Temperature-index models are based on a statistical relationship, between melting and near-surface air temperatures, using restricted number of input data (generally air temperature), hence do not possess extensive physical resolution. This approach was firstly used for an Alpine glacier by [Finsterwalder and Schunk \(1887\)](#). Air temperature data are usually the most widely available data; thus, temperature-index melt models have been applied in a variety of studies. Conversely, energy-balance models estimate melt based on sophisticated energy-balance equations ([Hock et al., 2007](#)) and in turn provide a detailed physical resolution but demand an extensive input dataset. It is still unclear how the empirical relationship between air temperature and melt holds under different climate conditions ([Hock, 2003](#)), but good performance of temperature-index models is generally attributed to the fact that many components of energy balance are strongly correlated with

temperature (Ohmura, 2001). Temperature-index models are known to perform better on mid-latitude glaciers than on low-latitude glaciers (Sicart et al., 2008). However, Chhota Shigri Glacier is similar to mid-latitude glaciers with an ablation season limited to the summer months and a mean vertical gradient of mass balance in the ablation zone similar to those reported in the Alps (Wagnon et al., 2007).

Consequently, in this study, a temperature-index model (e.g., Hock, 2003) together with an accumulation model is used to reconstruct B_a of Chhota Shigri Glacier since 1969 using meteorological data from Bhuntar meteorological station. The goals of this study are (1) to determine long-term time series of B_a and (2) to resolve them into winter (B_w) and summer (B_s) glacier-wide mass balances. This provides a basis for the study of climate-glacier interaction as well as some principles of B_a governing processes in the western Himalaya.

4.2 Study site

Chhota Shigri Glacier (32.28° N, 77.58° E) is a valley-type, non-surging glacier located in the Chandra-Bhaga river basin of Lahaul and Spiti valley, Pir Panjal range, western Himalaya (Fig. 4.1). It lies ~25 km (aerial distance) from the city of Manali. This glacier is located in the monsoon–arid transition zone and is influenced by two different atmospheric circulation systems: the Indian summer monsoon during summer and the Northern Hemisphere mid-latitude westerlies during winter (Bookhagen and Burbank, 2010). Chhota Shigri Glacier feeds Chandra River, one of the tributaries of Indus river system. This glacier is likely to be temperate and extends from 6263 to 4050 m a.s.l. with a total length of 9 km and area of 15.7 km² (Wagnon et al., 2007). Chhota Shigri Glacier is mainly oriented north-south in its ablation area but its tributaries and accumulation area have a variety of orientations (lower right inset in Fig. 4.1). Its snout is well defined, lying in a narrow valley and producing a single proglacial stream. The lower ablation area (<4500 m a.s.l.) is covered by debris representing 3.4% of the total surface area (Vincent et al., 2013). The debris layer is highly heterogeneous, ranging from few millimeter sand particles to big boulders sometimes exceeding several meters. The equilibrium-line altitude (ELA) for a zero net balance is close to 4900 m a.s.l. (Wagnon et al., 2007).

4.3 Data and climatic settings

4.3.1 Mass-balance data

Jawaharlal Nehru University, India, and Institut de Recherche pour le Développement (IRD), France, have been collaborating closely on Chhota Shigri Glacier since 2002, with B_a measurements being conducted by the direct glaciological method at the end of September or the beginning of October. Details of B_a measurements are provided by Wagnon et al. (2007) and Azam et al. (2012). Between 2002 and 2012, the glacier lost mass at a rate of -0.57 ± 0.40 m w.e. a⁻¹. Its volume change was also measured between 1988 and 2010 using in-situ geodetic measurements. Topographic measurements conducted in 1988 (Dobhal, 1992) were resurveyed in October 2010

using the carrier-phase GPS to determine the thickness variations of the glacier over 22 years. These thickness variations were converted to cumulative MB between 1988 and 2010 (-3.8 ± 2.0 m w.e. corresponding to -0.17 ± 0.09 m w.e. a^{-1}) (Vincent et al., 2013). Using satellite digital elevation models differencing and field measurements, a negative MB between 1999 and 2010 (-4.8 ± 1.8 m w.e., corresponding to -0.44 ± 0.16 m w.e. a^{-1}) was observed. Thus, a slightly positive or steady-state MB between 1988 and 1999 ($+1.0 \pm 2.7$ m w.e., corresponding to $+0.09 \pm 0.24$ m w.e. a^{-1}) was deduced.

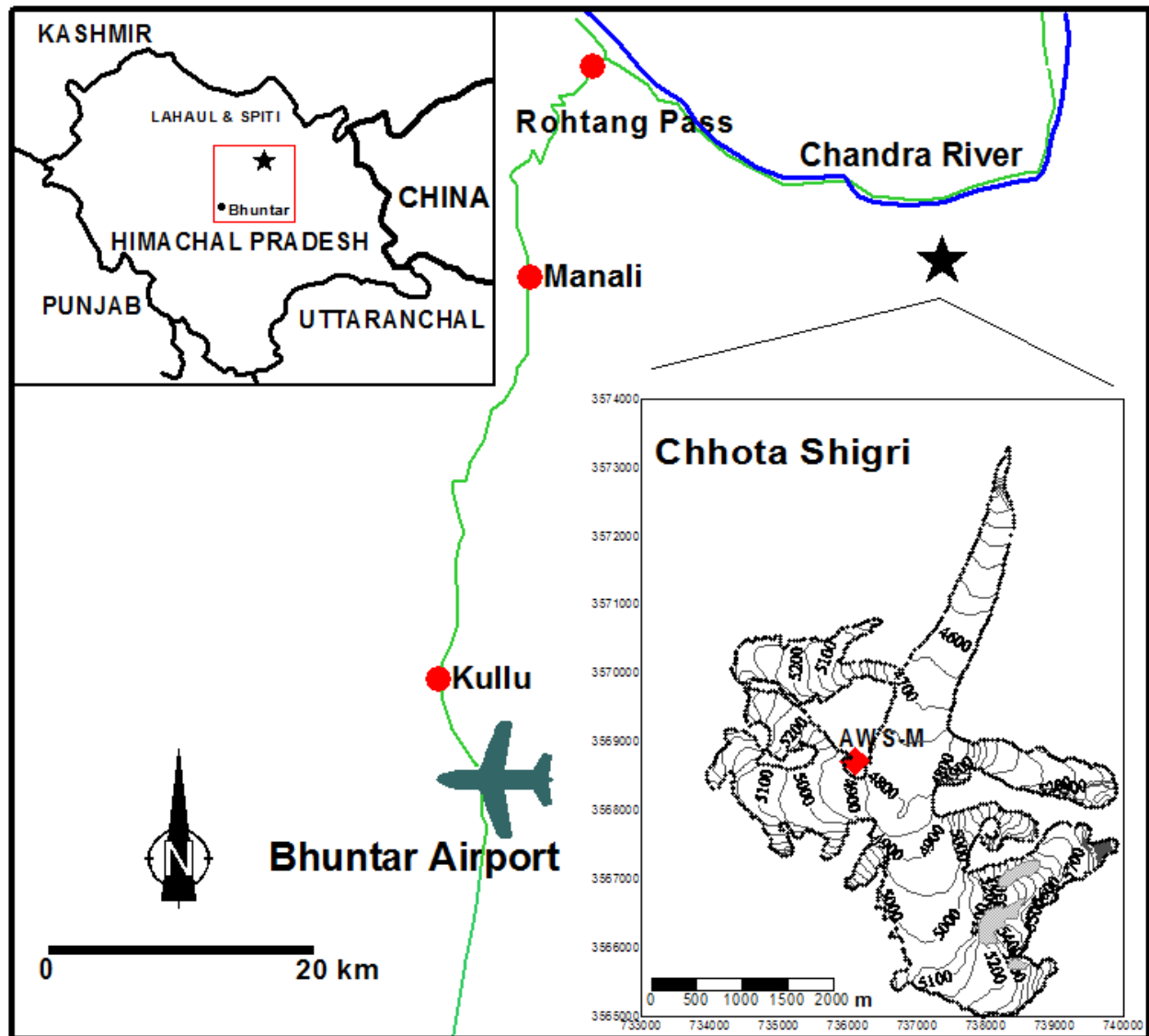


Figure 4.1. Location map of Chhota Shigri Glacier and its surroundings. Roads are shown in green, river in blue and Chhota Shigri Glacier as a star. The upper left inset shows a map of Himachal Pradesh, India, with the location of the Bhuntar meteorological station and glacier (star) indicated in the box. The lower right inset is a map of Chhota Shigri Glacier with the location of the AWS-M (red diamond). The map coordinates are in the UTM 43 (north) World Geodetic System 1984 (WGS84) reference system.

4.3.2 Meteorological data

At Chhota Shigri Glacier, in-situ meteorological data since 18 August 2009 are available from an Automatic Weather Station (AWS-M) located on a lateral moraine at 4863 m a.s.l. (lower right inset in Fig. 4.1). The nearest long-term meteorological record comes from Bhuntar meteorological station, Kullu Airport (31.5° N, 77.9° E, 1092 m a.s.l.). This meteorological station is located ~50 km (aerial distance) southwest of Chhota Shigri Glacier and belongs to the Indian Meteorological Department (IMD). The daily maximum, minimum temperature and precipitation data are available since January 1969.

4.3.2.1 Air temperature

Air temperatures (minimum and maximum) are recorded daily by traditional maximum-minimum thermometers at Bhuntar meteorological station. Daily mean temperature is calculated as a mean of daily maximum and minimum temperatures. This averaged temperature may differ slightly from a daily temperature derived from continuous measurements recorded at hourly or infra-hourly time-scale, but since this mean temperature is used to assess degree-day factors (see section 4.4.2.2), this difference does not impact MB results. The temperature series from Bhuntar meteorological station has some data gaps usually of some days to a couple of months. Out of 16010 days, a total of 1182 days are missing (7.3% data gaps). Short gaps of one or two days were filled by a linear interpolation method between data from the days immediate preceding and following the missing day. In the case of longer gaps (more than two days) a correlation is calculated between daily mean temperatures from Bhuntar meteorological station and daily re-analysis temperatures from the US National Centers for Environmental Prediction/US National Center for Atmospheric Research (NCEP/NCAR) (Kalnay et al., 1996). Given that the correlation is influenced by temperature seasonality, both temperature series were de-seasoned using a multiplicative decomposition model to remove the seasonality of the data. To achieve this task, before performing any correlation, any daily temperature value was divided by a mean daily index of the corresponding day. This index was computed 1. by dividing the daily temperature value by the 365 day moving average of the same date and 2. by averaging all resulting day-of-year index values over the whole studied period (e.g., averaging all values for 1 January over the 43 years to compute the mean index of 1 January). The NCEP/NCAR re-analysis data for temperature are available since 1948 for the grid point 32.5° N, 77.5° E (nearest grid point to Bhuntar meteorological station) at 925 hPa. The correlation coefficient is fairly low ($r=0.49$) and a t-test is done for the slope coefficient of the regression. The t-test suggests that relationship is statistically significant at a confidence level of 95%. The correlation is used to fill the gaps in Bhuntar temperature series and the seasonality was then added back to yield a continuous temperature series. Figure 4.2 shows the mean annual temperature since 1969.

4.3.2.2 Precipitation

The daily precipitation record since 1969 is available from Bhuntar meteorological station. At this meteorological station the precipitation measurements were collected by tipping-bucket rain gauges. The gaps (352 daily data are missing over 16010 days; 2.1% data gaps) are filled using the average value of the daily amount of rain of the same dates in the other years. Figure 4.2 shows the annual precipitation sums at Bhuntar meteorological station since 1969.

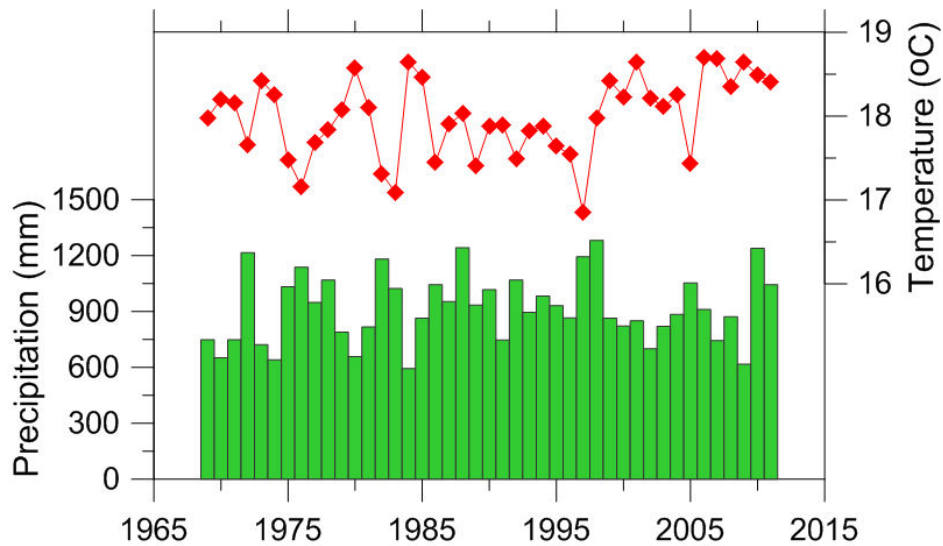


Figure 4.2. Annual mean temperature (red squares) and annual precipitation sums (green bars) recorded at Bhuntar meteorological station from January 1969 to October 2012.

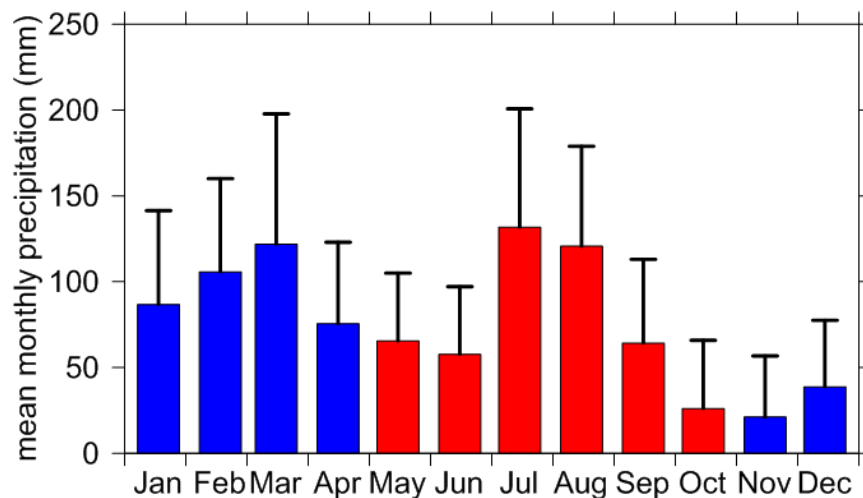


Figure 4.3. Mean monthly precipitations between 1969 and 2012 at Bhuntar meteorological station. Summer precipitation (red bars) predominantly derives from the Indian summer monsoon, whereas winter precipitation (blue bars) predominantly derives from mid-latitude westerlies. The error bars represent the standard deviation ($\pm 1\sigma$) of the monthly precipitation mean.

4.3.3 Climatic setting

Western Himalaya are characterized by, from west to east, the decreasing influence of the mid-latitude westerlies (MLW) and the increasing influence of the Indian summer monsoon (ISM) (Bookhagen and Burbank, 2010), leading to distinct accumulation regimes on glaciers depending on their location. Over the whole Himalayan range, summer precipitation (May to October) is predominantly of monsoonal origin, whereas in winter (November to April) precipitation accompanies MLW (Wulf et al., 2010). Mean monthly precipitations with monthly standard deviation at Bhuntar meteorological station are shown in Fig. 4.3. ISM (May to October) accounts for 51% of the average annual rainfall (916 mm a⁻¹) over 1969-2012, while MLW (November to April) contribute 49%. Almost equal precipitations from ISM and MLW, recorded since 1969 at Bhuntar meteorological station, suggest that Chhota Shigri Glacier is a good representative of a transition zone that is alternatively influenced by ISM and MLW.

4.4 Methods

4.4.1 Model description

B_a is computed using the temperature-index model (e.g., Hock, 2003) together with an accumulation model. The temperature-index model relates the amount of melt/ablation with positive air temperature sums (cumulated positive degree-days, CPDD) with a proportionality factor called the degree-day factor (DDF).

The Ablation M is computed by:

$$M = \begin{cases} DDF_{ice/snow/debris} \cdot T & : T > T_M \\ 0 & : T \leq T_M \end{cases} \quad (4.1)$$

where, DDF denotes the degree-day factor (mm d⁻¹ °C⁻¹), different for ice, snow and debris-cover surfaces, T is extrapolated daily mean temperature (°C) at glacier altitudes and T_M is the threshold temperature (°C) for melt.

The accumulation A is computed by:

$$A = \begin{cases} P & : T \leq T_P \\ 0 & : T > T_P \end{cases} \quad (4.2)$$

where, P and T are extrapolated daily precipitation (mm) and temperature (°C) at glacier altitudes, respectively and T_P is the threshold temperature (°C) for snow-rain.

Computations of the DDFs were performed at various altitudes using ablation stakes distributed over the glacier (see section 4.4.2.2). Temperature and precipitation at daily resolution are the required input data for the model. The MB is calculated at every altitudinal

range of 50 meters using temperature and precipitation from Bhuntar meteorological station since 1969 extrapolated at the mean altitude (e.g., for the 4400-4450 band, 4425 m a.s.l.). The model starts on 1 October of a year and calculates both accumulation and ablation for each altitudinal range at daily time-step for a full hydrological year (until 30 September the following year), taking into account the surface state (snow, bare ice or debris) and using the corresponding DDF. There was no option but to assume that the initial conditions (surface state, snow depth as a function of elevation) of 1 October 1969 were similar to those observed on 1 October 2002 in the field, but this assumption only impacted the B_a results of the first year of reconstruction. The sum of accumulation and ablation gives the specific B_a . Daily melt of snow-, ice- and debris-cover glacier was calculated when the air temperature was above the threshold melt temperature. Liquid precipitation is assumed not to contribute to glacier mass gain. Refreezing of melt water or rainfall is discounted as it is negligible for temperate glaciers (Braithwaite and Zhang, 2000). Given that the area loss for Chhota Shigri Glacier between 1980 and 2010 is only 0.47% of its area in 1980 (Pandey and Venkataraman, 2013) and mass wastage between 1988 and 2010 is mainly limited to the last decade (Vincent et al., 2013), the glacier hypsometry (surface elevation distribution) is considered to be unchanged over the whole modeling period and equal to the 2004-2005 hypsometry given by Wagnon et al. (2007).

4.4.2 Parameter analysis

Table 4.1 lists all the parameters used in the model. To achieve one of the main objectives of this study, *i.e.* to assess the temporal variability of B_a since 1969, it was decided to use a simple and robust model with as few calibration parameters as possible. In order not to multiply parameters, this model includes neither any radiation component nor a grid-based approach which could be used to assess the spatial variability of the MB but is less relevant for studying its temporal variability. Moreover, as far as possible, the model parameters are derived from available in situ measurements (temperature gradients as a function of elevation and DDFs for snow-, ice- and debris-covered surfaces). Threshold temperatures for melt and snow-rain limit have been chosen from the literature. Indeed, those temperatures are related to DDFs or temperature and precipitation altitudinal gradients through Eqs. (4.1) and (4.2), so selecting different values for these temperatures would have resulted in different values of DDFs or temperature and precipitation gradients but would not have significantly changed MB results. The only adjusted parameter, because of a lack of data, was the altitudinal precipitation gradient.

4.4.2.1 Temperature lapse rate (LR)

Daily LRs were calculated using daily mean temperatures from Bhuntar meteorological station (1092 m a.s.l.) and the glacier-side AWS-M (4863 m a.s.l.) for the overlapping period between 18 August 2009 and 31 October 2012. Although Bhuntar meteorological station is far away (~50

km) from the glacier, air temperature is relatively well correlated over large distances (Begert et al., 2005) and can therefore be extrapolated with confidence. There is a pronounced seasonal cycle in LRs, with the highest mean monthly LR ($7.03\text{ }^{\circ}\text{C km}^{-1}$) in March during winter and the lowest ($5.52\text{ }^{\circ}\text{C km}^{-1}$) in August during summer. The lower LRs over summer months are probably due to the strong monsoonal convectational activity producing an efficient mixing of the lower atmosphere.

Temperature-index models generally use a single constant value of LR for the whole modeling period (e.g., Jóhannesson et al., 1995; Vincent, 2002). In the present study the daily LRs were calculated for a full year to capture the annual temporal variability. A mean daily LR for every day of the year over the three hydrological years (1 October 2009 to 30 September 2012) was first calculated to remove the interannual variability and then fitted by an order-10 polynomial function (Fig. 4.4). This function was used to calculate the LR for every day of the year over the whole year. The daily air temperatures on glacier surface at each altitude range are computed from Bhuntar meteorological station temperatures using these LRs. The average LR is calculated as $6.4\text{ }^{\circ}\text{C km}^{-1}$.

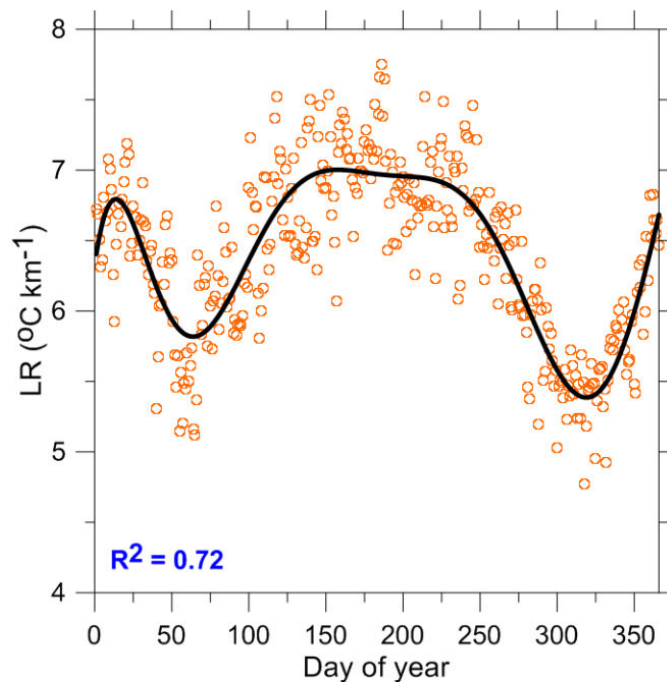


Figure 4.4. Polynomial fit (black line) for the day-of-year average values of LRs (orange circles). Day-of-year 1 corresponds to 1 October. Every dot stands for a daily value of LR for each day of the year, averaged over three hydrological years (1 October 2009 to 30 September 2012). Also shown is the correlation coefficient R^2 between LR daily values and the corresponding polynomial fit (95% confidence level).

4.4.2.2 Degree-day factors

On Chhota Shigri Glacier, the DDFs for ice-, snow-, and the debris-cover part were obtained by linear regression between point ablation measurements performed during the summers of 2009, 2011 and 2012 (June to October) between 4300 and 4900 m a.s.l. and the corresponding CPDD. The ablation was measured for different time periods, from a few days to a couple of weeks, at several stakes. These periods are sometimes short because they have been carefully selected to exclude significant snowfall events on the glacier (no observation of snowfalls at the permanent base camp (~3900 m a.s.l.) and no significant fresh snow reported at stake locations during measurements). For each ablation stake, the CPDD is computed from Bhuntar meteorological station (1092 m a.s.l.) applying the daily calculated LR between this meteorological station and the AWS-M (4863 m a.s.l.) close to the glacier. Around 500 measurements have been performed at most of the available stakes. Ablation and CPDD have always been compared over the same time period. Given the overall uncertainty of 140 mm w.e. in stake ablation measurements obtained from a variance analysis including all types of errors (ice/snow density, stake height determination, liquid-water content of the snow and snow height) (Thibert et al., 2008), all the measurements having ablation lower than 140 mm w.e. have been discarded for DDFs calculations of ice and debris. Given the limited number of measurements over snow surfaces (the glacier is inaccessible during winter), this threshold has been decreased to 100 mm w.e. to keep the number of measurements large enough for regression analysis. A total of 192 ablation measurements (13, 157 and 22 for snow, ice and debris respectively) were available for the analysis. Figure 4.5 provides the linear regression curves for snow, ice and debris, and the corresponding slopes are the respective DDFs. The y-intercept has been systematically forced to zero assuming the threshold temperature for ablation is always 0°C.

Figure 4.5 shows a linear increase in ablation as a function of CPDD except for debris-cover surfaces where dispersion is large. Over the debris-cover part, ablation strongly depends on the thickness of the debris, which is very variable in space, in turn, on the stake location which may change from one year to the next when new stakes are installed. The DDFs for debris- cover, snow and ice surfaces, with their respective uncertainties calculated following Taylor (1997, p. 188), were calculated as 3.34 ± 0.20 , 5.28 ± 0.14 and 8.63 ± 0.18 mm d⁻¹ °C⁻¹ respectively. The DDF for snow is 61% that of ice, a significantly lower value as expected given that melting is more efficient over ice surfaces than over snow surfaces due to albedo difference. Below 4400 m a.s.l., the glacier is debris-covered, which efficiently protects the ice against melting, explaining why its DDF is lower than the others.

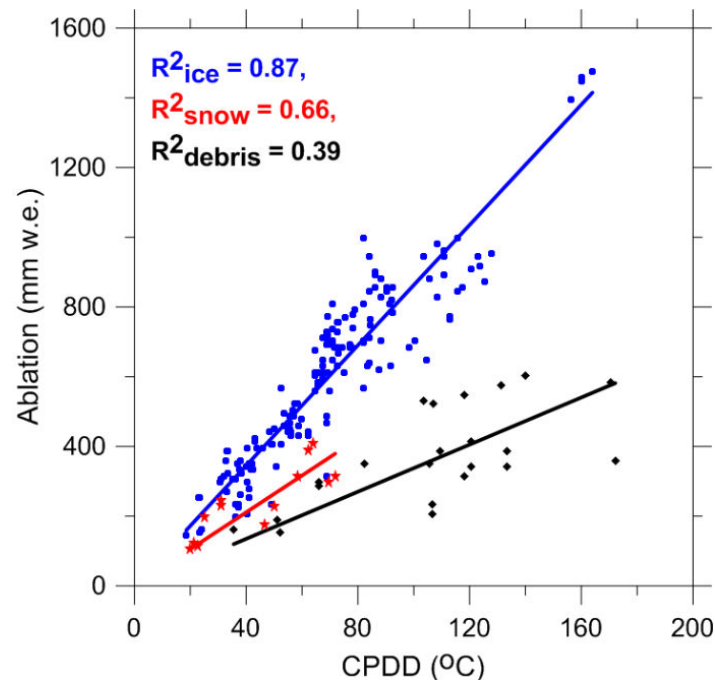


Figure 4.5. Measured ablation for debris (black squares), ice (blue dots) and snow (red stars) surfaces as a function of CPDD. In total 192 measurements performed between June and October 2009, 2011 and 2012 were selected for analysis. Also shown are the respective correlation coefficients R^2 (95% confidence level).

4.4.2.3 Precipitation gradient

The distribution of precipitation on the glacier is more complicated to handle than air temperature since precipitation amounts in mountainous regions are spatially non-uniform and have a strong vertical dependence (e.g., Immerzeel et al., 2012b). Sites only a few km away may receive significantly different amounts of rain or snow. Furthermore, limited information is available about precipitation amounts and gradients over the western Himalaya at glacier altitudes. Therefore, point MB measurements performed at 5550 m a.s.l. on Chhota Shigri Glacier seem to be the best available option to quantify the lower limit of the total annual accumulation and to try to derive the precipitation gradient between Bhuntar meteorological station and the glacier. Only the lower limit of annual accumulation is assessed because part of the total annual accumulated snow at 5550 m a.s.l. may have been removed by melting, sublimation or wind erosion. Temperature at 5550 m a.s.l. remains below the freezing point, suggesting that melting is insignificant. In addition, the measurement site is flat, and thus not submitted to over-accumulation due to avalanches. The correlation coefficient R^2 between point MB at 5550 m a.s.l. and precipitation at Bhuntar meteorological station over 9 years from 2002 to 2012 at annual time scale is equal to 0.57. The resulting precipitation gradient is positive with altitude at a rate of $0.10 \pm 0.03 \text{ m km}^{-1}$, in agreement with the gradient of $\sim 0.12 \text{ m km}^{-1}$ reported by Wulf et al. (2010) in Baspa Valley ($\sim 100 \text{ km SE}$ of Chhota Shigri Glacier). Considering that this

gradient has been derived using the lower limit of total annual accumulation at glacier elevation, it is probably underestimated here. Moreover, this gradient is known to be spatially highly variable (e.g., Immerzeel et al., 2012b). A calibration of this parameter is performed below to assess it better (see section 4.4.3).

Assuming that precipitation linearly increases with altitude, the precipitation gradient has been applied over the whole glacier to compute precipitation at every altitudinal range from Bhuntar meteorological station precipitation. Precipitation on the glacier is assumed to fall in the form of snow if the temperature at the corresponding altitude is below a specified threshold (typically 1 °C) (e.g., Jóhannesson et al., 1995; Lejeune et al., 2007).

4.4.3 Model calibration

In section 4.4.2, model parameters (temperature LRs, DDFs and precipitation gradient) have been obtained from field measurements. Threshold temperatures (T_P and T_M) have also been assigned as commonly used values. Among these parameters, DDF for debris-covered surfaces comes from a weak correlation ($R^2 = 0.39$) and precipitation gradient is not known with accuracy due the large spatial variability of these variables and paucity of field data. A calibration, therefore, is sought for better assessment of these parameters. As the lower part of Chhota Shigri Glacier is debris-covered (only 3.4% of its total area), melting from this area is insignificant compared to the whole glacier, suggesting that DDF for debris-covered area is not a sensitive parameter. Consequently, only precipitation gradient has been adjusted to match the modeled net MB with the observed MB data. The MB has been calculated step by step starting from the original measured underestimated precipitation gradient (0.10 m km^{-1} ; see section 4.4.2.3) and implementing it at each step with an additional 0.01 m km^{-1} until the best agreement between modeled and observed MBs was achieved. Annual point MB measurements between 2002 and 2012 and decadal geodetic MB observations over the 1988-2010 period (*i.e.* 1988-1999 and 1999-2010) have been used simultaneously for calibration. The model is tuned to minimize at the same time (1) the resulting root-mean-square errors (RMSE) between modeled and measured annual point MBs (averaged every 50 m altitudinal range) from 2002 to 2012 and (2) the difference between modeled MB and geodetic mass changes at decadal scale. The modeled B_a were cumulated over the periods when decadal geodetic MBs (Vincent et al., 2013) were available in order to make a comparison. The annual changing surface is not accounted for in this study, and all cumulative MBs are related to the 2004/05 surface area.

Table 4.1. List of the model parameters used for MB reconstruction

Melt-model parameter	Value
1. DDF for debris	3.34 mm d ⁻¹ °C ⁻¹
2. DDF for ice	8.63 mm d ⁻¹ °C ⁻¹
3. DDF for snow	5.28 mm d ⁻¹ °C ⁻¹
4. Precipitation gradient	0.20 m km ⁻¹
5. Temperature LRs	Mean daily LR* (°C km ⁻¹)
6. Threshold temperature for snow/rain (T_P)	1 °C
7. Threshold temperature for melting (T_M)	0 °C

* Averaged for each day of year using Bhuntar and AWS-M data between 1 October 2009 and 30 September 2012

4.5. Results

4.5.1. MB as a function of altitude

Figure 4.6 compares the modeled annual altitudinal gradient of MB (at each altitudinal range of 50 m from 4400 to 5400 m a.s.l.) with the observed gradient for each hydrological year between 2002 and 2012. Modeled and observed gradients show a good agreement, with an RMSE of 0.84 m w.e. a⁻¹ for 10 hydrological years between 2002 and 2012. The agreement is the best in 2009/2010 with an RMSE of 0.42 m w.e. a⁻¹, and worst in 2008/2009, with an RMSE of 1.66 m w.e. a⁻¹. The other eight years show RMSEs ranging between 0.49 and 0.95 m w.e. a⁻¹. The largest differences come from the ablation zone, below 4800 m a.s.l. (~22% glacier area) where for some years (2002-2008) modeled ablation is underestimated.

In fact, in the ablation area during summer, predominantly ice is exposed at the surface, hence the DDF for ice has probably been underestimated between 2002 and 2008 since it has been computed by regression analysis using data collected during the summers of 2009, 2011 and 2012 (section 4.4.2.2). The corresponding hydrological years 2008/2009, 2010/2011 and 2011/2012 had respective B_a of 0.13, 0.11 and -0.45 ± 0.40 m w.e. a⁻¹, which were above average compared to the prior years. In temperature-index models, DDFs are integrated factors taking into account all kinds of effects responsible for glacier melt. In the present study, the DDF for ice has perhaps been underestimated because some effects likely to enhance melting, such as longwave radiation emitted by the steep valley walls surrounding the glacier tongue below 4700 m a.s.l. (Wagnon et al., 2007) or progressive dust deposition at the glacier surface that might reduce the surface albedo (Oerlemans et al., 2009), have been minimized. Indeed, during positive B_a years, glacier surroundings may remain covered by snow longer even in summer, limiting longwave emission, and the dust deposition effect can be decreased when there are more frequent snowfalls than during negative B_a years.

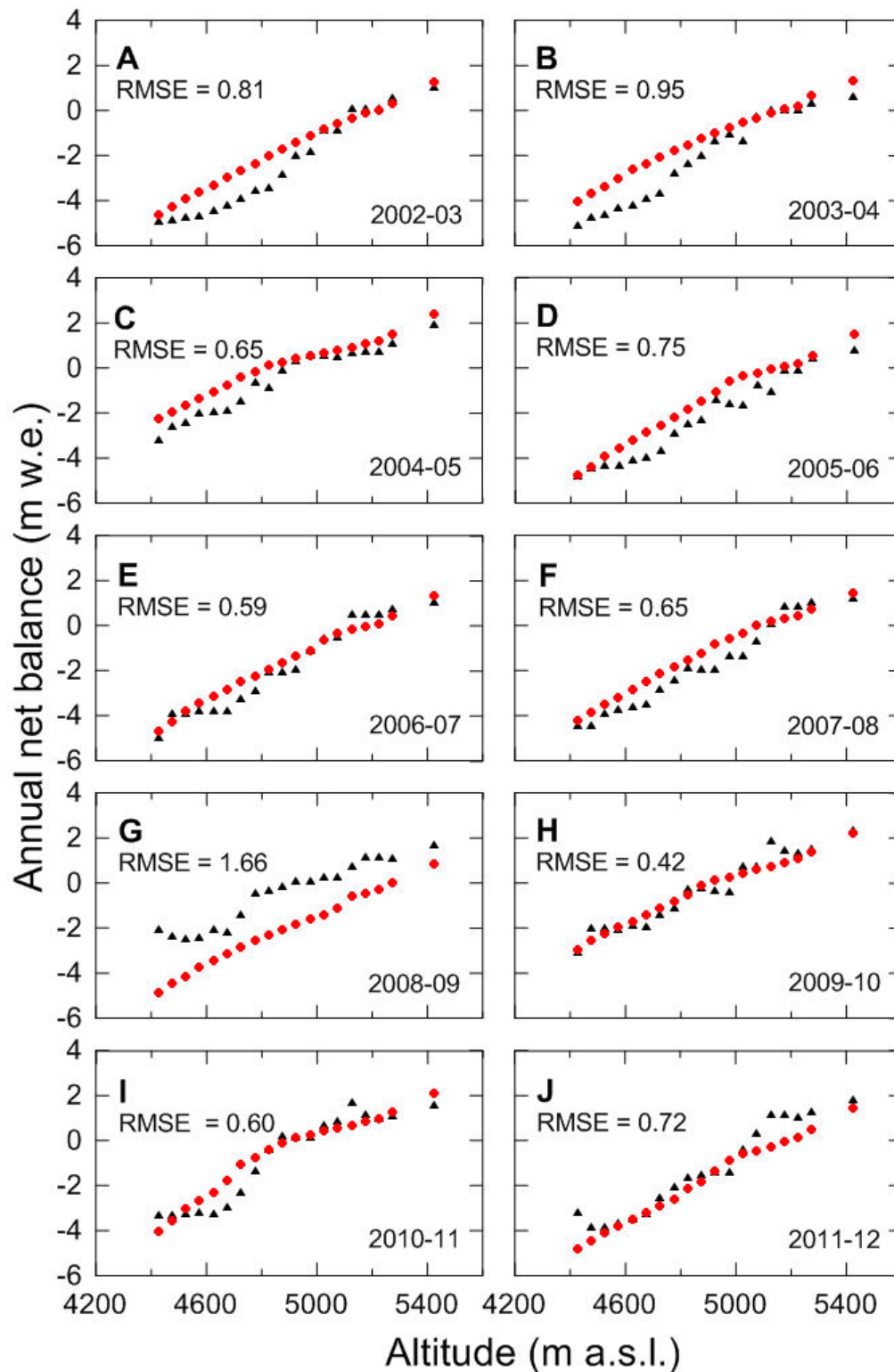


Figure 4.6. Comparison of reconstructed annual (red dots) with observed annual MBs (black triangles) as a function of elevation for 10 hydrological years 2002-2012. RMSE (m w.e. a⁻¹) for each year is also given.

In 2008/2009, the opposite is true, melting being sharply overestimated at every elevation by the model (Fig. 4.6G). The mismatch between modeled MBs as a function of elevation and observations is likely to be due to the large albedo spatio-temporal variability that sometimes occurs in the field. Brock et al. (2000) found that the albedo variations exert a significant control on the surface melt rate, and summer snowfall events are particularly important to the summer energy balance. During the 10 years of observations on Chhota Shigri Glacier, local observers reported some heavy summer snow falls usually in September (September 2005; 3-14 September 2009; 13-23 September 2010) and even in August (13 August 2011). These summer snow fall events sometimes deposit as much as 1 m of snow in a few days at the glacier snout. Consequently, melting is abruptly reduced or even stopped at the glacier surface for several weeks or even for the rest of the ablation season which usually ends around mid-October in years without such strong summer snowfalls. Such major and abrupt changes are probably difficult to simulate using the model, hence the mismatches between simulation and observation in some years. Moreover, during these specific events which are probably triggered by the orographic effect (Bookhagen and Burbank, 2010), precipitation amounts measured at Bhuntar meteorological station are not always representative of those occurring on the glacier. This may have been the case in 2008/2009. Nevertheless, additional measurements (e.g., systematic comparisons between precipitation at Bhuntar and at the glacier elevation) are still required to explain in details these discrepancies between modeled and observed MBs.

4.5.2 Annual mass balance

4.5.2.1 Cumulative mass balance since 1969

The 1969-2012 modeled B_a are displayed in Fig. 4.7 together with observed 2002-2012 B_a and 1988-2010 geodetic decadal MBs. Over the whole modeling period, B_a is negative 60% of the time and positive the rest of the time. The cumulative B_a is found to be -12.89 m w.e. (-0.30 m w.e. a^{-1}) between 1969 and 2012, which is a moderate mass loss over these 43 years. The hydrological year 1975/1976 shows the maximum B_a , 0.93 m w.e., whereas 1983/1984 shows the most negative B_a , -1.66 m w.e.

4.5.2.2 Error analysis

To assess the uncertainties in B_a , each sensitive parameter (precipitation gradient and DDFs for ice and snow) has been successively moved step by step from its initial value, the other parameters remaining unchanged, and the resulting cumulative B_a have been compared to observed geodetic MBs at decadal scale (1988-1999 and 1999-2010). Every parameter has been modified to allow the maximal variations of the resulting cumulative B_a within the limits prescribed by the uncertainty bounds of the observed geodetic MBs, *i.e.* ± 2.7 and ± 1.8 m w.e. for 1988-1999 and 1999-2010 respectively (Table 4.2; Fig. 4.7). Consequently, each parameter, as modified, provides two new 43 year series of B_a , one toward negative values and one toward

positive values. The resulting uncertainty in B_a is taken as the highest standard deviation calculated between these new series and the initial B_a series and is as high as ± 0.36 m w.e. a^{-1} .

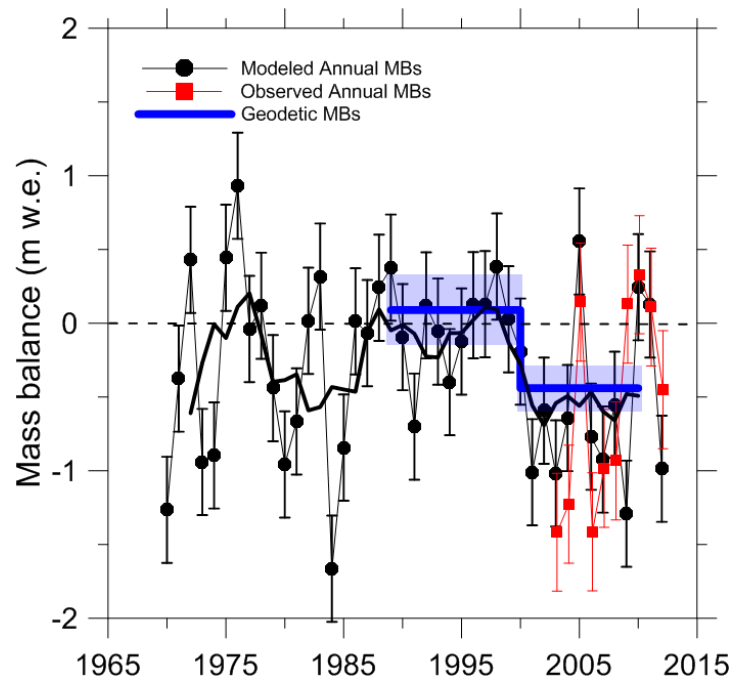


Figure 4.7. Comparison of modeled B_a (black points) with observed B_a (red squares) and decadal geodetic MBs (blue thick lines). The corresponding uncertainties in modeled, observed and geodetic MBs are also shown. Black thick line shows the 5 year running mean value since 1969.

In this study, given that the area loss is small as discussed in section 4.4.1, we have not considered the area change of Chhota Shigri Glacier over the studied period, and B_a changes are related to 2004/2005 glacier area and hypsometry (Wagnon et al., 2007). However, this assumption induces B_a errors due to temperature changes resulting from surface elevation changes that are not taken into account. Indeed, between 1969 and 2005 the calculated cumulative MB is as high as -8.74 m w.e., corresponding to ~ 9.7 m surface linear glacier-wide lowering between 1969 and 2005 (we assume no lowering at the highest point of the glacier, a maximum lowering at its snout and a linear lowering between these two points, leading to a MB of -8.74 m w.e.). Given a mean annual temperature lapse rate of 6.4 $^{\circ}\text{C km}^{-1}$ as obtained in section 4.4.2.1, we can recalculate the B_a for each year of this period, and the resulting error accounts for -0.06 m w.e. a^{-1} between 1969 and 2005. The same error analysis was performed between 2005 and 2012, where the cumulative MB is equal to -4.15 m w.e. (*i.e.* a rough estimate of 4.6 m surface glacier-wide lowering) and the MB error is $+0.03$ m w.e. a^{-1} . Combining both periods, a MB error of -0.03 m w.e. a^{-1} is calculated between 1969 and 2012, still low compared with the uncertainties associated to the modeling *i.e.* ± 0.36 m w.e. a^{-1} .

Table 4.2 compares the modeled cumulated B_a with the observed MB for the respective periods where the observed MBs are available. As expected (because these data served to calibrate the model) modeled B_a are in good agreement with geodetic decadal MBs since 1988 and cumulative glaciological B_a since 2002.

Table 4.2. Comparison of cumulative MBs (m w.e.)

	1988-1999	1999-2010	2002-2012	Source
Geodetic MB from field	1 ± 2.7	-4.8 ± 1.8		Vincent et al. (2013)
Glaciological B_a			-5.7 ± 0.4	Azam et al. (2012)
Modeled B_a	-0.2	-6.2	-5.3	Present study

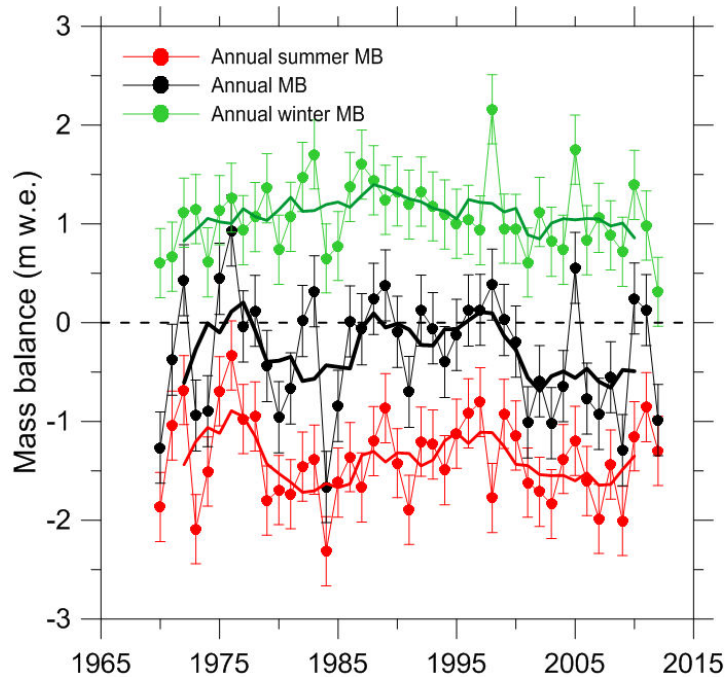


Figure 4.8. Annual and seasonal MB series of Chhota Shigri Glacier, 1969-2012. Black, green and red dots represent the annual, winter and summer MBs with their corresponding error bars respectively. The thick lines are the 5 day running means. The horizontal dotted line represents the zero MB.

4.5.3 Seasonal mass balance

Although B_a is of broad interest and has been determined in numerous glacier-monitoring programs (e.g., Dyurgerov and Meier, 2005), it does not provide insights into climate-glacier interaction. Seasonal MB offers the best insights to assess the effects of climatic drivers on glaciers (e.g., Ohmura, 2006). Every year the beginning and the end of the season were demarcated as the day when the MB was at its annual maximum (end of winter) or minimum

(end of summer) to retrieve the winter (B_w) and summer (B_s) glacier-wide mass balances from diurnal MB series. The model suggests that the average summer ablation period lasts from mid-June to the end of September, 96 ± 18 days. The computed B_s , B_w and B_a are shown in Fig. 4.8. Modeled seasonal MBs show large annual variability, with values from -2.31 to -0.33 m w.e. a^{-1} for B_s and 0.31 to 2.16 m w.e. a^{-1} for B_w . Over the whole simulation period the resulting B_a varies from -1.66 to 0.93 m w.e. a^{-1} . An error analysis for seasonal MBs similar to that conducted for B_a (section 4.5.2.2.) has been performed, leading to an error range of ± 0.35 m w.e. a^{-1} in B_s and B_w . The mean values for B_a , B_s and B_w for the 43 year period are -0.30 ± 0.36 , -1.38 ± 0.35 and 1.08 ± 0.35 m w.e. a^{-1} respectively.

4.6 Discussion

4.6.1 Mass balance pattern and climatic drivers

Over the whole simulation period (1969–2012), the cumulative B_a of Chhota Shigri Glacier was -12.89 m w.e., corresponding to a moderate mass loss rate of -0.30 ± 0.36 m w.e. a^{-1} . Three distinct periods (of 12–16 years) of this B_a series were distinguished according to the glacier mass gain or loss (Fig. 4.9). Student's t-tests, at 95% confidence level, have been performed to check whether periods I, II and III were statistically different from each other. The p-values (probability-values) for periods I and II and periods II and III are respectively 0.01 and 0.03, suggesting that period II statistically differs from the other periods, while p-value for periods I and III is 0.27, suggesting that the two periods are roughly similar. During periods I (1969–1985) and III (2001–2012), Chhota Shigri Glacier lost mass at B_a rates of -0.36 ± 0.36 and -0.57 ± 0.36 m w.e. a^{-1} respectively, whereas during period II (1986–2000) it remained close to steady-state conditions, with a mean B_a of -0.01 ± 0.36 m w.e. a^{-1} . The steady-state conditions over the nineties were qualitatively inferred by [Azam et al. \(2012\)](#) using a dynamical approach and quantified by [Vincent et al. \(2013\)](#) using geodetic in-situ measurements between 1988 and 2010. In this context, the present study enables determination of the exact time of glacier shifting from balance to imbalance conditions that [Vincent et al. \(2013\)](#) could not achieve.

For each period, the mean B_w , B_s and B_a are shown in Fig. 4.9 and Table 4.3, providing their respective values over the three periods and over a full 43-year period. In order to assess the climatic drivers, the average winter precipitations and summer temperatures at Bhuntar meteorological station are also plotted in Fig. 4.9 and reported in Table 4.3. Period I exhibits the largest inter-annual variability of the B_a of the 43 year reconstructed period, with the most positive (1975/76) and negative (1983/84) hydrological years (Fig. 4.8). This period also shows high mean B_s which is partially compensated by B_w , providing moderate mass loss. Period II is characterized by 56 mm a^{-1} higher precipitation and 0.2 °C lower summer mean temperature than 1969–2012 averages resulting in roughly equal B_w and B_s , leading to steady-state conditions (Table 4.3). Conditions for period III are diametrically opposite to those of period II, with 65 mm a^{-1} lower precipitation and 0.2 °C higher mean summer temperatures than 1969–2012 averages,

resulting in an accelerated mass loss due to reduced B_w and enhanced B_s . This comparison between these three periods suggests that winter precipitation and summer temperature are equally important drivers controlling the B_a pattern of Chhota Shigri Glacier at decadal scale.

Table 4.3. Mean annual, summer and winter MBs for periods I, II and III and for the whole 43 year period, with their corresponding mean summer temperatures and winter precipitations at Bhuntar meteorological station.

Period	B_a m w.e. a ⁻¹	B_s m w.e. a ⁻¹	B_w m w.e. a ⁻¹	Summer temperature °C	Winter precipitation mm
1969-1985	-0.36	-1.38	1.02	23.4	447
1986-2000	-0.01	-1.27	1.25	23.1	506
2001-2012	-0.57	-1.51	0.94	23.5	385
1969-2012	-0.30	-1.38	1.08	23.3	450

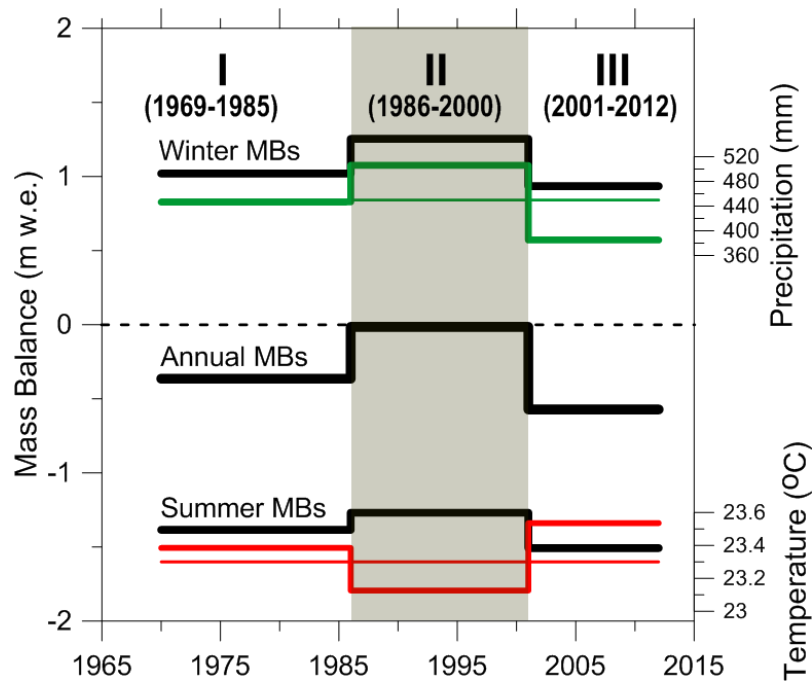


Figure 4.9. Mean winter, summer and annual MBs for all 3 periods since 1969 (black thick lines). Red thick line represents the summer mean temperatures (°C), while green line represents the annual winter precipitation sums (mm) at Bhuntar meteorological station. The continuous thin red and green lines represent the average summer temperatures (°C) and winter precipitation sums (mm) between 1969 and 2012 respectively. The black dotted line represents zero MB.

4.6.2 Comparison with other studies

This 43 year B_a series, the longest ever reconstructed in the Himalaya, provides the opportunity to make a comparison with other studies. In agreement with our results, showing a moderate mass loss over the last four decades, Panday and Venkataraman (2013) also reported moderate glacierized area shrinkage for the Chandra-Bhaga basin and a minor area loss (0.47%) for Chhota Shigri Glacier between 1980 and 2010. Balance conditions of the Chhota Shigri Glacier between 1986 and 2000 deviate from the most recent compilation for the entire Himalaya Karakoram region (Bolch et al., 2012). Bolch et al. (2012) reported ice wastage for this region over the past five decades, with increased rate of loss roughly after 1995 but with a high spatio-temporal variability. We would stress, as previously stated by Vincent et al. (2013), that Himalaya Karakoram MB averages between 1986 and 2000 should be regarded with caution, given the scarcity of MB data (Bolch et al., 2012) and result of this study testifying that the Chhota Shigri Glacier experienced a balanced mass budget between 1986 and 2000. Since 2000 an increased rate of mass loss is observed, in agreement with Bolch et al. (2012), with a B_a rate of -0.57 ± 0.36 m w.e. a^{-1} , representing 55% of the total mass loss of the last 43 years. This accelerated rate of B_a is in agreement with a mass wastage at -0.45 ± 0.13 m w.e. a^{-1} or -0.39 ± 0.18 m w.e. a^{-1} over 1999–2011, for Lahaul and Spiti region or Chhota Shigri Glacier respectively, calculated by Gardelle et al. (2013).

4.6.3 MB sensitivity to temperature and precipitation

Glacier-wide MB is a key variable widely used as a climate proxy in many environmental and climate change studies (e.g., Solomon et al., 2007). Temperature-index models are used worldwide to assess the modeled MB sensitivity to climate (e.g., De Woul and Hock, 2005; Braithwaite and Raper, 2007; Shea et al., 2009; Anderson et al., 2010; Wu et al., 2011) and estimate the future contribution of glaciers to sea-level rise (e.g., Raper and Braithwaite, 2006; Radic and Hock, 2011; Gardner et al., 2013). The sensitivity of a glacier MB to climate is usually assessed by rerunning the models with a uniform change in a specific variable, *i.e.* air temperature or precipitation throughout the year (e.g., Oerlemans et al., 1998; Braithwaite and Zhang, 2000), while the other variables and model parameters kept unchanged. These sensitivity tests were performed for Chhota Shigri Glacier, calculating B_a averaged over the period 1969–2012 firstly assuming a 1°C change in air temperature and secondly a 10% change in precipitation. The B_a sensitivity to temperature (dMB/dT) and precipitation (dMB/dP) are calculated following Oerlemans et al. (1998) as:

$$\frac{dMB}{dT} \approx \frac{MB(+1^\circ\text{C}) - MB(-1^\circ\text{C})}{2} \approx MB(1^\circ\text{C}) - MB(0^\circ\text{C}) \quad (4.3)$$

$$\frac{dMB}{dP} \approx \frac{MB(P+10\%) - MB(P-10\%) }{2} \approx MB(P + 10\%) - MB(P) \quad (4.4)$$

The sensitivity of the modeled B_a to temperature is $-0.52 \text{ m w.e. a}^{-1} \text{ } ^\circ\text{C}^{-1}$ which corresponds to the highest sensitivity recently reported by Rasmussen (2013) who investigated the meteorological controls on glacier MB in High Asia using NCEP/NCAR reanalysis data since 1948. It is also in agreement with the sensitivity of Zhadang Glacier, Tibet ($-0.47 \text{ m w.e. a}^{-1} \text{ } ^\circ\text{C}^{-1}$), calculated by Mölg et al. (2012) using an energy-balance model. The Chhota Shigri modeled MB sensitivity to temperature decreases with elevation from $-1.21 \text{ m w.e. a}^{-1} \text{ } ^\circ\text{C}^{-1}$ at 4400 m a.s.l. to $-0.05 \text{ m w.e. a}^{-1} \text{ } ^\circ\text{C}^{-1}$ at 6000 m a.s.l. (Fig. 4.10). It is consistent with the fact that ablation is mainly controlled by air temperature; in turn, in the lower part of the glacier where ablation is predominant, sensitivity of modeled MB to temperature is enhanced. Over the debris cover part (<4400 m a.s.l.) of the glacier, the sensitivity ($-0.52 \text{ m w.e. a}^{-1} \text{ } ^\circ\text{C}^{-1}$) is lower than over debris-free areas at the same elevation (not shown in Fig. 4.10). This is due to the low DDF for debris cover (40% of DDF for ice) which efficiently protects ice from fast melting. The dispersion in sensitivity is quite high close to the ELA ($\sim 4900 \text{ m a.s.l.}$), where it sharply changes from $-0.91 \text{ m w.e. a}^{-1} \text{ } ^\circ\text{C}^{-1}$ at 4850 m a.s.l. to $-0.56 \text{ m w.e. a}^{-1} \text{ } ^\circ\text{C}^{-1}$ at 5150 m a.s.l. This is likely due to the albedo pattern which can differ markedly from year to year close to the ELA (Vincent, 2002).

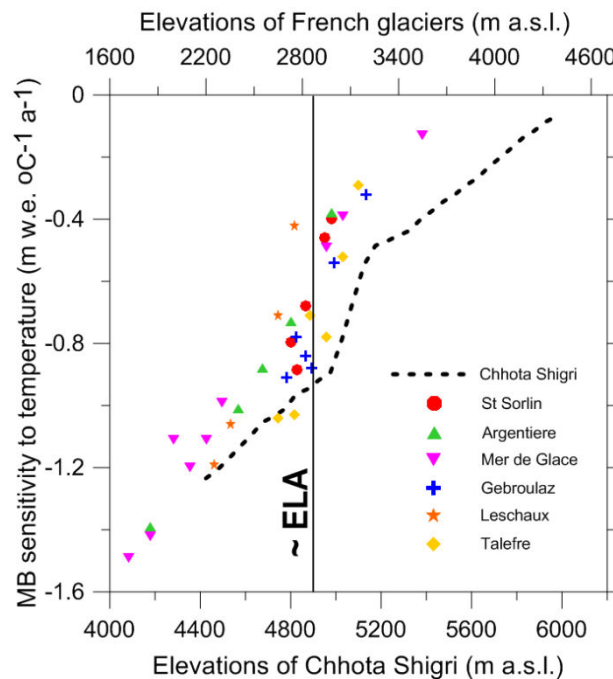


Figure 4.10. MB sensitivity of Chhota Shigri Glacier to temperature as a function of altitude (dotted line) compared to glaciers in the French Alps (various symbols) (Vincent, 2002). The lower and upper x-axis are the elevations for Chhota Shigri and French glaciers respectively and have been shifted to match their ELAs (thin vertical line).

Figure 4.10 compares the Chhota Shigri Glacier modeled MB sensitivity to temperature with summer ablation sensitivities of some monitored French glaciers (Vincent, 2002). These ablation sensitivities are calculated for the whole summer period by multiplying the DDF by the mean number of days for which temperature is higher than 0 °C at the observation elevation. The glacier altitudes are different, so they have been shifted to match the ELA of Chhota Shigri Glacier (~4900 m a.s.l.) to the mean ELA of the French Glaciers (~2900 m a.s.l.) in order to compare the sensitivity profiles with respect to elevation. The average sensitivity for Chhota Shigri Glacier at ~ELA is calculated as $-0.73 \text{ m w.e. a}^{-1} \text{ }^{\circ}\text{C}^{-1}$, while it is $-0.50 \text{ m w.e. a}^{-1} \text{ }^{\circ}\text{C}^{-1}$ for the French glaciers. Thibert et al. (2013) reported ablation sensitivity for another French glacier, Glacier de Sarnes, as $-0.62 \text{ m w.e. a}^{-1} \text{ }^{\circ}\text{C}^{-1}$ at 3000 m a.s.l. The sensitivity profile of Chhota Shigri Glacier with respect to altitude is in good agreement with those of French glaciers with maximum dispersion around ELAs.

A similar sensitivity test was performed for precipitation assuming a +10% increase. B_a sensitivity to precipitation is calculated as $0.16 \text{ m w.e. a}^{-1}$ for a 10% change, again in agreement with the value ($0.14 \text{ m w.e. a}^{-1}$ for a 10% change) reported by Mölg et al. (2012) on Zhadang Glacier. The model was run several times while changing successive total precipitation to discern the precipitation amount needed to compensate a 1 °C change in temperature. A 32% increase in precipitation results in the same change in B_a as a 1°C increase in temperature. Our results are in good agreement with Braithwaite et al. (2002) and Braithwaite and Raper (2007), who reported a 30–40% increase in precipitation to offset the effects of a +1 °C temperature change.

To test the relative importance of summer temperature and winter precipitation as drivers controlling the B_a of Chhota Shigri Glacier, we compared the sensitivity of the modeled MB to 1 standard deviation (1σ) of both variables ($0.49 \text{ }^{\circ}\text{C}$ for summer temperature and 145 mm for winter precipitation over the 43 year period). The respective sensitivities are -0.25 m w.e. for 1σ of temperature and $+0.30 \text{ m w.e.}$ for 1σ of precipitation confirming that both variables are almost equally important drivers controlling the B_a of Chhota Shigri Glacier at decadal scale.

4.7 Conclusion

B_a of Chhota Shigri Glacier has been measured annually using the glaciological method since 2002 and the geodetic method between 1988 and 2010. In the present study, B_a series of Chhota Shigri Glacier has been extended back to 1969 by a temperature-index model together with an accumulation model using daily records of precipitation and temperature from Bhuntar meteorological station. Model parameters were mostly derived from field measurements, except the vertical precipitation gradient whose lower limit was first obtained from field data to finally be calibrated because of the paucity of field measurements. The modeled and observed altitudinal MBs show an RMSE of $0.84 \text{ m w.e. a}^{-1}$ for the 10 years 2002-2012. Chhota Shigri Glacier experienced a moderate mass wastage at a rate of $-0.30 \pm 0.36 \text{ m w.e. a}^{-1}$ over 1969–2012

period. The reconstructed B_a time series shows two deficit periods (1969–1985 and 2000–2012) with moderate and accelerated mass loss respectively, and one steady-state period (1986–1999) when the B_a remained close to zero. The steady-state period is characterized by 56 mm a^{-1} higher precipitation and 0.2 °C lower summer mean temperature than 1969–2012 averages, resulting in roughly equal B_w and B_s . The sensitivity of B_a of Chhota Shigri Glacier to precipitation is 0.16 m w.e. a^{-1} for a 10% change and to temperature is -0.52 m w.e. a^{-1} °C $^{-1}$. This sensitivity to temperature ranges from -1.21 m w.e. a^{-1} °C $^{-1}$ at 4400 m a.s.l. to -0.05 m w.e. a^{-1} °C $^{-1}$ at 6000 m a.s.l., whereas it is -0.73 m w.e. a^{-1} °C $^{-1}$ around ELA (~4900 m a.s.l.), similar to the sensitivity of French glaciers relative to their ELA (Vincent, 2002). A 32% increase in precipitation compensates the effect of +1 °C change in temperature.

This study suggests that winter precipitation and summer temperature are almost equally important drivers controlling B_a pattern of Chhota Shigri Glacier at decadal scale. Comprehensive precipitation measurements at glacier elevation, presently in progress, will help us to confirm this finding as well as to understand the impact of summer sporadic heavy snowfalls on B_a precisely. Further investigations including energy balance studies at the glacier surface are also required to understand the role of different energy fluxes in B_a determination.

Acknowledgements

Authors thank Dr. E. Berthier, Dr. Qazi and Dr. Rajdeep and two anonymous referees for their constructive comments that led to a considerably improved manuscript. This work has been supported by IFCPAR/CEFIPRA project no. 3900-W1, the French Service d'Observation GLACIOCLIM as well as the Department of Science and Technology (DST), Government of India. M F Azam is grateful to IRD for providing financial support for his PhD. We thank Indian meteorological Department (IMD), New Delhi India to provide the data from Bhuntar meteorological station. A special thanks to our field assistant Adhikari Ji and the porters who have taken part in successive field trips, sometimes in harsh conditions. Authors thank Jawaharlal Nehru University for providing all the facilities to carry out this work.

Appendix

Hydrological year and mass balance evolution

The hydrological balance year is defined as the time between one minimum of glacier mass to the next, which, in mid-latitudes, generally occurs in autumn (Kaser et al., 2003). Ideally, the MB of a glacier should be monitored at the beginning of each hydrological year but this is almost impossible in the HKH region because of the harsh conditions that make the access difficult. Practically, the mass balance is calculated over a period slightly differing from the hydrological year. The hydrological demarcation is quite easy in the case of alpine/winter accumulation type glaciers (with distinct ablation and accumulation periods) but problematic over summer-accumulation type glaciers (ablation and accumulation periods coincide). Given that Chhota Shigri Glacier seems to be a winter accumulation type glacier, the hydrological year was arbitrarily defined from 1st October to 30th September of the next year (Wagnon et al., 2007). On Chhota Shigri Glacier, ablation season usually ends around mid-October if glacier does not receive any summer-monsoon snow falls in the month of August or September (section 4.5.1); therefore, 1st October is not the balance minimum of the hydrological year. The starting of the hydrological year from mid-October or 1st November would be more appropriate but the access to the glacier is not possible after 15th October as the road is closed by the state government. For similar reason winter MB measurements are taken between May and July months depending on the access in the corresponding year.

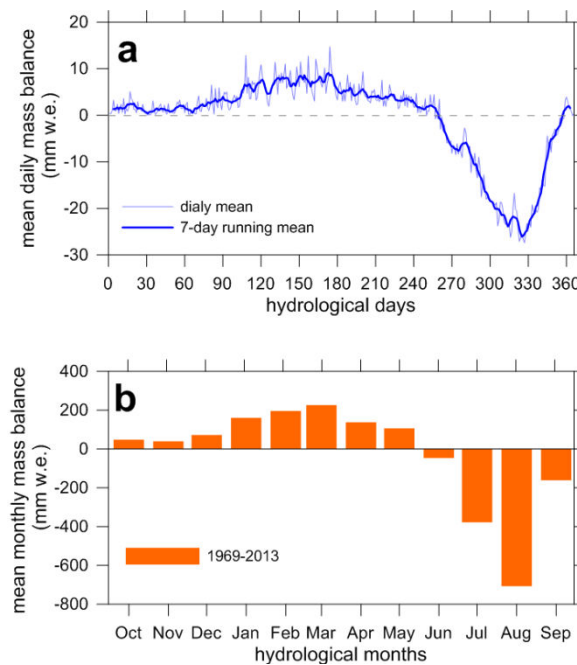


Figure 4.A1. A mean annual mass balance cycle at daily (a) and monthly (b) time-steps (data from 1969 to 2013 averaged every day (a) or month (b)). Hydrological year is defined between 1st October (day 0 on x-axis) and 30th September.

The least amount of mean monthly precipitations in the months of October and November at Bhuntar meteorological station (Fig. 4.3, section 4.3.2.2) as well as at the glacier base camp (Fig. 5.5, section 5.2.4.2) suggests that October and November are the driest months in this area in agreement with [Datt et al. \(2008\)](#) and [Prasad and Roy \(2005\)](#). Given the least precipitation amounts or almost balance conditions in October and November and the restricted accessibility to the glacier after mid-October, selecting 1st October as the starting date of the hydrological year seems to be the best available option. Besides, May shows the maximum MB conditions after accumulation period followed by June which is almost in balance conditions thus, 1st June seems to be the most justified date for starting the winter MB measurements. Chhota Shigri Glacier is a representative glacier for whole Lahaul and Spiti Valley ([Berthier et al., 2007](#); [Vincent et al., 2013](#)) in the western Himalaya; therefore, the hydrological year for annual and winter MBs assessed on Chhota Shigri Glacier may be adopted for other glaciers of the region. It is noteworthy to say that the delineation of the hydrological year for annual and winter MBs is assessed by a MB model output on Chhota Shigri Glacier which is calibrated using long term in-situ data. Consequently such delineation is likely to be relevant for Chhota Shigri Glacier, but it should be considered with caution when applied to other glaciers of the region.

CHAPTER 5

Processes governing the mass balance of Chhota Shigri Glacier

After:

[Azam, M. F.](#), Wagnon, P., Vincent, C., Ramanathan, AL., Favier, V., Mandal, A., and Pottakkal, J. G.: Processes governing the mass balance of Chhota Shigri Glacier (western Himalaya, India) assessed by point-scale surface energy balance measurements, *The Cryosphere*, 8, 2195-2217, doi:10.5194/tc-8-2195-2014, 2014b.

Executive summary

In chapter 4 the annual glacier-wide mass balance (B_a) series since 1969 was reconstructed and three different periods were distinguished between 1969 and 2012. Periods I (1969–85) and III (2001–12) showed moderate and high mass losses, respectively whereas period II (1986–2000) exhibited steady-state conditions of B_a . The reconstructed B_a series not only re-confirmed the steady B_a state of Chhota Shigri Glacier already inferred in chapter 3 (section 3.4.1) and approved by [Vincent et al. \(2013\)](#) but also defined the exact period of steady-state. Additionally the comparison of the mean B_a with the mean winter precipitation and summer temperature over each period suggested that winter precipitation and summer temperature are almost equally important drivers controlling B_a pattern of Chhota Shigri Glacier at decadal scale. Furthermore chapter 2 (section 2.5.5) and chapter 4 (section 4.5.1) qualitatively highlighted the vital role of the summer-monsoon snowfalls for B_a evolution by controlling the summer glacier-wide mass balance via surface albedo. Yet the quantitative analysis and in-depth understanding of physical processes behind B_a evolution remain the open questions.

Certainly these questions can only be addressed with a detailed physical surface energy balance approach. Consequently on 12 August 2012 a fully equipped Automatic Weather Station (AWS-G) was erected on the mid-ablation zone of Chhota Shigri Glacier. The 30-min mean data were analyzed to understand the meteorological conditions on the glacier surface at daily scale and used as input data in an energy balance model. The energy balance numerical modeling outputs provided the quantification of the surface energy fluxes and identification of the factors affecting B_a . Net energy was available for melt only during the summer-monsoon period when net radiation was the primary component of the surface energy balance accounting for 80% of the total heat flux followed by turbulent sensible (13%), latent (5%) and conductive (2%) heat fluxes. During post-monsoon and winter periods, sublimation predominated on Chhota Shigri Glacier.

In summer-monsoon, similar to other glaciers in High Mountain Asia which are affected by Indian Summer Monsoon circulation, latent heat flux brought a significant amount of energy at Chhota Shigri Glacier surface in the form of condensation/re-sublimation. Using the meteorological data and model outputs, the impact of the summer monsoon snowfalls on Chhota Shigri Glacier melt was assessed. This analysis, at point scale, quantitatively validated that the intensity of snowfall events during the summer-monsoon controls the surface albedo, in turn ablation, and therefore is among the most important drivers responsible for B_a evolution of Chhota Shigri Glacier. The summer-monsoon air temperature controlling the precipitation phase (rain versus snow and thus albedo), assigned, indirectly, also among the most important drivers. Following the point scale quantitative impact of summer-monsoon snowfalls, this analysis was also extended qualitatively for the whole glacier by analyzing the biggest daily summer-monsoon snowfall events, extrapolated from Bhuntar meteorological station, and B_a between 2002 and 2013. Both the quantitative point scale as well as the qualitative glacier-wide scale analysis suggested that the intensity of summer-monsoon snowfall events, together with winter precipitation and summer temperature, is one of the most important drivers controlling the B_a of Chhota Shigri Glacier. Given that the qualitative analysis at glacier scale, done using the extrapolated precipitation data from Bhuntar meteorological station which is separated by an orographic barrier; therefore, may not be the best representative of snowfalls on the glacier, needs further investigation with local precipitation data to support this analysis in the coming future.

Abstract

Some recent studies revealed that Himalayan glaciers have been shrinking at an accelerated rate since the beginning of the 21st century. However the climatic causes for this shrinkage remain unclear given that surface energy balance studies are almost nonexistent in this region. In this study, a point-scale surface energy balance analysis was performed using in-situ meteorological data from the ablation zone of Chhota Shigri Glacier over two separate periods (August 2012 to February 2013 and July to October 2013) in order to understand the response of mass balance (MB) to climatic variables. Energy balance numerical modeling provides quantification of the surface energy fluxes and identification of the factors affecting glacier MB. The model was validated by comparing the computed and observed ablation and surface temperature data. During the summer-monsoon period, net radiation was the primary component of the surface energy balance accounting for 80% of the total heat flux followed by turbulent sensible (13%), latent (5%) and conductive (2%) heat fluxes. A striking feature of the energy balance is the positive turbulent latent heat flux, suggesting re-sublimation of moist air at the glacier surface, during the summer-monsoon characterized by relatively high air temperature, high relative humidity and a continual melting surface. The impact of the Indian summer monsoon on Chhota Shigri Glacier MB has also been assessed. This analysis demonstrates that the intensity of snowfall events during the summer-monsoon plays a key role on surface albedo (melting is reduced in the case of strong snowfalls covering the glacier area), and thus is among the most important drivers controlling B_a of the glacier. The summer-monsoon air temperature, controlling the precipitation phase (rain versus snow and thus albedo), counts, indirectly, also among the most important drivers.

5.1 Introduction

Himalayan glaciers, located on Earth's highest mountain range, are source to numerous rivers that cater to the water needs of millions of people in Asia (e.g., Kaser et al., 2010; Immerzeel et al., 2013). Recent studies have reported negative MB over Himalayan glaciers (e.g., Bolch et al., 2012; Kääb et al., 2012; Gardelle et al., 2013), in line with the observation that the Himalayan glaciers (22,800 km²) have been shrinking at an accelerated rate since the beginning of the 21st century (Bolch et al., 2012). Glacial retreat and significant mass loss may not only cause natural hazards such as landslides and glacier lake outburst floods but also increase the specter of shrinking water resources in the long term (Thayyen and Gergan, 2010; Immerzeel et al., 2013).

Unfortunately, data on recent glacier changes in the Himalayan region are sparse and even sparser as we go back in time (Cogley, 2011; Bolch et al., 2012) and, thus, the rate at which these glaciers are changing remains poorly constrained (Vincent et al., 2013). The erroneous statement in the Intergovernmental Panel on Climate Change (IPCC) Fourth Assessment Report (Parry et al., 2007) about the future of the Himalayan glaciers dragged the attention of the scientific community towards the behavior of these glaciers in relation to climate. However, the IPCC Fifth Assessment Report (Stocker et al., 2013) stated *"Several studies of recent glacier velocity change (Azam et al., 2012; Heid and Kääb, 2012) and of the worldwide present-day sizes of accumulation areas (Bahr et al., 2009) indicate that the world's glaciers are out of balance with the present climate and thus committed to losing considerable mass in the future, even without further changes in climate"*. A reliable prediction of the responses of Himalayan glaciers towards future climatic change and their potential impacts on the regional population requires a sound understanding of the existing physical relationship between these glaciers and climate. This relationship can be addressed in detail by studying the glacier surface energy balance (hereafter SEB).

Comprehensive glacier SEB studies began in the early 1950s (e.g., Hoinkes, 1953) and since then our understanding of the glacier-climate relationship has substantially improved. SEB studies of the world's glaciers and ice sheets have been carried out extensively in the Alps (e.g., Klok and Oerlemans, 2002; Oerlemans and Klok, 2002), Antarctica (e.g., Favier et al., 2011; Kuipers Munneke et al., 2012), Greenland (e.g., Van den Broeke et al., 2011), and the tropics (e.g., Wagnon et al., 1999, 2001, 2003; Favier et al., 2004; Sicart et al., 2005, 2011; Nicholson et al., 2013). In High Mountain Asia, only a few studies have been carried out mainly in Tian Shan (Li et al., 2011), the Qilian mountains (Sun et al., 2014), the Tibetan Plateau (Fujita and Ageta, 2000; Yang et al., 2011; Mölg et al., 2012; Zhang et al., 2013) and the Nepalese Himalaya (Kayastha et al., 1999; Lejeune et al., 2013). Glacier SEB studies from the Indian Himalaya (covering western as well parts of central and eastern Himalaya) are not yet available. Such SEB studies are crucial because glaciers across the Himalayan range have different MB behaviors (Gardelle et al., 2013), depending on their different climatic setup. For example, glaciers in Nepal receive almost all their annual precipitation from the Indian summer monsoon (ISM), and are summer-accumulation

type glaciers (Ageta and Higuchi, 1984; Wagnon et al., 2013), while glaciers in western Himalaya receive precipitation both from the ISM in summer and from mid-latitude westerlies (MLW) in winter (Shekhar et al., 2010).

In this paper, we present a SEB analysis for Chhota Shigri Glacier, western Himalaya. This glacier is one of the best studied glaciers in Indian Himalaya in terms of MB. The first MB measurement on this glacier was performed in 1987. Unfortunately, it was abandoned in 1989 and restarted in 2002 (Ramanathan, 2011). Between 2002 and 2013, annual field measurements revealed that the glacier lost mass at a rate of -0.59 ± 0.40 m w.e. a^{-1} (Ramanathan, 2011; Azam et al., 2014a). The volume change of Chhota Shigri Glacier has also been measured between 1988 and 2010 using in-situ geodetic measurements by Vincent et al. (2013), revealing a moderate mass loss over this 2 decade-period (-3.8 ± 2.0 m w.e. corresponding to -0.17 ± 0.09 m w.e. a^{-1}). Combining the latter result with field measurements and digital elevation model differencing from satellite images, they deduced a slightly positive or near-zero MB between 1988 and 1999 ($+1.0 \pm 2.7$ m w.e. corresponding to $+0.09 \pm 0.24$ m w.e. a^{-1}). Further, Azam et al. (2014a) reconstructed B_a of Chhota Shigri Glacier between 1969 and 2012 using a degree-day approach and an accumulation model fed by long-term meteorological data recorded at Bhuntar meteorological station (~50 km south of the glacier, 1092 m a.s.l.) and discussed the MB pattern at decadal scale. They also compared the decadal timescale MBs with meteorological variables and suggested that winter precipitation and summer temperature are almost equally important drivers controlling the MB pattern of this glacier. A period of steady state between 1986 and 2000 and an accelerated mass wastage after 2000 were also defined.

Present studies on the climate sensitivity of western/Indian Himalayan glaciers either come from empirical analysis at decadal timescales (Azam et al., 2014a) or are based on basic comparison between meteorological variables and the glacier MB (Koul and Ganjoo, 2010), emphasizing the lack of physical understanding of the glacier-climate relationship in this region. Therefore, a detailed analysis of the SEB yet remains underway for the western/Indian Himalayan glaciers. Use of Automatic Weather Stations (AWSs) provides the opportunity to obtain long and continuous records of meteorological data and to study the seasonal and inter-annual variations in SEB at point locations (e.g., Oerlemans, 2000; Reijmer and Oerlemans, 2002; Mölg and Hardy, 2004). The present study is focused on the SEB analysis of Chhota Shigri Glacier, using in-situ AWS-G (located on mid-ablation area of the glacier) measurements. It involves two main objectives: (1) analysis of the glacier's micrometeorology, and (2) an analysis of the SEB components along with the change characteristic of each component so as to give an insight into the processes controlling the MB at point scale as well as glacier scale.

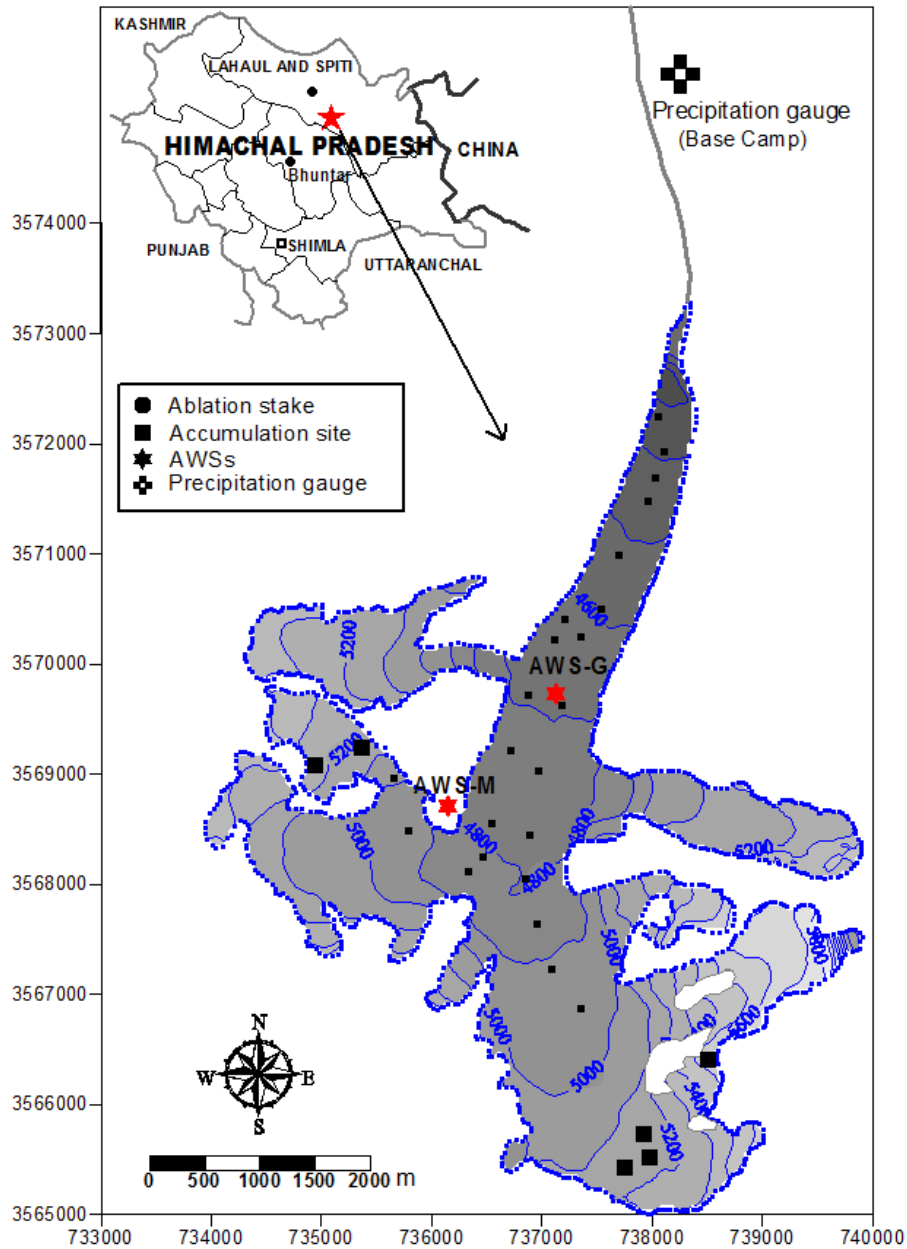


Figure 5.1. Map of Chhota Shigri Glacier showing the ablation stakes (black small squares), accumulation sites (black big squares), AWSs (red stars) and precipitation gauge (black cross). The map coordinates are in the UTM43 (north) World Geodetic System 1984 (WGS84) reference system.

5.2 Data and climatic settings

5.2.1 Study site and AWSs description

Chhota Shigri Glacier (32.28 N, 77.58 E) is a valley-type, non-surging glacier located in the Chandra-Bhaga river basin of Lahaul and Spiti valley, Pir Panjal range, western Himalaya (Fig. 5.1). It lies ~25 km (aerial distance) from the nearest town of Manali. This glacier feeds Chandra River, one of the tributaries of the Indus River system. Chhota Shigri Glacier extends from 6263

to 4050 m a.s.l. with a total length of 9 km and an area of 15.7 km² (Wagnon et al., 2007). The main orientation is north in its ablation area, but its tributaries and accumulation areas have a variety of orientations (Fig. 5.1). The lower ablation area (<4500 m a.s.l.) is covered by debris representing approximately 3.4% of the total surface area (Vincent et al., 2013). The debris layer is highly heterogeneous, from sand size to big boulders exceeding several meters. The snout is well defined, lying in a narrow valley and giving birth to a single pro-glacial stream. The equilibrium line altitude (ELA) for a zero net balance is 4960 m a.s.l. (Wagnon et al., 2007).

This glacier is located in the monsoon–arid transition zone and influenced by two different atmospheric circulation systems: the ISM during summer (July–September) and the Northern Hemisphere MLW during winter (January–April) (e.g., Bookhagen and Burbank, 2010). On Chhota Shigri Glacier, the hydrological year is defined from 1 October to 30 September of the following year (Wagnon et al., 2007). Since, the glacier sometimes experiences some melting even in October, it would have been more appropriate to start the hydrological year at the beginning of November. Nevertheless, for practical reasons (access to the glacier is impossible after mid-October) and in view of the fact that both October and November are usually characterized by a non-significant MB, starting the hydrological year at the beginning of October does not change the results.

Table 5.1. Measurement specifications for AWS-G located at 4670 m a.s.l. on the mid ablation zone of Chhota Shigri Glacier, AWS-M located on a moraine at 4863 m a.s.l., and precipitation gauge installed at base camp (3850 m a.s.l.). Accumulation/Ablation at AWS-G was measured by SR50A sensor (section 5.2.3). Variable symbols are also given. Sensor heights indicate the initial distances to the surface (12 August 2012).

Variable	symbol (unit)	Sensor	initial height (m)	stated accuracy
AWS-G				
air temperature	T_{air} (°C)	Campbell HMP155A ^a	0.8 & 2.5	±0.1 at 0 °C
relative humidity	RH (%)	Campbell HMP155A ^a	0.8 & 2.5	±1% RH at 15 °C
wind speed	u (m s ⁻¹)	A100LK, Vector Inst.	0.8 & 2.5	±0.1 m s ⁻¹ up to 10 m s ⁻¹
wind direction	WD (degree)	W200P, Vector Inst.	2.5	±2 deg
incoming and outgoing short wave radiations	SWI, SWO (W m ⁻²)	Kipp & Zonen CNR-4	1.8	±10% day total
incoming and outgoing long wave radiations	LWI, LWO (W m ⁻²)	Kipp & Zonen CNR-4	1.8	±10% day total
air pressure	P_{air} (hPa)	Young 61302V	1	±0.3 hPa
accumulation/ablation	SR50A (m)	Campbell SR50A ^b	1.6 ^c	±0.01 m or 0.4% to target
AWS-M				
air temperature	T_{air} (°C)	Campbell H3-S3-XT	1.5	±0.1 at 0 °C
relative humidity	RH (%)	Campbell H3-S3-XT	1.5	±1.5% RH at 23 °C
wind speed	u (m s ⁻¹)	Campbell 05103-10-L	3.0	±0.3 m s ⁻¹
incoming short wave radiation	SWI (W m ⁻²)	Kipp & Zonen CNR-1	2.5	±10% day total
incoming longwave radiation	LWI (W m ⁻²)	Kipp & Zonen CNR-1	2.5	±10% day total
Precipitation (base camp)	(mm)	Geonor T-200B	1.7 (inlet height)	±0.6 mm

^a aspirated during daytime with RM Young 43502 radiation shields,

^b mounted on a separate aluminum pole drilled into the ice,

^c 1.6 m was initial height for SR50A sensor

Two meteorological stations (AWS-G and AWS-M) have been operated on Chhota Shigri Glacier (Fig. 5.1). AWS-G was operated between 12 August 2012 and 4 October 2013, in the middle of ablation zone (4670 m a.s.l.) on an almost horizontal and homogeneous surface while AWS-M is located off-glacier on a western lateral moraine (4863 m a.s.l.), functioning continuously since 18 August 2009. At AWS-G and AWS-M, meteorological variables are recorded as half-hourly means with a 30 s time step, except for wind direction (half-hourly instantaneous values), and stored in a Campbell CR1000 data logger. AWS-G is equipped with a tripod standing freely on the glacier with wooden plates at the base of its legs and sinks with the melting surface. AWS-M provides pluri-annual meteorological data (from 2009 to 2013) allowing the characterization of the seasons as well as the analysis of the local climatic conditions on Chhota Shigri Glacier. Both AWS-G and AWS-M were checked and maintained every month during the summers (accessibility in winter was not possible). At the glacier base camp (3850 m a.s.l.), an all-weather precipitation gauge with a hanging weighing transducer (Geonor T-200B) has been operating continuously since 12 July 2012 (Fig. 5.1). The Geonor sensor is suitable for both solid and liquid precipitation measurements. Table 5.1 gives the list of meteorological variables used in this study, with the sensor specifications.

5.2.2 Meteorological data and corrections

Only AWS-G data were used for SEB calculations. During winter, the lower sensors (T_{air} , RH, u) were buried under heavy snowfalls on 18 January 2013, and AWS-G stopped operating completely on 11 February 2013 until 7 July 2013 when the glacier was again accessible and AWS-G could be repaired. To ensure good data quality, the period between 4 and 11 February 2013 was eliminated as this period was supposed to be influenced by near surface snow. Thus, complete data sets of 263 days in two separate periods (13 August 2012 to 3 February 2013 and 8 July to 3 October 2013) are available for analysis, except for the sensor SR50A, for which data are also missing from 8 September to 9 October 2012. The records from AWS-M have very few data gaps (0.003%, 0.29%, and 0.07% data gaps over the 4-year period for T_{air} , u and WD, respectively). These gaps were filled by linear interpolation using the adjacent data. Only one long gap exists for LWI data between 18 August 2009 and 22 May 2010.

Radiation fluxes are directly measured in the field (Table 5.1), however several corrections were applied to these data before using in the SEB model. Night values of SWI and SWO were set to zero. At high elevation sites, such as the Himalaya, measured SWO can be higher than SWI (2.6% of total data here) during the morning and evening time when the solar angle is low because of poor cosine response of the upward-looking radiation (SWI) sensor (Nicholson et al., 2013). Besides, as AWS-G was installed on the middle of the ablation area, the unstable glacier surface during the ablation season conceivably gave rise to a phase shift by mast tilt (Giesen et al., 2009). The SWO sensor mostly receives isotropic radiation and consequently is much less sensitive to measurement uncertainties of poor cosine response and mast tilt compared to the SWI sensor

(Van den Broeke et al., 2004). Therefore, SWI is calculated from SWO (raw) and accumulated albedo (α_{acc}) to avoid the impact of the phase shift because of tilting during the daily cycle of SWI and poor cosine response of the SWI sensor during the low solar angles. α_{acc} values were computed (Eq. 1) as the ratio of accumulated SWO (raw) and SWI (raw) over a time window of 24 hours centered on the moment of observation using the method described in Van den Broeke et al. (2004). The obvious shortcoming of the accumulated albedo method is the elimination of the clear-sky daily cycle in α_{acc} (Van den Broeke et al., 2004):

$$\alpha_{acc} = \frac{\sum_{24} SWO}{\sum_{24} SWI} \quad (5.1)$$

A correction has also been applied to longwave radiations as the air particles between the glacier surface and CNR-4 sensor radiate and influence LWI (underestimation of LWI at the surface) and LWO (overestimation). This generally occurs when T_{air} is higher than 0 °C during the summer-monsoon (July to September). Figure 5.2a reveals a linear relation between LWO and T_{air} above 0 °C. Measured LWO was often found to be substantially greater than 315.6 W m⁻², which is the maximum possible value for a melting glacier surface. Therefore, a correction can be done using LWO. We adopted the method described by Giesen et al. (2014) and fitted a linear function to the median values of the additional LWO (greater than 315.6 W m⁻²) for all 0.5 °C T_{air} intervals above 0 °C, assuming that the correction is zero at 0 °C. This correction was added to LWI and subtracted from LWO (Fig. 5.2b) when T_{air} was higher than 0 °C. Corrections have half-hourly values up to 22 W m⁻² for T_{air} of 11 °C. Over all half-hourly periods with T_{air} above 0 °C, the average correction was 6.3 W m⁻².

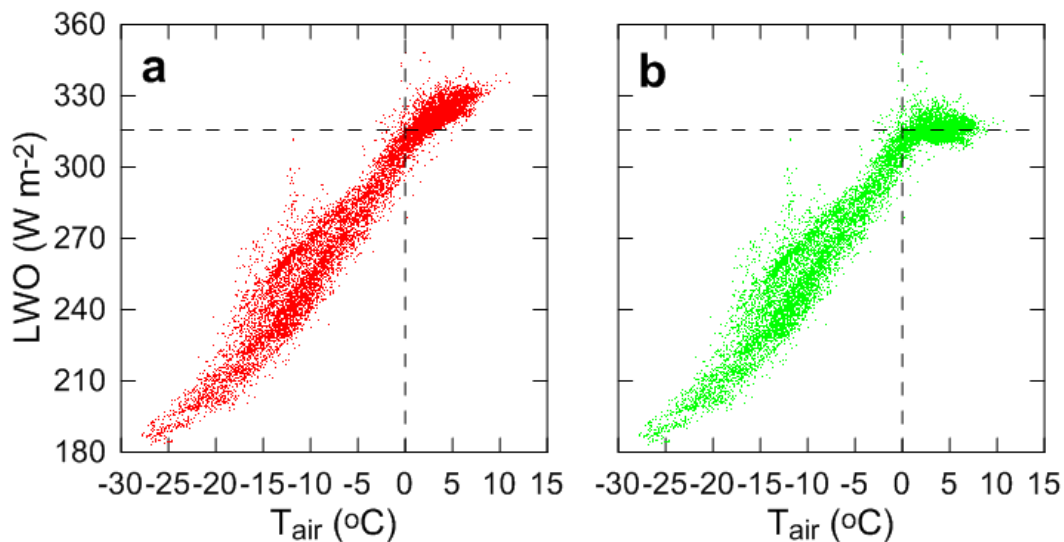


Figure 5.2. Half-hourly values of LWO as a function of T_{air} , (a) before and (b) after applying the correction for T_{air} above 0 °C. The dashed lines indicate 0 °C and 315.6 W m⁻², the maximum LWO for a melting surface.

In snow- and ice-melt models, cloud cover is investigated by computing 'cloud factors', defined as the ratio of measured and modeled clear-sky solar radiation (Greuell et al., 1997; Klok and Oerlemans, 2002; Mölg et al., 2009). In the present study cloud factor is calculated by comparing SWI with solar radiation at the top of atmosphere (STOA) according to the Eq.: cloud factor = $1.3-1.4 \cdot (\text{SWI}/\text{STOA})$ which represents a quantitative cloud cover estimate and ranges between 0 and 1. The values 1.3 (offset) and 1.4 (scale factor) were derived from a simple linear optimization process (Favier et al., 2004). The cloud factor is calculated between 11:00 and 15:00 local time (LT) to avoid the shading effect of steep valley walls during morning and evening time. The theoretical value of STOA is calculated for a horizontal plane following Iqbal (1983) and considering the solar constant equal to 1368 W m^{-2} .

5.2.3 Accumulation and ablation data

The SR50A sensor records the accumulation of snow (decreasing the sensor distance to the surface) or the melting of ice and melting or packing of snow (increasing the sensor distance from the surface) at 4670 m a.s.l. close to AWS-G (Fig. 5.3). This sensor does not involve an internal temperature sensor to correct for the variations in speed of sound as a function of T_{air} . Without this correction the measured distance may reduce during the evening, which could be misunderstood as a snowfall event (Maussion et al., 2011). Therefore, temperature corrections for the speed of sound were applied to the sensor output using T_{air} recorded at the higher level. Also, to reduce the noise, a 3-hour moving mean is applied to smooth the SR50A data. During the summer-monsoon on Chhota Shigri Glacier, sporadic snowfall events and follow-up melting may occur within hours. Therefore, the surface height variations from the 3-hour smoothed SR50A data should be calculated over a time interval long enough to detect the true height changes during the snowfalls and short enough to detect a snowfall before melting begins. Given that SR50A measurements have an uncertainty of $\pm 1 \text{ cm}$, an agreement was achieved with a 6-hour time step between smoothed SR50 data to extract surface changes greater than 1 cm.

Point MB was measured from ablation stake n° VI located at the same elevation and around 20 m south to AWS-G. Frequent measurements, with intervals of some days to a couple of weeks, were made at stake n° VI during summer expeditions. In summer 2012, three stake measurements with intervals of 10 to 15 days were performed from 8 August to 21 September 2012, while in summer 2013, six measurements with intervals of 7 to 30 days were carried out from 8 July to 3 October 2013. By subtracting the snow accumulation assessed from SR50A measurements at AWS-G (assuming a density of 200 kg m^{-3} for accumulated snow), the ablation was derived corresponding to every period between two stake measurements.



Figure 5.3. Photographs of AWS-G on Chhota Shigri Glacier taken on 09 October 2012 (left panel) and on 22 August 2013 (right panel) (copyright: Mohd. Farooq Azam). SR50A mounted on a separate pole drilled into the ice, is visible to the left of AWS-G.

5.2.4 Climatic settings

5.2.4.1 Characterization of the seasons

In this section, the meteorological conditions on Chhota Shigri Glacier, as derived from the measurements at AWS-M, are described. The Himalayan Mountains are situated in the subtropical climate zone, characterized by high annual thermal amplitude, that allows a separation into summer and winter seasons. The general circulation regime over Himalaya is controlled by the Inter-Tropical Convergence Zone (ITCZ) (Bookhagen and Burbank, 2006; 2010). Figure 5.4 shows the mean annual cycle of monthly T_{air} and RH during the four hydrological years, from 1 October 2009 to 30 September 2013, recorded at AWS-M. The standard deviations (STDs) of mean monthly measurements were 7.0 °C and 13% for T_{air} and RH, respectively, indicating that on Chhota Shigri Glacier, T_{air} and RH variations are large enough to characterize pronounced seasonal regimes. A warm summer-monsoon with high relative humidity from June to September and a cold winter season, comparatively less humid, from December to March were identified. A pre-monsoon from April to May and a post-monsoon from October to November could also be defined.

Daily mean T_{air} ranges between -22.0 and $+7.3$ °C with a mean T_{air} of -6.0 °C for the studied cycle (1 October 2009 to 30 September 2013), reflecting the high altitude of the AWS-M location (4863 m a.s.l.). The coldest month was January with a mean T_{air} of -15.8 °C and the warmest month was August with a mean T_{air} of 4.3 °C. Table 5.2 displays the mean seasonal values of all studied variables for the whole period (1 October 2009 to 30 September 2013). The summer-monsoon is warm (mean $T_{\text{air}} = 2.5$ °C) and calm (mean $u = 2.8$ m s⁻¹) with high humidity (mean RH = 68%), whereas the winter season is characterized by cold (mean $T_{\text{air}} = -13.4$ °C) and windy (mean $u = 5.5$ m s⁻¹) conditions with relatively less humidity (mean RH = 42%). The mean annual RH is 52%. An

increase (decrease) in mean monthly RH in June (October) shows the onset (end) of monsoon on Chhota Shigri Glacier. Pre-monsoon and post-monsoon seasons showed intermediate conditions for air temperature, moisture and wind speed (Table 5.2). Although the solar angle is at its annual maximum during the summer-monsoon, SWI is the highest during the pre-monsoon with a mean value of 299 W m^{-2} . The summer-monsoonal mean is 33 W m^{-2} lower than the pre-monsoonal mean because of high cloud coverage in the summer-monsoon. The comparatively low values of SWI, during the summer-monsoon, are compensated by high values of LWI (Fig. 5.4 and Table 5.2) mostly emitted from warm summer-monsoonal clouds. Post-monsoon and winter seasons are rather similar, receiving low and almost same SWI (176 and 161 W m^{-2} , respectively) and LWI (187 and 192 W m^{-2} , respectively). The low SWI and LWI values over these seasons are mainly related to the decreasing solar angle (for SWI), and low values of T_{air} , RH and cloudiness (for LWI), respectively.

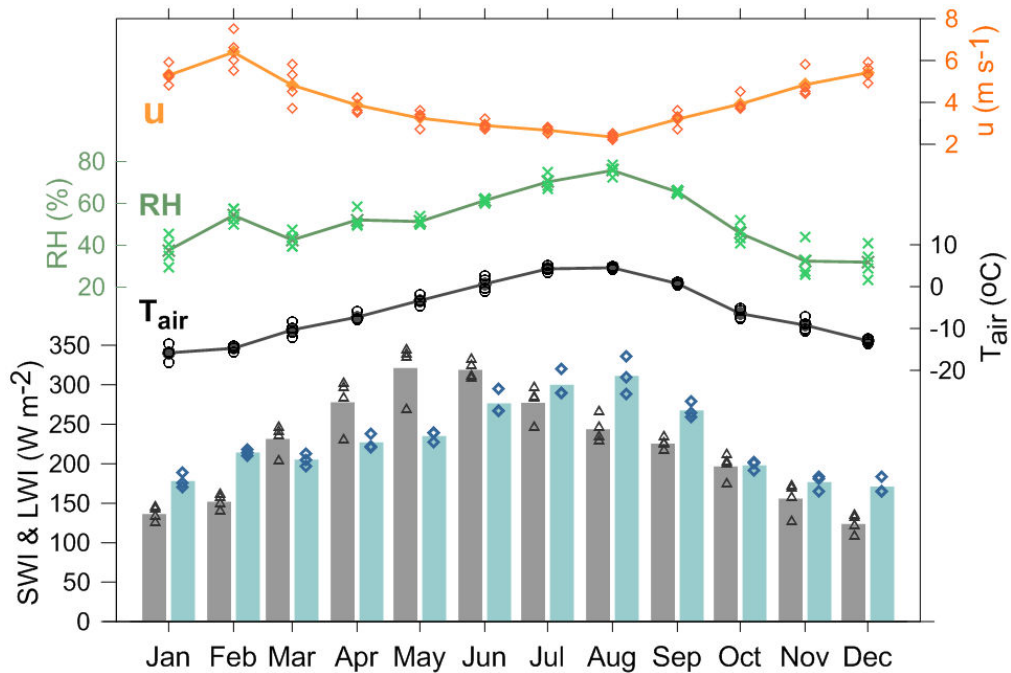


Figure 5.4. Mean monthly values of T_{air} (black dots), RH (green crosses), u (orange squares), SWI (grey bars) and LWI (light blue-green bars) at AWS-M (4863 m a.s.l.). T_{air} , RH, u and SWI are the mean monthly values of four hydrological years between 1 October 2009 and 30 September 2013 while LWI are the mean monthly values of three hydrological years between 1 October 2010 and 30 September 2013. Also shown are the monthly values of T_{air} (black circles), RH (light green crosses), u (orange hollow squares), SWI (black hollow triangles) and LWI (blue hollow squares) used to derive the mean monthly values.

Table 5.2. Seasonal means and annual mean (standard deviations) of T_{air} , RH, u and SWI over four hydrological years between 1 October 2009 and 30 September 2013 except for LWI (only three years between 1 October 2010 and 30 September 2013) at AWS-M (4863 m a.s.l.). P is the seasonal precipitation for one hydrological year between 1 October 2012 and 30 September 2013 at glacier base camp collected by the Geonor T-200B.

	Winter (DJFM)	Pre-monsoon (AM)	Summer-monsoon (JJAS)	Post-monsoon (ON)	Annual mean
T_{air} (°C)	-13.4 (0.9)	-5.3 (0.7)	2.5 (0.6)	-7.8 (1.4)	-5.8 (0.2)
RH (%)	42 (2)	52 (2)	68 (1)	39 (6)	52 (2)
u (m s ⁻¹)	5.5 (0.6)	3.5 (0.2)	2.8 (0.1)	4.4 (0.5)	4.1 (0.2)
SWI (W m ⁻²)	161 (12)	299 (34)	266 (7)	176 (18)	221 (14)
LWI (W m ⁻²)	192 (3)	231 (2)	289 (17)	187 (8)	230 (6)
P (mm w.e.)	679	148	117	32	976

5.2.4.2 Influence of ISM and MLW

The whole Himalayan range is characterized by, from west to east, the decreasing influence of the MLW and the increasing influence of the ISM (Bookhagen and Burbank, 2010), leading to distinct precipitation regimes on glaciers depending on their location.

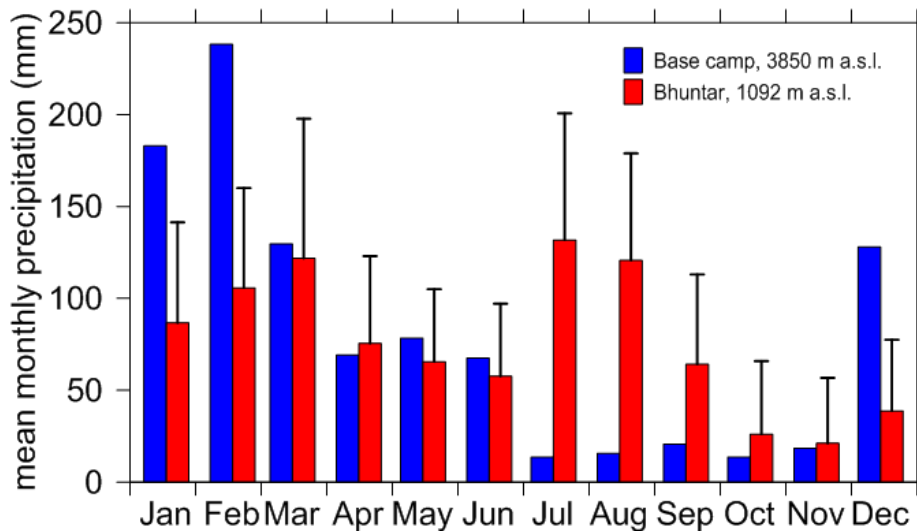


Figure 5.5. Comparison of monthly precipitations (blue bars) at Chhota Shigri base camp for 2012/13 hydrological year with the mean monthly precipitations (red bars) between 1969 and 2013 at Bhuntar meteorological station. The error bars represent the standard deviation (1σ) of the monthly precipitation mean.

Figure 5.5 shows the monthly precipitations for a complete hydrological year between 1 October 2012 and 30 September 2013 at Chhota Shigri Glacier base camp (3850 m a.s.l.) (Fig. 5.1).

Surprisingly, the months with minimum precipitation were July to November (mean value of 16 mm) and those with maximum precipitation were January and February (183 and 238 mm, respectively). For ease of understanding, Wulf et al. (2010) divided the distribution of precipitation over the same region into two periods: from May to October with precipitation predominantly coming from ISM and from November to April with precipitation coming from MLW. ISM contributed only 21% while MLW added 79% precipitation to the annual precipitation (976 mm) at Chhota Shigri base camp for the 2012/13 hydrological year. In Fig. 5.5, a comparison of 2012/13 monthly precipitation at base camp is also done with long-term (1969-2013) mean monthly precipitations at Bhuntar meteorological station, Beas Basin (Fig. 5.1). Although this station is only about 50 km (aerial distance) from Chhota Shigri Glacier, the precipitation regime is noticeably different because ISM and MLW equally contribute to the average annual precipitation (916 mm yr⁻¹). The different precipitation regimes in this region can be explained by the location of the orographic barrier which ranges between 4000 and 6600 m in elevation (Wulf et al., 2010). ISM, coming from Bay of Bengal in the southeast, is forced by the orographic barrier to ascend, enhancing the condensation and cloud formation (Bookhagen et al., 2005). Thus, it provides high precipitation on the windward side of the orographic barrier at Bhuntar meteorological station (51% of the annual precipitation) and low precipitations on its leeward side at Chhota Shigri Glacier (21% of annual precipitation). In contrast to the ISM, MLW moisture derived from the Mediterranean, Black, and Caspian seas is transported at higher tropospheric levels (Weiers, 1995). Therefore, the winter westerlies predominantly undergo orographic capture at higher elevations in the orogenic interior providing high precipitations at Chhota Shigri Glacier (79% of annual precipitation) compared to Bhuntar meteorological station on the windward side (49% of annual precipitation). Thus, Chhota Shigri Glacier seems to be a winter-accumulation type glacier receiving most of its annual precipitation during the winter season. This precipitation comparison between glacier base camp and Bhuntar meteorological station is only restricted to 2012/13 hydrological year, when precipitation records at glacier base camp are available. Long-term precipitation data at glacier site are still required to better understand the relationship between the precipitation regimes prevalent on the southern and northern slopes of Pir Panjal Range.

5.2.4.3 Representativeness of 2012/13 hydrological year

Given that long-term meteorological data at the glacier are unavailable, the representativeness of the meteorological conditions prevailing during the 2012/13 hydrological year is assessed at Bhuntar using T_{air} and precipitation data from the Bhuntar meteorological station. Figure 5.6a shows the comparison of 2012/13 T_{air} with the long-term mean between 1969 and 2013 at seasonal as well as annual scales. T_{air} in 2012/13 hydrological year was systematically higher for all seasons (0.5 °C, 0.5 °C and 0.6 °C in winter, pre-monsoon and summer-monsoon, respectively) except for post-monsoon when it was lower (0.4 °C) than the mean seasonal T_{air} over the 1969-2013 period.

At the annual scale, the 2012/13 hydrological year was 0.4 °C warmer with T_{air} close to the 75th percentile of the annual mean T_{air} between 1969 and 2013. Figure 5.6b compares the precipitation observed during the 2012/13 hydrological year with the mean over the 1969-2013 period. In the 2012/13 hydrological year, both ISM (May to October) and MLW (November to April) circulations brought an almost equal amount (49 and 51%, respectively) of precipitation at Bhuntar meteorological station. This year the ISM precipitation was equal to the mean ISM precipitation over 1969-2013 whereas MLW precipitation was 5% higher than the mean MLW precipitation over the 1969-2013 hydrological years (Fig. 5.6b); therefore, the annual precipitation for 2012/13 was found to be slightly higher (943 mm w.e.) than the mean annual precipitation (919 mm w.e.) over the 1969-2013 hydrological years. In conclusion, 2012/13 hydrological year was relatively warmer with slightly higher precipitation compared to the annual means over 1969-2013 period. Especially concerning precipitation, the 2012/13 hydrological year can be considered as an average year.

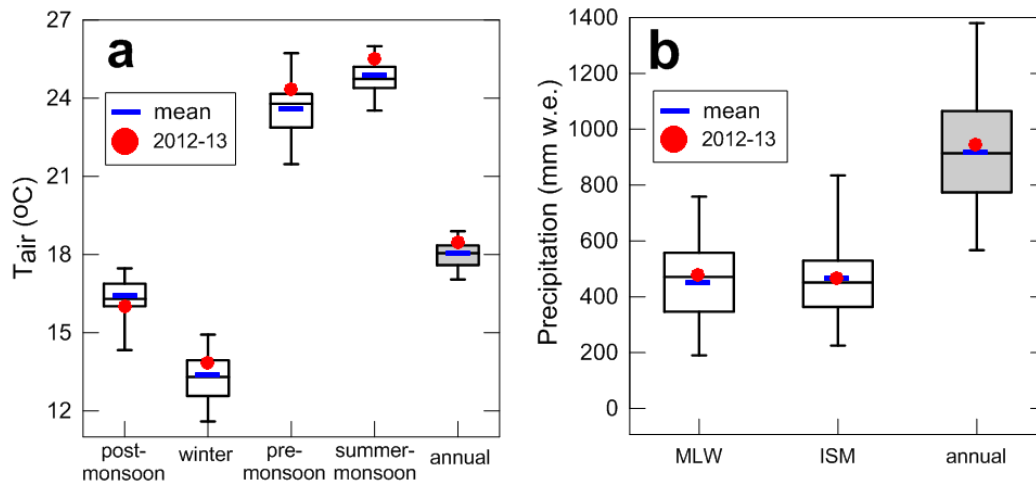


Figure 5.6. Boxplots of seasonal and annual T_{air} (a) and precipitation (b) obtained from 44 hydrological years (1969 to 2013) from Bhuntar meteorological station. Boxes cover the 25th to the 75th percentile of each distribution with a central line as the median. The blue thick horizontal line is the 1969-2013 mean, red dot is the 2012/13 hydrological year mean.

5.3 Methodology: SEB calculations

5.3.1 SEB equation

The meteorological data from AWS-G were used to derive the SEB at point scale. The incoming energy at the glacier surface ($F_{surface}$) is computed following Favier et al. (2011):

$$SWI - SWO + LWI - [(1 - \epsilon) LWI + \epsilon \sigma T_{s_mod}^4] + H + LE = F_{surface} \quad (5.2)$$

where SWI, SWO and LWI are the incident shortwave, outgoing shortwave and incoming longwave radiations, respectively and the term in square brackets is the modeled outgoing longwave radiation ($LW_{O_{mod}}$ hereafter) that was deduced from the Stefan-Boltzmann equation (ϵ is surface emissivity, assumed to be equal to 1 for snow and ice surfaces and $\sigma = 5.67 \cdot 10^{-8} \text{ W m}^{-2} \text{ K}^{-4}$ is the Stefan-Boltzmann constant) using modeled surface temperature $T_{s_{mod}}$. H and LE are the sensible and latent turbulent heat fluxes, respectively. The heat supplied by precipitation on glaciers is insignificant compared to the other fluxes (Oerlemans, 2001) and is therefore neglected here. The fluxes are assigned a positive value if directed towards the glacier surface or vice versa, except the outgoing radiation terms which are kept positive but assigned a negative sign as they are always directed away from the surface. For model validation, $T_{s_{mod}}$ was compared to the measured surface temperature ($T_{s_{obs}}$) which was derived from measured LWO using the Stefan-Boltzmann equation assuming again that the surface emissivity is unity and that it cannot exceed 273.15 K (section 5.4.3).

$F_{surface}$ is the energy available at the surface. Part of the shortwave radiation is actually not available for warming/cooling or melting processes at the surface, because a shortwave flux partially penetrates into the snow/ice. Hence, $F_{surface}$ is separated into two terms:

$$F_{surface} = G_0 + (1 - a) SWN = G_0 + SW_{sub} \quad (5.3)$$

where G_0 is the energy excess or deficit at the surface, $SWN (=SWI-SWO)$ is the net short wave radiation and SW_{sub} is the shortwave radiation penetrating in the ice. In this equation, a is the fractional amount of shortwave radiation that is absorbed in the top layer of the model (at the surface). When the modeled surface temperature, $T_{s_{mod}}$, is $0 \text{ }^\circ\text{C}$, the positive G_0 values represent the energy available for surface melt (m w.e.). Otherwise, this amount is used to cool/warm the frozen surface and underlying snow/ice, depending on its sign. If the subsurface ice/snow temperature exceeds $0 \text{ }^\circ\text{C}$, the corresponding energy excess is converted into melt to block $T_{s_{mod}}$ at $0 \text{ }^\circ\text{C}$, but liquid water is assumed to be retained in the ice. When a negative surface heat budget occurs, the subsurface temperature stays at $0 \text{ }^\circ\text{C}$ until this liquid water storage refreezes, and then temperature decreases. This is not the case for the surface layer where liquid water is assumed to run off and hence not be available for refreezing processes any more. Ablation is the sum of melt and sublimation (in m w.e.).

5.3.2 Conduction into the ice/snow

Considering that the energy conservation in the model is crucial, heat conduction (or conductive heat flux, G) into the ice/snow pack was also considered in the model. Assuming horizontal homogeneity, temperature distribution inside the ice is governed by the thermodynamic energy equation (Bintanja et al., 1997; Picard et al., 2009):

$$\rho C_{p-is} \frac{\partial T(z,t)}{\partial t} = -K_s \frac{\partial^2 T(z,t)}{\partial z^2} + \frac{\partial SW_{sub}(z,t)}{\partial z} \quad (5.4)$$

where t is the time, z is the coordinate normal to the surface (positive downward), ρ is the snow ($\rho_{snow} = 250 \text{ kg m}^{-3}$) or ice density ($\rho_{ice} = 910 \text{ kg m}^{-3}$), $T(z)$ is the ice/snow temperature at depth z , K_s is thermal conductivity, C_{p-is} is specific heat capacity of ice/snow at constant pressure, which depends on temperature [$C_{p-is}(z) = 185 + 7.037 T(z)$ (Dorsey, 1940)], and $SW_{sub}(z,t) = SWN(t)(1 - a) e^{-bz}$ is penetrated shortwave flux at depth z . Bintanja et al. (1997) suggested that a is 0.8 for blue ice and 0.9 for snow. Below the surface, the shortwave flux decreases exponentially with a constant extinction coefficient $b = 2.5 \text{ m}^{-1}$ (Bintanja et al., 1997). Distinct thermal conductivities were considered for ice ($K_{s-ice} = 2.0715 \text{ W m}^{-1} \text{ K}^{-1}$) and snow (K_{s-snow}). K_{s-snow} was computed according to Douville et al. (1995), as a function of snow density. Thermal diffusion was computed through an explicit scheme to a depth of 2 m, with a 2 cm layer resolution and a 20 s time step. Neumann limit condition was assumed at the surface (e.g., Picard et al., 2009). This boundary condition results into the following equation:

$$K_s \frac{\partial T(z,t)}{\partial z} = -F_{surface} \quad (5.5)$$

when G_0 is not used to produce surface melt; otherwise the right side of this boundary condition equation is $-SW_{sub}$. For initial conditions, we assumed that the ice was exposed (no snow at surface) and temperate (every layer was at 0°C) for both studied periods (in 2012 and in 2013).

5.3.3 Turbulent fluxes

5.3.3.1 Turbulent flux calculations

The major characteristic of katabatic flow is the wind speed maximum which is dependent on glacier size, slope, temperature, surface roughness and other forcing mechanisms (Denby and Greuell, 2000). Wind speed, T_{air} and RH were measured at two levels (0.8 and 2.5 m) at AWS-G. At AWS-G site, u at the upper level (initially at 2.5m) is always higher (99.6% of all half-hourly data) than that at the lower level (initially at 0.8m). For the turbulent heat flux calculations, the bulk method was used. Denby and Greuell (2000) showed that the bulk method gives reasonable results in the entire layer below the wind speed maximum even in katabatic wind conditions whereas the profile method severely underestimates these fluxes. In turn, the bulk method is applied in our present study as it has already been applied in various studies where katabatic winds dominate (e.g. Klok et al., 2005; Geisen et al., 2014).

The bulk method calculates the turbulent fluxes including stability correction. This method is usually used for practical purposes because it allows the estimation of the turbulent heat fluxes from one level of measurement (Arck and Scherer, 2002). In this approach, a constant gradient is assumed between the level of measurement and the surface; consequently, surface

values have to be evaluated. The stability of the surface layer is described by the bulk Richardson number, Ri_b (Eq. 5) which relates the relative effects of buoyancy to mechanical forces (e.g., Brutsaert, 1982; Moore, 1983; Oke, 1987):

$$Ri_b = \frac{g \frac{(T_{air} - T_{s_mod})}{(z - z_{0T})}}{T_{air} \left(\frac{u}{z - z_{0m}} \right)^2} = \frac{g(T_{air} - T_{s_mod})(z - z_{0m})^2}{T_{air} u^2 (z - z_{0T})} \quad (5.6)$$

where z is the level of measurements. T_{air} and u are taken from the upper level (2.5 m) that provides a longer period for investigation. The sensor heights were extracted from SR50A records except during a data gap between 8 September and 9 October 2012. Over this period sensor heights were assumed to be constant and set as 2.5 m, this being AWS-G in free-standing position. g is the acceleration of gravity ($g = 9.81 \text{ m s}^{-2}$). z_{0m} and z_{0T} are the surface roughness parameters (in m) for momentum and temperature, respectively. Assuming that local gradients of mean horizontal u , mean T_{air} and mean specific humidity q are equal to the finite differences between the measurement level and the surface, it is possible to give analytical expressions for the turbulent fluxes (e.g., Oke, 1987):

$$H = \rho \frac{C_p k^2 u (T_{air} - T_{s_mod})}{\left(\ln \frac{z}{z_{0m}} \right) \left(\ln \frac{z}{z_{0T}} \right)} (\Phi_m \Phi_h)^{-1} \quad (5.7)$$

$$LE = \rho \frac{L_s k^2 u (q - q_s)}{\left(\ln \frac{z}{z_{0m}} \right) \left(\ln \frac{z}{z_{0q}} \right)} (\Phi_m \Phi_v)^{-1} \quad (5.8)$$

where ρ is the air density (in kg m^{-3}) at 4670 m a.s.l. at AWS-G and calculated using the ideal gas equation ($\rho = \frac{P_{atm}}{R_a T}$, where R_a is the specific gas constant for dry air and P_{air} is given by the measurements and around 565 hPa). C_p is the specific heat capacity for air at constant pressure ($C_p = C_{pd} (1 + 0.84q)$ with $C_{pd} = 1005 \text{ J kg}^{-1} \text{ K}^{-1}$, the specific heat capacity for dry air at constant pressure), k is the von Karman constant ($k = 0.4$) and L_s is the latent heat of sublimation of snow or ice ($L_s = 2.834 \cdot 10^6 \text{ J kg}^{-1}$). Furthermore, q is the mean specific humidity (in g kg^{-1}) of the air at the height z and q_s is the mean specific humidity at surface. z_{0T} and z_{0q} are the surface roughness parameters for temperature and humidity, respectively. To compute turbulent fluxes (Eq. 7 and 8), it is assumed that the temperature is equal to T_{s_mod} at z_{0T} and that the air is saturated with respect to T_{s_mod} at z_{0q} . The last assumption helps to calculate surface specific humidity q_s . The non-dimensional stability functions for momentum (Φ_m), for heat (Φ_h) and moisture (Φ_v) can be expressed in terms of Ri_b (e.g., Favier et al., 2011).

$$\text{For } Ri_b \text{ positive (stable): } (\Phi_m \Phi_h)^{-1} = (\Phi_m \Phi_v)^{-1} = (1 - 5Ri_b)^2 \quad (5.9)$$

$$\text{For } Ri_b \text{ negative (unstable): } (\Phi_m \Phi_h)^{-1} = (\Phi_m \Phi_v)^{-1} = (1 - 16Ri_b)^{0.75} \quad (5.10)$$

The lower and upper limits of Ri_b were fixed at -0.40 and 0.23 , respectively beyond which all turbulence is suppressed (Denby and Greuell, 2000; Favier et al., 2011).

5.3.3.2 Roughness parameters

The aerodynamic (z_{0m}) and scalar roughness lengths (z_{0T} and z_{0q}) play a pivotal role in bulk method as the turbulent fluxes are very sensitive to the choice of these surface roughness lengths (e.g., Hock and Holmgren, 1996; Wagnon et al., 1999). In several studies (e.g., Wagnon et al., 1999; Favier et al., 2004), the surface roughness lengths were all taken to be equal ($z_{0m} = z_{0T} = z_{0q}$) and used as calibration parameters. In the present study, the z_{0m} was calculated assuming a logarithmic profile for wind speed between both the levels of measurements in neutral conditions (e.g., Moore, 1983):

$$z_{0m} = \exp\left(\frac{u_2 \ln z_1 - u_1 \ln z_2}{u_2 - u_1}\right) \quad (5.11)$$

where u_1 and u_2 are the wind velocities measured at the lower and higher levels z_1 and z_2 , respectively. For $-0.005 < Ri_b < 0.005$ (11% of our total data set, at half-hourly time step), it was assumed that conditions are neutral, and half-hourly values for z_{0m} were calculated using the Eq. (5.11). Half-hourly values of z_{0m} were assessed separately for ice and snow surfaces, based on field observations (snow-covered surface between 16/09/2012 and 17/01/2013 and ice-covered surface the rest of the time). The z_{0m} was calculated as 0.016 m (with STD of 0.026 m) and 0.001 m (0.003 m) for ice and snow surfaces, respectively. During the summer-monsoon, the surface is covered with hummocks and gullies and z_{0m} is large whereas in winter, snow covers all surface irregularities and fills up the gullies (Fig. 5.3) providing small values of z_{0m} . The ratio between roughness lengths (z_{0m}/z_{0q} and z_{0m}/z_{0T}) depends on the Reynolds number of the flow according to Andreas (1987) polynomials. For high Reynolds numbers (aerodynamically rough flows), the polynomials suggested by Smeets and Van den Broeke (2008) for hummocks were used. The respective mean values obtained for z_{0T} and z_{0q} are identical and equal to 0.004 m over rough icy surfaces, and 0.001 m over smooth snow surfaces. These values are similar to z_{0m} values for snow-smooth surfaces as already observed by Bintanja and Van den Broeke (1995) and lower for icy-rough surfaces as pointed out by many authors (e.g., Andreas, 1987; Hock and Holmgren, 1996; Meesters et al., 1997).

5.4 Results

5.4.1 Analysis of the meteorological conditions at AWS-G

In order to understand the seasonal evolution of the physical processes controlling the MB of the glacier, different representative periods for various seasons of 60 days duration were selected for

inter-seasonal comparisons, based on the meteorological conditions observed in section 5.2.4 and the available data set at AWS-G. The selected representative periods are post-monsoon (1 October 2012 to 29 November 2012), winter (1 December 2012 to 29 January 2013) and the summer-monsoon (8 July 2013 to 5 September 2013). The same length of 60 days of each representative period was chosen for justified comparison among different seasons. Unfortunately, data were not available for pre-monsoon. Measurements (T_{air} , RH, u and WD) recorded at the upper-level sensors were used for the analysis, since the records from the lower-level sensors have longer data gap because of early burial of sensors. A summary of the mean variables measured in different representative periods at AWS-G is given in Table 5.3.

Table 5.3. 60-day means (standard deviations) of meteorological and SEB variables measured or computed at AWS-G (4670 m a.s.l.) on Chhota Shigri Glacier for different representative periods. The symbols for variables are described either in the text or in Table 5.1. SWN, LWN, and R are net shortwave, longwave and all-wave radiations, respectively.

Variable	Post-monsoon (01/10/12-29/11/12)	Winter (01/12/12-29/01/13)	Summer-monsoon (08/07/13-05/09/13)
T_{air} (°C)	-8.6 (2.5)	-14.8 (3.7)	3.6 (1.2)
RH (%)	49 (12)	44 (17)	82 (5)
u (m s ⁻¹)	4.7 (0.7)	4.9 (1.1)	3.6 (0.5)
STOA (W m ⁻²)	276 (39)	216 (11)	458 (25)
SWI (W m ⁻²)	175 (46)	130 (44)	248 (67)
SWO (W m ⁻²)	127 (31)	101 (32)	47 (15)
α_{acc}	0.73 (0.04)	0.79 (0.04)	0.19 (0.02)
Cloud factor	0.28 (0.26)	0.29 (0.33)	0.36 (0.24)
LWI (W m ⁻²)	205 (23)	189 (36)	300 (20)
LWO _{mod} (W m ⁻²)	274 (9)	243 (16)	315 (1)
$T_{\text{s,mod}}$ (°C)	-9.7 (2.1)	-17.8 (4.3)	-0.2 (0.3)
SWN (W m ⁻²)	48 (17)	29 (13)	202 (53)
LWN (W m ⁻²)	-69 (19)	-54 (24)	-14 (19)
R (W m ⁻²)	-21 (19)	-25 (15)	187 (44)
H (W m ⁻²)	10 (13)	28 (23)	31 (10)
LE (W m ⁻²)	-45 (9)	-27 (11)	11 (13)
G (W m ⁻²)	1 (1)	0 (1)	4 (5)
SW _{sub} (W m ⁻²)	-10 (3)	-3 (2)	-40 (11)
$H+LE$ (W m ⁻²)	-36 (11)	1 (11)	42 (21)
F_{surface} (W m ⁻²)	-56 (16)	-24 (28)	233 (59)
Precipitation (mm w.e. d ⁻¹)	0.6 (1.0)	5.0 (8.9)	0.5 (0.9)
Snow (mm w.e. d ⁻¹)	5.3 (5.1)	6.3 (13.0)	1.4 (1.6)
Total melting (mm w.e. d ⁻¹)	0.6 (1.7)	0.0 (0.0)	61.3 (14.9)
Subl./re-subl. (mm w.e. d ⁻¹) ^a	-1.4 (0.3)	-0.8 (0.3)	0.3 (0.4)

^a negative for sublimation, positive for re-sublimation

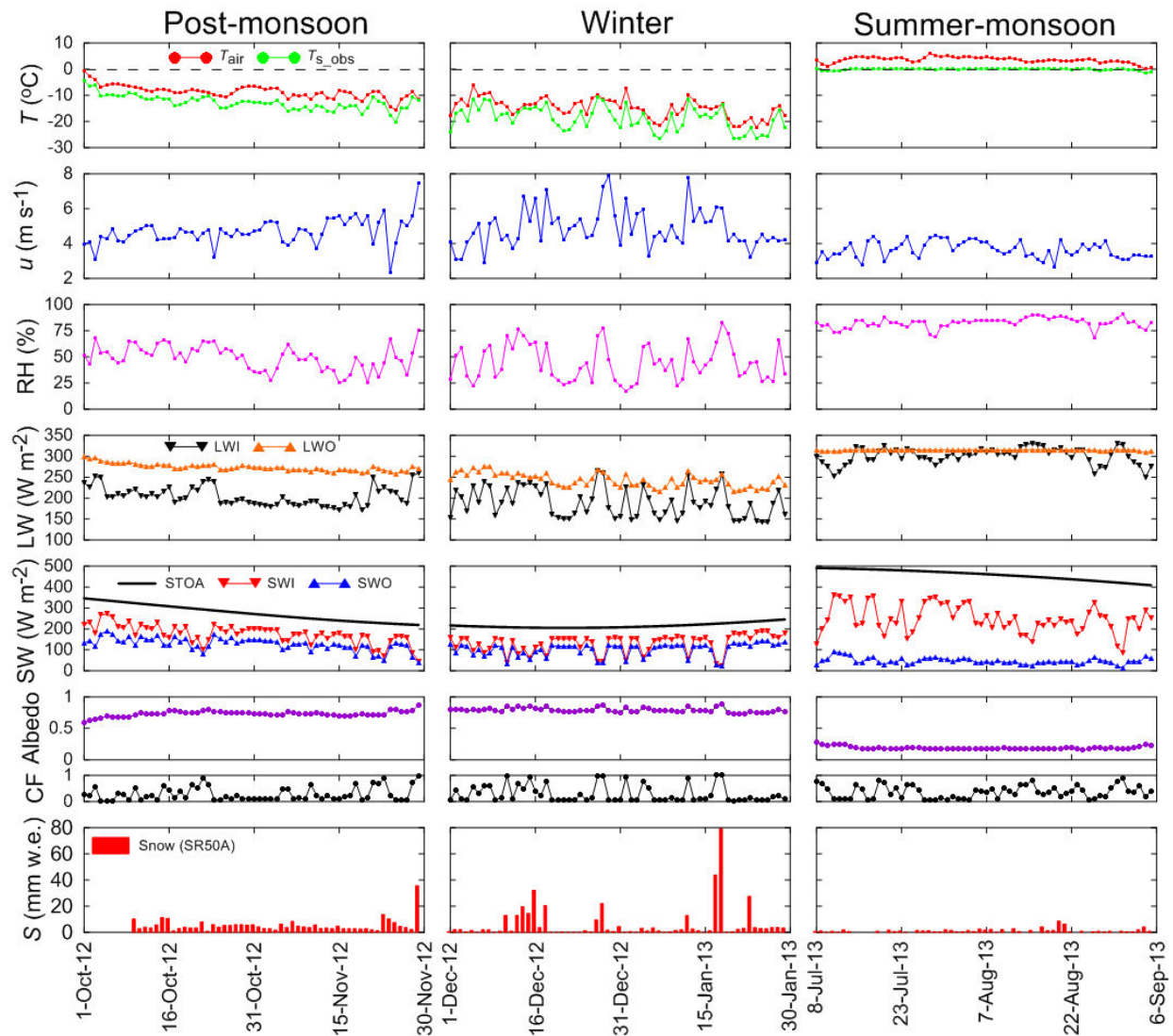


Figure 5.7. Daily meteorological variables recorded at AWS-G (4670 m a.s.l.) as representative of post-monsoon (1 October to 29 November 2012), winter (1 December to 29 January 2013) and summer-monsoon (8 July to 5 September 2013) periods. Also shown (lower panel) are the snowfalls derived from SR50A data at AWS-G.

Figure 5.7 shows the daily averages of T_{air} , u , RH, LWI, LWO, SWI, SWO, STOA, cloud factor, α_{acc} and snowfalls for all three representative periods. The meteorological variables show strong seasonality and day-to-day variability. The last panels of Fig. 5.7 represent the daily snowfall amounts (with a data gap between 1 and 8 October 2012) at AWS-G site extracted from SR50A data (by applying a fresh snow density of 200 kg m^{-3}). Post-monsoon and winter periods are cold with mean T_{air} and $T_{\text{s_obs}}$ always far below freezing point (Fig. 5.7 and Table 5.3). During the post-monsoon period mean u and α_{acc} progressively increased (mean $u = 4.7 \text{ m s}^{-1}$ and $\alpha_{\text{acc}} = 0.73$) and reached their highest values in the winter period (mean $u = 4.9 \text{ m s}^{-1}$ and $\alpha_{\text{acc}} = 0.79$). α_{acc}

remains almost constant in the winter period showing the persistent snow cover. Snowfalls in the post-monsoon period were frequent but generally very light (<10 mm w.e.), whereas the winter period received a substantial amount of snow (the heaviest snowfalls were observed on 16 December 2012, and 17, 18 January 2013 with 32, 44 and 80 mm w.e., respectively). These snowfall events are associated with high RH, α_{acc} , cloud factor and LWI values. Obviously, an abrupt decrease of SWI (consequently low SWO) is noticed during snowfall events. Most of the time, due to very cold and dry high-elevation atmosphere, LWI remains very low during both the periods, with mean values of 205 and 189 $W m^{-2}$ in post-monsoon and, respectively (Table 5.3). An analysis of Fig. 5.7 showed that overcast days with high cloud winter periods factor, high RH, increased LWI and decreased SWI are evident during all three representative periods.

The summer-monsoon period is warm and calm with relatively high humidity (Fig. 5.7 and Table 5.3). SWI is high during the summer-monsoon period (however, the maximum SWI is expected in pre-monsoon, section 5.2.4.1) with a mean value of 248 $W m^{-2}$ (Table 5.3). Most SWI (81%) is absorbed by the glacier because of the lowest values of α_{acc} (mean value = 0.19) consequently low SWO. The low and almost constant α_{acc} indicates that the glacier ice was exposed all the time. The surface remains almost continuously in melting condition, as shown by constantly maximal LWO values. Although the summer-monsoon period is characterized by the highest value of cloud factor (0.4), few snowfall events are observed from the SR50A at AWS-G site. Given that T_{air} was above freezing point, the precipitation might have occurred in the form of rain most of the time. Due to warm, humid and cloudy conditions, LWI is much higher in the summer-monsoon than during the other two studied seasons, with a mean value of 300 $W m^{-2}$ (Table 5.3).

Post-monsoon and winter periods are characterized by high wind speeds (mean u values of 4.7 and 4.9 $m s^{-1}$, respectively; Table 5.3). In the summer-monsoon period u is quite stable (STD = 0.5 $m s^{-1}$) and gusts at minimum strength with a mean value of 3.6 $m s^{-1}$. Chhota Shigri Glacier is situated in an almost north-south oriented valley and the AWS-G site is bounded by steep valley walls to the east and west (Fig 5.1). The scatter plots of u with T_{air} and WD over all of the observation periods at half-hourly timescale were plotted following [Oerlemans \(2010\)](#). Figure 5.8a mostly shows a linear relationship between T_{air} above melting point and u at AWS-G site showing that increasing u is associated with increasing near-surface T_{air} , indicative of katabatic forcing, whereas Fig. 5.8b reveals a mean down-glacier wind (WD of 200-210°) most of the time.

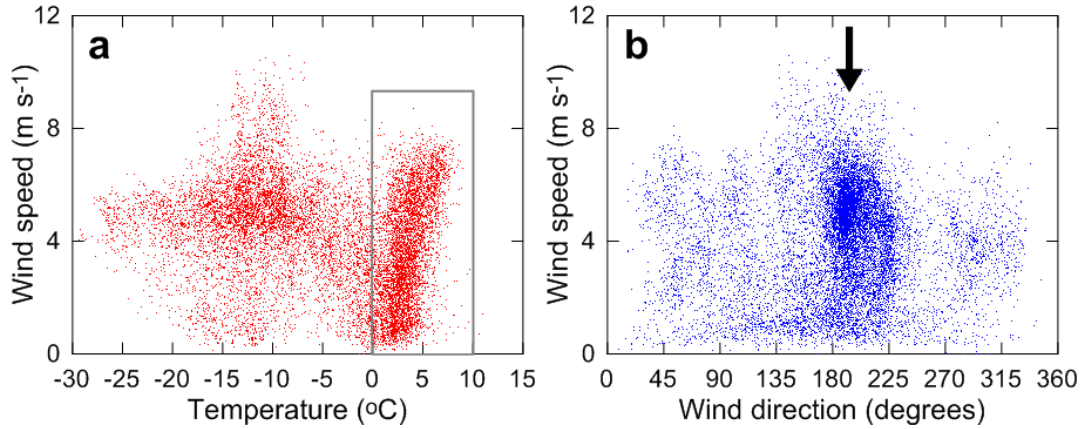


Figure 5.8. Scatter plots showing relations between u , T_{air} and WD . In both panels (a and b) all the available measurements are shown, and every dot represents a half-hourly mean value. The inset in (a) highlights the relationship between u and T_{air} above 0 °C. The arrow in (b) indicates the direction of the local flow line of the glacier.

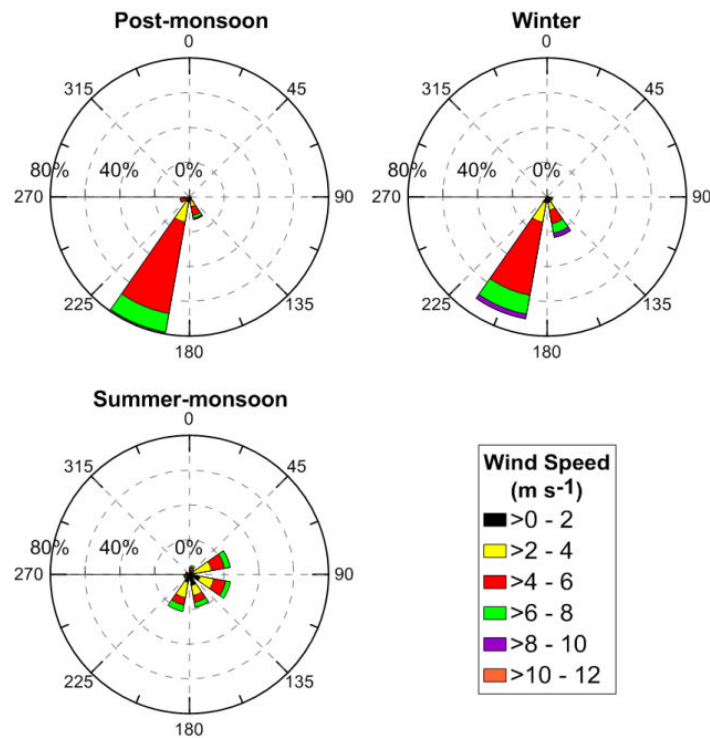


Figure 5.9. WD and u (half-hourly means) at AWS-G for post-monsoon, winter and summer-monsoon representative periods. The frequency of WD is expressed as percentage over the entire observational period (indicated on the radial axes).

Wind direction, measured at AWS-G, indicates that there is a persistent down-glacier wind coming from south to southwest (200-210°) during the post-monsoon and winter periods (Fig. 5.9). In winter, the half-hourly mean u reaches up to 10 m s⁻¹ compared to 8 m s⁻¹ in the post-monsoon period. During both post-monsoon and winter periods the glacier surface is snow covered (with high α_{acc} , Fig. 5.7) and a down-glacier wind is maintained by the negative radiation budget (section 5.4.2) of the snow surface which gives rise to cooling to the near-surface air, generating katabatic flow (Grisogono and Oerlemans, 2002). Further, on Chhota Shigri Glacier, in the summer-monsoon period the wind regime is quite remarkable. During the summer-monsoon, the down-glacier wind, coming from south to southwest (200-210°) is relatively weak and might be the result of katabatic forcing, which is typical for many valley glaciers (Van den Broeke, 1997). Occasionally, wind also tends to come from the southeast (160°), in the direction of a large hanging glacier (Fig. 5.1). The upcoming valley wind coming from the northeast (50°), blowing against the down-glacier wind, is weak at the AWS-G site and appears only during the summer-monsoon periods when the down-glacier wind is comparatively weak. As a cumulative result of upcoming valley and down-glacier winds, a wind from 110° is also observed.

AWS-G is surrounded by steep N-S valley walls. In order to analyze the impact of synoptic-scale circulation at AWS-G site, we compared the wind directions at AWS-G with those at 450 hPa pressure level obtained from High Asia Reanalysis data (HAR, Maussion et al., 2014) at hourly scale. HAR wind data are available at 10 km resolution for different pressure levels for the 2001-2012 period. The pressure level of 450 hPa (equivalent to ~6350 m a.s.l.) has been chosen as representative of the synoptic circulation above the glacier (whose highest elevation is 6263 m a.s.l.). Synoptic (HAR, 450 hPa) wind comes mainly from the west or southwest directions, depending on the season. Given that on its eastern side the glacier is bordered by a high N-S ridge (often above 6000 m a.s.l.), this synoptic wind may be deflected down to the valley providing winds parallel to the katabatic flow at AWS-G. Therefore at AWS-G site the wind coming from south to southwest is probably the result of both katabatic and synoptic effects.

5.4.2 Mean values of the SEB components

Mean SEB values for three representative periods are presented in Fig. 5.10 and are reported in Table 5.3. The results indicate that the mean seasonal net short wave radiation (SWN) is highly variable from 29 W m⁻² in winter to 202 W m⁻² in the summer-monsoon (Table 5.3). Besides the seasonal changes in sun inclination, the main reason for the seasonal variability of SWN is the contrast in surface albedo in different periods (Table 5.3). Seasonal variations in net longwave radiations (LWN=LWI-LWO_{mod}) are rather low; post-monsoon and winter periods show minimum values of LWN (mean = -69 and -54 W m⁻², respectively), while the maximum was obtained for the summer-monsoon period (mean = -14 W m⁻²) when T_{s_mod} (mean = -0.2 °C) remains close to the melting point and coincides with warm and humid conditions associated with dense cloud cover leading to high values of LWI. The net radiation heat flux R (=SWN +

LWN) was negative in post-monsoon and winter periods, giving rise to near-surface air cooling, with mean values of -21 and -25 W m^{-2} , respectively whereas in the summer-monsoon, it was the main heat source with a mean value of 187 W m^{-2} .

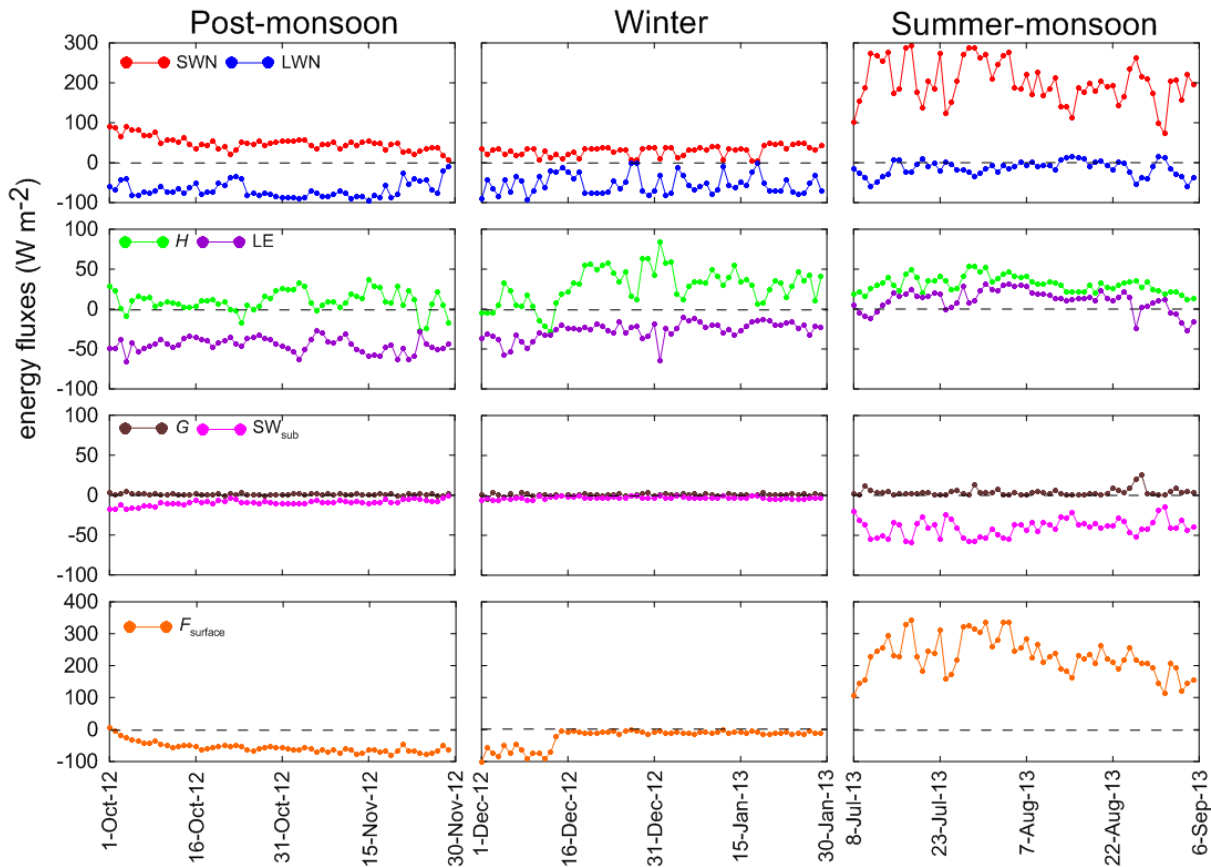


Figure 5.10. Daily values of the surface energy fluxes at AWS-G (4670 m a.s.l.) as representative of post-monsoon (1 October to 29 November 2012), winter (1 December to 29 January 2013) and summer-monsoon (8 July to 5 September 2013) periods. SWN, LWN, H , LE, G , SW_{sub} and $F_{surface}$ are the net shortwave radiation, the net longwave radiation, the turbulent sensible and latent heat fluxes, the conductive heat flux, the shortwave radiation penetrating below the surface, and the amount of energy available at the surface, respectively.

During all representative periods, the atmosphere transported heat towards the glacier surface in the form of H . The highest contribution of H (associated with the highest $T_{s,mod}$, Table 5.3) was in the summer-monsoon with a mean value of 31 W m^{-2} (Table 5.3). LE was continuously negative in post-monsoon and winter periods with mean values of -45 and -27 W m^{-2} , respectively. Therefore, the surface lost mass through sublimation (corresponding to respective mean daily rates of -1.4 and -0.8 mm w.e. d^{-1}). However, in the summer-monsoon period, a sign shift in LE from negative to positive occurred. The relatively high T_{air} and RH (Table 5.3) led to a reversal of the specific humidity gradient and therefore a positive LE for a melting valley glacier

(Oerlemans, 2000). Because of this positive LE, the glacier gained mass through condensation or re-sublimation of moist air at the surface (Table 5.3). Assuming re-sublimation as the main process, an amount of 0.3 mm w.e. d⁻¹ mass gain is calculated during the summer-monsoon period. The amount of shortwave radiation penetrating below the surface (SW_{sub}) is slightly negative during post-monsoon and winter seasons while in the summer-monsoon it was highest in agreement with the highest values of SWN. When subsurface ice layers were at 0°C, this energy amount was converted into subsurface melt occurring in the first layer of the model, leading to runoff. At daily timescale, the conductive heat flux (G) was mostly negligible except during the summer-monsoon when it was slightly positive and was responsible for a small energy gain during the night in the upper layers of the glacier, which resulted in melt when these layers were at melting point soon after sunrise.

As a result of SEB, positive melt heat flux ($F_{surface}$), with almost the same seasonal oscillation as SWN (Fig. 5.10), occurred only in the summer-monsoon period when melting conditions were prevailing all the time, leading to a mean daily melt rate of 61.3 mm w.e. d⁻¹. During the summer-monsoon period SWN accounted for 87% of the total heat flux and was the most important heat-flux component for surface melting. R was estimated as 80% of the total heat flux that was complemented with turbulent sensible, latent and conductive heat fluxes with a share of 13%, 5% and 2%, respectively. During post-monsoon period the glacier started cooling down (mean $F_{surface} = -56 \text{ W m}^{-2}$) with a little melting (mean daily rate of 0.6 mm w.e. d⁻¹) occurring during the noon hours only, when occasionally T_{s_mod} reached 0 °C, while in winter period the glacier was too cold (the highest half hourly T_{s_mod} was -4.23 °C) to experience any melting (mean $F_{surface} = -24 \text{ W m}^{-2}$).

5.4.3 Model validation

The model provides a heat transfer at half-hourly time step to the glacier superficial layers that can be turned into melt when the modeled surface temperature, T_{s_mod} , is at 0 °C. When the computed snow or ice temperature exceeds 0°C, the corresponding energy excess is also converted into melt. Subsurface melt contributes to runoff when it occurs in the first layer of the model. Another way to lose/gain mass is from sublimation/re-sublimation. The amount of sublimation/re-sublimation (m w.e.) was computed from calculated LE divided by the latent heat of sublimation ($2.834 \cdot 10^6 \text{ J kg}^{-1}$) and the density of water (1000 kg m^{-3}) when the half-hourly mean LE flux was negative/positive. During the summer-monsoon, the glacier lost mass at a daily mean melt rate of 61.3 mm w.e. d⁻¹, while a mass gain of 0.3 mm w.e. d⁻¹ was observed through re-sublimation (Table 5.3). Sublimation was negligible during the summer-monsoon.

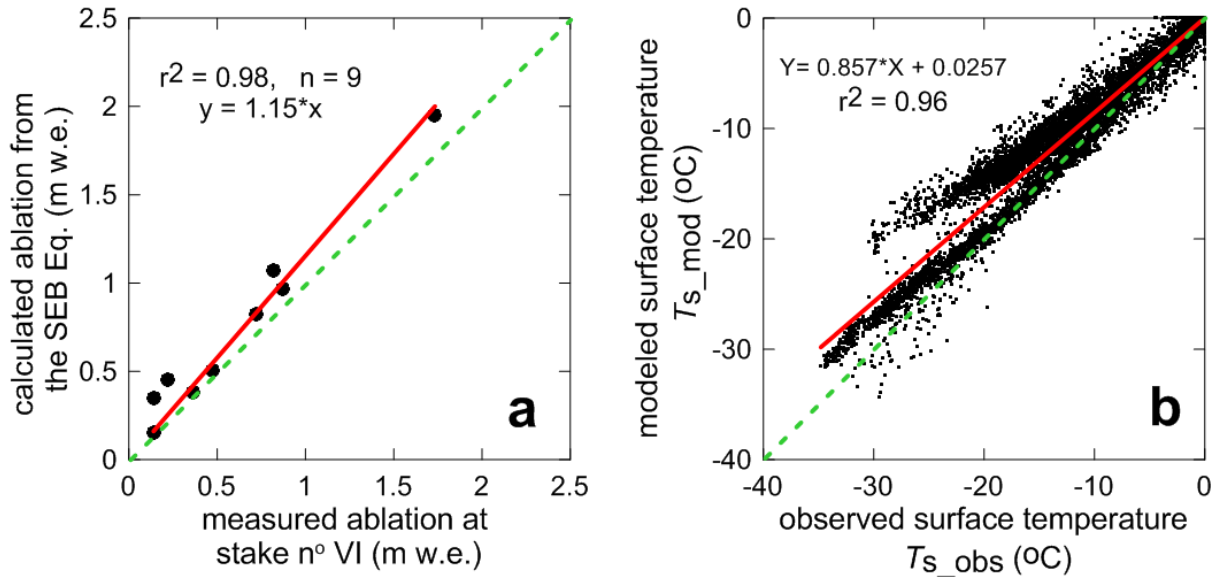


Figure 5.11. Comparison between ablation computed from the SEB Eq. and measured at stake n° VI (a) during several few-day to few-week periods of 2012 and 2013 summers where field measurements are available. (b) Comparison between modeled half-hourly (T_{s_mod}) and observed (T_{s_obs}) surface temperatures over the whole simulation period. Also shown are the 1:1 line (dashed line) and the regression line (solid line).

To validate the SEB model, computed ablation (melt + sublimation – re-sublimation) was compared with the ablation measured at stake n° VI in the field (section 5.2.3). The correlation between computed ablation from the SEB Eq. and measured ablation at stake n° VI is strong ($r^2 = 0.98$, $n = 9$ periods), indicating the robustness of the model. Although the computed ablation is 1.15 times higher than the measured one (Fig. 5.11a), this difference (15% overestimation) is acceptable given the overall uncertainty of 140 mm w.e. in stake ablation measurements (Thibert et al., 2008). Furthermore, surface temperatures at half-hourly time step (T_{s_mod}) were calculated by the model without using measured LWO (or associated surface temperatures, T_{s_obs}). Figure 5.11b shows that the half-hourly T_{s_obs} and T_{s_mod} are highly correlated ($r^2 = 0.96$), with an average difference of 1.2 °C. This temperature difference corresponds to a mean difference of 4.6 W m⁻² between LWO_{mod} and observed LWO, showing that the modeled surface heat budget is reasonably computed. Moreover, if we run the model with an additional 2-cm snow layer at the surface when measured albedo values are higher than 0.7, the mean difference between T_{s_mod} and T_{s_obs} drops to 0.2°C, showing that this difference does not come from a bad performance of the model, but from a bad estimation of the surface state (snow or ice) and thus of precipitation during low-intensity events (explaining the bi-modal scatter observed in Fig. 5.11b *i.e.* surface state correctly reproduced or not). Thus when the surface state is appropriately assessed, the model provides a good estimation of T_{s_mod} . In conclusion, given that the model is able to properly

compute surface temperature or ablation at point scale, we believe that it can reasonably calculate all the SEB fluxes.

5.4.4 Mean diurnal cycle of the meteorological variables and SEB components

The mean diurnal cycles of the meteorological variables and SEB components for all three representative periods are shown in Fig. 5.12. Mean diurnal cycles of T_{s_mod} (equivalent to LWO_{mod}) and T_{air} showed that the glacier was in freezing conditions during post-monsoon and winter periods all the time (Fig. 5.12) while in the summer-monsoon, T_{s_mod} is always at melting point in agreement with consistently positive T_{air} . Occasionally, for some days, half-hourly mean T_{air} (not shown here) may drop below freezing point during the night in the summer-monsoon and climb above freezing point during noon hours in the post-monsoon period. A wind speed maximum is observed in the afternoon hours during all the representative periods, which is consistent with T_{air} . This is a common phenomenon on valley glaciers, with u increasing in the afternoon (e.g., [Van den Broeke, 1997](#); [Greuell and Smeets, 2001](#)) as a consequence of an increased glacier wind due to a stronger T_{air} deficit in the afternoon. A wind speed minimum is observed in the morning time of post-monsoon but no reason for this could be identified.

For all the representative periods, R is negative at night (indicating longwave radiative cooling of the surface) and positive during the day time. However, during the summer-monsoon period the night values of R are slightly less negative as the radiative cooling is attenuated due to enhanced RH, T_{air} , cloudiness, and in turn high LWI. In daytime, R is much higher during the summer-monsoon than other periods, mainly because of exposed low-albedo ice at the glacier surface enhancing the absorption of solar radiation, which is already high due to annual maximum of the solar angle.

H and LE show similar daily cycles in post-monsoon and winter periods. During the night, H remains permanently high ($\sim 50 \text{ W m}^{-2}$) and starts decreasing in the morning as the surface is heated up with R (Fig. 5.12). This daily cycle of H is in agreement with the daily cycle of R_{ib} , showing stable conditions almost all day long ($R_{ib} > 0$ except 4 hours in the middle of the afternoon in winter), with very stable conditions in the night, and moderately stable during the day or even unstable in the afternoon in winter. LE is negative in the night, decreases in the morning and shows the minimum values during early afternoon hours which are in agreement with increasing wind speed and stronger vertical gradients of specific humidity in the vicinity of the surface. During the summer-monsoon, both H and LE are positive (heat supplied to the surface) and follow a similar trend, but H attains its peak approximately 2 hours before LE. H shows a peak at $\sim 14:00$ LT with positive T_{air} and wind speed maximum (Fig. 5.12) whereas LE remains close to 0 W m^{-2} until noon and increases with an afternoon wind speed maximum. The stability of the surface boundary layer is not very different from that observed during the other periods, highly stable at night, but moderately stable during the day due to the occurrence of warm up-valley

winds blowing over a melting surface in summer-monsoon. Thus, LE is positive during the summer-monsoon giving rise to re-sublimation in afternoon and early night hours.

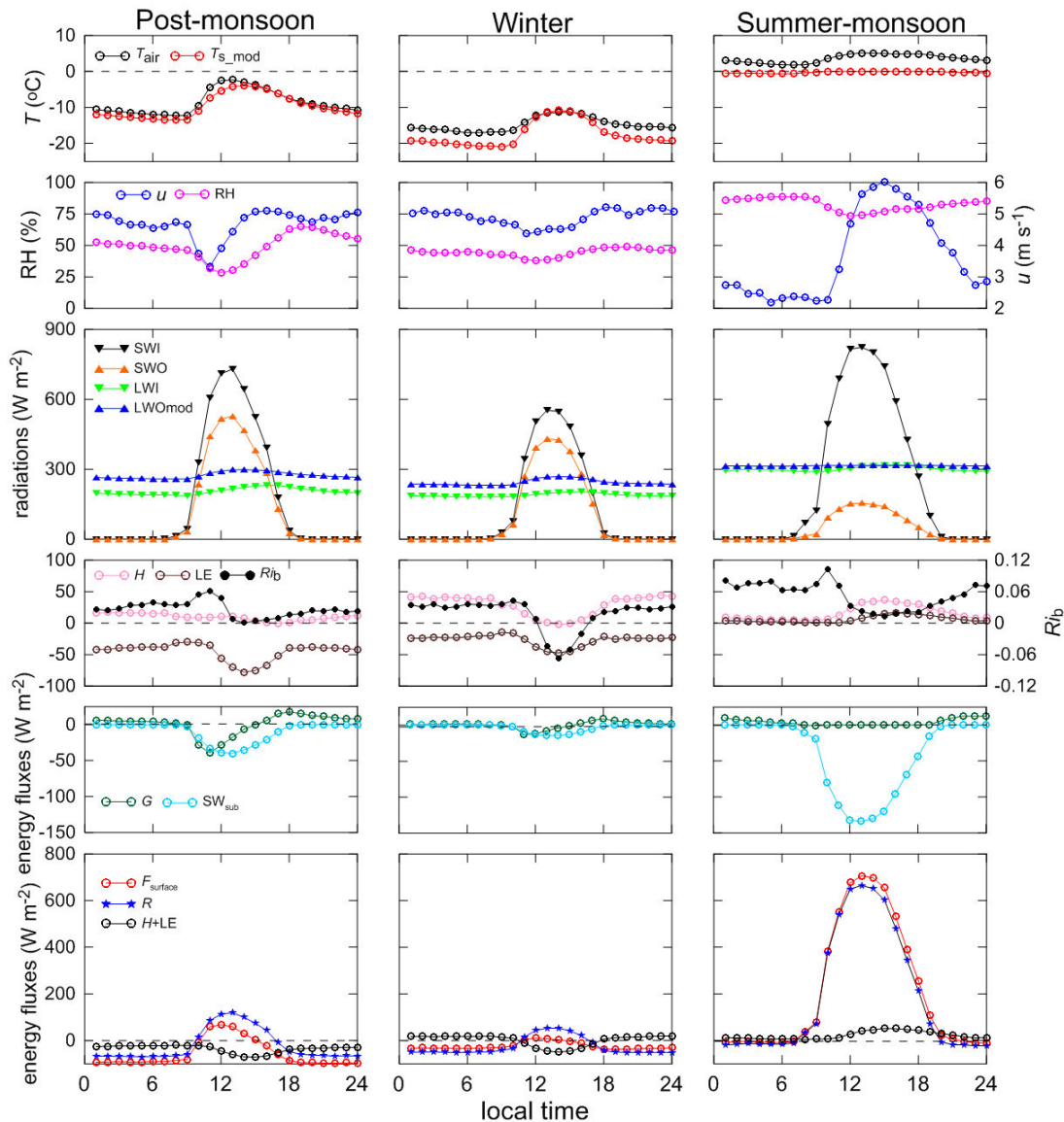


Figure 5.12. Mean diurnal cycle of meteorological and SEB variables at AWS-G (4670 m a.s.l.) as representative of post-monsoon (1 October to 29 November 2012), winter (1 December to 29 January 2013) and summer-monsoon (8 July to 5 September 2013) periods.

SW_{sub} mirrors the daily cycle of SWN but is attenuated as part of SWN is absorbed by the surface, and part is transferred to the underlying layers, following an exponential extinction. During winter and post-monsoon, negative values of G are compensated by positive values in the afternoon (after 16:00 LT, when surface temperature begins to decrease) or early night hours, leading to insignificant values of this heat flux at daily scale. During the summer-monsoon, G is

equal to zero during daytime and only positive at night when internal layers of the glacier at the melting point try to compensate the nocturnal surface cooling and thus bring energy to the surface.

During post-monsoon and winter periods, in the night, F_{surface} is negative, and a cold front penetrates into the superficial layers of the glacier. However, F_{surface} is rather low as R is mostly compensated by $H+LE$ except during noon hours when F_{surface} switches to slightly positive values. Heat is then transferred during a few hours of the day to the ice/snow pack whose temperature rises but not enough to reach melting conditions ($T_{\text{s_mod}}$ remains below 0 °C) (Fig. 5.12). During the summer-monsoon period, F_{surface} follows the diurnal cycle of R providing energy up to 710 W m⁻² to the glacier surface at around 12:00 LT. This energy is consumed for melting process as the surface is melting continuously (Fig. 5.12). Unfortunately, the data set does not cover the pre-monsoon. But during this season, the heat transferred to the glacier progressively increases as net shortwave radiation enhances in agreement with the rise in solar angle, as well as the decreasing surface albedo. This heat is first used to warm up the surface layers of the glacier until $T_{\text{s_mod}}$ reaches 0 °C, then melting starts.

5.5 Discussion

5.5.1 Control of the summer-monsoon snowfalls on melting

5.5.1.1 Comparison between 2012 and 2013 melting periods

The impact of ISM has already been analyzed on Tibetan glaciers (e.g., [Fujita and Ageta, 2000](#); [Yang et al., 2011](#); [Mölg et al., 2012 & 2014](#)) but it is still not well understood in the Himalaya. Previously, based on a degree-day approach, [Azam et al. \(2014a\)](#) suggested that winter precipitation and summer temperature are almost equally important drivers controlling the MB pattern of Chhota Shigri Glacier. Here this topic is addressed by analyzing the surface melting on Chhota Shigri Glacier with the summer-monsoon precipitations using a more detailed SEB approach. Based on the available data set, we selected the same length of the summer-monsoon period (15 August to 30 September) from 2012 and 2013 years to compare the evolution of the computed cumulative melting (Fig. 5.13). Given that the SR50A at AWS-G site has a data gap between 8 September and 9 October 2012 and that this sensor cannot record rain events, daily precipitations, collected at glacier base camp (3850 m a.s.l.), are used in this analysis. These precipitation values are extrapolated at AWS-G assuming a zero-precipitation gradient and are considered as rain (snow) at AWS-G site when T_{air} at AWS-G is above (below) 1 °C (e.g., [Wagnon et al., 2009](#)). In the summer-monsoon 2012, Chhota Shigri Glacier received one important snowfall of 25 mm w.e. (equivalent to 125 mm of fresh snow applying a density of 200 kg m⁻³) during the period 17-19 September. This snowfall abruptly changed the surface conditions by varying the surface albedo from 0.19 to 0.73 (Fig. 5.13a). Therefore, the energy F_{surface} available at the glacier surface suddenly dropped from 123 W m⁻² on 16 September to 14 W m⁻² on 17 September as shown by the sharp change in the melting rate (slope of the melting curve on Fig. 5.13a) associated with

this specific snowfall event. The effect is also evident on T_{s_mod} evolution. The daily number of hours with $T_{s_mod} > -1$ °C decreased from 24 to 6 hours and remained around this value throughout, showing that melting, which was continuous before the snowfall event, is reduced to a few hours of the day. During the summer-monsoon 2013, the situation was different as the snowfalls were more sporadic and never big enough to efficiently slow down the melting. Consequently, a shift in the slope in the melting curve is not observed as was the case in mid-September 2012. Indeed, the light snowfalls, observed from 13 to 16 September 2013 and from 24 to 30 September 2013, were only able to protect the glacier from high melting for some days but could not maintain a persistent snow cover as in mid-September 2012. Ice was again exposed at the surface as revealed by low albedo values (~ 0.38) observed again a few days after the snowfalls. Mean T_{air} and the daily number of hours with $T_{s_mod} > -1$ °C again rose up, maintaining the high melt rates. As a consequence, at point scale, although the cumulative melting between 15 August and 30 September was very similar in 2012 and 2013 (2.08 and 1.96 m w.e., respectively), the main difference comes from the distribution of the melting along the considered period. Although the melt rates in 2012 were higher than 2013 during the first 31 days, an early snowfall efficiently slowed down the melting, however it was slightly less intense but more regular in 2013.

In order to better quantify the albedo effect of the mid-September 2012 snowfalls on the glacier melting, the model was run again assuming a constant albedo ($=0.19$) over the entire 2012 summer period, all other meteorological variables being unchanged meanwhile (Fig. 5.13a). As expected, the overall melting with constant albedo is enhanced (2.44 m w.e.) with a moderate difference of 0.36 m w.e. (+17% compared to a simulation with real albedo) between 15 August and 30 September 2012, but very significant when considering only the period when the observed albedo differs from 0.19 (*i.e.* after 17 September 2012). Certainly, between 17 and 30 September, the computed melting using a constant albedo (0.19) is 0.48 m w.e., 4 times higher than that with the observed albedo (0.12 m w.e.). Even though Chhota Shigri Glacier receives maximum accumulation in winter season, this analysis highlights and quantifies the role of snowfall events during the summer-monsoon on albedo and, in turn on melting.

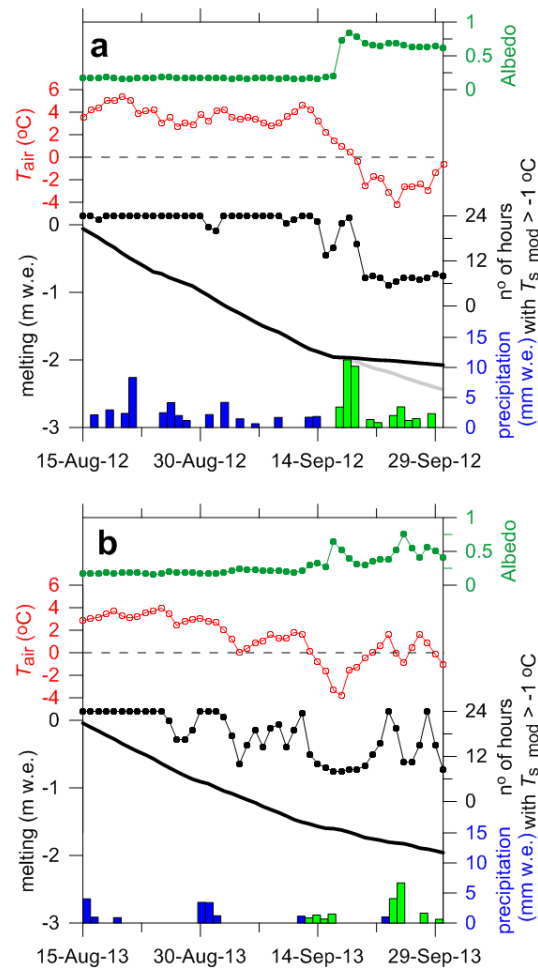


Figure 5.13. Comparison of computed cumulative melting (black thick line) between 15 August and 30 September from summers 2012 (a) and 2013 (b). Also shown are the mean T_{air} (red open dots), the number of hours in a day when T_{s_mod} is > -1 °C (black dots), daily albedo (dark green dots) and the precipitations as rain/snow obtained from records at base camp (blue and green bars, respectively). The grey line in panel (a) is the computed cumulative melting between 15 August and 30 September 2012 assuming a constant surface albedo of 0.19.

This effect has already been described in other parts of the world. [Sicart et al. \(2011\)](#) suggested that melting on Zongo Glacier, Bolivia is reduced by wet season snowfalls via the albedo effect during the melt season. In the central Tibetan Plateau, [Fujita and Ageta, \(2000\)](#), [Fujita \(2008a & 2008b\)](#) and [Zhang et al. \(2013\)](#) indicated that the glacier surface MB was closely related to the summer-monsoon precipitation seasonality and phase (snow versus rain). [Mölg et al. \(2012\)](#) analyzed the impact of ISM on Zhadang Glacier using their fully distributed SEB/MB model between 2009 and 2011 and concluded that the timing of monsoon onset leaves a clear footprint on the glacier via the albedo effect. Recently [Mölg et al. \(2014\)](#) extended this analysis at the

decadal scale and opined that the intensity of ISM onset together with MLW dynamics are important in determining the annual MB of Zhadang Glacier.

5.5.1.2 Impact of the summer-monsoon snowfalls on glacier-wide mass balance

In order to investigate the impact of the summer-monsoon snowfalls on glacier-wide MB, B_a between 2002 and 2013 were compared with the largest summer-monsoon daily snowfalls of the corresponding season. These snowfalls have been extrapolated using daily precipitation data from Bhuntar meteorological station (1092 m a.s.l.), assuming no precipitation gradient and applying the daily lapse rate between Bhuntar and glacier calculated by [Azam et al. \(2014a\)](#) with the idea that if the precipitation is in the form of snow (threshold temperature equal to 1°C) at 4400 m a.s.l. (below 4400 m a.s.l. the glacier is totally debris covered), the whole glacier is covered by summer-monsoonal snow.

The choice of using precipitation data from Bhuntar meteorological station to assess precipitation on the glacier might seem unfortunate at first glance because, as already discussed in section 5.2.4.2., both sites are separated by an orographic barrier inducing a different precipitation distribution. However, these sites are only 50 km away from each other, and we believe that meteorological conditions are not totally decoupled between the windward and the leeward side of the mountain range, especially in the case of precipitation events strong enough to cross this orographic barrier. Fortunately, [Wulf et al. \(2010\)](#) conducted a thorough study using the precipitation data of 80 stations from the Northwest Himalaya including Chhota Shigri area and concluded that in Baspa Valley (~100 km southeast to Chhota Shigri Glacier) “The two most prominent 5-day-long erosional events account for 50% of the total 5-year suspended sediment flux and coincide with synoptic scale monsoonal rainstorms. This emphasizes the erosional impact of the ISM as the main driving force for erosion processes in the orogenic interior, despite more precipitation falling during the winter season”.

The best relationship is obtained when considering the sum of the three most important daily snowfall records of the corresponding summer-monsoon (Fig. 5.14). The correlation is strong ($r^2 = 0.88$, $n = 11$ years) and suggests that the summer-monsoon snowfall events play a key role in controlling the B_a of the glacier. Such snowfalls cover the whole glacier implying that the albedo of the whole ablation area can suddenly switch from low to high values (ice to snow surfaces). Consequently, melting is abruptly reduced or even stopped at the glacier surface for several weeks or even for the rest of the ablation season that usually ends around mid-October in years without such strong summer-monsoon snowfalls. Thus, the intensity of such summer-monsoon snowfalls is among the most important drivers controlling B_a of Chhota Shigri Glacier.

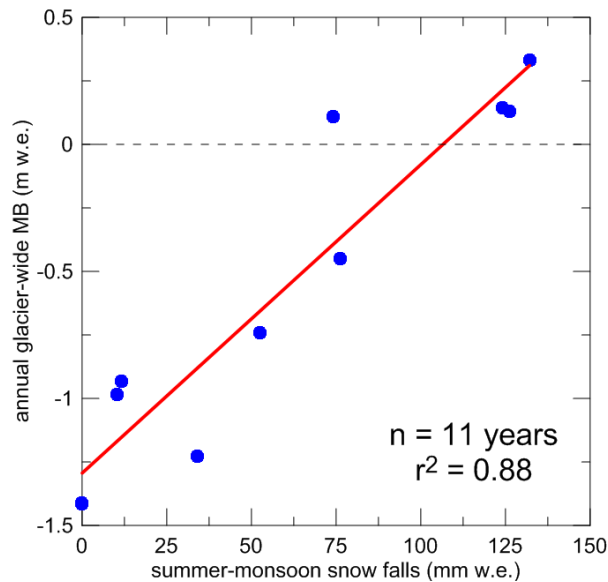


Figure 5.14. Annual glacier-wide mass balance as a function of the sum of the 3 largest summer-monsoon daily snowfalls assessed from precipitation record from Bhuntar meteorological station (see text for details) between 2002 and 2013.

Azam et al. (2014a), using a degree-day approach, showed that winter precipitation and summer temperature are equally important drivers controlling B_a of Chhota Shigri Glacier. This present analysis extends this knowledge a step further, showing that the summer-monsoon snowfalls also play an important role in controlling B_a of Chhota Shigri Glacier. Indeed, the summer-monsoon air temperature is as crucial as summer precipitation mainly because it controls the amount of rain versus snow received at the glacier surface and in turn, has an important control on glacier albedo and thus on the amount of shortwave radiation absorbed by the glacier surface, which is the main heat source for Himalayan glaciers.

5.5.2 Comparison of the SEB of Chhota Shigri Glacier with that of other glaciers in High Mountain Asia

In this section some key features of the energy fluxes responsible for the ablation on glaciers in High Mountain Asia are discussed in the light of the SEB results obtained on Chhota Shigri Glacier, as well as from some previously published studies. Table 5.4 shows an up-to-date compilation of SEB studies from High Mountain Asia glaciers coming from ablation zones of different glaciers during summer ablation periods.

Table 5.4. Comparison of SEB components on different glaciers in High Mountain Asia. All fluxes are in $W m^{-2}$, Values in brackets are the % contribution of each energy flux.

Glacier	Altitude (m a.s.l.)	Region (ISM dominated, Y or N)	Period of observation	R ($W m^{-2}$)	H ($W m^{-2}$)	LE ($W m^{-2}$)	Rest ($W m^{-2}$)	$F_{surface}$ ($W m^{-2}$)	Reference
Glacier AX010	4960	central Himalaya, Nepal (Y)	25 May- 25 Sep 1978	64 (85)	8 (10)	4 (5)	n/a	74 (100)	Kayastha et al., 1999
Glacier AX010	5080	central Himalaya, Nepal (Y)	25 May- 25 Sep 1978	55 (83)	8(12)	3 (5)	n/a	63 (100)	Kayastha et al., 1999
Xixibangma	5700	south central TP ^a (N)	23 Aug- 11 Sep 1991	28 (200)	5(33)	-19 (133)	n/a	14(100)	Aizen et al., 2002
Parlung No. 4	4800	southeast TP (Y)	21 May- 8 Sep 2009	150 (86)	28 (16)	-1 (1)	-1 (1)	176 (100)	Yang et al., 2011
Zhadang	5660	central TP (N)	1 May - 30 Sep 2010	62 (103)	10 (17)	-8 (13)	-4 (7)	61 (100)	Zhang et al., 2013
Zhadang	5660	central TP (N)	1 May - 15 Sep 2011	27 (117)	8 (35)	-10 (43)	-2 (9)	23 (100)	Zhang et al., 2013
Keqicar	4265	southwest Tianshan (N)	16 June-7 Sep 2005 ^b	63 (274)	14 (61)	-54 (235)	n/a	23 (100)	Li et al., 2011
Laohugou No. 12	4550	western Qilian, China (N)	1 June-30 Sep 2011	81 (108)	7 (9)	-13 (17)	n/a	75 (100)	Sun et al., 2014
Chhota Shigri	4670	western Himalaya, India (Y)	8 July-5 Sep 2013	187 (80)	31 (13)	11 (5)	4(2)	230 (100)	Present study

^aTP = Tibetan Plateau, ^bwith a gap of 1 July to 7 Aug 2005, n/a = not available

As already highlighted on High Mountain Asia glaciers (Yang et al., 2011; Mölg et al., 2012; Zhang et al., 2013; Sun et al., 2014), the present study also showed that SWN is the largest source of energy to the glacier surface and mainly controls the temporal variability of melting, whereas LWN is the greatest energy loss moderate during the summer-monsoon when $LW_{O_{mod}}$ is almost compensated by maximum LWI due to warm, humid and cloudy atmosphere, and high during the rest of the year when LWI reaches minimum values (Fig. 5.10 and Table 5.3). SWN is inversely dependent on surface albedo. At AWS-G site on Chhota Shigri Glacier, during the summer-monsoon period, precipitation often occurs in liquid form and surface albedo is relatively constant (Fig. 5.7). During such conditions SWN is driven by cloud factor (Fig. 5.7). However when precipitation occurs in solid phase (Fig. 5.13), the surface albedo abruptly changes and controls the SWN and in turn, melting. The sum of SWN and LWN, R , provides >80% energy flux to the glacier surface during the summer-monsoon for all High Mountain Asia glaciers (Table 5.4).

All the studied sites, described in Table 5.4, are on the debris-free ablation area. A negative contribution (in %) is assigned to negative heat fluxes in order to have the resulting flux $F_{surface}$ equal to 100%. Sensible turbulent heat flux is always positive and provides energy to the glacier surface, complementing net radiation flux. However, its contribution to R ranges from 7% on Laohugou Glacier No. 12, western Qilian, China, to the maximum of 23% on Zhadang Glacier, central Tibetan Plateau over the corresponding observation periods (Table 5.4). During the summer-monsoon, LE is positive on Chhota Shigri Glacier due to warm and humid air at the glacier surface, giving rise to re-sublimation at the surface. This phenomenon has already been observed on AX010 Glacier located in an ISM-dominated region, central Himalaya, Nepal, where Kayastha et al. (1999) measured a positive LE between 25 May and 25 September 1978 in the ablation area. On Parlung Glacier No. 4, Southeast Tibetan Plateau, however, the mean LE was slightly negative from 21 May to 8 September 2009 (Table 5.4), while it was continuously positive with a mean value of 8 W m^{-2} during the core summer-monsoon between 25 June and 21 August 2009 because of the considerably high temperature and relative humidity associated with the summer-monsoon circulation over this period (Table 2 in Yang et al., 2011). Conversely, in the central Tibetan Plateau, where dry conditions prevail, on Zhadang Glacier, LE is continuously negative at the monthly scale (Mölg et al., 2012) but at daily timescale it was slightly positive during the core monsoon for a few days when the air temperature and relative humidity were the highest (Fig. 2 and 5 in Zhang et al., 2013). Sun et al. (2014) also showed that on Laohugou Glacier No. 12, western Qilian Mountains, LE is negative throughout the summer season (1 June to 30 September 2011), and rarely becomes positive (only on 2 and 3 July). Similarly on Xixibangma Glacier, south central Tibetan Plateau, and Keqicar Glacier, Southwest Tianshan, LE was found to be negative during the observation period, indicating sublimation. From the present analysis (Table 5.4), it can be surmised that, on High Mountain Asia glaciers, sublimation predominates in the summer-monsoon over the ablation zone of the glaciers that are less affected

by the ISM and submitted to drier conditions than those directly affected like Chhota Shigri Glacier, where LE brings a significant amount of energy at the glacier surface, in the form of re-sublimation. The conductive heat flux is most of the time negligible compared to the other terms of the SEB, even during the summer-monsoon where it slightly contributed to melt.

5.6 Conclusion

In the Indian Himalaya where meteorological observations are short and scarce, the meteorological data set recorded since August 2009 at 4863 m a.s.l. on a lateral moraine of Chhota Shigri Glacier (AWS-M) is one of the longest ever recorded data sets at high elevation. Mean monthly meteorological conditions at AWS-M show large month-to-month variability. A warm and calm summer-monsoon with high relative humidity from June to September and a cold and windy winter season with comparatively less humidity from December to March were identified. A pre-monsoon from April to May and a post-monsoon from October to November with intermediate conditions were also defined. Precipitation records at glacier base camp suggest that Chhota Shigri Glacier receives maximum seems to be a winter accumulation type glacier receiving around 80% of its annual precipitation from MLW in winter and 20% from ISM; but longer precipitation records at glacier site are still needed to confirm this feature.

A physically based energy balance experiment, using a model computing surface and subsurface heat fluxes, was carried out to understand the melting processes on Chhota Shigri Glacier based on the forcing data over two separate periods from 13 August 2012 to 3 February 2013 and from 8 July to 3 October 2013 recorded at an in-situ meteorological station (AWS-G, 4670 m a.s.l.) in the ablation zone. The roughness length for momentum was calculated separately for ice and snow surfaces as 0.016 m and 0.001 m, respectively whereas roughness lengths for temperature and humidity were derived from the Reynolds number and the roughness length for momentum. Net short wave radiation was highly variable with the lowest mean value (29 W m^{-2}) in winter to the highest (202 W m^{-2}) in the summer-monsoon period, while net longwave radiation exerted lower seasonality with minimum values in post-monsoon and winter periods (-69 and -54 W m^{-2} , respectively) and maximum in the summer-monsoon period (-14 W m^{-2}). During the summer-monsoon period the melting conditions with high T_{s_mod} (mean = $-0.2 \text{ }^{\circ}\text{C}$) coincides with warm and humid conditions, associated with intense cloud covers, leading to high values of LWI and thus high net longwave radiation is observed. Net all-wave radiation was negative in post-monsoon and winter periods, indicative of radiative cooling of the glacier surface, whereas in the summer-monsoon, it was the main heat source for melting. Through the entire observation period, the atmosphere transported heat towards the glacier surface in the form of sensible heat flux. An interesting feature observed in latent heat flux evolution was it being continuously negative in post-monsoon and winter periods, indicating predominantly sublimation; while in the summer-monsoon period, it switched to positive values indicating re-sublimation at the glacier surface. The result from the SEB equation suggests that energy was

available for melting in the summer-monsoon period only. Net all-wave radiation was the main heat flux towards surface with 80% contribution while H , LE and G shared 13%, 5% and 2% of total heat flux, respectively.

This study highlights the impact of the summer-monsoon snowfalls on glacier MB. Snowfall events during the summer-monsoon play an important role on melting via surface albedo. The intensity of these snowfalls during ablation period abruptly changes the surface conditions from ice to snow, slowing down the melting rates. Therefore, these snowfall events are among the most important drivers controlling B_a of Chhota Shigri Glacier. The summer-monsoon air temperature, controlling the precipitation phase (rain versus snow and thus albedo), also counts indirectly, among the most important drivers for the glacier MB.

A comparison of the SEB measured at the ablation zone of Chhota Shigri Glacier with those of other glaciers in High Mountain Asia shows that net short wave radiation flux is the largest energy source and mainly controls the melt energy to the glacier surface whereas net longwave radiation flux is the greatest energy loss. In High Mountain Asia, sublimation predominates in the summer-monsoon over the ablation zone of the glaciers less affected by the ISM and submitted to drier conditions than those directly affected like Chhota Shigri Glacier, where LE brings a significant amount of energy at the glacier surface in the form of re-sublimation.

The good validation of the present model (comparison between modeled and observed ablation and surface temperature data) indicates that the model is reliable enough to make robust calculations of surface energy balance. In the future, this study would be useful to calibrate spatially distributed energy- and mass-balance models at glacier as well as regional scale. These models can be used to predict the future of water supply using different climate change projections.

Acknowledgements. This work has been supported by IRD as a part of M F Azam's PhD. Authors are also grateful to DST-IFCPAR/CEFIPRA project no. 3900-W1, the French Service d'Observation GLACIOCLIM as well as the Department of Science and Technology (DST), Government of India. We thank the Indian meteorological Department (IMD), New Delhi India for providing the data from Bhuntar meteorological station. We thank Jawaharlal Nehru University, New Delhi for providing all the facilities to carry out this work. M F Azam is grateful to Dr. Rajdeep Singh for improving the content of the paper, Mr. Romain Biron for sharing his knowledge and experience about AWS assembling and Dr. Fabien Maussion for his kind help to provide the High Asia Reanalysis data. We are also grateful to the two anonymous referees, whose thorough comments significantly improved the paper as well as Dr. Mauri Pelto, Dr. Thomas Mölg, Dr. Koji Fujita and one anonymous reviewer for providing constructive comments and suggestions.

CHAPTER 6

General conclusions and perspectives

In the Hindu-Kush Karakoram Himalaya (HKH), the historical knowledge of the glaciers primarily comes from the snout fluctuation records. In-situ glaciological mass balance measurements are available for a limited number of glaciers (22 glaciers covering only ~110 km² out of 40,800 km² of glacierized area of the HKH region) and generally come from the last four decades. The developments in remote sensing techniques significantly improved our knowledge of the region-wide glacier mass changes in the HKH region. These region-wide mass changes, generally limited to the last decade, revealed a contrasting pattern of glacier mass change over the entire HKH region, depending on the climatic settings of these ranges. From east to west, increasingly negative region-wide glacier mass changes were observed in the Himalaya, whereas to the west in the Karakoram a slight mass gain or balanced mass budget were reported between 1999 and 2011. Unfortunately these geodetic mass changes do not allow us to analyze the accumulation and ablation terms, which are directly related to climatic variables. Besides, the meteorological data from glacier altitudes are scarce making it difficult to understand the glacier-climate relationship or the physical processes governing the melting of the large glacierized areas of the HKH region.

In this present study, Chhota Shigri Glacier was chosen to analyze the sensitivity of its mass balance to climate change and to understand which meteorological variables drive the mass balance of the glaciers in the western Himalayan region. The meteorological dataset recorded at Automatic Weather Station (AWS-M, 4863 m a.s.l. on a western moraine) since 2009 was used to characterize the seasons on Chhota Shigri Glacier. A warm summer-monsoon with high humidity from June to September and a cold winter season, relatively less humid, from December to March were identified. A pre-monsoon from April to May and a post-monsoon from October to November were also demarcated. The meteorological variables suggested a clear onset of the monsoon in June and the sharp decline in September on Chhota Shigri Glacier. The one year (1 October 2012 to 30 September 2013) precipitation record at glacier base camp suggested that the maximum precipitation (71% of the total annual precipitation) was received during the winter season whereas post-monsoon received the minimum precipitation (3% of the annual amount). The contributions of the pre-monsoon and summer-monsoon to annual precipitation were only 15% and 12%, respectively.

In reality, the field observations are challenging because of remoteness and difficult access to the glaciers in the HKH region. Consequently, the glaciers have never been monitored on a

long term basis and the longest available mass balance series (eleven years) is for Chhota Shigri Glacier, Lahaul and Spiti Valley (western Himalaya). Chhota Shigri Glacier experienced mass wastage with a cumulative glacier-wide mass balance of -6.45 m w.e. and a mean annual glacier-wide mass balance of -0.59 ± 0.40 m w.e. a^{-1} between 2002 and 2013. The negative mean glacier-wide mass balance revealed strong unsteady-state conditions since 2002. During the period 1999 to 2004, the satellite derived geodetic glacier-wide mass balance was approximately -1.02 m w.e. a^{-1} ; therefore, the unsteady-state conditions can be extended back to 1999. In the present as well as previous studies, the annual mass balance calculations of Chhota Shigri Glacier since 2002 have been performed using 2004/2005 glacier area; thus some errors associated with the surface area change are obviously inherited in the mass balances. Besides, this series may also has some systematic biases similar to any other glaciological mass balance series. Thanks to latest Pléiades image of Chhota Shigri Glacier, one of our colleagues Etienne Berthier is going to calculate the geodetic mass balance between 2004 and 2014. The geodetic results will be available by the end of this year and will be used to reanalyze the glaciological annual mass balances.

The lower ablation area (<4500 m a.s.l.) of Chhota Shigri Glacier is highly debris covered and lies in a deep-narrow valley reducing the ablation by $2-3$ m w.e. a^{-1} despite the low altitude. In the main ablation zone of the glacier, between 4400 and 5200 m a.s.l., the mean vertical annual mass balance gradient of 0.66 m w.e. $(100\text{m})^{-1}$ over 2002-2013 period was similar to those observed in the Alps, Nepalese Himalaya and other mid-latitude glaciers. Equilibrium line altitude for a zero glacier-wide mass balance was calculated as 4950 m a.s.l. corresponding to an accumulation area ratio of 62% between 2002 and 2013. The analysis of the seasonal glacier-wide mass balances since 2009 with the air temperature collected at off-glacier AWS-M and precipitation obtained from Bhuntar meteorological station suggested that the intensity of summer snowfall events controls the annual glacier-wide mass balance evolution by controlling the summer glacier-wide mass balances. This analysis, conducted over 4 years only, needs to be strengthened with long term analyses between seasonal glacier-wide mass balances and meteorological variables. Besides, field measurements are very limited in the HKH region and Chhota Shigri Glacier is a representative glacier in the Lahaul and Spiti Valley (2110 km²), western Himalaya; therefore, the seasonal and annual mass balance observations on this glacier must be continued in the future in spite of the challenges involved.

In October 2009, Ground Penetrating Radar (GPR) surveys at five different cross sections on Chhota Shigri Glacier confirmed that the ice thicknesses obtained by gravimetric method in 1989 were almost two fold underestimated. These ice thicknesses together with surface ice velocity measurements of 2003/04 provided the kinematic ice flux at each cross section. In contrast to the unsteady-state conditions revealed from negative mass balances since 1999, the kinematic fluxes corresponding to 2003/04 year were close to the theoretical ice fluxes calculated from the mass balance method assuming the glacier to be in equilibrium. This ice flux comparison proposed that the dynamic behaviour of the glacier in 2003/04 was representative of steady-state

conditions suggesting that during one or two decades preceding 2003/04, the glacier was in steady-state. In 2003/2004, the ice fluxes had not adjusted yet to the negative mass balances observed since 1999 but in-situ observations of decreasing surface velocities or thinning of the glacier between 2003/04 and 2009/10 suggested that the glacier was progressively adjusting to the last-decade negative mass balances. This analysis was also supported by the similar ice velocities measured in 1987/88 and in 2003/04 as well as the limited terminus retreat of 7 m a^{-1} between 1988 and 2010 suggesting that the dynamic behaviour did not change much between 1988 and 2010. Although some adjustments had been observed since 2004, but the dynamic behaviour of this glacier was far from the glacier-wide mass balance and climatic conditions between 2002 and 2010, and hence an accelerated thinning as well as a large terminus retreat are expected in the coming decades.

Since October 2009, the annual thickness measurements on ~12 cross sections, including 5 GPR cross sections over the ablation and lower accumulation areas have been conducted. Besides, during 2011-2013 an additional dense network of stakes was set up on the longitudinal center line of the glacier in order to compare the annual velocity changes at the same points from year to year. Hence it is recommended to continue these measurements in the future. These GPR, thickness and surface velocity change data can be used either in the detailed ice flow models or in simplified thickness change parameterized models in order to understand the past glacier fluctuations and to validate the past mass balance reconstruction on Chhota Shigri Glacier. Moreover, with the different climatic scenarios the future thinning and snout retreat can also be predicted. Indeed such analysis will give an opportunity to understand how the dynamics of Chhota Shigri Glacier is adjusting with the cumulative mass wastage.

The annual and seasonal glacier-wide mass balances of Chhota Shigri Glacier were reconstructed between 1969 and 2012 applying a degree-day model together with an accumulation model fed by long-term meteorological data recorded at Bhuntar meteorological station (~50 km south of the glacier, 1092 m a.s.l.). This reconstruction allowed us to examine the mass balances since 1969. A period of steady-state between 1986 and 2000 sandwiched between a moderate mass loss period (between 1969 and 1985) and an accelerated mass wastage period (between 2001 and 2012) was defined. The respective mean mass balances for these 3 periods were $-0.36 \pm 0.36 \text{ m w.e. a}^{-1}$ (1969-85), $-0.01 \pm 0.36 \text{ m w.e. a}^{-1}$ (1986-2000) and $-0.57 \pm 0.36 \text{ m w.e. a}^{-1}$ (2001-12) corresponding to a moderate mean mass wastage at a rate of $-0.30 \pm 0.36 \text{ m w.e. a}^{-1}$ over the 1969–2012 period. This reconstructed mass balance series not only re-confirmed the steady-state of Chhota Shigri Glacier already inferred by the ice flux analysis and proved by [Vincent et al. \(2013\)](#) but also defined the exact period of steady-state. The steady-state period between 1986 and 2000 was characterized by 56 mm a^{-1} higher winter precipitation and $0.2 \text{ }^{\circ}\text{C}$ lower summer mean temperature than 1969–2012 averages, resulting in roughly equal winter and summer mass balances. This analysis of decadal scale mass balances with meteorological variables suggested that winter precipitation and summer temperature are almost equally important drivers

controlling the mass balance pattern of this glacier. The sensitivity of the reconstructed annual glacier-wide mass balance of Chhota Shigri Glacier to precipitation was $0.16 \text{ m w.e. a}^{-1}$ for a 10% change and to temperature is $-0.52 \text{ m w.e. a}^{-1} \text{ }^{\circ}\text{C}^{-1}$.

In August 2012, an in-situ meteorological station (AWS-G) was installed on the ablation zone (4670 m a.s.l.) of Chhota Shigri Glacier. Using the data from this station, a physically-based energy balance experiment was carried out to understand the melting processes on this glacier. The model, computing surface and sub-surface heat fluxes, was run over two separate periods from 13 August 2012 to 3 February 2013 and from 8 July to 3 October 2013. The results from the surface energy balance equation suggested that energy was available for melting in the summer-monsoon only. Net all-wave radiation was the main heat flux towards surface with 80% contribution while sensible, latent heat and conductive heat fluxes shared 13%, 5% and 2% of total heat flux, respectively. Interestingly, the latent heat flux switched from continuously negative values in post-monsoon and winter periods, indicating sublimation, to positive values in the summer-monsoon period indicating condensation/re-sublimation at the glacier surface. The impact of the summer-monsoon snowfalls on the glacier mass balance was studied using detailed surface energy balance approach. In line with the qualitative comparison of seasonal mass balances with meteorological variables, the point scale analysis of the modeled melting with meteorological data quantitatively validated that the intensity of snowfall events during the summer-monsoon control the surface albedo, in turn ablation. Therefore, together with winter precipitation and summer temperature, intensity of snowfall events during the summer-monsoon is among the most important drivers responsible for glacier-wide mass balance evolution of Chhota Shigri Glacier.

After the provoking statement of IPCC Fourth Assessment Report about the future of the Himalayan glaciers, several studies, generally remote sensing, were conducted in the HKH region. Chhota Shigri Glacier showed a negative mass budget since 1999 and a moderate mass loss since 1969 with an almost steady-state between 1986 and 2000. [Vincent et al. \(2013\)](#) proposed Chhota Shigri Glacier as a representative glacier for the Lahaul and Spiti region (2110 km²) with similar mass balances during 1999-2011; therefore, a similar behaviour may have been experienced by the other glaciers in the Lahaul and Spiti region during 1986 and 2000 when Chhota Shigri Glacier was in balanced conditions. The balanced conditions of Chhota Shigri Glacier between 1986 and 2000 contrasts with the most recent compilation ([Bolch et al., 2012](#)) of mass balance data in the Himalaya. [Bolch et al. \(2012\)](#) indicated ice wastage over the past five decades with an increased rate of loss roughly after 1995, but with a high spatiotemporal variability and almost no mass balance measurements between 1986 and 2000 for the western Himalaya. In agreement with regional ([Bolch et al., 2012](#); [Gardelle et al., 2013](#)) and global ([Zemp et al., 2009](#)) mass budget estimations, the field as well as reconstructed mass balances of Chhota Shigri Glacier confirm more negative mass budgets since 1999. The controversial statement about the Himalayan glaciers to be vanished by 2035 was found to be wrong ([Cogley et al., 2010](#)).

Certainly the topic of future projections of the HKH glaciers needs to be addressed in detail. Given the contrasting pattern of mass balance behaviour in the HKH region, the best way to project the future of these glaciers is to select some representative glaciers from the regions and perform detailed studies about future mass budgets. In this context Chhota Shigri Glacier is a very good option to assess the future mass budgets in the Lahaul and Spiti region.

Chhota Shigri Glacier has been studied extensively for its mass balances and meteorological drivers since 1969 but the hydrological studies, which were initially part of the PhD project, could not be covered because of the time limitation. Thanks to the field as well as modelling based research conducted in this study, a strong foundation for stream flow-climate change assessment has been laid. A fully distributed high resolution glacio-hydrological model for Chhota Shigri Glacier as well as for the Lahaul-Spiti region is needed in order to understand the runoff evolution in the western Himalaya. In the present work melt models are used to understand the mass balance-climate relationship. Indeed the understanding of different energy fluxes on Chhota Shigri Glacier and involvement of sublimation/condensation processes will significantly improve the quality of the glacio-hydrological model. However working at catchment scale, including the nonglacierized area, needs the involvement of hydrological processes such as evapotranspiration, infiltration, ground-surface water interactions etc. Furthermore, probably the most crucial is to know the spatial distribution of precipitation over the basin. These parameters have to be constrained in the field. When the model outputs at Chhota Shigri Glacier basin scale are validated/calibrated using the in-situ data from this glacier, the model can be used at regional scale. With an established understanding of glacio-hydrological processes and the precipitation distribution I propose to use the model to simulate the future runoff using the forcing data from the latest climate model “Coupled Model Intercomparison Project 5” ensemble (Taylor et al., 2012). The available data can be downscaled using the statistical downscaling approach (Immerzeel et al., 2012). The relative percentage of the glacier melt water to the total river runoff is an indicator of vulnerability of the river systems to the future climate changes; therefore, the output from the high resolution glacio-hydrological model will help us to assess the water availability in the future under different future climate scenarios. The future glacier changes will be simulated by applying a recently developed parameterization for the glacier changes at the large river basin scale (Lutz et al., 2013).

In this study the precipitation data from the nearest meteorological station at the township of Bhuntar was often used to understand the mass balance processes at glacier. At Bhuntar meteorological station, the mean contribution of Indian summer monsoon (May to October) and mid-latitude westerlies (November to April) to the annual precipitation was almost same with 51% and 49%, respectively between 1969 and 2012, whereas the 2012/13 precipitation record from the glacier base camp showed contributions of Indian summer monsoon and mid-latitude westerlies as 21% and 79%, respectively. Bhuntar meteorological station and Chhota Shigri Glacier are separated by an orographic barrier; hence some differences in the precipitation

amounts are obvious. Given that the glacier base camp data was available only for 2012/13 year, the precipitation distribution over this region needs to be further analyzed with long term data. There is a network of meteorological stations running over almost last three decades across the orographic barrier in the Bhuntar Valley and Lahaul & Spiti Valley. These meteorological stations were established by *Snow and Avalanche Study Establishment (SASE)*, Manali, which is a unit of *Defense Research Organization (DRDO)*, Ministry of Defense, Government of India. Unfortunately, the data from these stations are not available in public domain and thus could not be used in the present study. In the upcoming future, it is highly recommended to analyze the spatial distribution of precipitation over a long time period using precipitation records from several gauges. Chhota Shigri Glacier is 9 km long; consequently we propose to install more precipitation gauges on the glacier moraines up to the AWS-M site (4863 m a.s.l.) and one gauge in the Bhuntar valley around 2 km south to Sara-Umga pass (Fig. 2.1) in order to understand (1) the distribution of precipitation over the glacier and (2) across the orographic barrier.

References

- Ageta, Y. and Higuchi, K.: Estimation of mass balance components of a summer-accumulation type glacier in the Nepal Himalaya, *Geogr. Ann. A*, 66, 249–255, 1984.
- Ageta, Y., Naito, N., Nakawo, M., Fujita, K., Shankar, K., Pokhrel, A. P. and Wangda, D.: Study project on the recent rapid shrinkage of summer-accumulation type glaciers in the Himalayas, 1997-1999, *Bull. Glaciol. Res.*, 18, pp.45–49, 2001.
- Aizen, V. B., Aizen, E. M. and Nikitin S. A.: Glacier regime on the northern slope of the Himalaya (Xixibangma glaciers), *Quat. Int.*, 97–98, 27–39, doi:10.1016/S1040-6182(02)00049-6, 2002.
- Anderson, B., Mackintosh, A., Stumm, D., George, L., Kerr, T., Winter-Billington, A., and Fitzsimmons, S.: Climate sensitivity of a high-precipitation glacier in New Zealand, *J. Glaciol.*, 56, 114–128, 2010.
- Andreas, E. L.: A theory for the scalar roughness and the scalar transfer coefficients over snow and sea ice, *Bound.-Lay. Meteorol.*, 38, 159–184, 1987.
- Arck, M. and Scherer, D.: Problems in the determination of sensible heat flux over snow. *Geogr. Ann. A*, 84, 157–169, 2002.
- Armstrong, R. L.: The glaciers of the Hindu Kush-Himalayan region: a summary of the science regarding glacier melt/retreat in the Himalayan, Hindu Kush, Karakoram, Pamir, and Tien Shan mountain ranges, CIRES/NSIDC, University of Colorado, Boulder, USA, 2010.
- Ashwell, I. Y.: Glacier mapping in Iceland by the British Schools Exploring Society. *The Geographical Journal* 148, 308–16, 1982.
- Auden, J. B.: Snout of the Gangotri Glacier, Tehri Garhwal. *Records of the Geological Survey of India*, 72, 135–40, 1937.
- Azam, M. F., Wagnon, P., Ramanathan, AL., Vincent, C., Sharma, P., Arnaud, Y., Linda, A., Pottakkal, J. G., Chevallier, P., Singh, V. B., and Berthier, E.: From balance to imbalance: a shift in the dynamic behaviour of Chhota Shigri Glacier (Western Himalaya, India), *J. Glaciol.*, 58, 315–324, doi:10.3189/2012JoG11J123, 2012.
- Azam, M. F., Wagnon, P., Vincent, C., Ramanathan, AL., Linda, A., and Singh, V. B.: Reconstruction of the annual mass balance of Chhota Shigri Glacier (Western Himalaya, India) since 1969, *Ann. Glaciol.*, 55(66), 69-80, doi: 10.3189/2014AoG66A104, 2014a.
- Azam, M. F., Wagnon, P., Vincent, C., Ramanathan, AL., Favier, V., Mandal, A., and Pottakkal, J. G.: Processes governing the mass balance of Chhota Shigri Glacier (western

- Himalaya, India) assessed by point-scale surface energy balance measurements, *The Cryosphere*, 8, 2195-2217, doi:10.5194/tc-8-2195-2014, 2014b.
- Bahr, D. B., Dyurgerov, M., and Meier, M. F.: Sea-level rise from glaciers and ice caps: A lower bound, *Geophys. Res. Lett.*, 36, L03501, doi:10.1029/2008GL036309, 2009.
- Bajracharya, S. R. and Mool, P.: Glaciers, glacial lakes and glacial lake outburst floods in the Mount Everest region, Nepal. *Ann. Glaciol.*, 50 (53), 81-86, 2009.
- Bali, R., Ali, S. N., Agarwal, K. K., Rastogi, S.K., Krishna, K. and Srivastava, P.: Chronology of late Quaternary glaciation in the Pindar valley, Alaknanda Basin, Central Himalaya (India) *J. Asian Earth Sci.*, 66, 224-233, 2013.
- Baral, P., Kayastha, R. B., Immerzeel, W. W., Pradhananga, N. S., Bhattarai, B. C., Shahi, S., Galos, G., Springer, C., Joshi, S. P. and Mool P. K.: Preliminary results of mass-balance observations of Yala Glacier and analysis of temperature and precipitation gradients in Langtang Valley, Nepal, *Ann. Glaciol.* 55 (66), 9-14, doi: 10.3189/2014AoG66A106, 2014.
- Barnett, T. P., Adam, J. C. and Lettenmaier, D. P.: Potential impacts of a warming climate on water availability in snow-dominated regions, *Nature*, 438(7066), 303–309, 2005.
- Begert, M., Schlegel, T., and Kirchhofer, W.: Homogeneous temperature and precipitation series of Switzerland from 1864 to 2000, *Int. J. Climatol.*, 25, 65–80, 2005.
- Benn, D. I. and Owen, L. A.: The role of the Indian summer monsoon and the mid-latitude westerlies in Himalayan glaciation: review and speculative discussion, *J. Geo. Soc.*, 155 (2): 353-363, 1998.
- Benn, D. I. and Lehmkuhl, F.: Mass balance and equilibrium-line altitudes of glaciers in high mountain environments, *Quatern. Int.*, 65/66, 15–29, 2573, 2000.
- Berthier, E., Vadon, H., Baratoux, D., Arnaud, Y., Vincent, C., Feigl, K. L., Remy, F. and Legresy, B.: Surface motion of mountain glaciers derived from satellite optical imagery, *Remote Sens. Environ.*, 95(1), 14-28, 2005.
- Berthier, E., Arnaud, Y., Kumar, R., Ahmad, S., Wagnon, P., and Chevallier, P.: Remote sensing estimates of glacier mass balances in the Himachal Pradesh (Western Himalaya, India), *Remote Sens. Environ.*, 108, 327–338, 2007.
- Bhambri, R. and Bolch, T.: Glacier mapping: a review with special reference to the Indian Himalayas, *Prog. Phys. Geog.*, 33, 672–702, 2009.
- Bhambri, R., Bolch, T., Chaujar R. K., and Kulshreshtha, S. C.: Glacier changes in the Garhwal Himalayas, India 1968-2006 based on remote sensing, *J. Glaciol.*, 57(203), 543-556, 2011.

- Bhambri, R., Bolch, T., and Chaujar, R. K.: Frontal recession of Gangotri Glacier, Garhwal Himalayas, from 1965 to 2006, measured through high resolution remote sensing data, *Current Science*, Vol. 102, No. 3, 2012.
- Bhambri, R., Bolch, T., Kawishwar, P., Dobhal, D. P., Srivastava, D. and Pratap, B.: Heterogeneity in glacier response in the upper Shyok Valley, northeast Karakoram, *The Cryosphere*, 7, 1385–1398, 2013, doi:10.5194/tc-7-1385-2013.
- Bhutiyan, M. R.: Mass balance studies on Siachen Glacier in the Nubra valley, Karakoram Himalaya, India. *J. Glaciol.*, Vol. 45, No. 149, 1999.
- Bhutiyan, M. R., et al.: Long-term trends in maximum, minimum and mean annual air temperatures across the Northwestern Himalaya during the twentieth century, *Journal of Climatic Change*, 85 (1-2): 159-177, 2007.
- Bhutiyan, M. R., et al.: Climate change and the precipitation variations in the northwestern Himalaya: 1866–2006, *International Journal of Climatology*, 30 (4): 535-548, 2010.
- Bintanja, R. and Van den Broeke, M. R.: The surface energy balance of Antarctic snow and blue ice, *J. Appl. Meteorol.*, 34, 902–926, 1995.
- Bintanja, R., Jonsson, S. and Knap W.: The annual cycle of the surface energy balance of Antarctic blue ice, *J. Geophys. Res.*, 102(D2), 1867–1881, doi:10.1029/96JD01801, 1997.
- Bolch, T., Buchroithner, M. F., Pieczonka, T., and Kunert, A.: Planimetric and volumetric glacier changes in Khumbu Himalaya since 1962 using Corona, Landsat TM and ASTER data, *J. Glaciol.*, 54, 592–600, 2008.
- Bolch, T., Pieczonka, T., and Benn, D. I.: Multi-decadal mass loss of glaciers in the Everest area (Nepal Himalaya) derived from stereo imagery, *The Cryosphere*, 5, 349–358, doi:10.5194/tc-5-349-2011, 2011.
- Bolch, T., Kulkarni, A., Käab, A., Huggel, C., Paul, F., Cogley, J. G., Frey, H., Kargel, J. S., Fujita, K., Scheel, M., Bajracharya, S., and Stoffel, M.: The State and Fate of Himalayan Glaciers, *Science*, 336, 310–314, 2012.
- Bookhagen, B., Thiede, R. C., and Strecker, M. R.: Abnormal monsoon years and their control on erosion and sediment flux in high, arid northwest Himalaya; *Earth Planet. Sci. Lett.*, 231, 131–146, 2005.
- Bookhagen, B. and Burbank, D. W.: Topography, relief, and TRMM-derived rainfall variations along the Himalaya, *Geophys. Res. Lett.*, 33, L08405, doi:10.1029/2006GL026037, 2006.
- Bookhagen, B. and Burbank, D. W.: Toward a complete Himalayan hydrological budget: Spatiotemporal distribution of snowmelt and rainfall and their impact on river discharge, *J. Geophys. Res.*, 115, F03019, doi:10.1029/2009JF001426, 2010.

- Braithwaite, R. J. and Zhang, Y.: Sensitivity of mass balance of five Swiss glaciers to temperature changes assessed by tuning a degree-day model, *J. Glaciol.*, 46(152), 4–14, 2000.
- Braithwaite, R. J., Zhang, Y. and Raper S. C. B.: Temperature sensitivity of the mass balance of mountain glaciers and icecaps as a climatological characteristic. *Z. Gletscherkd. Glazialgeol.*, 38, 35–61, 2002.
- Braithwaite, R. J. and Raper S. C. B.: Glaciological conditions in seven contrasting regions estimated with the degree day model. *Ann. Glaciol.*, 46, 297–302, doi:10.3189/172756407782871206, 2007.
- Brock, B., Willis, I., Sharp, M., and Arnold, N.: Modelling seasonal and spatial variations in the surface energy balance of Haut Glacier d'Arolla, Switzerland, *Ann. Glaciol.*, 31, 53–62, 2000.
- Brun, F., Dumont, M., Wagnon, P., Berthier, E., Azam, M. F., Shea, J. M., Sirguey, P., Rabatel, A., and Ramanathan, Al.: Seasonal changes in surface albedo of Himalayan glaciers from MODIS data and links with the annual mass balance, *The Cryosphere Discuss.*, 8, 3437–3474, doi:10.5194/tcd-8-3437-2014, 2014.
- Brutsaert, B.: *Evaporation in the Atmosphere: Theory, History and Application*, 299, Kluwer Acad., Norwell, Mass, 1982.
- Chaturvedi, R. K., Kulkarni, A., Karyakarte, Y., Joshi, J. and Bala, G.: Glacial mass balance changes in the Karakoram and Himalaya based on CMIP5 multi-model climate projections, *Climatic Change*, Volume 123, Issue 2, pp 315–328, DOI 10.1007/s10584-013-1052-5, 2014.
- Chaujar, R. K.: Glacial geomorphology – a case study of Chhota Shigri Glacier. In *Proceedings of National Meet on Himalayan Glaciology*, New Delhi: Ministry of Science and Technology, Government of India, 173–85, 1989.
- Cogley, J. G.: Geodetic and direct mass-balance measurements: comparison and joint analysis, *Ann. Glaciol.*, 50(50), 96–100, 2009.
- Cogley, J. G., Kargel, J. S., Kaser, G. and van der Veen, C. J.: Tracking the Source of Misinformation, *Science* 29 January 2010: 522. DOI:10.1126/science.327.5965.522-a, 2010.
- Cogley, J. G.: Present and future states of Himalaya and Karakoram glaciers, *Ann. Glaciol.*, 52 (59), 69–73, 2011.
- Cotter, G. D. and Brown, J. C.: Notes on certain glaciers in Kumaon. *Rec. Geol. Survey of India* 35 (4), 1907.
- Cuffey, K. and Paterson, W. S. B.: *The physics of glaciers*, 5th Edn., Massachusetts Academic Press, Burlington, 2010.
- Dash, S. K., Jenamani, R. K., Kalsi, S. R. and Panda, S. K.: Some evidence of climatic change in twentieth century India. *Clim Chang* 85, 299–321, 2007.

- Datt, P., Srivastava, P. K., Negi, P. S. and Satyawali, P. K.: Surface energy balance of seasonal snow cover for snow-melt estimation in N-W Himalaya *J. Earth Syst. Sci.* 117 567–73, 2008.
- De Woul, M. and Hock, R.: Static mass-balance sensitivity of Arctic glaciers and ice caps using a degree-day approach, *Ann. Glaciol.*, 42, 217–224, 2005.
- Denby, B. and Greuell, W.: The use of bulk and profile methods for determining surface heat fluxes in the presence of glacier winds, *J. Glaciol.*, 46, 445–452, 2000.
- Dimri, A. P.: Impact of horizontal model resolution and orography on the simulation of a western disturbance and its associated precipitation, *Meteorol. Appl.* 11 (2), 115–127, 2004.
- Dimri, A. P. and Dash, S. K.: Winter temperature and precipitation trends in the Siachen Glacier *Current Science*, Vol. 98, No. 1620 12, 2010.
- Dimri, A. P. and Dash, S. K.: Wintertime Climatic Trends in the Western Himalayas, *Climatic Change*, 111, 3-4, 775-800, 2012.
- Dobhal, D. P.: Ph.D. thesis, Inventory of Himachal glaciers and glaciological studies of Chhota Shigri Glacier, Himachal Pradesh: a case history, Garhwal University, Srinagar, 1992.
- Dobhal, D. P., Kumar, S. and Mundepi, A. K.: Morphology and glacier dynamics studies in monsoon–arid transition zone: an example from Chhota Shigri glacier, Himachal Himalaya, India. *Current Science*, 68(9), 936–944, 1995.
- Dobhal, D. P., Gergan, J. G. and Thayyen, R. J.: Mass balance studies of the Dokriani Glacier from 1992 to 2000, Garhwal Himalaya, India, *Bull. Glaciol. Res.*, 25, 9-17, 2008.
- Dobhal, D. P., Mehta, M. and Srivastava, D.: Influence of debris cover on terminus retreat and mass changes of Chorabari Glacier, Garhwal region, central Himalaya, India, *J. Glaciol.*, 59 (217), 961–971, 2013.
- Dorsey, N. E.: *Properties of Ordinary Water-Substance in All Its Phases: Water-Vapor, Water, and All the Ices*, Reinhold, New York, 1940.
- Douville, H., Royer, J. F. and Mahfouf, J. F.: A new snow parameterization for the Météo-France climate model, Part I: Validation in standalone experiments, *Clim. Dyn.*, 12, 21–35, doi:10.1007/BF00208760, 1995.
- Dyurgerov, M. B., and Meier, M. F.: Twentieth century climate change: evidence from small glaciers. *Proceedings of National Academy of Sciences, USA*, 97 (4), 1406–1411, 2000.
- Dyurgerov, M. B. and Meier, M. F.: *Glaciers and the changing Earth System: a 2004 snapshot*, Boulder, CO, Arctic, Antarc. Alp. Res., Occasional Paper 58, 2005.
- Eriksson, M. et al.: The changing Himalayas: impact of climate change on water resources and livelihoods in the greater Himalayas. ICIMOD, 2009.

- Favier, V., Wagnon, P., Chazarin, J. P., Maisincho, L., and Coudrain, A.: One-year measurements of surface heat budget on the ablation zone of Antizana Glacier 15, Ecuadorian Andes, *J. Geophys. Res.*, 109, D18105, doi:10.1029/2003JD004359, 2004.
- Favier, V., Agosta, C., Genthon, C., Arnaud, L., Trouvillez, A., and Gallée, H.: Modeling the mass and surface heat budgets in a coastal blue ice area of Adelie Land, Antarctica, *J. Geophys. Res.*, 116, F03017, doi:10.1029/2010JF001939, 2011.
- Finsterwalder, S. and Schunk, H.: Der Suldenferner. *Zeitschrift des Deutschen und Oesterreichischen Alpenvereins*, 18, 72–89, 1887.
- Fowler, H. J., and Archer, D. R.: Hydro-climatological Variability in the Upper Indus Basin and Implications for Water Resources. *Regional Hydrological Impacts of Climatic Change—Impact Assessment and Decision Making*, 295, 131–138, 2005.
- Fowler, H. J. and Archer, D. R.: Conflicting Signals of Climatic Change in the Upper Indus Basin." *Journal of Climate*, 19, 4276–4293, 2006.
- Fujita, K. and Ageta, Y.: Effect of summer accumulation on glacier mass balance on the Tibetan Plateau revealed by mass-balance model, *J. Glaciol.*, 46(153), 244–252, 2000.
- Fujita, K. et al.: Shrinkage of Glacier AX010 in Shorong region, Nepal Himalayas in the 1990s. *Bulletin of Glaciological Research*, 18, pp.51–54, 2001a.
- Fujita, K. et al.: Glaciological observations on Rikha Samba Glacier in Hidden Valley, Nepal Himalayas, 1998 and 1999, *Bull. of Glaciol. Res.*, 18, pp.31–35, 2001b.
- Fujita, K.: Influence of precipitation seasonality on glacier mass balance and its sensitivity to climate change, *Ann. Glaciol*, 48, 88–92, 2008a.
- Fujita, K.: Effect of precipitation seasonality on climatic sensitivity of glacier mass balance, *Earth and Planetary Science Letters*, 276, 14–19, 2008b.
- Ganjoo, R. K. and Koul, M. N.: Is Siachen glacier melting? *Current Science*, 97 (3), 87–94, 2009.
- Ganjoo, R. K.: Are secular movements in the glaciers of Ladakh Mountains, Ladakh (J & K State, India) a response to climate change? *International Symposium Benefiting from Earth Observation, ICIMOD, Kathmandu (Oct. 4–6)*, 2010.
- Gardelle, J., Arnaud, Y., and Berthier, E.: Contrasted evolution of glacial lakes along the Hindu Kush Himalaya mountain range between 1990 and 2009, *Global Planet. Change*, 75, 47–55, 2011.
- Gardelle, J., Berthier, E., and Arnaud, Y.: Slight mass gain of Karakoram glaciers in the early twenty-first century, *Nat. Geosci.*, 5, 322–325, 2012.
- Gardelle, J., Berthier, E., Arnaud, Y., and Käab, A.: Region-wide glacier mass balances over the Pamir-Karakoram-Himalaya during 1999–2011, *The Cryosphere*, 7, 1263–1286, doi:10.5194/tc-7-1263-2013, 2013.

- Gardner, A. S., Moholdt, G., Cogley, J. G., Wouters, B., Arendt, A. A., Wahr, J., Berthier, E., Pfeffer, T., Kaser, G., Hock, R., Ligtenberg, S. R. M., Bolch, T., Sharp, M., Hagen, J. O., van den Broeke, M. R., and Paul, F.: A consensus estimate of glacier contribution to sea level rise: 2003 to 2009, *Science*, 340, 852–857, 2013.
- Garratt, J. R.: *The Atmospheric boundary layer*, Cambridge Univ. Press, New York, 316p., 1999.
- Gautam, C. K. and Mukherjee B. P.: Mass-balance vis-à-vis snout position of Tipra bank glacier District Chamoli, Uttar Pradesh, *Proc. Natl. Meet Himalayan Glaciol*, 5–6 June 1989, 141–148, 1989.
- Gautam, R., et al.: Enhanced pre-monsoon warming over the Himalayan–Gangetic region from 1979 to 2007, *Geophysical Research Letters* 36 (L07704): doi:10.1029/2009GL037641, 2009.
- Gautam, R., et al.: Pre-monsoon aerosol characterization and radiative effects over the Indo-Gangetic Plains: Implications for regional climate warming, *J. Geophys. Res.* 115 (D17): D17208, 2010.
- Geological Survey of India (GSI): Annual general report, Part 8. Volume 133, 1999.
- Geological Survey of India (GSI): Chapter 8, Annual Report 1991–1992, 175–176, 1992.
- Geological Survey of India (GSI): Chapter 8, Annual Report 2010–2011, 69–70, 2011.
- Geological Survey of India (GSI): Glaciological studies on Dunagiri Glacier, district Chamoli (Field Seasons 1983-84 to 1991-92), Final Report 1992, 5–9, 1992.
- Giesen, R. H., Andreassen, L. M., Van den Broeke, M. R., and Oerlemans, J.: Comparison of the meteorology and surface energy balance at Storbreen and Midtdalsbreen, two glaciers in southern Norway, *The Cryosphere*, 3, 57-74, doi:10.5194/tc-3-57-2009, 2009.
- Giesen, R. H., Andreassen, L. M., Oerlemans, J. and Van den Broeke, M. R.: Surface energy balance in the ablation zone of Langfjordjøkelen, an arctic, maritime glacier in northern Norway. *J. Glaciol.*, 60, 57-70, doi: 10.3189/2014JG13J063, 2014.
- Godwin-Austen, H. H.: On the glaciers of the Mustagh Range. *J. Royal Geog. Soc.*, 34, 19–56, 1864.
- Govindha Raj, K.B.: Recession and reconstruction of Milam glacier, Kumaon Himalaya, observed with satellite imagery. *Current Science*, 100(9), 1420-1425, 2011.
- Govindha Raj, K. B., Remya, S. N. and Kumar, K. V.: Remote sensing-based hazard assessment of glacial lakes in Sikkim Himalaya, *Current Science*, 104(3), 2013.
- Greuell, W. and Smeets, P.: Variations with elevation in the surface energy balance on the Pasterze (Austria), *J. Geophys. Res.*, 106, 31717–31727, 2001.
- Greuell, W., Knap, W. H., and Smeets, P. C.: Elevational changes in meteorological variables along a mid-latitude glacier during summer, *J. Geophys. Res.*, 102(D22), 25941–25954, 1997.

- Grisogono, B. and Oerlemans, J.: Justifying the WKB approximation in pure katabatic flows, *Tellus A* 54, 453-463, 2002.
- Haerberli, W. and Hoelzle, M.: Application of inventory data for estimating characteristics of and regional climate-change effects on mountain glaciers: a pilot study with the European Alps. *Ann. Glaciol.*, 21, 206–212, 1995.
- Heid, T. and Käab, A.: Repeat optical satellite images reveal widespread and long term decrease in land-terminating glacier speeds, *The Cryosphere*, 6, 467-478, doi:10.5194/tc-6-467-2012, 2012.
- Hewitt, K.: The Karakoram anomaly? Glacier expansion and the “elevation effect,” *Karakoram Himalaya, Mt. Res. Dev.*, 25 (4), 332–340, 2005.
- Hewitt, K.: Glacier change, concentration, and elevation effects in the Karakoram Himalaya, upper Indus basin, *Mt. Res. Dev.*, 31, 188–200, 2011.
- Hock, R. and Holmgren, B.: Some aspects of energy balance and ablation of Storglaciaren, Northern Sweden, *Geogr. Ann. A*, 78, 121–131, 1996.
- Hock, R.: Temperature index melt modelling in mountain areas, *J. Hydrol.*, 282, 104–115, 2003.
- Hock, R. and Holmgren, B.: A distributed surface energy-balance model for complex topography and its application to Storglaciaren, Sweden, *J. Glaciol.*, 51, 25–36, 2005.
- Hock, R., Radic', V. and De Woul, M.: Climate sensitivity of Storglaciaren, Sweden: an intercomparison of mass-balance models using ERA-40 re-analysis and regional climate model data, *Ann. Glaciol.* 46, 342-348, 2007.
- Hoinkes, H.C.: Measurements of ablation and heat balance on alpine glacier. *J. Glaciol.*, 2, 497–501, 1953.
- Hubbard B. and Glasser, N.: *Field Techniques in Glaciology and Glacial Geomorphology*, Wiley & Sons Ltd, Chichester, England, 400 pp, 2005.
- Huss, M., Sugiyama, S., Bauder, A. and Funk, M.: Retreat scenarios of Unteraargletscher, Switzerland, using a combined ice-flow mass-balance model, *Arctic, Antarc. Alp. Res.*, 39 (3), 422-431, 2007.
- Huss, M., Bauder, A., Funk, M., and Hock, R.: Determination of the seasonal mass balance of four Alpine glaciers since 1865, *J. Geophys. Res.*, 113, F01015, 2008.
- Huss, M., Bauder, A. and Funk, M.: Homogenization of long-term mass-balance time series, *Ann. Glaciol.*, 50, 198-206, 2009.
- Immerzeel, W. W.: Historical Trends and Future Predictions of Climate Variability in the Brahmaputra Basin. *International Journal of Climatology* 28: 243-254, 2008.

- Immerzeel, W. W., van Beek, L. P. H., and Bierkens, M. F. P.: Climate Change Will Affect the Asian Water Towers, *Science*, 328, 1382–1385, 2010.
- Immerzeel, W.W. and Bierkens, M. F. P.: Asia's water balance, *Nature Geosci.*, 5, 841-842, 2012a.
- Immerzeel, W. W., Pellicciotti, F., and Shrestha, A. B.: Glaciers as a proxy to quantify the spatial distribution of precipitation in the Hunza Basin, *Mt. Res. Dev.*, 32, 30–38, doi:10.1659/MRDJOURNAL-D-11-00097.1, 2012b.
- Immerzeel, W. W., Pellicciotti, F. and Bierkens, M. F. P.: Rising river flows throughout the twenty-first century in two Himalayan glacierized watersheds, *Nat. Geosci.*, 6 (9), 742–745, 2013.
- Intergovernmental Panel on Climate Change (IPCC): Contribution of Working Group II to the Fourth Assessment Report of the Intergovernmental Panel on Climate Change, 2007. In ML Parry, OF Canziani, JP Palutikof, PJ van der Linden and CE Hanson (Eds). Cambridge University Press, Cambridge, United Kingdom and New York, NY, USA, 2007.
- Iqbal, M.: An introduction to solar radiation, Academic Press, New York, 1983.
- Jacob, T., Wahr, J., Pfeffer, W. T. and Swenson, S.: Recent contributions of glaciers and ice caps to sea level rise, *Nature* 482, 514–518 (23 February 2012) doi:10.1038/nature10847, 2012.
- Jangpangi, B. S.: Study of some of the central Himalayan glaciers, *Journal of Scientific and Industrial Research*, Vol. 17A, No. 12, 1958.
- Jiawen, R., Zhefan, J., Jianchen PU., and Xiang, Q.: Glacier variations and climate change in the central Himalaya over the past few decades. *Ann. Glaciol.*, 43, 218-222, 2006.
- Jóhannesson, T., Sigurdsson, O., Laumann, T., and Kennett, M.: Degree-day glacier mass-balance modelling with applications to glaciers in Iceland, Norway and Greenland, *J. Glaciol.*, 25 41(138), 345–358, 1995.
- Kääb, A., Berthier, E., Nuth, C., Gardelle, J. and Arnaud, Y.: Contrasting patterns of early 21st century glacier mass change in the Himalaya, *Nature*, 488(7412), 495–498, doi:10.1038/nature11324, 2012.
- Kalnay, E., Kanamitsu, M., Kistler, R., et al.: The NCEP/NCAR 40-year reanalysis project, *B. Am. Meteorol. Soc.*, 77, 437–471, 1996.
- Kamp, U., Byrne, M., Bolch, T.: Glacier Fluctuations between 1975 and 2008 in the Greater Himalaya Range of Zaskar, Southern Ladakh, *J. Mt. Sci.*, 8, 374-389, DOI: 10.1007/s11629-011-2007-9, 2011.
- Kargel, J. S., Cogley, J. G., Leonard, G. J., Haritashya, U., Byers, and Byers, A.: Himalayan glaciers: the big picture is a montage, *Proc. Natl. Acad. Sci. USA*, 108 (36), 14709–14710, 2011.

- Kaser, G., Fountain, A. G., and Jansson, P.: A manual for monitoring the mass balance of mountain glaciers with particular attention to low latitude characteristics. A contribution to the UNESCO HKH-Friend programme, Paris, France, 107 pp., 2003.
- Kaser, G., Großhauser, M. and Marzeion, B.: Contribution potential of glaciers to water availability in different climate regimes, *Proc. Natl. Acad. Sci.*, 107(47), 20223–20227, doi:10.1073/pnas.1008162107, 2010.
- Kayastha, R. B., Ohata, T., and Ageta, Y.: Application of mass balance model to a Himalayan glacier, *J. Glaciol.*, 45, 559–567, 1999.
- Klok, E. J. L. and Oerlemans, J.: Model study of the spatial distribution of the energy and mass balance of Morteratschgletscher, Switzerland, *J. Glaciol.*, 48, 505–518, 2002.
- Klok, E. J., Nolan, M., and Van den Broeke, M. R.: Analysis of meteorological data and the surface energy balance of McCall Glacier, Alaska, USA, *J. Glaciol.*, 51, 451–461, 2005.
- Klok, E., and J. Oerlemans.: Deriving historical equilibrium-line altitudes from a glacier length record by linear inverse modelling, *Holocene*, 13 (3), 343–351, 2003.
- Koul, M. N. and Ganjoo R. K.: Impact of inter- and intra-annual variation in weather parameters on mass balance and equilibrium line altitude of Naradu Glacier (Himachal Pradesh), NW Himalaya, India, *Clim. Change*, 99, 119–139, doi:10.1007/s10584-009-9660-9, 2010.
- Kuipers Munneke, P., Van den Broeke, M. R., King, J. C., Gray, T., and Reijmer, C. H.: Near-surface climate and surface energy budget of Larsen C ice shelf, Antarctic Peninsula, *The Cryosphere*, 6, 353–363, doi:10.5194/tc-6-353-2012, 2012.
- Kulkarni, A. V.: Mass balance of Himalayan glaciers using AAR and ELA methods, *J. Glaciol.*, 38, 101–104, 1992.
- Kulkarni, A. V. et al.: Glacial retreat in Himalaya using Indian remote sensing satellite data, *Current Science*, 92(1), 69–74, 2007.
- Kumar, S.: Chhota Shigri Glacier: its kinematic effects over the valley environment, in the northwest Himalaya, *Current Science*, 77(4), 594–598, 1999.
- Leclercq, P. W. and Oerlemans, J.: Global and hemispheric temperature reconstruction from glacier length fluctuations, *Clim. Dyn.*, 38:1065–1079 DOI 10.1007/s00382-011-1145-7, 2012.
- Lejeune, Y., Wagnon, P., Bouilloud, L., Chevallier, P., Etchevers, P., Martin, E., Sicart, J. E. and Habets, F.: Melting of snow cover in a tropical mountain environment: processes and melting, *J. Hydrometeorol.*, 8, 922–937, doi: 10.1175/JHM590.1, 2007.
- Lejeune, Y., Bertrand, J.-M., Wagnon, P., and Morin, S.: A physically based model of the year-round surface energy and mass balance of debris-covered glaciers, *J. Glaciol.*, 59, 327–344, doi:10.3189/2013JogG12J149, 2013.

- Leysinger Vieli, G. J.-M. C., and G. H. Gudmundsson.: On estimating length fluctuations of glaciers caused by changes in climatic forcing, *J. Geophys. Res.*, 109, F01007, doi:10.1029/2003JF000027, 2004.
- Li, J., Liu, S., Zhang, Y., and Shangguan, D.: Surface energy balance of Keqicar Glacier, Tianshan Mountains, China, during ablation period, *Sciences in Cold and Arid Regions*, 3, 197–205, doi: 10.3724/SP.J.1226.2011.00197, 2011.
- Liu, S., Xie, Z., Song, G., Ma, L. and Ageta, Y.: Mass balance of Kangwure (flat-top) Glacier on the north side of Mt. Xixiabangma, China, *Bulletin of Glacier Research*, 14, 37-43, 1996.
- Longstaff, T. G.: Dr. Longstaff's Himalayan expedition, 1909. *The Geographical Journal* 35, 64–65, 1910.
- Luthcke, S. B., Arendt, A. A., Rowlands, D. D., McCarthy, J. J. and Larsen, C. F.: Recent glacier mass changes in the Gulf of Alaska region from GRACE mascon solutions. *J. Glaciol.* 54, 767–777, 2008.
- Lüthi, M. P., and Bauder, A.: Analysis of Alpine glacier length change records, *Geogr. Helv.*, 2, 92–102, 2010.
- Lüthi, M. P., A. Bauder, and M. Funk.: Volume change reconstruction of Swiss glaciers from length change data, *J. Geophys. Res.*, 115, F04022, doi:10.1029/2010JF001695, 2010.
- Lutz, A. F., Immerzeel, W.W., Gobiet, A., Pellicciotti, F. & Bierkens, M. F. P.: Comparison of climate change signals in CMIP3 and CMIP5 multi-model ensembles and implications for Central Asian glaciers. *Hydrol. Earth Syst. Sci.* 17, 3661-3677, 2013.
- Lutz, A. F., Immerzeel, W. W., Shrestha, A. B. and Bierkens, M. F. P.: Consistent increase in High Asia's runoff due to increasing glacier melt and precipitation, *Nature climate change*, 4 587-592, doi: 10.1038/NCLIMATE2237, 2014.
- Machguth, H., Eisen, O., Paul, F. and Hoelzle, M.: Strong spatial variability of snow accumulation observed with helicopter-borne GPR on two adjacent Alpine glaciers, *Geophys. Res. Lett.*, 33, L13503, (10.1029/2006GL026576.), 2006.
- Mason, K.: Karakoram nomenclature, *The Himalayan Journal*, 10, 86–125, 1938.
- Mattson, L. E., Gardner, J. S. and Young, G. J.: Ablation on debris covered glacier, Punjab, Himalaya. *IAHS Publ.*, 218, 289-296, 1993.
- Maussion, F., Wei, Y., Huintjes, E., Pieczonka, T., Scherer, D., Yao, T., Kang, S., Bolch, T., Buchroithner, M., and Schneider, C.: Glaciological field studies at Zhadang Glacier (5500–6095 m), Tibetan Plateau, in: *Workshop on the use of automatic measuring systems on glaciers – Extended abstracts and recommendations of the IASC Workshop*, edited by: Tijm-Reijmer, C. H. and Oerlemans, J., 23–26 March 2011, Pontresina (Switzerland), 62–68, Institute for Marine and Atmospheric Research, Utrecht University, 2011.

- Maussion, F., Scherer, D., Mölg, T., Collier, E., Curio, J. and Finkelburg, R.: Precipitation Seasonality and Variability over the Tibetan Plateau as Resolved by the High Asia Reanalysis, *J. Climate*, 27, 1910–1927, doi:10.1175/JCLI-D-13-00282.1, 2014.
- Mayewski, P. A. and Jeschke, P. A.: Himalayan and Trans-Himalayan Glacier Fluctuations Since AD 1812, *Arctic and Alpine Research*, 11 (3), pp.267–287, 1979.
- Meesters, A. G. C. A., Bink, N. J. H., Vugts, F., Cannemeijer, F. and Henneken, E. A. C.: Turbulence observations above a smooth melting surface on the Greenland Ice Sheet, *Boundary Layer Meteorol.*, 85, 81 – 110, 1997.
- Mehta, M., Dobhal, D. P., and Bisht, M. P. S.: Change of Tipra glacier in the Garhwal Himalaya, India, between 1962 and 2008, *Prog. Phys. Geog.*, 30, 1–18, 2011.
- Mölg, T. and Hardy, D. R.: Ablation and associated energy balance of a horizontal glacier surface on Kilimanjaro, *J. Geophys. Res.*, 109, 1-13, doi:10.1029/2003JD004338, 2004.
- Mölg, T., Cullen, N. J., and Kaser, G.: Solar radiation, cloudiness and longwave radiation over low-latitude glaciers: implications for mass-balance modelling, *J. Glaciol.*, 55, 292–302, doi:10.3189/002214309788608822, 2009.
- Mölg, T., Maussion, F., Yang, W., and Scherer, D.: The footprint of Asian monsoon dynamics in the mass and energy balance of a Tibetan glacier, *The Cryosphere*, 6, 1445–1461, doi:10.5194/tc-6-1445-2012, 2012.
- Mölg, T., Maussion, F., and Scherer, D.: Mid-latitude westerlies as a driver of glacier variability in monsoonal High Asia, *Nature Climate Change*, 4, 68-73, 2014.
- Moore, R.: On the use of bulk aerodynamic formulae over melting snow. *Nordic Hydrol.*, 14, 193–206, 1983.
- Mukhtar, M. A. and Prakash, O.: Glacio-geomorphological studies in the pro-glacial region of Gepang Gath Glacier, Lahaul and Spiti district, Himachal Pradesh on expedition basis 2012-13, Geological survey of India, 2013.
- Naithani, A. K., Nainwal, H. C., Sati, K. K. and Prasad, C.: Geomorphological evidences of retreat of the Gangotri glacier and its characteristics. *Current Science*, 80, 87–94, 2001.
- Narod, B. B. and Clarke, G. K. C.: Miniature high-power impulse transmitter for radio-echo sounding, *J. Glaciol.*, 40(134), 190-194, 1994.
- Nemec, J., Huybrechts, P., Rybak, O., and Oerlemans, J.: Reconstruction of the annual balance of Vadret da Morteratsch, Switzerland, since 1865, *Ann. Glaciol.*, 50(50), 126–134, 2009.
- Nicholson, L. I., Prinz, R., Mölg, T., and Kaser, G.: Micrometeorological conditions and surface mass and energy fluxes on Lewis Glacier, Mt Kenya, in relation to other tropical glaciers, *The Cryosphere*, 7, 1205-1225, doi:10.5194/tc-7-1205-2013, 2013.

- Nijampurkar, V. N. and Rao, D. K.: Accumulation and flow rates of ice on Chhota Shigri Glacier, central Himalaya, using radio-active and stable isotopes, *J. Glaciol.*, 38(128), 43–50, 1992.
- Nuimura, T., Fujita, K., Yamaguchi, S., and Sharma, R.: Elevation changes of glaciers revealed by multitemporal digital elevation models calibrated by GPS survey in the Khumbu region, Nepal Himalaya, 1992–2008, *J. Glaciol.*, 58, 648–656, doi:10.3189/2012JoG11J061, 2012.
- Nye, J. F.: The flow of a glacier in a channel of rectangular, elliptic or parabolic cross section, *J. Glaciol.*, 5(41), 661–690, 1965.
- Odell, N. E.: The Kolahoi Northern Glacier, Kashmir, *J. Glaciol.*, Vol. 4, pp. 633–635, 1963.
- Oerlemans, J., Anderson, B., Hubbard, A., Huybrechts, P., Jóhannesson, T., Knap, W. H., Schmeits, M., Stroeven, A. P., van de Wal, R. S. W., Wallinga, J., and Zuo, Z.: Modelling the response of glaciers to climate warming, *Clim. Dynam.*, 14, 267–274, 1998.
- Oerlemans, J.: Analysis of a 3 year meteorological record from the ablation zone of Morteratschgletscher, Switzerland: energy and mass balance, *J. Glaciol.*, 46, 571–579, 2000.
- Oerlemans, J.: *Glaciers and climate change*. Lisse, etc., A.A. Balkema, Brookfield, Vt., 2001.
- Oerlemans, J. and Klok, E.: Energy balance of a glacier surface: analysis of automatic weather station data from Morteratschgletscher, Switzerland, *Arct., Antarct. Alp. Res.*, 34, 477–485, 2002.
- Oerlemans, J.: Extracting a climate signal from 169 glacier records, *Science*, 308 (5477), 270–277, doi:2010.1126/science.1107046, 2005.
- Oerlemans, J., Giesen, R., and Van den Broeke, M.: Retreating alpine glaciers: increased melt rates due to accumulation of dust (Vadret da Morteratsch, Switzerland), *J. Glaciol.*, 55, 729–736, 2009.
- Oerlemans, J.: *The Microclimate of Valley Glaciers*. Igitur, Utrecht University, 138 pp., ISBN 987-90-393-5303-5, Utrecht Publishing & Archiving Services, The Netherlands, 2010.
- Ohmura, A.: Physical Basis for the Temperature-Based Melt-Index Method, *J. Appl. Meteorol.*, 40, 753–761, 2001.
- Ohmura, A.: Changes in mountain glaciers and ice caps during the 20th century, *Ann. Glaciol.*, 43, 361–368, 2006.
- Ohmura, A., Bauder, A., Müller, H. and Kappenberger, G.: Long-term change of mass balance and the role of radiation, *Ann. Glaciol.*, 46, 367–374, 2007.
- Oke, T. R.: *Boundary Layer Climates*. Second Edition, Routledge, 1987.
- Østrem, G. and Brugman, M.: *Glacier mass-balance measurements: A manual for field and office work*, NHRI Science Report, Saskatoon, Canada, 224 pp., 1991.

- Pandey, A. C., Ghosh, S. and Nathawat, M. S.: Evaluating patterns of temporal glacier changes in Greater Himalayan Range, Jammu & Kashmir, India, *Geocarto International* 26, 321-338, 2011.
- Pandey, P., and Venkataraman. G.: Changes in the glaciers of Chandra–Bhaga basin, Himachal Himalaya, India, between 1980 and 2010 measured using remote sensing, *Inter. J. Rem. Sens.*, 34(15), 5584-5597, 2013.
- Parry, M. L., Canziani, O. F., Palutikof, J. P., van der Linden, P. J. and Hanson C. E.: Contribution of Working Group II to the Fourth Assessment Report of the Intergovernmental Panel on Climate Change, 2007, Cambridge University Press, Cambridge, United Kingdom and New York, NY, USA, 2007.
- Paterson, W. S. B.: *The physics of glaciers*, Third edition. Oxford, etc., Elsevier, 1994.
- Paul, F., Kääb, A., and Haeberli, W.: Recent glacier changes in the Alps observed by satellite: Consequences for future monitoring strategies, *Global Planet. Change*, 56, 111–122, 2007.
- Paul, F.: The influence of changes in glacier extent and surface elevation on modeled mass balance, *The Cryosphere*, 4, 569-581, doi:10.5194/tc-4-569-2010, 2010.
- Pellicciotti, F., Brock, B., Strasser, U., Burlando, P., Funk, M., and Corripio, J.: An enhanced temperature-index glacier melt model including the shortwave radiation balance: development and testing for Haut Glacier d'Arolla, Switzerland, *J. Glaciol.*, 51, 573–587, 2005.
- Picard, G., Brucker, L., Fily, M., Gallée, H. and Krinner, G.: Modeling time series of microwave brightness temperature in Antarctica, *J. Glaciol.*, 55(191), 537–551, doi:10.3189/002214309788816678, 2009.
- Prasad, V. H. and Roy, P., Estimation of snowmelt runoff in Beas Basin, India. *Geocarto Int.*, 20(2), 41–47, 2005.
- Prasch, M., Mauser, W., and Weber, M.: Quantifying present and future glacier melt-water contribution to runoff in a central Himalayan river basin, *The Cryosphere*, 7, 889-904, doi:10.5194/tc-7-889-2013, 2013.
- Purdon, W.: On the trigonometrical survey and physical configuration of the Valley of Kashmir, *Journal of the Royal Geographical Society of London*, 31, 14–30, 1861.
- Rabatel, A., Dedieu, J.-P., and Vincent, C.: Using remote-sensing data to determine equilibrium-line altitude and mass-balance time series: validation on three French glaciers, 1994–2002, *J. Glaciol.*, 51, 539–546, doi:10.3189/172756505781829106, 2005.
- Racoviteanu, A., Armstrong, R., and Williams, M.: Evaluation of an ice ablation model to estimate the contribution of melting glacier ice to annual discharge in the Nepal Himalaya, *Water Resour. Res.*, 49, 5117–5133, 2013.

- Racoviteanu, A., Arnaud, Y., Williams, M., and Manley, W. F.: Spatial patterns in glacier area and elevation changes from 1962 to 2006 in the monsoon-influenced eastern Himalaya, *The Cryosphere Discuss.*, 8, 3949-3998, doi:10.5194/tcd-8-3949-2014, 2014.
- Radić, V. and Hock, R.: Regionally differentiated contribution of mountain glaciers and ice caps to future sea-level rise, *Nat. Geosci.*, 4, 91–94, 2011.
- Raina, V. K., Kaul M. K. and Singh, S.: Mass balance studies of Gara Glacier, *J. Glaciol.* 18(80), 415-423, 1977.
- Raina, V. K. and Srivastava, D.: *Glacier atlas of India*, Geological Society of India, Bangalore, 2008.
- Raina, V. K.: *Himalayan glaciers, A state-of-art review of glacial studies, glacial retreat and climate change*, Ministry of Environment and Forests, India, <http://go.nature.com/pLgJ6D>, 2009.
- Ramanathan, AL.: *Status Report on Chhota Shigri Glacier (Himachal Pradesh)*, Himalayan Glaciology Technical Report No. 1, Department of Science and Technology, Ministry of Science and Technology, New Delhi, 88 pp., 2011.
- Raper, S. C. B. and Braithwaite, R. J.: Low sea level rise projections from mountain glaciers and icecaps under global warming, *Nature*, 439, 311–313, 2006.
- Rasmussen, L. A.: Meteorological controls on glacier mass balance in High Asia, *Ann. Glaciol.*, 54 (63), 352-359 (doi:10.3189/2013AoG63A353), 2013.
- Reijmer, C. H. and Oerlemans, J.: Temporal and spatial variability of the surface energy balance in Dronning Maud Land, East Antarctica, *J. Geophys. Res.*, 107, 4759–4770, doi:10.1029/2000JD000110, 2002.
- Riva, R. E. M., Bamber, J. L., Lavallee, D. A. and Wouters, B.: Sea-level fingerprint of continental water and ice mass change from GRACE, *Geophys. Res. Lett.* 37, L19605, 2010.
- Roy, S. S. and Baling, R. C.: Analysis of trends in maximum and minimum temperature, diurnal temperature range, and cloud cover over India, *Geophys. Res. Lett.*, 32(12), L12702, (10.1029/2004GL022201.), 2005.
- Sangewar, C. V. and Siddiqui, M. A.: *Thematic compilation of mass balance data on glaciers of Satluj catchment in Himachal Himalaya*, Geol. Surv. India, (Unpub.), 2007.
- Sangewar, C. V.: *Remote sensing applications to study Indian glaciers*, Geocarto International, doi:10.1080/10106049.2011.617841, 2011.
- Sarikaya, M. A. et al.: Space-Based Observations of Eastern Hindu Kush Glaciers between 1992 and 2007, Afghanistan and Pakistan, *Remote Sensing Letters*, 3(1), pp.77–84, 2012.
- Schaner, N., Voisin, N., Nijssen, B. and Lettermaier, D. P.: The contribution of glacier melt to streamflow, *Environ. Res. Lett.* 7, 034029, 2012.

- Scherler, D., Bookhagen, B., Strecker, M. R.: Spatially variable response of Himalayan glaciers to climate change affected by debris cover, *Nature Geoscience*, 4, 156–159, doi: 10.1038/ngeo1068, 2011.
- Schmidt, S. and Nüsser, M.: Fluctuations of Raikot Glacier during the past 70 years: a case study from the Nanga Parbat massif, northern Pakistan, *J. Glaciol.*, 55 (194), 949, 2009.
- Shea, J. M., Moore, R. D., and Stahl, K.: Derivation of melt factors from glacier mass-balance records in western Canada, *J. Glaciol.*, 55, 123–130, 2009.
- Shea, J. M., Menounos, B., Moore, R. D., and Tennant, C.: An approach to derive regional snow lines and glacier mass change from MODIS imagery, western North America, *The Cryosphere*, 7, 667–680, doi:10.5194/tc-7-667-2013, 2013.
- Shekhar, M., Chand, H., Kumar, S., Srinivasan, K., and Ganju, A.: Climate-change studies in the western Himalaya, *Ann. Glaciol.*, 51, 105–112, doi:10.3189/172756410791386508, 2010.
- Shrestha, A. B. et al.: Maximum Temperature Trends in the Himalaya and Its Vicinity: An Analysis Based on Temperature Records from Nepal for the Period 1971–94, *Journal of the American Meteorological Society*, 12, 2775 – 2786, 1999.
- Shrestha, M. L. and Shrestha, A. B.: Recent trends and potential climate change impacts on glacier retreat/glacier lakes in Nepal and potential adaptation measures, Paper presented at the OECD Global Forum on Sustainable Development: Development and Climate Change; ENV/EPOC/GF/SD/RD (2004)6/Final, OECD, Paris, 2004.
- Srivastava, D., Sangewar C. V., Kaul, M. K., and Jamwal, K. S.: Mass balance of Rulung Glacier—a Trans-Himalayan glacier, Indus basin, Ladak. *Proc. Symp. Snow, Ice and Glacier*, March 1999, *Geol. Surv. India, Special Publication*, 53, 41–46, 2001.
- Sicart, J. E., Wagnon, P., and Ribstein, P.: Atmospheric controls of the heat balance of Zongo Glacier (16° S, Bolivia), *J. Geophys. Res.*, 110, D12106, doi:10.1029/2004JD005732, 2005.
- Sicart, J. E., Ribstein, P., Francou, B., Pouyaud B. and Condom T.: Glacier mass balance of tropical Glaciar Zongo, Bolivia, comparing hydrological and glaciological methods. *Global Planet. Change*, 59(1–4), 27–36, 2007.
- Sicart, J. E., Hock, R., and Six, D.: Glacier melt, air temperature, and energy balance in different climates: the Bolivian Tropics, the French Alps, and northern Sweden, *J. Geophys. Res.*, 113, D24113, 2008.
- Sicart, J. E., Hock, R., Ribstein, P., Litt, M., and Ramirez, E.: Analysis of seasonal variations in mass balance and meltwater discharge of the tropical Zongo Glacier by application of a distributed energy balance model, *J. Geophys. Res.*, 116, D13105, doi:10.1029/2010JD015105, 2011.
- Singh P., Jain, S. K. and Kumar, N.: Estimation of snow and glacier-melt contribution to the Chenab River, western Himalaya, *Mount. Res. Dev*, 17(1), 49-56, (10.1029/2004GL022201.), 1997.

- Singh, P., Umesh, K. H. and Kumar, N.: Modelling and estimation of different components of streamflow for Gangotri Glacier basin, Himalayas/Modélisation et estimation des différentes composantes de l'écoulement fluvial du bassin du Glacier Gangotri, Himalaya. *Hydrological Sciences Journal*, 53: 309-322, 2008.
- Singh, S. P., Bassignana-Khadka, I., Karky, B. S. and Sharma, E.: *Climate change in the Hindu Kush-Himalayas: The state of current knowledge*, Kathmandu: ICIMOD, 2011.
- Smeets, C. J. P. P. and Van den Broeke, M. R.: The parameterisation of scalar transfer over rough ice surfaces, *Bound.-Lay. Meteorol.*, 128, 339–355, 2008.
- Solomon, S., Qin, D., Manning, M., Chen, Z., Marquis, M., Averyt, K. B., Tignor, M., and Miller, H. L.: *IPCC: Climate Change 2007: The Physical Science Basis. Contribution of Working Group I to the Fourth Assessment Report of the Intergovernmental Panel on Climate Change*, Cambridge University Press, Cambridge, United Kingdom and New York, NY, USA, 2007.
- Span, N. and Kuhn, M.: Simulating annual glacier flow with a linear reservoir model, *J. Geophys. Res.*, 108(D10), 4313, (10.1029/2002JD002828.), 2003.
- Steiner, D., Pauling, A., Nussbaumer, S. U., Nesje, A., Luterbacher, J., Wanner, H. and Zumbühl, H. J.: Sensitivity of European glaciers to precipitation and temperature—two case studies, *Clim. Change*, 90, 413–441, doi:10.1007/s10584-008-9393-1, 2008.
- Stocker, T. F., Qin, D., Plattner, G.-K., Tignor, M., Allen, S. K., Boschung, J., Nauels, A., Xia, Y., Bex, V., and Midgley, P. M.: *IPCC: Climate Change 2013: The Physical Science Basis. Contribution of Working Group I to the Fifth Assessment Report of the Intergovernmental Panel on Climate Change*, Cambridge University Press, Cambridge, United Kingdom and 10 New York, NY, USA, in press, 2013.
- Sun, W., Qin, X., Du, W., Liu, W., Liu, Y., Zhang, T., Xu, Y., Zhao, Q., Wu, J., and Ren, J.: Ablation modeling and surface energy budget in the ablation zone of Laohugou glacier No. 12, western Qilian mountains, China, *Ann. Glaciol.*, 55(66), 111-120, 10.3189/2014AoG66A902, 2014.
- Survey of India 2005: National map policy. <http://www.surveyofindia.gov.in/tenders/nationalmappolicy/nationalmappolicy.pdf>
- Tangborn, W. and Rana, B.: Mass balance and runoff of the partially debris-covered Langtang Glacier, Nepal. *IAHS Publ. 264 (Symposium at Seattle 2000 – Debris-Covered Glaciers)*, 99–108, 2000.
- Taylor, J. R.: *An introduction to error analysis: the study of uncertainties in physical measurements*. University Science Books, Sausality, California. 2nd ed., 1997.
- Taylor, K. E., Stouffer, R. J. and Meehl, G. A.: An overview of CMIP5 and the experiment design. *Bull. Am. Meteorol. Soc.* 93, 485-489, 2012.

- Tewari, A. P.: Recent changes in the snout of Pindari glacier (Kumaun Himalayas), The role of snow and ice in hydrology, Proceedings of Banff Symposia, Sept. 1972, UNESCO-WHOIAHS, 1973.
- Thayyen, R. J. and Gergan, J. T.: Role of glaciers in watershed hydrology: a preliminary study of a "Himalayan catchment", *The Cryosphere*, 4, 115-128, doi:10.5194/tc-4-115-2010, 2010.
- Thibert, E., Blanc, R., Vincent, C. and Eckert, N.: Glaciological and volumetric mass-balance measurements: error analysis over 51 years for Glacier de Sarennes, French Alps. *J. Glaciol.*, 54(186), 522–532, 2008.
- Thibert, E., Eckert, N., and Vincent, C.: Climatic drivers of seasonal glacier mass balances: an analysis of 6 decades at Glacier de Sarennes (French Alps), *The Cryosphere*, 7, 47-66, doi:10.5194/tc-7-47-2013, 2013.
- Third Pole Environment: Report of TPE Glacial Mass Balance Flagship Station, Workshop in Guangzhou, By TPE Glacial Mass Balance Flagship Station Working Group, February 20-21, 2012.
- Van den Broeke, M. R.: Momentum, heat and moisture budgets of the katabatic wind layer over a mid-latitude glacier in summer, *Journal of Applied Meteorology* 36, 763-774, 1997.
- Van den Broeke, M. R., Van As, D., Reijmer, C. H., and Van de Wal, R. S. W.: Assessing and Improving the Quality of Unattended Radiation Observations in Antarctica, *J. Atmos. Ocean. Tech.*, 21, 1417–1431, 2004.
- Van den Broeke, M. R., Smeets, C. J. P. P., and Van de Wal, R. S. W.: The seasonal cycle and interannual variability of surface energy balance and melt in the ablation zone of the west Greenland ice sheet, *The Cryosphere*, 5, 377-390, doi:10.5194/tc-5-377-2011, 2011.
- Vincent, C., Vallon, M., Reynaud, L. and Le Meur, E.: Dynamic behaviour analysis of glacier de Saint Sorlin, France, from 40 years of observations, 1957–97, *J. Glaciol.*, 46(154), 499–506, 2000.
- Vincent, C.: Influence of climate change over the 20th century on four French glacier mass balances, *J. Geophys. Res.*, 107(D19), 4375. (10.1029/2001JD000832.), 2002.
- Vincent, C., Kappenberger, G., Valla, F., Bauder, A., Funk, M., and Le Meur, E.: Ice ablation as evidence of climate change in the Alps over the 20th century, *J. Geophys. Res.*, 109, D10, D10104, doi:10.1029/2003JD003857, 2004.
- Vincent, C., Le Meur, E., Six, D. and Funk, M.: Solving the paradox of the end of the Little Ice Age in the Alps, *Geophys. Res. Lett.*, 32(9), L09706, (10.1029/2005GL022552.), 2005.
- Vincent, C., Soruco, A., Six, D. and Le Meur, E.: Glacier thickening and decay analysis from 50 years of glaciological observations performed on Glacier d'Argentière, Mont Blanc area, France, *Ann. Glaciol.* 50, 73-79, 2009.

- Vincent, C., Ramanathan, A., Wagnon, P., Dobhal, D. P., Linda, A., Berthier, E., Sharma, P., Arnaud, Y., Azam, M. F., Jose, P. G., and Gardelle, J.: Balanced conditions or slight mass gain of glaciers in the Lahaul and Spiti region (northern India, Himalaya) during the nineties preceded recent mass loss, *The Cryosphere*, 7, 569-582, doi:10.5194/tc-7-569-2013, 2013.
- Wagnon, P., Ribstein, P., Francou, B., and Pouyaud, B.: Annual cycle of energy balance of Zongo Glacier, Cordillera Real, Bolivia, *J. Geophys. Res.*, 104, 3907-3923, 1999.
- Wagnon, P., Ribstein, P., Francou, B., and Sicart, J. E.: Anomalous heat and mass balance budget of Glaciar Zongo, Bolivia, during the 1997/98, El Nino year, *J. Glaciol.*, 47, 21-28, 2001.
- Wagnon, P., Sicart, J.-E., Berthier, E., and Chazarin, J.-P.: Wintertime high-altitude surface energy balance of a Bolivian glacier, Illimani, 6340 m above sea level, *J. Geophys. Res.*, 108, 4177, doi:10.1029/2002JD002088, 2003.
- Wagnon, P., Linda, A., Arnaud, Y., Kumar, R., Sharma, P., Vincent, C., Pottakkal, G. J., Berthier, E., Ramanathan, A., Hasnain, S. I. and Chevallier, P.: Four years of mass balance on Chhota Shigri Glacier, Himachal Pradesh, India, A New Benchmark Glacier In the western Himalaya, *J. Glaciol.*, 53(183), 603-610, 2007.
- Wagnon, P., Lafaysse, M., Lejeune, Y., Maisincho, L., Rojas, M., and Chazarin, J. P.: Understanding and modeling the physical processes that govern the melting of snow cover in a tropical mountain environment in Ecuador, *J. Geophys. Res.*, 114, D19113, doi:10.1029/2009JD012292, 2009.
- Wagnon, P., Vincent, C., Arnaud, Y., Berthier, E., Vuillermoz, E., Gruber, S., Ménégoz, M., Gilbert, A., Dumont, M., Shea, J. M., Stumm, D., and Pokhrel, B. K.: Seasonal and annual mass balances of Mera and Pokalde glaciers (Nepal Himalaya) since 2007, *The Cryosphere*, 7, 1769-1786, doi:10.5194/tc-7-1769-2013, 2013.
- Weiers, S.: Zur Klimatologie des NW-Karakoram und angrenzender Gebiete. Statistische Analysen unter Einbeziehung von Wettersatellitenbildern und eines Geographischen Information systems (GIS), *Bonner Geographische Abhandlungen*, 92, Geographisches Institut, Universität Bonn, Bonn, Germany, 1995.
- Wu, L., Li, H., and Wang, L.: Application of a degree-day model for determination of mass balance of Urumqi Glacier No. 1, eastern Tianshan, China, *J. Earth Sci.*, 22(4), 470-481, doi:10.1007/s12583-011-0201-x, 2011.
- Wulf, H., Bookhagen, B., and Scherler, D.: Seasonal precipitation gradients and their impact on fluvial sediment flux in the Northwest Himalaya, *Geomorphology*, 118, 13-21, 2010.
- Yadav, R. R., Park, W. K., Singh, J. and Dubey, B.: Do the western Himalayas defy global warming? *Geophys. Res. Lett.*, 31(17), L17201, (10.1029/2004GL020201.), 2004.
- Yang, X., Zhang, Y., Zhang, W., Yan, Y., Wang, Z., Ding, M. and Chu, D.: Climate Change in Mt. Qomolangma Region since 1971, *Journal of Geographical Sciences*, 16, 326-336, 2006.

Yang, W., Guo, X., Yao, T., Yang, K., Zhao, L., Li, S., and Zhu, M.: Summertime surface energy budget and ablation modeling in the ablation zone of a maritime Tibetan glacier, *J. Geophys. Res.*, 116, D14116, doi:10.1029/2010JD015183, 2011.

Zemp, M., Hoetzle, M. and Haeberli, W.: Six decades of glacier mass-balance observations: a review of worldwide monitoring network, *Ann. Glaciol.*, 50(50), 101-111, 2009.

Zemp, M., Thibert, E., Huss, M., Stumm, D., Rolstad Denby, C., Nuth, C., Nussbaumer, S. U., Moholdt, G., Mercer, A., Mayer, C., Joerg, P. C., Jansson, P., Hynek, B., Fischer, A., Escher-Vetter, H., Elvehøy, H., and Andreassen, L. M.: Reanalysing glacier mass balance measurement series, *The Cryosphere*, 7, 1227–1245, doi:10.5194/tc-7-1227-2013, 2013.

Zhang, Y., Liu, S., and Ding, Y.: Observed degree-day factors and their spatial variation on glaciers in western China, *Ann. Glaciol.*, 43, 301-306, 2006.

Zhang, G., Kang, S., Fujita, K., Huintjes, E., Xu, J., Yamazaki, T., Haginoya, S., Wei, Y., Scherer, D., Schneider, C., Yao, T.: Energy and mass balance of the Zhadang Glacier surface, central Tibetan Plateau, *J. Glaciol.*, 213, 137-148, doi:10.3189/2013JoG12J152, 2013.

List of Tables

Table 1.1	Snout fluctuation records for some selected glaciers from the HKH region. See Fig. 1.3 for recession evolution	10
Table 1.2	Glacier-wide mass balance observations from the HKH region	13
Table 2.1	Measurement specifications for AWS-M located at 4863 m a.s.l. on the western lateral moraine of Chhota Shigri Glacier and precipitation gauge installed at base camp (3850 m a.s.l.). Variable symbols are also given.....	21
Table 2.2	Mean seasonal values of T_{air} , RH, u , SWI and LWI at AWS-M. T_{air} , RH, u and SWI are the mean seasonal values of four hydrological years between 1 October 2009 and 30 September 2013 while LWI are the mean seasonal values between 1 June 2010 and 30 September 2013. P is the seasonal precipitation for one hydrological year between 1 October 2012 and 30 September 2013 at glacier base camp collected by the precipitation gauge.....	27
Table 2.3	Annual and 11-year mean glacier-wide mass balances (B_a), ELA, AAR and MB gradients db/dz (m w.e. $(100m)^{-1}$) for Chhota Shigri Glacier. The standard deviation (STD) is also displayed for every variable. The uncertainty range for B_a is ± 0.40 m w.e.....	37
Table 3.1	Calculated ice flux, mean surface ice velocity and maximum ice depth at each cross section. The mean surface horizontal ice velocities are from DGPS measurements performed in 2003/04. The satellite-derived mean ice velocities are from the correlation of satellite images acquired on 13 November 2004 and 21 September 2005 (NA: Not available).	49
Table 3.2	Ice fluxes (in 10^6 m ³ ice a ⁻¹), inferred at each cross section from annual mass-balance data.	53
Table 3.3	Ice fluxes (in 10^6 m ³ ice a ⁻¹), obtained at every cross section, using steady state mass-balance assumption for every surveyed year.....	53
Table 3.4	Thickness and surface velocity changes between 2003 and 2010 on 5 longitudinal cross sections (NA: Not available).....	56
Table 4.1	List of the model parameters used for MB reconstruction.....	72
Table 4.2	Comparison of cumulative MBs (m w.e.).....	76

Table 4.3	Mean annual, summer and winter MBs for periods I, II and III and for the whole 43 year period, with their corresponding mean summer temperatures and winter precipitations at Bhuntar meteorological station.	78
Table 5.1	Measurement specifications for AWS-G located at 4670 m a.s.l. on the mid ablation zone of Chhota Shigri Glacier, AWS-M located on a moraine at 4863 m a.s.l., and precipitation gauge installed at base camp (3850 m a.s.l.). Accumulation/Ablation at AWS-G was measured by SR50A sensor (section 2.3). Variable symbols are also given. Sensor heights indicate the initial distances to the surface (12 August 2012).	91
Table 5.2	Seasonal means and annual mean (standard deviations) of T_{air} , RH, u and SWI over four hydrological years between 1 October 2009 and 30 September 2013 except for LWI (only three years between 1 October 2010 and 30 September 2013) at AWS-M (4863 m a.s.l.). P is the seasonal precipitation for one hydrological year between 1 October 2012 and 30 September 2013 at glacier base camp collected by the Geonor T-200B.	97
Table 5.3	60-day means (standard deviations) of meteorological and SEB variables measured or computed at AWS-G (4670 m a.s.l.) on Chhota Shigri Glacier for different representative periods. The symbols for variables are described either in the text or in Table 5.1. SWN, LWN, and R are net short-wave, long-wave and all-wave radiations, respectively.	104
Table 5.4	Comparison of SEB components on different glaciers in the High Mountain Asia. All fluxes are in $W m^{-2}$, Values in brackets are the % contribution of each energy flux.	119

List of Figures

Figure 1.1	Map of the Hindu-Kush Karakoram Himalayan range showing the location of three major river basins. The base map comes from Google Earth, the basin boundaries are provided by <i>International Centre for Integrated Mountain Development (ICIMOD)</i> and the boundary shape is provided by Dr. Tobias Bolch. The balloons A-W show the location of the glaciers surveyed by glaciological method in the whole HKH region.....	2
Figure 1.2	The processes determining the energy flux at the glacier-atmosphere interface	6
Figure 1.3	The recession evolution for some selected glaciers in the HKH region over the last 170 years	11
Figure 1.4	Glacier annual glacier-wide mass balances in the Hindu-Kush Karakoram Himalayan region. (a) Annual B_a of glaciers with more than one year of observations. The dark brown and blue thick lines correspond to the pentadal Himalaya–Karakoram averages from Cogley (2011) and decadal MBs of Chhota Shigri Glacier from Vincent et al. (2013), respectively (b) cumulative MBs.....	14
Figure 2.1	Map of Chhota Shigri Glacier showing the ablation stakes in eastern flank (blue dots), western flank (green dots), debris cover area (black dots), accumulation sites (red squares), AWS-M (black star) and precipitation gauge (black cross). The map coordinates are in the UTM43 (north) World Geodetic System 1984 (WGS84) reference system	22
Figure 2.2	Daily means of (a) T_{air} ($^{\circ}C$), (b) RH (%), (c) u ($m\ s^{-1}$), (d) SWI ($W\ m^{-2}$) and (e) LWI ($W\ m^{-2}$) at AWS-M. T_{air} , RH, u and SWI are the daily means for the full observation period between 18 August 2009 and 30 September 2013 while LWI are the daily means between 23 May 2010 and 30 September 2013. The lowest panel (f) shows the daily precipitation (mm w.e.) between 12 July 2012 and 30 September 2013 at glacier base camp collected by the precipitation gauge. The thick line in panels a-e is the 15 day running mean.....	26
Figure 2.3	Wind rose (direction and intensity of half-hourly average data) at AWS-M for post-monsoon, winter, pre-monsoon and the summer-monsoon over four hydrological years of observation. The data is hourly average between 1 September 2009 and 22 May 2010. The frequency of wind	

direction is expressed as percentage for each season (indicated on the radial axes).....28

Figure 2.4 Panels a–g show the annual point MB (dots) as a function of altitude derived from field measurements (stakes, drillings or pits) on Chhota Shigri Glacier for seven hydrological years between 2006 and 2013. The black, blue and green dots are the annual point MBs over debris cover area (<4400 m a.s.l.), eastern flank and western flank of glacier, respectively whereas red dots are the MBs at 5500/5550 m a.s.l. B_a and ELA for every year are also displayed on the corresponding panel. Panel h shows the hypsometry (50-m altitudinal ranges) and mean altitudinal MBs (brown dots) of Chhota Shigri Glacier. The mean altitudinal MBs are mean MBs for each 50-m range (e.g., 4400 MB represents the mean MB for 4400–4450 range), except for at 4250 and 5400 where the mean MB are for 4050–4300 and 5400–6250 range, respectively31

Figure 2.5 Cumulative (blue line) and annual glacier-wide mass balances (red (-) and green (+) histograms) of Chhota Shigri Glacier between 2002 and 2013. Black error bars represent the uncertainty in annual glacier-wide mass balance calculated in Azam et al. (2012)33

Figure 2.6 The equilibrium line altitude (m a.s.l.) and accumulation area ration (%) as a function of annual glacier-wide mass balance34

Figure 2.7 Annual, winter and summer mass balances are shown by light black, light blue and light orange histograms. The annual, winter and summer precipitations (temperatures) are shown by black, blue and orange histograms (dots). The mean temperatures are from AWS-M while the precipitations sums are from Bhuntar meteorological station36

Figure 3.1 Map of Chhota Shigri Glacier with the measured transverse cross-sections (lines 1-5), the ablation stakes (dots) and the accumulation sites (squares). Also shown are longitudinal sections (lines A-E) used to calculate thickness and ice velocity variations (see section 2.4.2). The map (contour lines, glacier delineation) was constructed using a stereoscopic pair of SPOT5 (Système Pour l’Observation de la Terre) images acquired 12 and 13 November 2004 and 21 September 2005 (Wagnon et al., 2007). The map coordinates are in the UTM43 (north) World Geodetic System 1984 (WGS84) reference system44

Figure 3.2 Cumulative (blue line) and annual glacier-wide mass balances (red (-) and green (+) histograms) of Chhota Shigri Glacier between 2002 and 201046

Figure 3.3	The 2002–10 average mass-balance profile and hypsometry of Chhota Shigri Glacier. Altitudinal ranges are of 50m (e.g., 4400 stands for the range 4400–4450 m), except for 4250 and 5400 which stand for 4050–4300 and 5400–6250m respectively	48
Figure 3.4	Radargram of cross section 2: radar signals plotted side by side from west to east in their true spatial relationship to each other (interval between each signal of 10 m). The x-axis gives the amplitude of each signal (50 mV per graduation); the y-axis is the double-time interval (μ s)	49
Figure 3.5	Ice depth and surface topography of cross-sections 1-5. The horizontal and vertical scales are the same for all cross-sections. All cross sections are oriented from west to east except cross section 5 which is north-south oriented.....	50
Figure 3.6	Measured ice velocities plotted as a function of the distance from the 2010 terminus position. Measurements were collected along the central flow line.....	51
Figure 3.7	Ice fluxes at every cross section derived (i) from 2003/04 ice velocities and section areas (red open squares) and (ii) from mass balance method for a glacier-wide MB = 0 m w.e. (black squares) or a glacier-wide MB = -0.67 m w.e. (blue triangles).....	54
Figure 3.8	Elevation (dots) and surface ice velocity (triangles) between 2003 (continuous lines) and 2010 (dashed lines) along the longitudinal sections A, B, C, D and E shown in Fig. 3.1	56
Figure 4.1	Location map of Chhota Shigri Glacier and its surroundings. Roads are shown in green, river in blue and Chhota Shigri Glacier as a star. The upper left inset shows a map of Himachal Pradesh, India, with the location of the Bhuntar meteorological station and glacier (star) indicated in the box. The lower right inset is a map of Chhota Shigri Glacier with the location of the AWS-M (red diamond). The map coordinates are in the UTM 43 (north) World Geodetic System 1984 (WGS84) reference system.....	63
Figure 4.2	Annual mean temperature (red squares) and annual precipitation sums (green bars) recorded at Bhuntar meteorological station from January 1969 to October 2012.....	65
Figure 4.3	Mean monthly precipitations between 1969 and 2012 at Bhuntar meteorological station. Summer precipitation (red bars) predominantly derives from the Indian summer monsoon, whereas winter precipitation (blue bars) predominantly derives from mid-latitude westerlies. The	

	error bars represent the standard deviation ($\pm 1\sigma$) of the monthly precipitation mean.....	65
Figure 4.4	Polynomial fit (black line) for the day-of-year average values of LRs (orange circles). Day-of-year 1 corresponds to 1 October. Every dot stands for a daily value of LR for each day of the year, averaged over three hydrological years (1 October 2009 to 30 September 2012). Also shown is the correlation coefficient R^2 between LR daily values and the corresponding polynomial fit (95% confidence level).....	68
Figure 4.5	Measured ablation for debris (black squares), ice (blue dots) and snow (red stars) surfaces as a function of CPDD. In total 192 measurements performed between June and October 2009, 2011 and 2012 were selected for analysis. Also shown are the respective correlation coefficients R^2 (95% confidence level).....	70
Figure 4.6	Comparison of reconstructed annual (red dots) with observed annual MBs (black triangles) as a function of elevation for 10 hydrological years 2002-2012. RMSE (m w.e. a ⁻¹) for each year is also given.....	73
Figure 4.7	Comparison of modeled B_a (black points) with observed B_a (red squares) and decadal geodetic MBs (blue thick lines). The corresponding uncertainties in modeled, observed and geodetic MBs are also shown. Black thick line shows the 5 year running mean value since 1969.....	75
Figure 4.8	Annual and seasonal MB series of Chhota Shigri Glacier, 1969-2012. Black, green and red dots represent the annual, winter and summer MBs with their corresponding error bars respectively. The thick lines are the 5 day running means. The horizontal dotted line represents the zero MB.....	76
Figure 4.9	Mean winter, summer and annual MBs for all 3 periods since 1969 (black thick lines). Red thick line represents the summer mean temperatures (°C), while green line represents the annual winter precipitation sums (mm) at Bhuntar meteorological station. The continuous thin red and green lines represent the average summer temperatures (°C) and winter precipitation sums (mm) between 1969 and 2012 respectively. The black dotted line represents zero MB.....	78
Figure 4.10	MB sensitivity of Chhota Shigri Glacier to temperature as a function of altitude (dotted line) compared to glaciers in the French Alps (various symbols) (Vincent, 2002). The lower and upper x-axis are the elevations for Chhota Shigri and French glaciers respectively and have been shifted to match their ELAs (thin vertical line).....	80

Figure 4.A1	A mean annual mass balance cycle at daily (a) and monthly (b) time-steps (data from 1969 to 2013 averaged every day (a) or month (b). Hydrological year is defined between 1 st October (day 0 on x-axis) and 30 th September	83
Figure 5.1	Map of Chhota Shigri Glacier showing the ablation stakes (black small squares), accumulation sites (black big squares), AWSs (red stars) and precipitation gauge (black cross). The map coordinates are in the UTM43 (north) World Geodetic System 1984 (WGS84) reference system	90
Figure 5.2	Half-hourly values of LWO as a function of T_{air} , (a) before and (b) after applying the correction for T_{air} above 0 °C. The dashed lines indicate 0 °C and 315.6 W m ⁻² , the maximum LWO for a melting surface.....	93
Figure 5.3	Photographs of AWS-G on Chhota Shigri Glacier taken on 09 October 2012 (left panel) and on 22 August 2013 (right panel) (©: Mohd. Farooq Azam). SR50A mounted on a separate pole drilled into the ice, is visible to the left of AWS-G.....	95
Figure 5.4	Mean monthly values of T_{air} (black dots), RH (green crosses), u (orange squares), SWI (grey bars) and LWI (light blue-green bars) at AWS-M (4863 m a.s.l.). T_{air} , RH, u and SWI are the mean monthly values of four hydrological years between 1 October 2009 and 30 September 2013 while LWI are the mean monthly values of three hydrological years between 1 October 2010 and 30 September 2013. Also shown are the monthly values of T_{air} (black circles), RH (light green crosses), u (orange hollow squares), SWI (black hollow triangles) and LWI (blue hollow squares) used to derive the mean monthly values	96
Figure 5.5	Comparison of monthly precipitations (blue bars) at Chhota Shigri base camp for 2012/13 hydrological year with the mean monthly precipitations (red bars) between 1969 and 2013 at Bhuntar meteorological station. The error bars represent the standard deviation (1σ) of the monthly precipitation mean	97
Figure 5.6	Boxplots of seasonal and annual T_{air} (a) and precipitation (b) obtained from 44 hydrological years (1969 to 2013) from Bhuntar meteorological station. Boxes cover the 25 th to the 75 th percentile of each distribution with a central line as the median. The blue thick horizontal line is the 1969-2013 mean, red dot is the 2012/13 hydrological year mean	99
Figure 5.7	Daily meteorological variables recorded at AWS-G (4670 m a.s.l.) as representative of post-monsoon (1 October to 29 November 2012), winter (1 December to 29 January 2013) and summer-monsoon (8 July to 5	

	September 2013) periods. Also shown (lower panel) are the snow falls derived from SR50A data at AWS-G.....	105
Figure 5.8	Scatter plots showing relations between u , T_{air} and WD. In both panels (a and b) all the available measurements are shown, and every dot represents a half-hourly mean value. The inset in (a) highlights the relationship between u and T_{air} above 0 °C. The arrow in (b) indicates the direction of the local flow line of the glacier	107
Figure 5.9	WD and u (half-hourly means) at AWS-G for post-monsoon, winter and summer-monsoon representative periods. The frequency of WD is expressed as percentage over the entire observational period (indicated on the radial axes).....	107
Figure 5.10	Daily values of the surface energy fluxes at AWS-G (4670 m a.s.l.) as representative of post-monsoon (1 October to 29 November 2012), winter (1 December to 29 January 2013) and summer-monsoon (8 July to 5 September 2013) periods. SWN, LWN, H , LE, G , SW_{sub} and F_{surface} are the net short-wave radiation, the net long-wave radiation, the turbulent sensible and latent heat fluxes, the conductive heat flux, the short-wave radiation penetrating below the surface, and the amount of energy available at the surface, respectively.....	109
Figure 5.11	Comparison between ablation computed from the SEB Eq. and measured at stake n° VI (a) during several few-day to few-week periods of 2012 and 2013 summers where field measurements are available. (b) Comparison between modeled half-hourly ($T_{\text{s,mod}}$) and observed ($T_{\text{s,obs}}$) surface temperatures over the whole simulation period. Also shown are the 1:1 line (dashed line) and the regression line (solid line).....	111
Figure 5.12	Mean diurnal cycle of meteorological and SEB variables at AWS-G (4670 m a.s.l.) as representative of post-monsoon (1 October to 29 November 2012), winter (1 December to 29 January 2013) and summer-monsoon (8 July to 5 September 2013) periods.....	113
Figure 5.13	Comparison of computed cumulative melting (black thick line) between 15 August and 30 September from summers 2012 (a) and 2013 (b). Also shown are the mean T_{air} (red open dots), the number of hours in a day when $T_{\text{s,mod}}$ is > -1 °C (black dots), daily albedo (dark green dots) and the precipitations as rain/snow obtained from records at base camp (blue and green bars, respectively). The grey line in panel (a) is the computed cumulative melting between 15 August and 30 September 2012 assuming a constant surface albedo of 0.19	116

Figure 5.14 Annual glacier-wide mass balance as a function of the sum of the 3 largest summer-monsoon daily snowfalls assessed from precipitation record from Bhuntar meteorological station (see text for details) between 2002 and 2013.....118